

FLOATING MEGASTRUCTURES

Future world's largest tidal power plant

The Tidal Bridge

An analysis of the dynamic response
of the Palembang Tidal Bridge.

Hydraulic Engineering Master's thesis by

F. F. H. M. Hoogsteder



Cover image by Henriëtte Teeuwen (2018)
Labuan Bajo, Komodo National Park, Flores, Indonesia

The Tidal Bridge

An analysis of the dynamic response of The Palmerah Tidal Bridge

Future world's largest tidal power plant and floating bridge.
(Strait of Larantuka, Indonesia.)

by

F.F.H.M. Hoogsteder

to obtain the degree of Master of Science
in Civil Engineering - Hydraulic Engineering
at the Delft University of Technology.

Student number: 4 227 956
Project duration: September 2018 – June 2019
Thesis committee: Dr. ir. J. D. Bricker Delft University of Technology, chair
Dr. ing. M. Z. Voorendt Delft University of Technology
Dr. ir. H. Hendrikse Delft University of Technology
Ir. M. Meijer BAM Infraconsult

This thesis is confidential and cannot be made public until June 2021.

An electronic version of this thesis is available at <http://repository.tudelft.nl/>.



Acknowledgements

Since I was just a little kid, I have always been keen to craft with any material I was given, and Lego of course was a wonderful tool to express my imagination. Little did I know, that 20 years later walking on a construction site makes me feel like that enthused child on a large playground with unlimited crafting materials. Large constructions have always fascinated me, which is why I started my bachelor in Civil Engineering at the Delft University of Technology in 2012. The wise words of Albert Einstein, "*Time flies when your having fun*", showed nothing but the truth. Time flew by the last 6,5 years and, without a doubt, I would do it all over again with even more pleasure.

My final task as a student is practically finished by writing these words; the last words of my graduation thesis. The final step before obtaining the degree of Master of Science at Delft University of Technology in the field of Hydraulic Engineering. The thesis subject combines my enthusiasm for hydraulic structures with my other passions: creativity, sustainability and ingenuity. A completely new design with a lot of exciting challenges: *The Tidal Bridge*.

First of all, I would like to thank the *Delta Marine Constructions* department within *BAM Infraconsult* that they trusted me with this challenging mission. Martijn, you always believed in my capabilities and was always very keen to answer my questions. Erik and Michiel, you were my Ansys Aqwa heroes, without your expertise my model would have never made it past the 'Solve Aborted' stage. And of course, all other colleagues deserve a gratitude, especially Andre, Ivo, Marko and Ruud. Everytime I encountered a problem it was solved within seconds with quick brainstorm sessions. Furthermore, I would like to thank the whole team that they adopted me in their BAM family and for all the wonderful weeks we've spent together.

At last, I would like to thank the committee members of the TU Delft for accepting my challenge at BAM Infraconsult and that they were willing to share their view, knowledge and experience with me. Mark, without your insight in rapportation techniques and formulating project proposals, my thesis would have been considerably more chaotic. Hayo, your view on dynamics and the Ansys Aqwa software resulted in understanding what I was actually doing. At last, Jeremy, thanks for asking sharp in-depth questions that improved the content of my report significantly.

Last thanksgiving goes to all family and friends that were always open to listen to all my stories, even without any knowledge of the subject. Their support made the whole thesis journey delightful. All in all, I experienced a wonderful and enlightening time working on my research the past months. Rewarded with a Masters degree on Civil Engineering, it was definitely worth it. I am looking forward to what the future is going to bring and I hope that you enjoy reading my report.

Fiona Hoogsteder

The Hague,
June 12, 2019

Abstract

The objective of this master thesis is to gain knowledge regarding the dynamic behaviour of *The Palmerah Tidal Bridge* to hydraulic loads. The Palmerah Tidal Bridge will become future's largest tidal power plant and a floating bridge between two islands in the Flores region, Indonesia. A combination of the two functions requires a dynamic design that allows movements and a design that is able to withstand severe loads. A pre-feasibility design is proposed, however the technical feasibility is not proven yet. Safety and stability are two key concepts to substantiate the technical feasibility. In addition, an estimation of the probable motions and accelerations may indicate whether traffic is able to cross the bridge safely.

The Tidal Bridge concept idea is complete different to other floating bridges. The bridge will be located in highly dynamic waters with flow speeds up to 7,5 m/s and a semi diurnal tidal range of 3 m. The resistance of the tidal water power turbines increases the drag force even more. To limit the maximum displacement a pendulum mooring system is proposed. A steel pendulum is connected with hinges to the seabed and the pontoons and regulates the motion induced by the tidal range. The main components are visualised in Figure 1. The floating bridge is highly dynamic and will be constantly in motion.

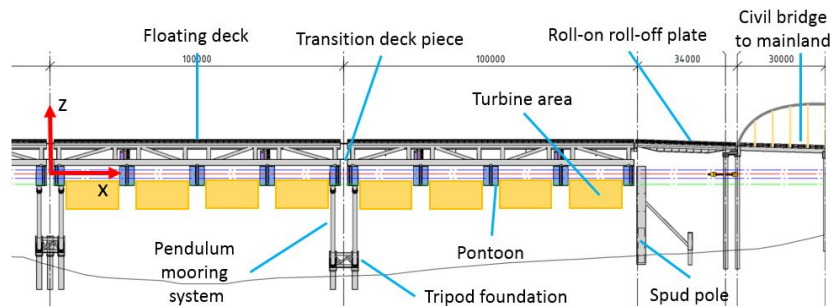


Figure 1: Front view of half of the Tidal Bridge design including main nomenclature of main components.

The aim of the project is to create insight in the behaviour of the coupled floating bridge structure. Obtaining information regarding the most sensitive structural parameters of the system may suggest design changes that result in an increase in stability of the bridge. This leads to a research question that is answered in the report: "*Is the dynamic response of the present design of the Palmerah Tidal Bridge induced by waves and currents of an acceptable magnitude regarding traffic serviceability?*". An answer to the research question is found by substantiating the following questions:

1. What data is required to compute the likely motion of the Palmerah Tidal Bridge?
2. Is the Palmerah Tidal Bridge stable enough to allow traffic safely across the bridge?

First, data is acquired that is required to create a virtual bridge model. The project location and present bridge design are analysed with available data, literature and calculations. Serviceability limits are estimated that allow traffic safely across the bridge. Governing loads that act on the bridge are determined and the structural properties of the bridge are calculated. The desired downtime of the bridge is 5% of its lifetime. Waves present during 5% of the lifetime have a significant wave height of 0,80 m, a frequency of 0,22 Hz and are coming from the north-east. The maximum flow velocity is based on the requirement regarding the maximum allowable roll-moment (2,1 MNm/m) and on a static CFD-model of the turbine-pontoon structure. The data implied a drag coefficient of $C_d = 2,11$, which is proportional to a flow speed of 5,2 m/s. The natural frequencies and hydrostatic properties of a single freely floating floater are calculated. The hydrostatic stiffness is used to calculate a first estimation of the roll-rotation as a result of current-induced pressures. During a positive and negative flow speed the maximum roll-rotations is 6,7 degrees. The software programs used for the data computations are Matlab, Matrixframe, MathCad and Excel.

Secondly, the data is converted into a virtual bridge model in the software package Ansys Aqwa. Ansys Aqwa is globally used to indicate the dynamic response of offshore maritime structures to wave induced pressures. The software has limitations regarding the current velocity implementation. The drag force should be defined manually and acts at the centre of gravity of the structure. As a result, the force 'moves' with the structure and the application point of the drag force can be located above the waterline. The virtual bridge model seems realistic for waves and positive flow speeds. However, the response to negative flow speeds is unrealistic, indicating that the Ansys Aqwa model is inaccurate. The model can not be calibrated as knowledge about the likely motion of the bridge is unknown, but the roll-rotation during a positive current is of the same magnitude as the stability calculation, visualised in Figure 2.

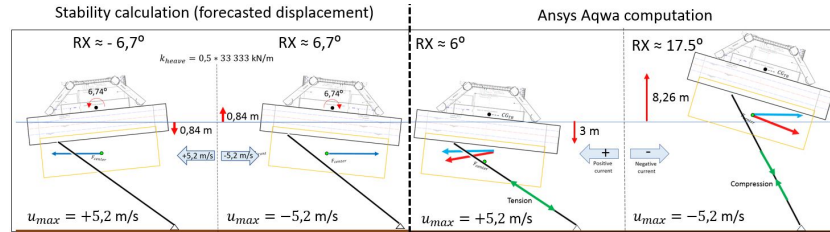


Figure 2: Forecasted displacement versus displacement computed by Ansys Aqwa. Both seen with respect to the middle two floaters

The sensitivity study indicated that the bridge is most vulnerable to north-eastern low frequency waves directed perpendicular to the bridge deck. The mooring system reduces the magnitude of induced motion with a factor 2,5. For the flow sensitivity study the spudpole characteristics are iterated. An increased bending stiffness results in a decrease in rotation and a more probable dynamic response. Motion of the bridge is mainly induced by the current velocity and the accelerations are a result of the wave induced pressures, substantiated in Table 1. The bridge experiences gradual current-induced rotations. On top of these rotations the wave-induced motion fluctuates, generating continuous movement and accelerations of the bridge that cause sincere discomfort for traffic. The dynamic response of the present design of the Tidal Bridge exceeds the estimated serviceability limits heavily and is not acceptable.

		Surge		Sway		Heave		Roll		Pitch		Yaw	
		Along x-axis		Along y-axis		Along z-axis		Around x-axis		Around y-axis		Around z-axis	
		[m]	[m/s ²]	[m]	[m/s ²]	[m]	[m/s ²]	[°]	[°/s ²]	[°]	[°/s ²]	[°]	[°/s ²]
Serviceability limits		-	0,50	-	0,50	3,00	0,70	2,52	6,13	2,01	4,01	3,44	2,86
Waves	Current												
from SW	No	0,13	0,01	3,51	0,08	0,06	0,07	0,12	0,25	0,10	0,08	0,03	0,04
from NE	No	0,14	0,09	3,36	0,28	0,49	0,83	1,70	2,96	0,41	0,61	0,11	0,16
No	Yes	0,15	0,02	20,27	0,15	8,41	0,05	19,68	0,28	4,38	0,09	8,16	0,10
from SW	Yes	0,15	0,02	20,25	0,17	8,42	0,40	19,65	0,57	4,44	0,54	8,16	0,20
from NE	Yes	0,17	0,37	20,47	0,32	8,53	0,78	20,49	2,87	4,44	0,90	8,26	0,33

Table 1: Overview of estimated serviceability limits and the maximum dynamic response to a combination of waves and current.

Substantiated on the previous information, seven design suggestions are proposed. The two most promising alternatives are implemented in the virtual model: the improved spudpole design and a complete rotation of the present bridge design. The results are favourable, all magnitudes of motion for the critical degrees of freedom decreased with approximately 70%. The peak values of the dynamic response are given in Table 2. The improved design approaches the serviceability limits and the technical feasibility becomes more realistic. Nonetheless, the estimated serviceability limits are still exceeded and the likely motion of the present Tidal Bridge design is still not acceptable for traffic.

		Surge		Sway		Heave		Roll		Pitch		Yaw	
		Along x-axis		Along y-axis		Along z-axis		Around x-axis		Around y-axis		Around z-axis	
		[m]	[m/s ²]	[m]	[m/s ²]	[m]	[m/s ²]	[°]	[°/s ²]	[°]	[°/s ²]	[°]	[°/s ²]
Serviceability limits		-	0,50	-	0,50	3,00	0,70	2,52	6,13	2,01	4,01	3,44	2,86
Original design		0,17	0,37	20,47	0,32	8,53	0,78	20,49	2,87	4,44	0,90	8,26	0,33
Improved spudpole		0,16	0,51	9,10	0,32	6,60	0,78	7,90	2,86	3,68	0,82	4,48	0,21
Rotation & spudpole		0,19	0,71	2,49	0,36	3,32	0,79	6,84	3,46	2,64	0,77	1,71	0,30

Table 2: Overview of the maximum dynamic response to the governing current and north-eastern waves.

Contents

Acknowledgements	i
Abstract	iii
I Introduction	1
1 The Tidal Bridge concept	3
1.1 Introduction of the Palmerah Tidal Bridge	4
1.2 Floating bridges.	5
1.2.1 Floating bridges versus general bridges	5
1.2.2 Mooring systems for floating bridges.	5
1.2.3 Technical challenges	6
1.3 Ocean energy	6
1.4 The Palmerah Tidal Bridge	7
1.4.1 General requirements	8
1.4.2 Mainland connection	8
1.4.3 Floating bridge components	9
2 Project specification	13
2.1 Problem statement	13
2.2 Objective	13
2.3 Scope	13
2.4 Project questions	14
2.5 Methodology	14
2.6 Reading guide.	15
II Data analysis	17
3 General design conditions	19
3.1 Serviceability limits	19
3.2 Boundary conditions	20
3.2.1 Bathymetry	21
3.2.2 Wind data	21
3.2.3 Significant wave height	23
3.2.4 Tidal level	23
3.2.5 Current profile	24
4 Load inventory	27
4.1 Static loads	27
4.2 Wave induced pressures.	29
4.3 Current induced pressures	30
4.3.1 Morison drag on mooring system	30
4.3.2 Drag forces: pontoon and turbines.	31
5 Structural properties of the Tidal Bridge	35
5.1 Analysis type	35
5.2 Structural dynamics.	36
5.3 System characteristics	38
5.3.1 Geometry	38
5.3.2 Stiffness properties.	38
5.3.3 Natural frequencies	39
5.4 Stability calculation of floater	40

III	Motion analysis	43
6	Virtual model of the Tidal Bridge	45
6.1	Modelling software	45
6.2	Model implementation steps	47
6.3	Accuracy of virtual bridge model	48
6.3.1	Hydrostatics of 'floaters'	49
6.3.2	Sea spectrum	49
6.3.3	Current implementation	50
6.3.4	Simulation of mainland connection	54
6.4	Evaluation of the Ansys Aqwa Tidal Bridge model	55
7	Sensitivity analysis	59
7.1	Static traffic load cases	59
7.2	Wave sensitivity	61
7.2.1	Response amplitude operators of individual floaters	61
7.2.2	Irregular waves	64
7.2.3	Time response analysis for the governing waves	66
7.3	Current sensitivity	70
7.3.1	Spudpole bending stiffness	71
7.3.2	Spudpole 'connection' sleeve	74
7.3.3	Improved spudpole design	76
7.4	Response to extreme load combinations	77
8	Design suggestions	83
8.1	Possible design alternatives	83
8.1.1	Improved spudpole design	83
8.1.2	Rotation of Tidal Bridge design	84
8.1.3	Initial deck tilting	86
8.1.4	Increase in mass	86
8.1.5	Limit vertical displacement	87
8.1.6	Adjust pendulum angle	87
8.1.7	Use of hydraulic springs	88
8.2	Deliberation of alternatives	89
IV	Outcome of the research	93
9	Conclusions and recommendations	95
9.1	Answers to project questions	95
9.1.1	Subquestion 1	96
9.1.2	Subquestion 2	97
9.1.3	Conclusion to research question	101
9.2	Recommendations	103
V	Appendices	105
A	The Palmerah Tidal Bridge	107
B	Determination of serviceability limits	109
B.1	Introduction to motion limits	109
B.2	International standard	110
B.3	Requirements obtained from test results (University of Singapore)	110
B.4	E39 Coastal Highway Project (Norway)	112
B.5	Serviceability limits of the Tidal Bridge	113
C	Boundary conditions	115
C.1	Seismic activity	115
C.2	Bathymetry	116
C.3	Wind	117
C.4	Wave height	123

C.5	Tidal data	126
C.6	Current profile	127
D	Load index	129
D.1	Static loads	129
D.2	Traffic	130
D.3	Wave induced loads	132
D.4	Current induced loads	134
D.4.1	Drag on 'tube-elements'	134
D.4.2	Drag on pontoons	135
D.4.3	Turbine induced loads	138
E	Structural dynamics	141
E.1	Introduction to dynamics	141
E.1.1	Example: floating body in water	142
E.1.2	Floating pontoon bridge	144
E.2	System properties	145
E.3	Connections	147
E.3.1	Connection between elements	147
E.3.2	Upper pendulum hinge	147
E.3.3	Lower pendulum hinge	148
E.3.4	Spudpoles to mainland	149
E.4	Stiffness characteristics	150
E.5	Rotation of individual floater	152
E.6	MathCad file	154
F	Ansys Aqwa	157
F.1	Purpose of the Ansys Aqwa model	157
F.2	Wave conditions	157
F.2.1	Linear regular wave (Airy wave)	158
F.2.2	Second order Stokes waves	158
F.2.3	Irregular waves	159
F.3	Current	159
F.4	Wave and current interaction	160
G	Model set-up	161
G.1	Geometry	161
G.1.1	Mesh	162
G.1.2	Connections	163
G.2	Wave implementation	164
G.3	Current implementation	166
G.3.1	Drag force on 'tube-elements'	166
G.3.2	Drag force on floating bodies	166
G.3.3	Implementation of mainland connection	173
H	Wave results	175
H.1	Hydrostatics	175
H.2	Response amplitude operators	176
H.3	Determination of critical waves	182
H.4	Time response analysis	184
I	Current results	187
I.1	Initial problems	187
I.2	Cable properties	188
I.3	Spudpole design iterations	191
	Lists of symbols	193
	References	195

I

Introduction

The first part introduces the future world's largest floating tidal power plant: *The Palmerah Tidal Bridge*. Furthermore, the content, aim and purpose of the graduation thesis are defined and explained.

The Tidal Bridge concept

Currently, the world strives towards sustainability, durability and renewable energy to reduce the ecological footprint of the world. Climate agreements resulted in the cooperation between 195 countries to reduce emissions in order to decelerate climate change (European Commission, 2015). *The Tidal Bridge* concept idea adapts to this mindset and combines renewable energy and sustainability with an innovative idea: a floating bridge that produces energy with tidal water power turbines. The main goal is to design a bridge with floating, standard elements that can be coupled and serve as a roadway for traffic and as a tidal power plant, illustrated in Figure 1.1. The bridge is highly dynamic, which makes it able to adapt to the tidal range and horizontal displacements, induced by large currents and waves. Several types of free flow turbine designs can be mounted directly onto the bridge elements. The main advantage of combining a floating bridge with a tidal power plant is that the weight of the bridge, including the turbines, is 'carried' by the water, avoiding the need for large and expensive foundations. In addition, the power generation increases with 10-25 % compared to turbines mounted on the sea bottom as the flow speed at the water surface level is higher than at the bottom. The need for maintenance is reduced by selecting maintenance-free components and by providing easy maintenance access. From a financial perspective, the installation and maintenance costs reduce the investment by 40-50% compared to a turbine on the seabed (Vos, 2017).



Figure 1.1: The two main functions of the Tidal Bridge: a connection and a power plant (Tidal Bridge, 2018)

The concept of the Tidal Bridge design is still in an early design stage and develops continuously. The first design originates from a collaboration between the enterprise Tidal Bridge, the construction company Strukton and the private equity firm Dutch Expansion Capital. After indicating locations with high flow speeds and limited cross-sectional spans, the design idea was proposed to the Indonesian government. The government is keen to evolve the Tidal Bridge project even more and to boost the local economy. Antea Group performed a limited pre-feasibility study for the project in Indonesia. BAM International bought the shares of Strukton, as the new policy of Strukton is to focus on national instead of international projects. BAM continues with the design study of the Tidal Bridge and decide whether the project is technically feasible and should proceed to the Front End Engineering Design (FEED) phase.

1.1. Introduction of the Palmerah Tidal Bridge

The proposed location of the pilot version of the Tidal Bridge project is in The Nusa Tenggara Timur (NTT) region in the south-east of Indonesia, Figure 1.2. The location is challenging as earthquakes occur frequently, high flow speeds are present, the infrastructure is outdated and an electricity network is absent. Nevertheless, the conclusion of the feasibility study stated that the project area is suitable. Yet, the technical feasibility of the Tidal Bridge concept should be proven (Bitter and Hoogeveen, 2014).

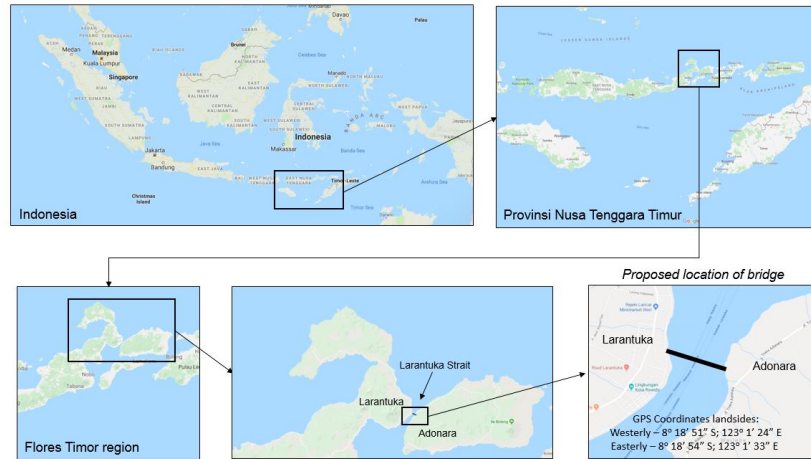


Figure 1.2: Location of the Palmerah Tidal Bridge

The NTT government has the vision to develop the NTT Region and to connect the islands Larantuka and Adonara with a bridge. Every year, numbers of citizens think that they can swim the 800 m long Strait of Larantuka and many of them drown according to the COO of Tidal Bridge, van den Eijnden and Middelweerd (2017). According to Van den Eijnden, local fisherman are still able to pass the bridge near the land and the fisherman can use the generated electricity to create cool cells for their fish. He also stated that the environmental impact on the biodiversity will be 'very limited'. The vision resulted in a Japanese pre-feasibility study conducted in 2015, however with estimated project costs of \$ 400 million the project was considered not feasible. After the rejection of the Japanese bridge design, Figure 1.3, Tidal Bridge presented an alternative solution that enhances the economic growth of the NTT region even more: *The Palmerah Tidal Bridge*, Figure 1.4. A floating bridge that produces renewable energy with tidal water power turbines and improves the infrastructure. The project costs were estimated at \$ 225 million, resulting in a feasible project. On April 16th of 2016 a "Head of Agreement" was signed between Tidal Bridge, the Indonesian government and NTT region, confirming the interest and commitment to develop the project (Vos, 2017). Publications and news articles regarding the Tidal Bridge are presented in Appendix A.

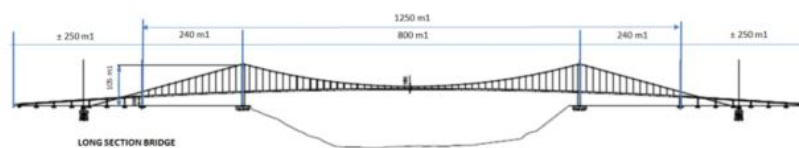


Figure 1.3: Japanese bridge design (Antea Group, 2018)

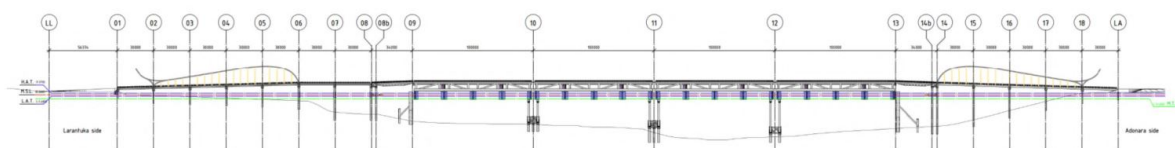


Figure 1.4: Floating bridge design of Tidal Bridge (Antea Group, 2018)

1.2. Floating bridges

Floating bridges are unique civil works of art and trending since the beginning of this era. In total more than fifty operational floating bridges are present today, most of them located in American lakes or between fjords in Norway. The *Evergreen Point Floating Bridge* in Seattle, USA, has currently the record of the largest floating bridge in the world with a floating length of 2 350 m. Nevertheless, the first floating bridge was build more than 4 000 years ago by King Xerxes of Persia.

1.2.1. Floating bridges versus general bridges

In general, bridges are constructed as permanent infrastructure with a certain design lifetime. However, when emergencies arise or during war time, temporary structures are required. The origin of a floating bridges traces back to about 2 000 BC and was constructed as a temporary structure. King Xerxes of Persia created a floating bridge, "*The Hellespont*", by aligning over 300 boats and wooden planks to be able to lead his army across the Dardanelles Strait to fight the Greeks (Herodotus, 450 BC). Nowadays, floating bridges are constructed with materials such as steel, light-weight concrete, composites and aluminium alloys.

One of the advantages of a floating bridge, compared to a civil bridge, is the ease of construction. The bridge elements can be pre-fabricated on land and sailed to the project location. In addition, the upwards water pressure is in balance with the weight of the bridge and additional vertical forces, implying that enormous foundations are not obligatory. Hence, lighter and reduced mooring systems are designed. This makes floating bridges an excellent alternative to cross deep waters and harsh seabed conditions such as soft peat or very hard rock. In addition, floating bridges are less disruptive to the environment and at the end of the lifetime, the bridge can be readily removed and deconstructed (Wang and Wang, 2015).

The design challenges for floating bridges differ from general bridges. Normally, bridges are designed to transfer vertical loads, while the governing loads for floating bridges are horizontal. The horizontal loads, induced by waves, currents, winds and tides, need to be transferred to land without initiating undesired vibrations in the structure. The horizontal movements are restricted by a mooring system or a stiff superstructure. The solutions to transfer forces to the land are continuously improved by the increase in knowledge of hydrodynamic behaviour of floating bridges. Nowadays, the most common type of floating bridges are pontoon bridges. Two different types of pontoon bridges can be distinguished; continuous and separate pontoon bridges. The separate pontoon bridge consists of multiple pontoons connected to a superstructure supported by discrete pontoon foundations, Figure 1.5. A continuous pontoon bridge has full surface contact with the water and experiences higher horizontal loads, Figure 1.6.



Figure 1.5: Separate floating pontoon bridge (Vicili et al., 2014) Figure 1.6: Continuous floating pontoon bridge (Vicili et al., 2014)

1.2.2. Mooring systems for floating bridges

The movement of floating bridges can be restricted and limited by multiple types of mooring systems. Mooring systems are attached to the seabed and require a foundation. Often, the characteristics of the bed are harsh: large depths, soft soil, hard rock or high current velocities. For this reason, mooring of floating structures is realised with cables, anchors, dolphins and abutments and not with significant large foundations. The most used mooring methods are dolphin frame-guide, chain/cable, pier wall, mooring piles, tension leg and jerk-free moorings, see Figure 1.7. Depending on the hydraulic conditions, the best suiting mooring system is selected.

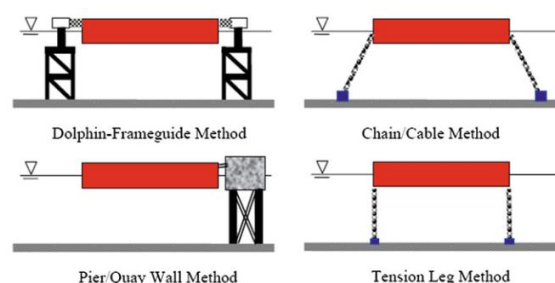


Figure 1.7: Mooring methods(Wang and Wang, 2015)

1.2.3. Technical challenges

In the design of large floating structures, multiple technical challenges arise. A floating bridge is more vulnerable to oceanographic and meteorological conditions than a regular bridge. Preferably, calm conditions such as a low current velocity, small waves, weak winds and limited tidal range, best suiting for floating bridges. The motion of the bridge should be studied extensively to reflect whether the local conditions are accurately incorporated in the design and if the riding comfort and driving safety of vehicles is met. Deformations and accelerations of the deck caused by waves, winds and tidal flux should be indicated. In addition, the connections to the abutments or for the interlocking bodies should provide a smooth passage for traffic. To limit the reaction forces, strong connections should be applied that are able to transfer the loads. The solutions for the technical challenges are project dependent and realised through an iterative process where the designs are continuously adapted and recalculated. The Tidal Bridge design is controversial compared to other floating bridges, introducing new technical challenges. The major differences are the heavy environmental conditions, strong currents are required for sufficient energy output, yet strong currents increase horizontal forces and decrease stability. Next to that, the failure mechanism fatigue has an increased probability as more vibrations are induced by the tidal power turbines and the 'stiff' mooring system of Tidal Bridge.

1.3. Ocean energy

Renewable energy is an enormous type of energy generated by the power of on-going natural processes without leaving a footprint for future generations, examples are wind, solar power, flowing water and biological processes. The most common types of renewable or 'green' energy are solar and wind energy. Nevertheless, both types are dependent on weather conditions. Luckily, a constant source of energy does exist: the tides of the oceans.

Due to the gravitational pull of the sun and moon, the rotation of the earth and the presence of water, the oceans are constantly in motion. The tides are long-period waves generated offshore and progressing towards the coasts. The tides result in a harmoniously varying high and low water level each day, respectively filling and emptying water basins such as the North Sea. Tidal currents have enormous power and are highly predictable. A study of *Ocean Energy Systems (2011)* estimated the worldwide theoretical tidal energy potential at 7 800 TWh/year, which can supply over 65 times the annual energy consumption of the Netherlands (based on data of CBS (2018)). Currently, tidal power is expensive, 150 €/MWh, while the price of general power in the Netherlands is approximately 30-55 €/MWh (Brito e Melo and Luis Vilate, 2016). However, increasing the amount and efficiency of water power turbines, the price can drop significantly. Multiple types of ocean energy devices are in use, Figure 1.9, tidal power turbines are indicated in Figure 1.8.

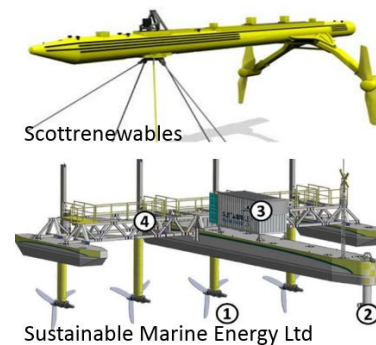


Figure 1.8: Floating tidal energy projects (Jarquin-Laguna, 2018)

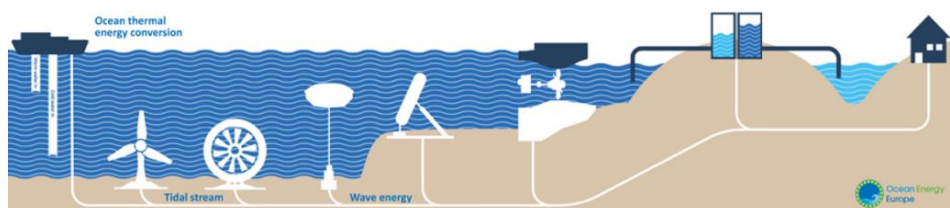


Figure 1.9: Ocean energy (Jarquin-Laguna, 2018)

The type of ocean energy that is applicable for the Tidal Bridge is tidal stream. The tidal range induces high flow speeds, especially if narrow passages are present. The project location is located in such a narrow passage: The Strait of Larantuka. The indication of the worldwide tidal potential is presented in Figure 1.10. The project location is indicated with the black arrow.

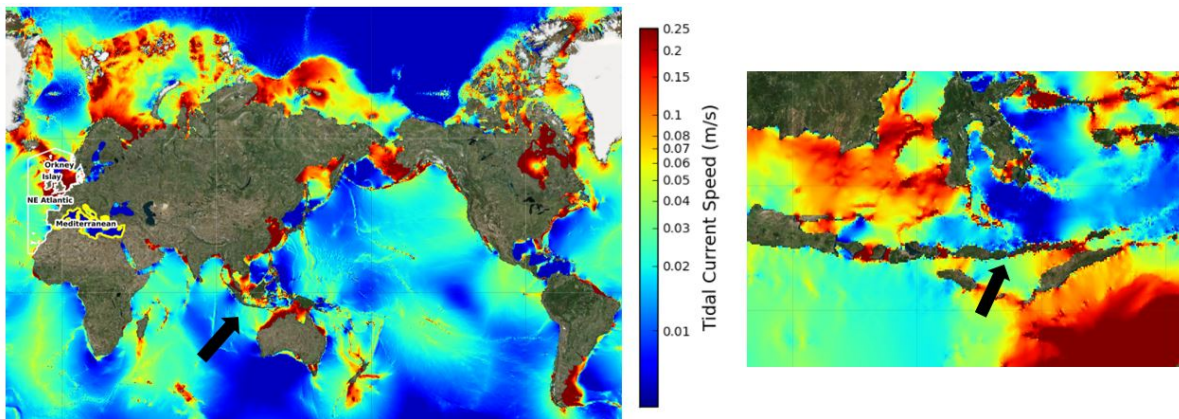


Figure 1.10: Tidal potential around the world, black arrow indicates project location (Noveltis, 2015)

1.4. The Palmerah Tidal Bridge

The floating bridge that will be constructed by BAM in Indonesia is the *Palmerah Tidal Bridge*. The main function of the bridge is to connect the islands Larantuka and Adonara in the Flores Timor Region, Figure 1.2. The selected project location is a result of an analysis conducted by Antea Group (2018) that combined and optimised multiple design requirements such as: minimum length, maximum viable energy production area, optimum current alignment, current infrastructure and desired hydraulic conditions. To cross the Larantuka Strait, the span of the bridge is approximately 860 meters. The Palmerah bridge consists of two major parts, a civil bridge and a floating Tidal Bridge (Figure 1.11 and 1.12). The bows on the civil bridge are aesthetic elements designed by a local architect, representing the shape of fish. Underneath the floating bridge the water power turbines will be installed, the area is shaded in blue in Figure 1.12 (Vos, 2017). An overview of all individual components that will be discussed is presented in Figure 1.13.



Figure 1.11: Visualisation Palmerah Tidal Bridge design (Antea Group, 2018)

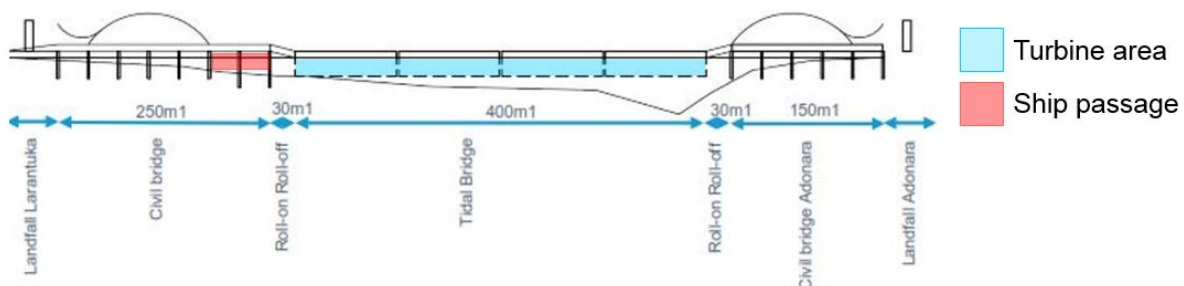


Figure 1.12: Schematic Palmerah Tidal Bridge design (Antea Group, 2018)

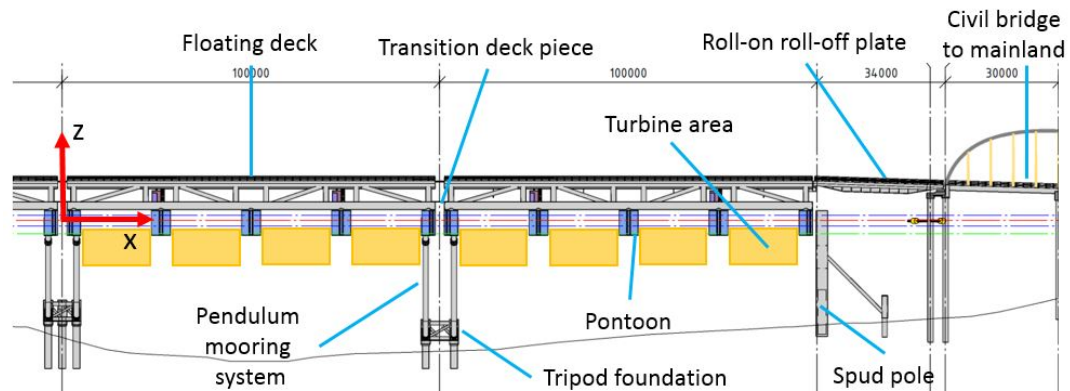


Figure 1.13: Overview of individual elements of the Tidal Bridge

1.4.1. General requirements

High requirements are set by the Nusa Tenggara Timur (NTT) government for the Palmerah Tidal Bridge. The NTT government functions as the client, hence the requirements should be fulfilled. Next main stakeholder is the company Tidal Bridge, their starting points for the design considers functional and structural statements.

Nusa Tenggara Timur Government

Minimum turbine output	18 MW (including electricity losses)
Maximum turbine output	23 MW
Safety	Traffic should be able to cross the bridge safely.
Design	The bridge should have an Indonesian appearance.
Costs	Budget available of approximately €225 million.

Tidal Bridge

Concept	Deliver a high-end product that can be implemented at multiple locations.
Design	Use of prefab and normalised structure elements.
Construction	Off-site construction of main parts.
Transport	Construction parts are transported over sea.
Maintenance	Use of maintenance-free materials and create easy access to critical elements.
Function bridge	The bridge serves as a connection and a power plant.

Design life

In general, bridges are designed for a lifetime of approximately 100 years. Yet, fatigue is suspected to occur, all elements are rotating and vibrating and maintenance possibilities are limited due to the strong current. Hence, the stakeholders agreed on a lifetime of 50 years. The applied consequence class according to the Eurocode for the complete bridge is CC3, the consequence class where consequences of failure are high. In general, the consequence class is accompanied by a lifetime of 100 years. The Tidal Bridge assumes an adjusted lifetime for this consequence class of 50 years, with a return period of once every 100 years (de Rijke et al., 2017).

1.4.2. Mainland connection

The civil bridge functions as the connection between the mainland and the floating Tidal Bridge. The bridge, according to the present designs, will be constructed by a concrete girder type bridge with steel a pile foundation, precast concrete girders, concrete capping beam, a roadway and side walks. On the Larantuka side, ships will be able to pass underneath the bridge, Figure 1.12. The bows in the form of a half fish are purely aesthetic. Additional technical drawings and information of the civil bridge and the deck structure are provided in Appendix A.

1.4.3. Floating bridge components

The Tidal Bridge uses standard floating bodies that, if coupled, function as a tidal power plant. Each body consists out of five floating pontoons, rigidly connected to a steel frame, Figure 1.14. The frame serves as the connection point of the tidal turbines. The structure is standardized, existing of identical floating elements with a length of 100 m each. The use of identical 'standard' prefabricated elements is the main concept of the Tidal Bridge as scale production reduces costs. Nevertheless, exact dimensions of elements are dependent on project specific conditions and requirements. The Palmerah Tidal Bridge consists of four coupled Tidal Bridge elements. The elements are moored with a tripod pendulum mooring system, Figure 1.15. A schematic mechanic overview of the coupled elements is provided in Figure 1.18.

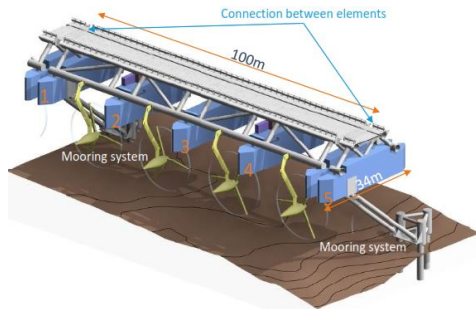


Figure 1.14: Visualisation Tidal Bridge element with initial turbine design (Vos, 2017)

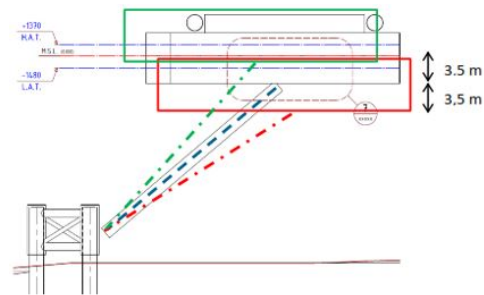


Figure 1.15: Indication of displacement induced by the tidal range and the secondary effect of the mooring system (Vos, 2017)

The floating part of the Pahlemerah Tidal Bridge has a length of 400 m. Regarding the pre-feasibility study conducted by Antea Group, the part should be able to withstand vertical and horizontal displacements in a order-size of 7 metres (absolute distance), Figure 1.16 and 1.17 (Vos, 2017). The values are based on an estimation of the sum of extreme forces on the mechanical structure (not exposed to water) and function as an appropriate assumption of the maximum order size of the displacement. Next to the major displacements, waves, current, wind, the turbines and traffic result in additional vibrations, accelerations and rotations. Traffic should be able to drive safely on the bridge deck, hence the movements of the bridge should be restricted. The Eurocode is considered as guideline to indicate the dynamic response of the Tidal Bridge. The Indonesian guidelines will suit better, yet these are written in Indonesian and a translated version is not present. The regulations of the Eurocode are assumed to be conservative compared to Indonesian standards.

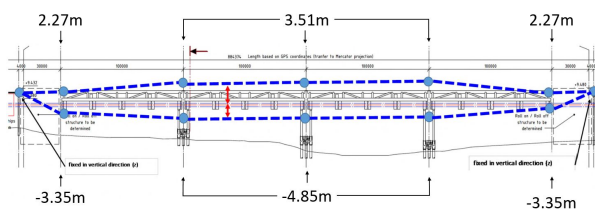


Figure 1.16: Sideview Tidal Bridge; indication of the amount of vertical motion according to Antea Group (2017) (not drawn to scale) (Vos, 2017)

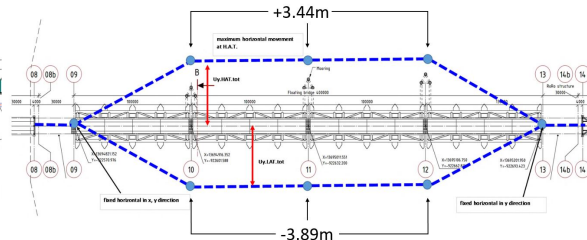


Figure 1.17: Topview Tidal Bridge; Horizontal motion according to Antea Group (2017) (not drawn to scale) (Vos, 2017)

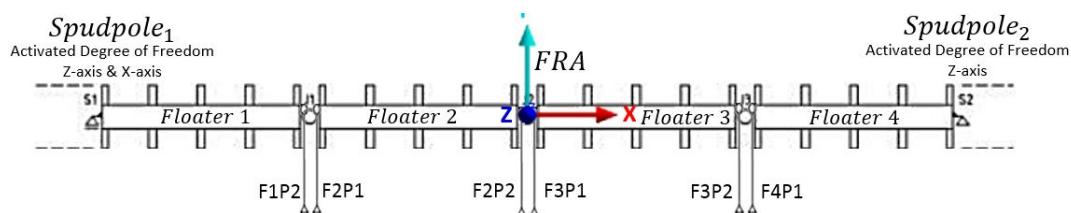


Figure 1.18: Schematic representation Tidal Bridge (Vos, 2017)

Mooring system

The horizontal and vertical displacements are limited by developing an innovative a mooring system. The system is a combination of static spudpoles with mooring pendulums that can rotate through hinges. The shape of the response of the coupled system is analogous to the motion of a skipping-rope, Figure 1.19. The mooring pendulums consist of a tripod foundation with small diameter foundation piles. The foundation is connected with hinges to a steel 'tube' and to the pontoon, Figure 1.20. To enhance stability, the pontoons at both ends of one Tidal Bridge element are supported with such a mooring system, presented in Figure 1.18. The individual elements of the pendulum system are indicated in Figure 1.21 and discussed in Appendix A. The connections are designed by the offshore mechanical connection company *Drie-D*, a specialist in constructing strong and flexible connections with very limited friction because of the use of lubricant material D-glide, a strong and maintenance free material. At the tripod foundation, on the bottom of the seabed, an uni-joint hinge is designed. The connection between the pendulum and pontoon is realised with point-hinges, able to rotate in every direction. The connections are generally used on offshore platforms and are able to transfer a force of ten times the magnitude of forces acting on the Tidal Bridge (Drie-D, 2017).

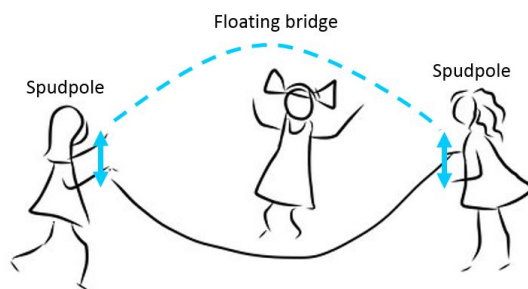


Figure 1.19: The shape of the dynamic response of the Tidal Bridge can be compared to the shape of a skipping-rope or necklace

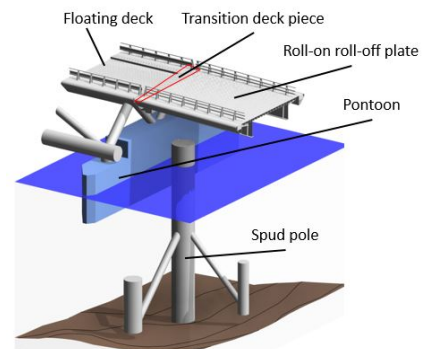


Figure 1.20: Spudpole that allows vertical motion at the Adonara side of the bridge (Vos, 2017)

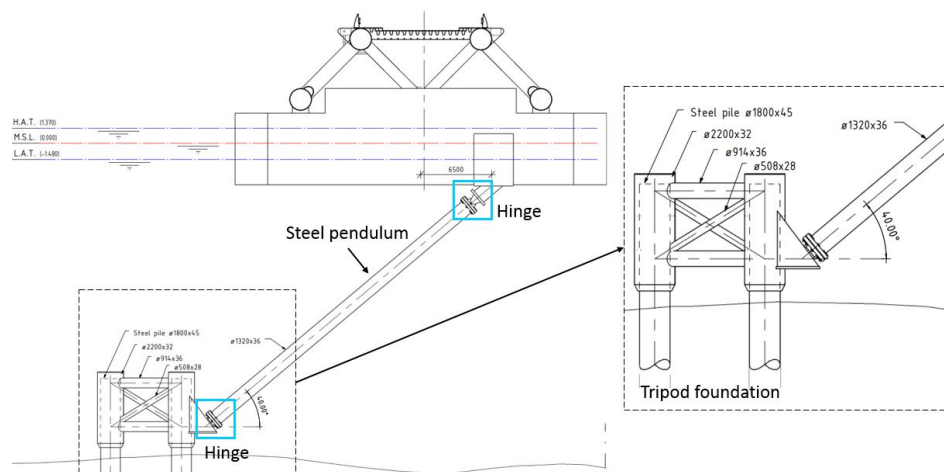


Figure 1.21: Technical drawing of the mooring system (Drie-D, 2017)

Spudpoles

Spudpoles are designed to function as the coupling element between the civil bridge and the floating bridge. The connecting hinge of the spudpoles can translate vertically along the pile to adapt to the water level of the tides. One of the piles allows limited horizontal motion to allow the possibility of 'elongation' of the floating span. The spudpoles are connected to the outer pontoon, as is indicated in Figure 1.20. A smooth deck transition between the floating deck and the rigid bridge deck is realised with of a roll-on roll-off plate and interlocking deck plates.

Pontoons

The 100 metres long Tidal Bridge elements float on partly submerged pontoons. Each element has five pontoons: three large pontoons in the middle and two small pontoons at the ends. The pontoons are 34 m long, 6,55 m high, 5 m (large pontoons) or 3 m (small pontoons) wide and have an additional surface layer to protect against corrosion.

Roll-on roll-off

A roll-on roll-off connection is used for a smooth transition between the civil bridge deck and the floating deck, Figure 1.22. The connection functions as the transition piece between the moving floating deck and the secure civil deck. The roll-on roll-off plate should be able to withstand deformations and large forces. The precise design will be created by the construction company *Maurer*.

Intersection piece between decks

Conform the Dutch traffic guideline ASVV 2004 (CROW, 2004), the allowed vertical angle for traffic on the roll-on roll-off bridge is 11%. Nevertheless, extra deck transitions create a more smooth interface between both decks. The design for the intersection piece between the decks originates from the offshore industry. The intersection piece can be simplified as a girder section with interlocked deck supported on pontoons, Figure 1.23. The piece needs to be flexible and deformable to prevent gaps between the decks.

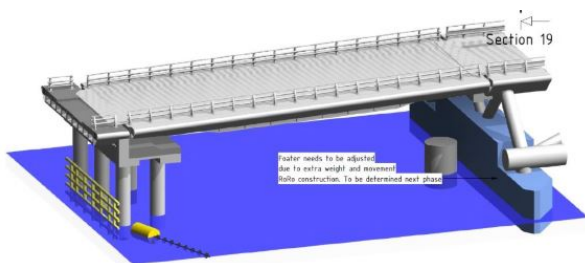


Figure 1.22: Roll-on Roll-off section (Vos, 2017)

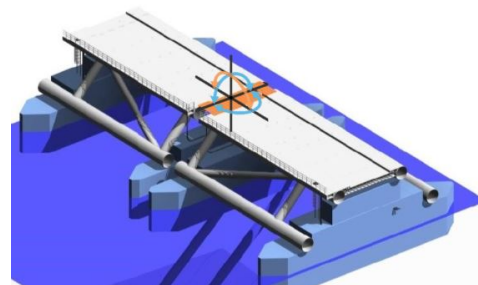


Figure 1.23: Girder section with intersection piece (Vos, 2017)

Turbines

For the Tidal Bridge concept, three different tidal turbine types proposed; Tocardo T2si, FishFlow FFI Free Flow Turbine and Schottel SIT250, Figure 1.24. The turbines are designed according to the requirements set by Tidal Bridge;

1. The minimum required power output is 18 MW (inc. losses) and the maximum output is 23 MW.
2. The maximum moment due to the turbines, acting midpoint on the bridge, is 21 000 kNm.
3. The accepted draught is maximum 21m and decreasing on both sides of the channel.
4. The turbines can be maintained easily and efficiently. Near the project location no harbour facilities or shipyards are present.
5. Prevention of the disruption of the environment.

The final turbine type for the Palmerah Tidal Bridge is depended on site specific conditions. However, the preferable turbine type is FishFlow, an enterprise of BAM. FishFlow is an innovative turbine system that allows fish to pass safely, reducing the environmental footprint. The concept idea is considered in the next paragraph.

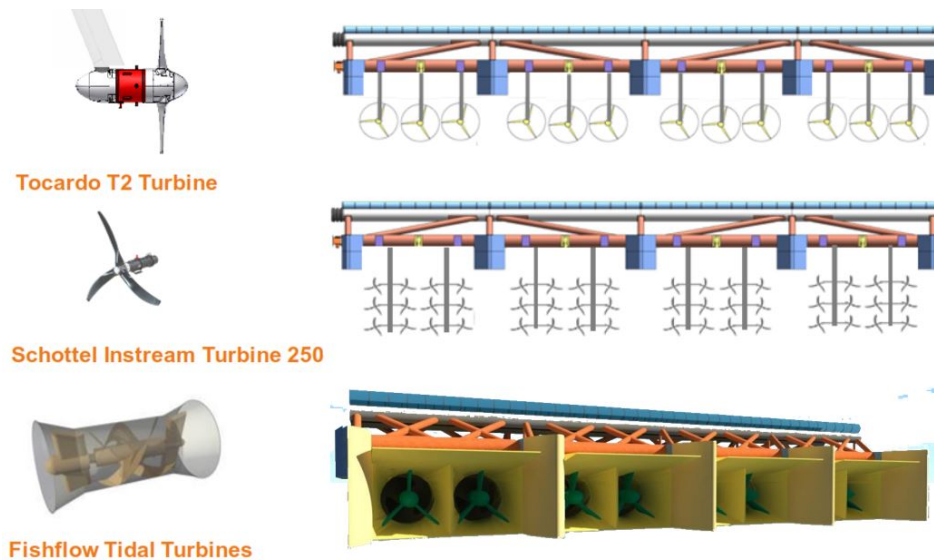


Figure 1.24: Possible turbine types for the Tidal Bridge (Tidal Bridge, 2018)

FishFlow

The unique shape of the 'rotor blades' of FishFlow create a fish-friendly design, Figure 1.26. A safe passage for fish is provided and a very limited amount of noise is initiated. The shape of the rotor blades is comparable with *Archimedes' screw*, Figure 1.25. Another advantage is that the FishFlow generates power rotating clockwise and counter-clockwise, being able to generate electricity during flood and ebb tides. No blades need to be flipped, which means fewer moving parts and less need for maintenance. The water output of the turbine induces little cavitation and is released in an almost straight beam, increasing the stability of the floating bridge structures. The turbines can be placed on the construction site or offshore and replaced relatively easily. Placement is done by floating the turbines underneath the bridge and removing the ballast. When in place, the turbines are secured. The dimensions of one FishFlow turbine are 10 x 9,5 x 28 m. This allows the fitting of two turbines in between two pontoons. The 'closed' structure area results in an estimated channel flow blockage of 37% and the average water depth below the bottom of the turbines is 13 m (Vos, 2017). An earlier design of the built-in FishFlow turbines in the Brouwersdam, Grevelingen, is presented in Figure 1.27. The type of tidal turbines in the Tidal Bridge is the same, but a significant difference is the aspect that the the turbines in The Tidal Bridge will be attached to the dynamic bridge frame and not secured in a dam or on the seabed.

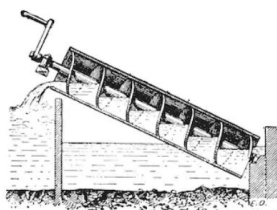
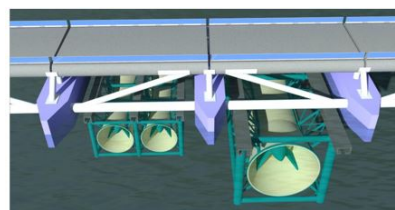


Figure 1.25: Archimedes' screw (Larive, 1895)



Two application possibilities

Figure 1.26: FishFlow implemented in Tidal Bridge element (Tidal Bridge, 2018)

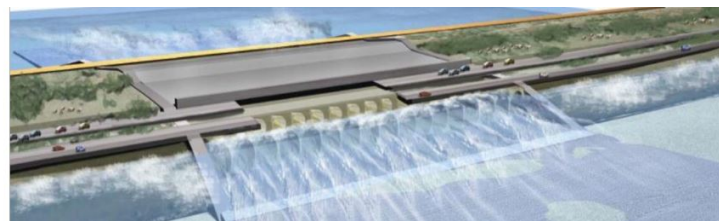
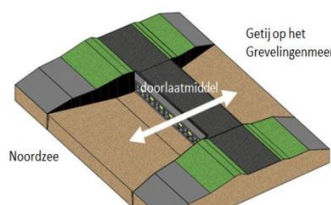


Figure 1.27: Illustration of design plan for FishFlow turbines in the Brouwersdam, Grevelingen (Tidal Bridge, 2018)

2

Project specification

2.1. Problem statement

The Tidal Bridge is a combination of a tidal power plant and a floating bridge. The main functions of the bridge are to generate electricity and to serve as a connection between two islands in Indonesia. A safe, stable and feasible design is required to fulfil both functions. Currently, questions arise about the probable behaviour of the floating bridge. What magnitude of motions and accelerations are induced by hydraulic loading? Will the dynamic response of the bridge exceed serviceability limit states? During what time will traffic be able to cross the bridge safely? A study on the likely bridge motion is not conducted and any realistic response estimation is absent. Supplementary, allowable serviceability limits are not defined for an equivalent type of dynamic floating bridge. Hence, the downtime of the bridge can not be indicated or even estimated. Consequently, the technical feasibility of the design is still not confirmed. The main problem is the lack of knowledge regarding the dynamic response of the present Tidal Bridge design.

2.2. Objective

The problem statement leads to the objective of the research: determine the dynamic response of the present design of the Tidal Bridge. What motion will the external wave and current loads induce on the floating bridge? The aim is to create insight in the displacement, rotations and accelerations of the coupled floating bridge structure. In addition, obtaining information regarding the most sensitive structural parameters of the system may lead to design changes that result in an increase in stability.

2.3. Scope

The Tidal Bridge concept is still in the preliminary development stage. Many aspects are uncertain and data is not conducted yet or incomplete. Hence, the extent of the research is limited, lots of (literature-based) assumptions are made and the limited amount of available data is assumed as correct.

Location	-	<i>The Palmerah Tidal Bridge</i> in Indonesia is considered as a reference case and will form the base of the research.
Design	-	The proposed preliminary design is considered as <i>complete and fixed</i> . New adjustments in the design are not implemented in the research.
	-	Dimensions of the system are set according to the present <i>technical drawings</i> .
Project stage	-	The construction, transport and assembling stage are not considered, solely the <i>constructed bridge</i> with a <i>lifetime of 50 years</i> is analysed.
Loads	-	The dynamic response due to variable <i>wave and current induced pressures</i> is analysed. Implementation of all correlated loads will become too complex, traffic is considered as a static point load.
	-	Difference in water level (tidal range) is not analysed.
	-	<i>Fatigue</i> and other long-term failure mechanisms are <i>excluded</i> , the influence on the structural integrity is expected to be crucial.

	-	<i>Extreme scenarios</i> such as accidental loads, ship collision, earthquakes, ice and abandonment are not considered.
	-	The turbine suppliers are assumed to deliver a product that fulfils the requirements set by Tidal Bridge. The <i>reliability of the turbines</i> is not checked.
Data	-	<i>Data is limited</i> , it is assumed that the available data is correct. If specific data is obligatory for the research, yet not conducted or confirmed, an <i>assumption</i> is estimated based on (literature) research.
Field	-	The focus of the project is the <i>dynamic response</i> of the Tidal Bridge, aspects as durability, design of the steel frame and economical feasibility are not elaborated.
Model	-	The structural elements of the system are considered as <i>infinitely stiff</i> .
	-	The bathymetry of the Strait of Lantoka is simplified to a <i>rectangular uniform 'box'</i> with constant depth and width.
	-	<i>Critical limitations</i> in the modelling software are tried to be solved by counterfeiting the problem. This reduces the validity of the model.

2.4. Project questions

The objective of the thesis is formulated into one main *research question* and two *subquestions*:

Research Question

Is the dynamic response of the present design of the Palmerah Tidal Bridge induced by waves and currents of an acceptable magnitude regarding traffic serviceability?

1. *What data is required to compute the likely motion of the Palmerah Tidal Bridge?*
 - (a) What are the governing hydraulic conditions at the project location?
 - (b) What types of loads are probable to induce significant motion?
 - (c) What are the dynamic properties of the Palmerah Tidal Bridge?
2. *Is the Palmerah Tidal Bridge stable enough to allow traffic safely across the bridge?*
 - (a) How can the Tidal Bridge be implemented in a virtual model?
 - (b) What is the dynamic response of the Tidal Bridge and what loads induce governing motion?
 - (c) What are design suggestions that improve the stability of the bridge?

The first subquestion considers the project characteristics and elaborates upon the data that is obligatory to determine the dynamic response of the Tidal Bridge. The subquestion is split into three categories: the hydraulic conditions at the project location, the governing loads and the structural properties of the bridge.

The second subquestion indicates whether the dynamic response of the Tidal Bridge is in an allowable motion range. The gathered data and the present Palmerah Tidal Bridge design are converted into a virtual floating bridge model that is used to estimate the likely response. This is realised by selecting a suitable software package and discussing the applicability of the software to compute the dynamic response. The model set-up is defined, implemented and elaborated. The accuracy of the computer model is examined and, if possible, verified. Next, an indication of the most intense bridge response is found with a sensitivity study. At last, design improvements, based on the results of the sensitivity study, that may influence the stability of the Tidal Bridge positively are proposed. The results indicate whether the dynamic response of the Tidal Bridge seems realistic and acceptable for traffic.

2.5. Methodology

The first subquestion is substantiated by consulting literature sources, study material, the online library of BAM, interviews with the COO of the enterprise *Tidal Bridge* and calculations. A variety of meetings between the companies BAM, Tidal Bridge, FishFlow, Antea Group, Drie-D and Dynasim provided secondary knowledge on the Tidal Bridge components. Literature, previous education and online data platforms supplied data that is converted into hydraulic conditions with *Matlab*. Loads that may act on the bridge are calculated according to knowledge obtained in the Bachelor Civil Engineering and Master Hydraulic Engineering, the expertise of the graduation committee and Eurocodes. The dynamic properties of the Tidal

Bridge are indicated with insight in structural dynamics and structural mechanics. The calculations are conducted in *MathCad*, *Matlab*, *Excel*, *Maple* and *Matrixframe*.

The second subquestion focusses on the implementation of the data into a computer model. First, a suitable model is chosen based on the expertise of the Coastal Dynamics department of *BAM Infraconsult* and the available software licenses of *Delft University of Technology* and *BAM*. The model geometry is defined in *Design Modeller* according to technical drawings of the Palmerah Tidal Bridge design provided by *Antea Group* and *BAM*. The implementation of the model is checked with previous calculations and by consultation of various *BAM* employees. The estimation of the dynamic response is based on the computational capabilities of the software package of *Ansys Aqua* and processed in *Excel*. The design suggestions are formed by combining the gathered motion results with literature, creativity and existing stabilising measures.

The final research question is answered by evaluating and discussing the results found in both analyses. An advise on the technical feasibility with respect to the likely motion of the Palmerah Tidal Bridge is proposed. At last, recommendations regarding the uncertainties, assumptions and inaccuracies in the research are listed.

2.6. Reading guide

The structure of the report is based on *parts*, the first part introduces the research topic, the second and third part answer respectively subquestions 1 and 2. The last part forms the conclusion to the research question. Each part is divided in multiple *chapters* with corresponding *appendices*. The chapters in part II and part III answer a sub-subquestion in every chapter. For example, subquestion 1a: "What are the governing hydraulic conditions at the project location?" is devoted to Chapter 3: *General design conditions*. Figure 2.1 illustrates the reading guide of the report. Next to each part, the considered chapters and appendices for this part are presented.

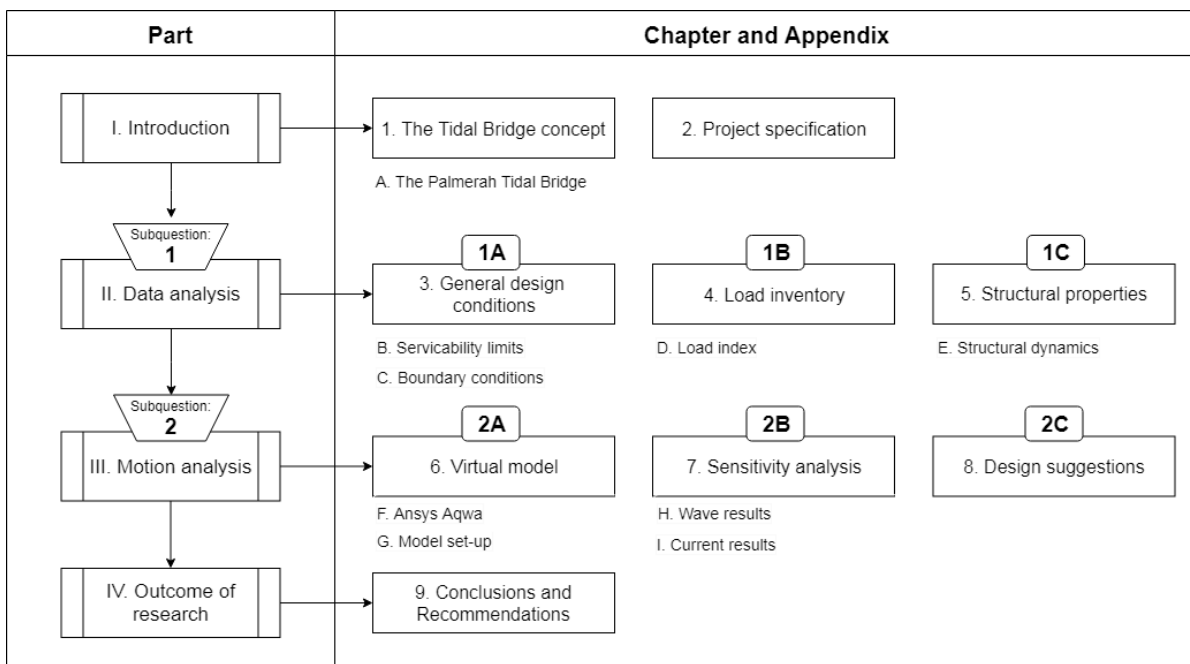


Figure 2.1: Reading guide of the report

II

Data analysis

The second part indicates, analyses, computes, estimates and determines the characteristic properties of the environmental conditions in the Strait of Larantuka (Indonesia) and the structural properties of the present Palmerah Tidal Bridge design. The data that is acquired will form the base of the virtual Tidal Bridge model. An overview of the part is presented in Figure 2.2.

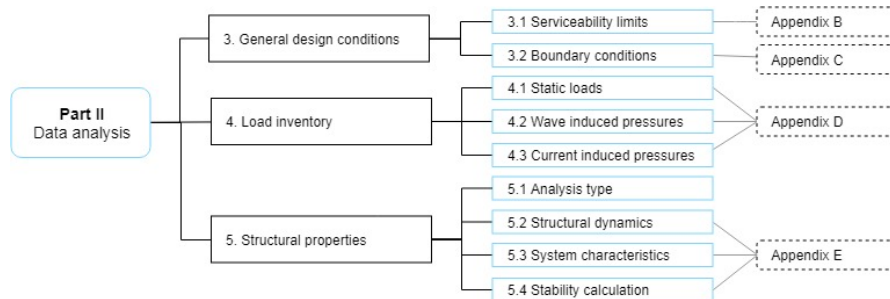


Figure 2.2: Part outline with corresponding sections

3

General design conditions

This chapter considers the design requirements and the boundary conditions and answers subquestion 1a: "What are the governing hydraulic conditions at the project location?". First, the serviceability limits are determined and second the general conditions for The Palmerah Tidal Bridge located in the Strait of Larantuka are analysed.

3.1. Serviceability limits

To guarantee safe traffic passage, serviceability limits should be defined for operational conditions. The serviceability limits should be valid if the bridge is open for traffic. In heavy weather the bridge is closed. Nevertheless, the aim is to limit the downtime of the bridge to 5%, suggesting that during 95% of the 50-year lifetime the bridge should remain open. This corresponds to a closure of the bridge of approximately 18 days per year or a total of 912 days in the lifetime.

If the bridge is open, the motion of the bridge should not exceed the serviceability limits that allow traffic to pass safely without discomfort. Compared to existing floating bridges, the motion of the Tidal Bridge is of a different magnitude and extent. People are mostly used to vertical motion, for example speed bumps, and not to horizontal motion. The Tidal Bridge moves in every degree of freedom and a sequence of combinations of motions may be present, an illustration of motions is presented in Figure 3.1. An example of the combined motion is the displacements induced by the tides, the vertical displacement is accompanied by a horizontal displacement and rotation induced by the mooring system.

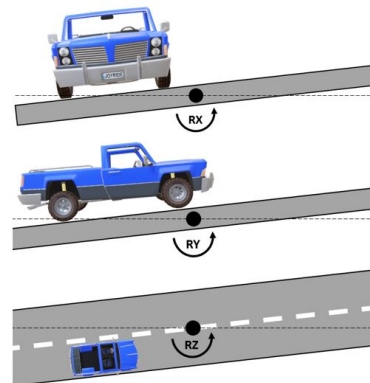


Figure 3.1: Visualisation of induced motion planes

At the moment, no serviceability limits are estimated or computed for the Tidal Bridge. An additional study is requested to verify allowable limits for the specific case of the Palmerah Tidal Bridge. The Tidal Bridge is of another extent than general floating bridges. An indication of the order size of allowable limits is obligatory to verify and validate the outcome of the dynamic response of the bridge. Therefore, an analysis of the serviceability limits of four different reference cases is conducted and discussed in Appendix B. The estimated and assumed serviceability limits for the Tidal Bridge are primarily based on floating bridges in Norway. Yet, the results may be conservative as the bridges are designed for a highway with speed limits of 120 km/h. The speed limit on the Tidal Bridge is set to 20 km/h. An overview of the reference cases and the serviceability limits that are elaborated in Appendix B is given in Table 3.1. It is strongly suggested to conduct extended research to verify the estimated serviceability limits.

Four reference cases are studied to indicate serviceability limits of the Tidal Bridge. An overview of the nomenclature and the directions of the degrees of freedom is presented in Figure 3.2.

1. NEN-ISO 2613: The design code for floating bridges.
2. Research of the University of Singapore. Studybook *Large Floating Structures* by Wang and Wang (2015).
3. The Sognefjord bridge: A design for a floating bridge that will serve as a part of a highway in Norway.
4. The Bergsøysund bridge: A floating bridge that is part of the E39 highway in Norway.

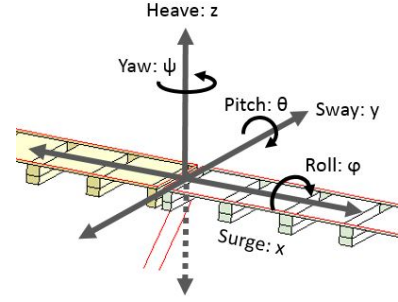


Figure 3.2: Six degrees-of-freedom-system with motion abbreviations and directions

	Surge		Sway		Heave		Roll		Pitch		Yaw	
	Along x-axis [m]	[m/s ²]	Along y-axis [m]	[m/s ²]	Along z-axis [m]	[m/s ²]	Around x-axis [rad]	[rad/s ²]	Around y-axis [rad]	[rad/s ²]	Around z-axis [rad]	[rad/s ²]
NEN-ISO 2613	-	-	0,3	0,5	0,3	0,5	0,010	0,050	-	-	-	-
University of Singapore	-	-	-	3	-	3,0	0,010	0,040	-	-	-	-
Sognefjord	-	0,5	L/200	0,5	L/200	0,7	0,044	0,107	0,006	0,07	0,06	0,05
Bergsøysund	-	-	L/350	0,5	L/350	0,7	0,044	0,107	0,035	0,07	0,03	0,05
-	-	-	-	-	-	-	-	-	-	-	-	-
Tidal Bridge (rad)	-	0,5	-	0,5	3,0	0,7	0,044	0,107	0,035	0,07	0,06	0,05
(degrees)	-	0,5	-	0,5	3,0	0,7	2,521	6,131	2,005	4,01	3,44	2,86

Table 3.1: Overview of all serviceability limits of floating bridges

The serviceability limits of the Tidal Bridge are estimated through an analysis of the correlation and applicability of reference cases. The NEN-ISO norm and the floating bridges in Norway are expected to be conservative and, for that reason, seen as the lower limits. The study of professor Wang is assumed to be an over-estimation of realistic limits. The results of his research are located in the unbearable range of the motion sickness graph that is used by sailors, Figure 3.3. The graph represents the tolerable heave motion, the estimated serviceability limits is 0,70 m/s² and proportional to 0,07g and thus located in the "bearable" part of the graph. It should be stated that the computed motion limits are solely used as a tool to validate the order-size of the outcome of the model and that the serviceability limits are not substantiated.

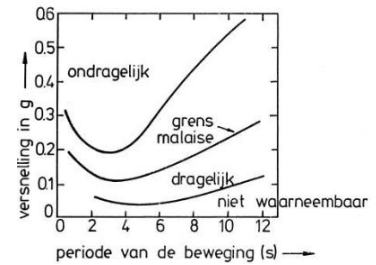


Figure 3.3: Human valuation of accelerations with specific periods (Gerritsma, 2003)

3.2. Boundary conditions

Indonesia is located south of the equator and has a tropical savanna climate with an average temperature of 27,8 °C. The clear dry season is from May till October, the wet season from November till April. The annual rainfall is 1 341 mm and wind speeds up to 40 km/h (11 m/s) arise yearly. Furthermore, Indonesia is located in "The Ring of Fire", four tectonic plates intersect, resulting in frequent earthquakes and floods. The *Disaster Risk Index* indicates a high tsunami risk factor of 9,6 out of 10. Nevertheless, when in 1992 a tsunami hit Flores Island, Larantuka was hardly affected due to the protected position in the Larantuka Strait. An overview of the data that forms the base of the boundary conditions is provided in Appendix C. The impact and consequences of a tsunami is not included in the scope of the research. The available data, conducted by Aquatera and Bintang Subsea, is retrieved during only three days (12th till the 14th of June 2017) of measurements and is therefore not significant, yet assumed as correct in the report.

3.2.1. Bathymetry

The bathymetry profile of the Larantuka Strait is indicated in Figure 3.4, Figure 3.5 and in Appendix C. Scour holes in bathymetry profile might possibly change the current pattern and create eddies. This may result in a non-uniform flow profile that can influence the dynamic response of the floating elements as well as the turbine efficiency. The average depth underneath the floating part of the bridge is 25 m with a maximum depth of 34 m, both seen from MSL. The percentage of flow blockage through the turbines decreases with an increasing depth. A constant average depth of 25 m is used in the research to simulate a realistic flow velocity blockage of the system.

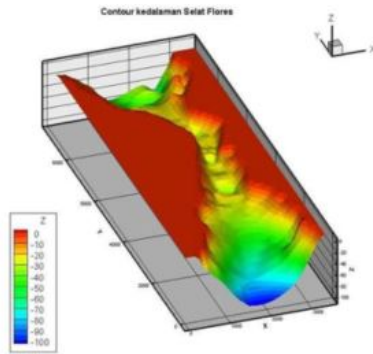


Figure 3.4: Bathymetry Larantuka Strait (Indonesian Hydrodynamics Laboratory)

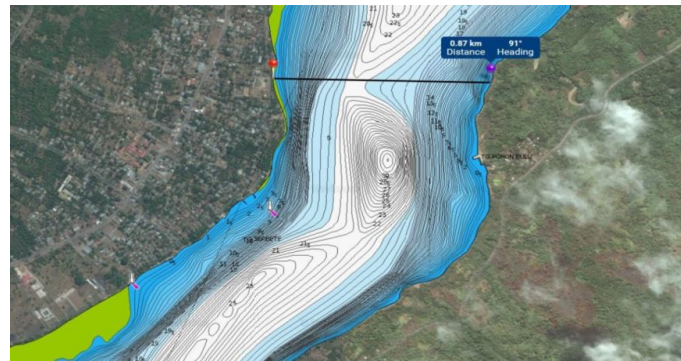


Figure 3.5: Bathymetric Strait of Larantuka (Indonesian Hydrodynamics Laboratory)

3.2.2. Wind data

An probability analysis is conducted to estimate the wind speeds for a return period once every year, 50 years and 100 years. Wind data is conducted during a period of twelve years by the company *EMD International A/S* (2017). Every hour the maximum wind speed at a height of 10 meter is measured and saved in an annual base over the years 2007 till 2015. The datasets are be downloaded from <http://indonesia.windprospecting.com>. The 105 000 datapoints are analysed in Appendix C.3. The maximum measured wind speed over a period of 12 years is 11,56 m/s, indicated on the Beaufort scale with an index of 6, 'a strong breeze'. The average wind speed is approximately 3 m/s 'a light breeze'. The probability of a certain wind speed magnitude with a specific return period is estimated with the Gumbell, Weibull and the Generalized Extreme Value (GEV) distributions (Jonkman et al. (2017)). An overview of the distribution of the total dataset is provided in the histogram in Figure 3.6. In the figure the three considered distribution types for the dataset are plotted as well. The second figure, Figure 3.7, indicates that the GEV-distribution is the best approximation with respect to the actual data. The distribution is used to estimate the maximum magnitudes of the 1, 50 and 100 year wind velocities with the dataset of 12 years.

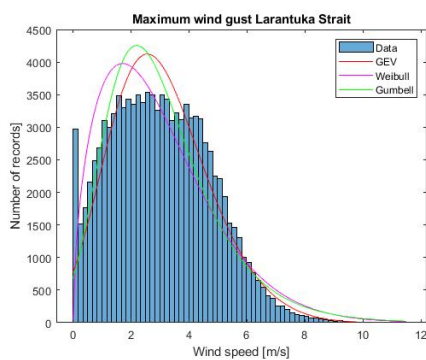


Figure 3.6: Histogram with maximum wind gusts in the Larantuka Strait

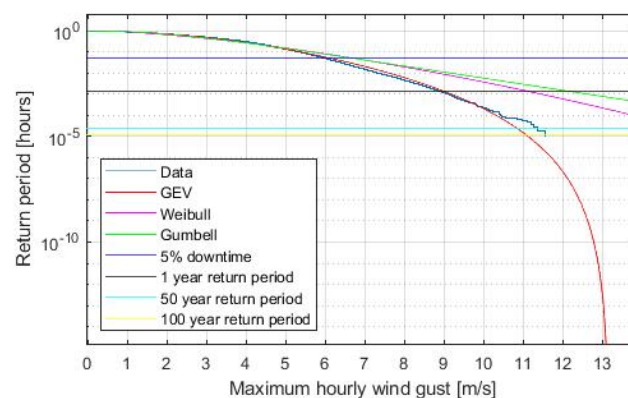


Figure 3.7: Extrapolation of the Gumbel, Weibull and GEV distributions

Next, the dataset is narrowed to indicate the winds in a specific direction range. For every 20 degrees the maximum wind velocities are computed according to the best fitting distribution type for that narrowed dataset. The estimated maximum wind speeds, Table 3.2, are used to compute the significant wave height in the Strait of Larantuka.

Direction [°]	Records [-]	$U_{10,max} 5\%$ [m/s]	$U_{10,max} 1\text{ year}$ [m/s]	$U_{10,max} 50\text{ year}$ [m/s]	$U_{10,max} 100\text{ year}$ [m/s]
Total dataset	105141	6,12	10,26	11,53	11,68
0-20	9548	5,49	7,80	9,56	9,83
20-40	6556	5,73	7,48	8,37	8,67
40-60	3092	3,94	5,48	8,93	9,54
60-80	1844	3,24	9,04	12,49	13,10
80-100	1646	3,78	4,76	7,81	8,35
100-120	2358	5,64	5,46	8,14	8,57
120-140	5353	6,01	8,06	9,90	10,14
140-160	11000	6,30	7,77	8,43	8,49
160-180	17536	6,59	8,21	8,83	8,89
180-200	11839	4,66	8,87	9,82	9,91
200-220	4422	4,66	7,14	9,75	10,15
220-240	2986	3,92	6,22	9,65	10,24
240-260	3074	4,77	7,75	12,27	13,08
260-280	4310	6,93	9,50	10,50	11,00
280-300	5225	7,66	10,40	12,12	12,31
300-320	4000	7,30	10,50	13,00	12,50
320-340	3469	5,51	8,96	14,01	14,88
340-360	6883	5,42	8,08	10,39	10,77

Table 3.2: Approximation of the maximum wind gusts with a return period of respectively 1, 50 and 100 years.

The determined wind speeds are used to estimate the significant wave heights of wind generated waves that may arise. The governing wind directions are directed over land, restricting the possibility for wind waves to develop, this is indicated in Figures 3.8 and 3.9. The 'yellow' areas correspond to the governing directions that allow wind waves to develop. In reality, effects such as diffraction, refraction and shoaling will effect the wave spectrum. Hence, additional data surveys of the wave spectrum are strongly suggested. The next section converts the wind speeds to significant wave heights.

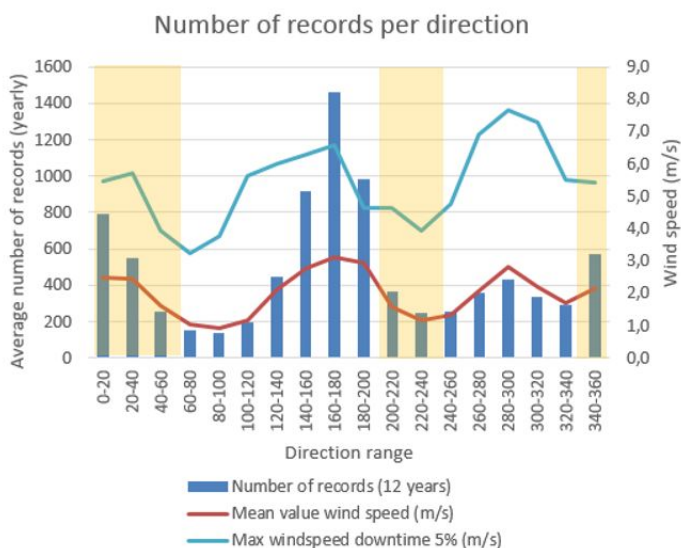


Figure 3.8: Overview of average amount of yearly records compared with measured maximum mean wind gusts and maximum windgust that is probable to arise during 5% of the time. Yellow areas correspond to yellow sections in Figure 3.9.

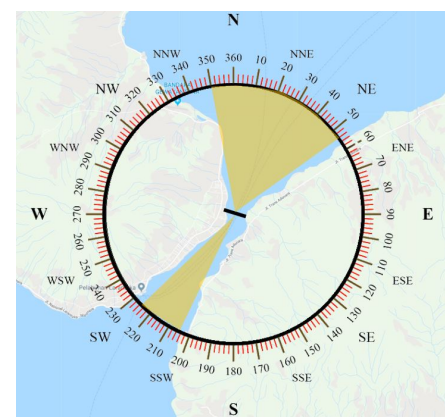


Figure 3.9: Governing directions for wind generated waves

3.2.3. Significant wave height

Actual wave records are not available, hence an estimation of the significant wave height is computed with the formula's of Young and Verhagen, Appendix C.4. The maximum wind speeds of the previous section are used along with an estimated fetch length and an averaged water depth over the fetch length. The significant wave heights that are found are plotted in Figure 3.10.

The incoming significant wave fronts are primarily parallel to the bridge deck due to diffraction and refraction induced by the topography, Figure 3.11. The range of directions where a wind wave is able to develop is in between 0-50 degrees and 200-230 degrees. The wave heights in the range of directions are provided in Table 3.3 and considered as governing in the research. In the table, the maximum wave height is calculated according to the ratio $H_{max} \approx 2H_s$ (Wulff Wathne (2012)).

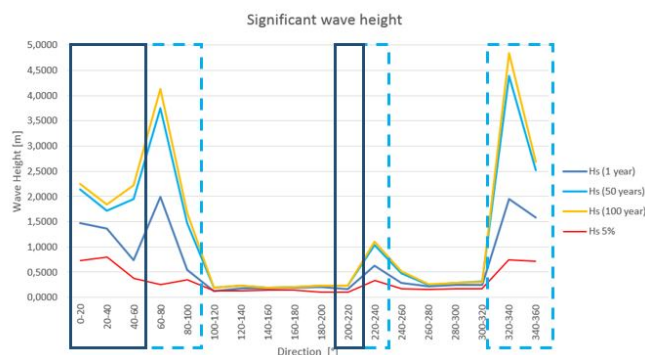


Figure 3.10: Computed wave heights per direction. Squared areas correspond with direction ranges indicated in Figure C.30.

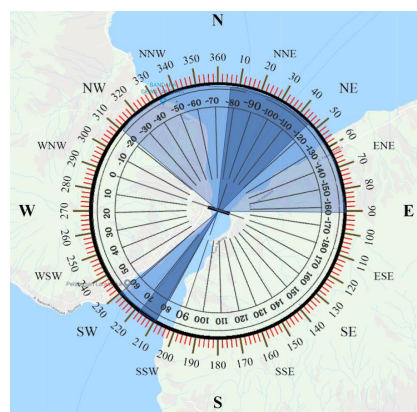


Figure 3.11: Significant incoming wave angles area (blue) according to Table C.29

	Direction [°]	U_{max} [m/s]	H_s [m]	H_{max} [m]	T_p [s]	L [m]	f [Hz]
Downtime of 5%	0-20	5,49	0,74	1,47	4,30	28,86	0,23
	20-40	5,73	0,80	1,61	4,49	31,49	0,22
	200-220	4,66	0,10	0,20	1,14	2,02	0,88
	220-240	3,92	0,33	0,67	2,66	11,01	0,38
1 year	0-20	7,80	1,473	2,95	6,06	57,35	0,16
	20-40	7,48	1,370	2,74	5,87	53,73	0,17
	200-220	7,14	0,162	0,32	1,38	2,99	0,72
	220-240	6,22	0,630	1,26	3,32	16,35	0,30
50 year	0-20	9,56	2,147	4,29	7,14	79,62	0,14
	20-40	8,37	1,713	3,43	6,56	67,20	0,15
	200-220	9,75	0,228	0,46	1,60	3,96	0,63
	220-240	9,65	1,039	2,08	4,06	17,33	0,25
100 year	0-20	9,83	2,256	4,51	7,28	82,76	0,14
	20-40	8,67	1,836	3,67	6,79	72,04	0,15
	200-220	10,15	0,238	0,48	4,09	4,09	0,62
	220-240	10,24	1,109	2,22	17,34	17,34	0,24

Table 3.3: Significant waves with corresponding characteristics for governing directions. Highest wave is highlighted in blue.

3.2.4. Tidal level

The English company Aquatera conducted a survey in June 2017 to indicate the environmental conditions in the Strait of Larantuka. Considering the data, the type of tide in the Larantuka Strait is mixed, mainly semidiurnal (Form Factor of 0,454). This represents two low and two high tides of a different size every day, Figure 3.12. The highest astronomical tide [HAT] is MSL + 1,37 m and the lowest astronomical tide [LAT] is at MSL - 1,48 m, together implying a tidal range of 2,85 m. The tidal levels are presented in Table C.7 in Appendix C. The measurements had a time span of a week and occurred simultaneously with the apogean spring tide, just after a Micro Full Moon, resulting in an underestimation of the tidal range, Appendix C.5.

A tidal range of 3 metres is assumed. Set-up and set-down, induced through waves that are obstructed by the bridge, are not included in the environmental data as the software of the computer model determines this directly. The tides can be simplified to a long-period wave with a very gradual varying slope. The slope induces a rotation of the floating parts of the bridge around the x-axis. The slope of the wave is approximated with the derivative of surface elevation formula, Appendix C equation C.13. The maximum angle is $2,1 * 10^{-9}$ degrees, indicating a negligible amount of induced rotation.

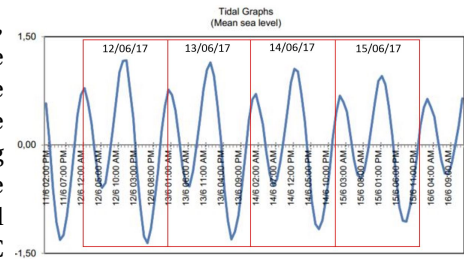


Figure 3.12: Tidal graph Larantuka Strait (Aqatera, 2017)

3.2.5. Current profile

The variation of the water level is related to a flow velocity induced by the displaced water body. Large current velocities occur due to the combination of the tidal range and the narrow passage of the Larantuka Strait. During high and low tides, the velocity of the current reduce to zero while at MSL maximum current velocities of 5 m/s arise. The maximum current depends on the water depth, near surface the current approaches 5,5 m/s, while at a depth of 25 m the maximum current is 4,5 m/s, elaborated in Appendix C. The maximum velocities occur just a fraction of the time and the average current speed is approximately 2,5 m/s. The survey measured the tidal flow velocity during 28 days with two Acoustic Doppler Current Profilers (ACDP). The instruments are able to indicate flow speeds along the whole depth profile. The results of the current magnitude at 0 to 5 m below MSL at both ADCP locations is presented in Figure 3.14. In the image the arrows indicate the direction of the flow. The distribution of the flow per direction implies that the governing current is directed perpendicular to the bridge, Figure 3.13. The small current that is present in (south)east and (north) west direction is neglected. The relationship between the current and the tide is analysed in Appendix C.5.

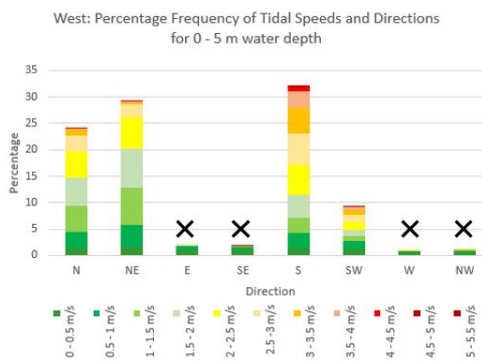


Figure 3.13: Current distribution along different directions on the Western survey point, crosses indicate omitted directions (Vos, 2017)

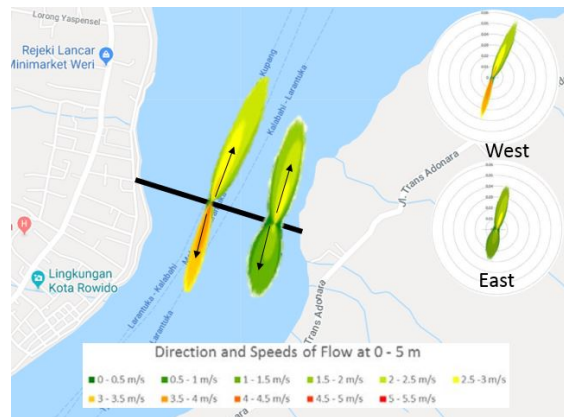


Figure 3.14: Current speed at 0-5m depth at both survey points (Aqatera, 2017)

Combining all survey data from Aquatera the average and extreme flow velocities can be found and analysed. The maximum extreme values measured at the ADCP stations are given in Appendix C. The maximum speed of 7,48 m/s arises during 0,0001 % of the measurements and is present at a small local spot. The considered maximum flow speed is a flow speed that is present at least 0,011 % of a day, respectively a flow speed of 5,2 m/s (Figure C.35). The maximum magnitude is based upon the requirement regarding the maximum moment around the x-axis induced by the drag force. Chapter 4 determines the drag coefficients with the use of a CFD-model and with this value the maximum flow velocity is computed. The forces induced by the flow speed are dependent on many unknown factors, for example the turbine resistance and behaviour. Therefore, the 'maximum' flow velocity is based upon a 'maximum' allowable moment instead of the maximum measured flow speed. When the maximum flow speed arises, it is assumed that the turbine resistance can be lowered to decrease the drag forces.

Summary: Chapter 3: General design conditions

This chapter elaborates upon the subquestion: "What are the governing hydraulic conditions at the project location?". Together with previous chapter, the data will form the basis of the load cases that will be tested to indicate the dynamic response of the Tidal Bridge. The next chapter will convert the data into forces and pressures that are acting on the bridge.

The Tidal Bridge is designed according to requirements set by the local Nusa Tenggara Timur Government and by the company Tidal Bridge. The government implies that a turbine electricity output should be in between 18 - 23 MW. In addition, traffic should be able to cross the bridge safely and the bridge should have an local Indonesian appearance.

The company Tidal Bridge has construction related requirements. The design should function as the template design that can be implemented at future project locations. The production costs of the bridge should be minimised with the use of prefab normalised structure elements and off-site construction. The lifetime of the bridge is relatively short and set to 50 years. The reduced lifetime is chosen as fatigue is suspected to occur. In addition, the desired downtime of the bridge is set to 5% within the lifetime of 50 years.

For safe traffic passage, serviceability limits are estimated. The limits are based upon reference cases and not analytical substantiated or proven. The main difference with existing floating bridges is that the type of roadway and corresponding speed limit. The Tidal Bridge has a speed limit of 20 km/h, while most floating bridges are designed as highways with a speed limits of 120 km/h. Nevertheless, the limits functions as an indication of an allowable amount of motion. An overview of the assumed serviceability limits is given in Table 3.4.

Tidal Bridge	Surge		Sway		Heave		Roll		Pitch		Yaw	
	Along x-axis [m]	Along y-axis [m/s ²]	Along y-axis [m]	Along x-axis [m/s ²]	Along z-axis [m]	Along z-axis [m/s ²]	Around x-axis [rad]	Around x-axis [rad/s ²]	Around y-axis [rad]	Around y-axis [rad/s ²]	Around z-axis [rad]	Around z-axis [rad/s ²]
(radians)	-	0,5	-	0,5	3,0	0,7	0,044	0,107	0,035	0,07	0,06	0,05
(degrees)	-	0,5	-	0,5	3,0	0,7	2,521	6,131	2,005	4,01	3,44	2,86

Table 3.4: Overview of estimated serviceability limits of the Tidal Bridge

The project location in Indonesia is considered as the frame of reference for the model. In the Strait of Larantuka, a tropical savanna climate with a wet and a dry season is present. During wet season, environmental conditions are heavier than during dry season. Indonesia is located on four tectonic plates and earthquakes occur frequently. Fortunately, the project location is sheltered by the neighbour-islands which reduces the probability and impact of a tsunami wave.

Environmental data sources are limited, hence the available data is elaborated and assumed as valid. The bathymetry of the project location indicates a maximum depth of MSL - 37 m and an average depth underneath the floating part of the bridge of MSL - 25 m. A constant average depth of 25 m is used in the model.

With twelve years of hourly maximum wind data, the wind characteristics are analysed. The wind speeds that may occur once every 1, 50 and 100 years are computed with the *Gumbel*, *Weibull* and *Generalised Extreme Value* distributions. The maximum measured wind speed in the dataset is 11,56 m/s, a strong breeze on the Beaufort scale. The maximum wind speed in 100 years is estimated as 14,8 m/s may arise from a direction of 320-330 degrees.

The significant wave height is calculated for every direction according to the theory of Young and Verhagen. The topography of the project location limits wind wave generation in some directions. Hence, the waves perpendicular to the bridge deck are considered as significant. Table 3.5 presents an overview of the significant and maximum wave heights during respectively 1, 50 and 100 years.

Summary: Chapter 3: General design conditions

	Direction [°]	U_{max} [m/s]	H_s [m]	H_{max} [m]	T_p [s]	L [m]	f [Hz]
Downtime of 5%	0-20	5,49	0,74	1,47	4,30	28,86	0,23
	200-220	4,66	0,10	0,20	1,14	2,02	0,88
1 year	0-40	7,80	1,473	2,95	6,06	57,35	0,16
	200-240	6,22	0,630	1,26	3,32	16,35	0,30
50 year	0-40	9,56	2,147	4,29	7,14	79,62	0,14
	200-240	18,53	1,039	2,08	4,06	17,33	0,25
100 year	0-40	9,83	2,256	4,51	7,28	82,76	0,14
	200-240	10,24	1,109	2,22	17,34	17,34	0,24

Table 3.5: Significant waves with corresponding characteristics for governing directions

A tidal range of 3 m is present, the fluctuation in water level results in two high and low tides every day and a tidal current. The maximum measured current during a three-day survey is 7,48 m/s. Yet, this current occurred less than 0,0001 % of the day and is neglected. In general the current varies harmonically between 0 and 4,5 m/s. The current velocity and directions measured with two *Acoustic Doppler Current Profilers* are indicated in Figure 3.15.

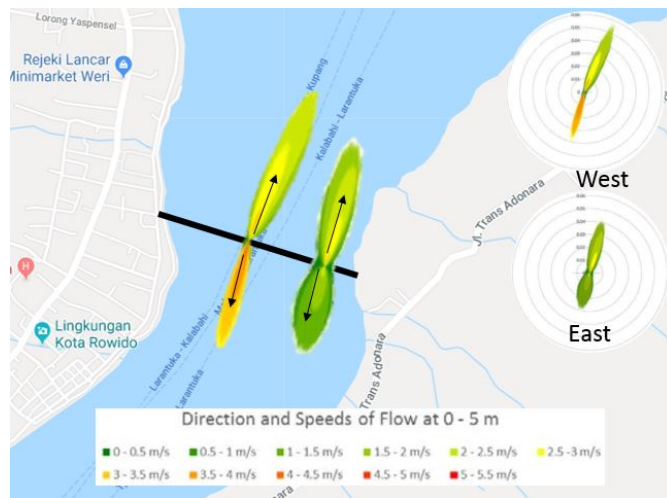


Figure 3.15: Current speed at 0-5m depth at both survey points (Aquatara, 2017)

4

Load inventory

In the chapter the loads acting on the submerged parts of the Tidal Bridge are indicated and quantified. In the way subquestion 1b: *"What types of loads are probable to induce significant motion?"*, can be answered. Appendix D elaborates upon the in-depth calculations and the estimation of the forces, loads and pressures.

First, the loads that act on the bridge in equilibrium conditions are indicated. Next, the external loads are elaborated and determined. A division is made between three main external load types: current loads, wave loads and static traffic loads, Figure 4.1. In the end, a combination of the input values for the sensitivity analysis are formulated.

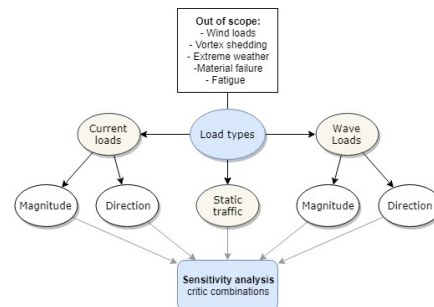


Figure 4.1: Overview of chapter outline

4.1. Static loads

A wide variety of loads act on the bridge in its lifetime. The scope of the report is set to wave and current induced variable loads only. Nevertheless, a short description of some of the environmental loads acting on the bridge is stated. Expressing the loads as static forces and pressures is done to simplify the situation and to be able to check the influence of a force quickly, in reality the forces will vary. The significance of the forces is discussed to check whether the actual dynamic response of the bridge differs from the situation with waves and current only.

Buoyancy force

The largest vertical load is the weight of the system, determined in Appendix D as $2,32 \cdot 10^6$ kg. When the system is in equilibrium and not exposed to external forces, an upwards water pressure is acting on the pontoons to balance with the self-weight: the buoyancy force. The buoyancy force is linear dependent on the displaced water volume, the pontoon volume under the water line. For the equilibrium situation, without external forces and pressures, this force has a magnitude of $2,27 \cdot 10^4$ kN. Yet, if for example traffic is present, the draught of the pontoons increases through additional weight, for that reason the buoyancy force is presented with a variable draught. For the modelling software, the geometry is created with a draft of 3,03 m, respectively the draught when the bridge is in equilibrium and not exposed to any forces. Additional forces can be applied on the structure, increasing the draught of the virtual pontoons in the software.

$$d_p = \frac{M_{TB}}{\rho_w A_p} \quad (4.1)$$

$$F_{buoy} = \rho_w g A_p d_p \quad (4.2)$$

d_p	Draught of pontoon	[m]
M_{TB}	Total mass of one Tidal Bridge element	[kg/100 m]
A_p	Cross-sectional area of all five pontoons	[m ²]
F_{buoy}	The buoyancy force	[kN/m]

Wind induced pressures

The *Indonesian Standard BMS bridge design manual, Volume 1* is considered for the determination of the maximum wind loads. An uniform wind pressure on the superstructure of 1,06 kPa in U.L.S. is present and an uniform line load at deck level of 2,12 kN/m in U.L.S. (Bridge Management System, 1992). Wind induced vortex shedding is not accounted for in the research. The wind load on the bridge is not studied, but wind generated waves are analysed.

Traffic

Vehicles, bicycles and pedestrians will be crossing the bridge from Larantuka to Adonara. Currently, the infrastructure near the bridge location is very remote and vehicles are not able to cross from island to island. This makes the forecasting of the traffic intensity questionable. The speed limit is restricted to 20 km/h to anticipate on vibrations induced by traffic and comfort when driving on the floating bridge.

Traffic intensity	Undetermined, estimated according to Dutch norms.
Speed limit on bridge	20 km/h.
Downtime of bridge	5 % in the 50-year lifetime.

The weight of traffic along one 100 m long Tidal Bridge element has a maximum force of 5 700 kN (Appendix table D.2). If the traffic is evenly distributed the draught of the pontoons will increase to 3,78 m instead of 3,03 m. In this scenario all lanes are fully occupied, which will not occur often. However, a more critical situation arises if only the outer lane is fully occupied. Then a maximum moment of 9 931 kNm may be present. The moment can be transformed to a point load of 3 825 kN with an eccentricity of 2,60 m of the centre of the bridge deck. The motion induced by asymmetric traffic point loads on the bridge is analysed. Three cases are analysed and case 1 and 2 are illustrated in Figure 4.2:

1. Maximum rotation around the y-axis: Point forces of 5 700 kN acting at points 2 and 4
2. Maximum rotation around the y-axis: Point forces of 2 705 kN acting on points 1 and 5
3. Maximum rotation around the x-axis: The eccentric point load of 3 825 kN, with an eccentricity of 2,60 m acting in the middle of each floater.

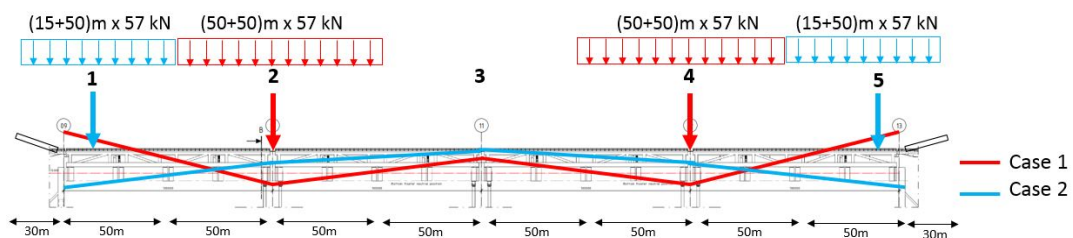


Figure 4.2: Traffic attachment points (rotation is not drawn to scale)

4.2. Wave induced pressures

The wave characteristics are uncertain and based upon wind velocities and fetch length. The actual wave spectrum in the Strait of Larantuka is unknown. The wind generated waves, computed with the Young and Verhagen formula's, are used to calculate the wave loads. If waves coincide with a structure, multiple scenarios can happen. Short standing waves collapse or break and long progressive waves will gradual flow underneath the structure. The analysis about the interaction of waves and structures is the *Hydrodynamic Diffraction Analysis* of Ansys Aqwa, elaborated in Appendix D.3.

First, the type of waves is determined to find the applicable wave theory. The steepness and shallowness characteristics lead to the corresponding wave theory: *Third Order Stokes theory*. The complexity of the wave theory increases according to the order size of the theory. The formula to compute the surface elevation (η) of a Third order Stokes wave is in the form of equation 4.3 (Holthuijsen, 2007).

$$\eta(x, t) = a \left(\left[1 - \frac{1}{16} (ka)^2 \right] \cos(\theta) + \frac{1}{2} (ka) \cos(2\theta) + \frac{3}{8} (ka)^2 \cos(3\theta) \right) + \mathcal{O}((ka)^4) \quad (4.3)$$

$$\text{With:} \quad \theta(x, t) = kx - \omega t \quad (4.4)$$

In which;

$\eta(x, t)$	Surface elevation in time (t) and space (x) domain	[m,s]
ω	Radian frequency	[rad/s]
a	Amplitude (H/2)	[m]
k	Wave number	[-]
θ	Wave expression	
t	Time	[s]
L	Wave length	[m]
\mathcal{O}	Order size	[-]

The wave height of a third order Stokes wave can be computed with equation 4.5 (Holthuijsen, 2007). The wave height is the difference between the surface elevation of the trough and the crest. In the equation a is the linear first order wave amplitude. The wave number k is a function of the wave length (λ). The difference in wave height between a linear and a third order Stokes wave is checked for the highest significant wave that may be present according to the wave heights estimations. The governing wave is $H_s = 2,25$ m with a proportional wave length of $\lambda = 82,762$ m. Hence, the wavenumber $k = 0,08$ and $a : H_s/2 = 1,13$ m (equation 4.6), Appendix C.4.

$$H_{3^{th} Stokes} = 2a \left(1 + \frac{3}{8} k^2 a^2 \right) = 2 \cdot 1,13 \left(1 + \frac{3}{8} \cdot 0,08^2 \cdot 1,13^2 \right) = 2,26693 \text{ m} \quad (4.5)$$

$$k = 2\pi/\lambda \quad (4.6)$$

The difference between the wave height of a linear wave and a Stokes wave is 0,017 m. This increase in wave height is small compared to the dimensions of the bridge. In addition, the applied wave characteristics are based upon uncertain data, suggesting that the error-size in the wave height estimation is of a larger extent than the influence of the increased height of a third order Stokes wave. For that reason, the linear wave theory is assumed as applicable in the research. The shape of a Stokes wave is more steep than a linear wave, the effect of the different wave shape is analysed for a second order Stokes wave in Ansys Aqwa. An estimation of the wave pressure (p) according to linear wave theory is calculated with equation 4.7 (Holthuijsen, 2007).

$$p_{wave, 2,06m} = \frac{1}{2} \rho_w g H_s = 5028 \cdot H_s = 10 351 Pa \quad (4.7)$$

4.3. Current induced pressures

The current is a result of the varying water levels of the tide. The tide in the Strait of Larantuka can be formulated as a sinus function in space with an amplitude of 1,5 m and a period of approximately 12 hours. The tidal wave that approaches the function is predictable and harmonic with a very gradual wave slope. The flow velocity of the tidal wave is analysed in Appendix C.5. The current is non-uniform and varies in distribution over the depth and along the span of the bridge. Friction and turbulence lower the magnitudes of the flow speed near the seabed and the bathymetry influences the flow velocity potential. In addition, the flow distribution along the Strait is uncertain. Therefore, the current profile that will be analysed is according to Figure 4.4. The maximum measured flow velocities present during 5% of the time is a flow of 4,5 m/s. The absolute maximum flow speed measured has a value of 7,5 m/s and occurs approximately less than 0,0001% of the time. The current approaches the bridge mostly perpendicular directed or slightly oblique with a small angle, Figure 4.3. The current velocities result in a drag force on the submerged structure elements. The drag force is determined in next sections.

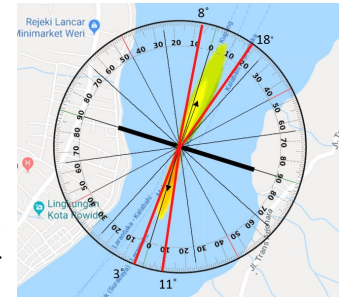


Figure 4.3: Flow velocity with maximum incoming angle (Dynasim Engineering (2017))

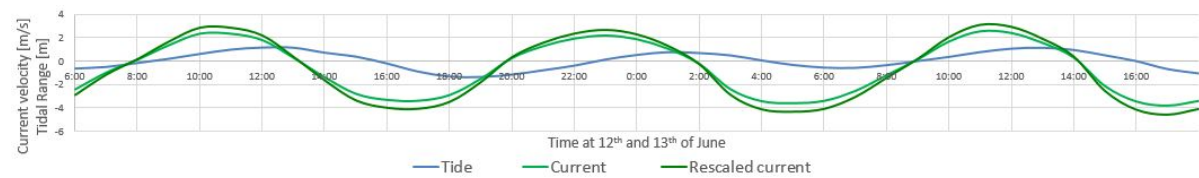


Figure 4.4: Current velocity versus Tidal Range during the 12th and 13th of June 2017 (Antea Group, 2018)

4.3.1. Morison drag on mooring system

The mooring system exists of cylindrical piles reaching along the whole depth. In hydraulic engineering, the Morison equation is often used to estimate the drag force on this type of 'tube-elements'. Yet, according to the expertise of *H. Hendrikse (2019)* calculating drag with the equation can be solely considered as an estimation and not as an exactly corresponding value. Nevertheless, the size of the pendulums is small compared to the submerged area of the pontoons and turbines, suggesting that the influence of the pendulum drag is limited.

The Morison equation is a combination of an equation for the inertia force, a force that includes the added mass, and the drag force. Both equations are depending on shape-dependent coefficients that are estimated in Appendix D.4. The drag on the 'tube-elements' is dependent on the flow speed and flow acceleration. Hence, the Morison equation calculated as a function of the flow speed u (Ansys Inc., 2015).

$$\begin{aligned}
 F_{drag, tube} &= \rho_w C_m \frac{\pi D^2}{4} \dot{u} + 0,5 \rho_w C_d D u |u| \\
 &= 2805 \dot{u} + 676,5 u |u|
 \end{aligned} \tag{4.8}$$

$F_{drag, tube}$	Force inline with the current direction	[N]
C_m	The inertia coefficient, $C_m = 1 + C_a$	[-]
C_a	Added mass coefficient	1,0 [-]
C_d	Drag coefficient of tube	1,0 [-]
\dot{u}	Flow acceleration $\frac{du}{dt}$	[m/s ²]
u	Flow velocity	[m/s]
D	Diameter of tube	1,32 [m]

4.3.2. Drag forces: pontoon and turbines

The main area that is exposed to the current is the combined pontoon-FishFlow structure, Figure 4.5. A high drag force will be present as a result of the large structure that is blocking the flow. The drag coefficients of the system are very complex to estimate and uncertain to indicate without (scale) model-tests. Multiple methods and literature sources are elaborated to indicate the individual and combined influence of the drag on both the pontoons and the turbines, Appendix D.4. Factors such as the draught-depth ratio and span-channel-to-width ratio complicate and reduce the amount of available information.

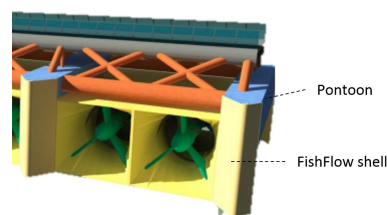


Figure 4.5: Combined pontoon - FishFlow structure (Dynasim Engineering (2017))

In addition, the modelling software *Ansys Aqua* is not able to replicate the estimated drag force entirely, but allows multiple input methods. Next chapter will discuss the various implementation methods in the *Ansys Aqua* software. The general equation to compute drag on a submerged element is equation 4.9. In the formula two variables should be defined: A_n and C_D . A_n is the area of the submerged part that is perpendicular to the flow, the area differs if the flow is directed under an angle. The A_n can be computed with equation 4.10 (Holthuijsen, 2007).

$$F_d = \frac{1}{2} C_D \rho_w A_n u^2 \quad (4.9)$$

$$A_n = \cos(\alpha) \cdot A_{front} + \sin(\alpha) \cdot A_{side} \quad (4.10)$$

In which,

F_d	Drag force parallel to flow direction		[N]
ρ_w	Density of water	1025	[kg/m ³]
u	Incident current velocity		[m/s]
C_D	Drag coefficient		[-]
A_n	Area normal to the current		[m ²]
α	Angle of incoming current		[°]
A_{front}	Submerged area parallel to the x-axis (100 m element)	1235	[m ²]
A_{side}	Submerged area parallel to the y-axis (100 m element)	442	[m ²]

The other variable of importance is the drag coefficient. The drag coefficient can solely be confirmed with model tests and only estimated with literature. The drag coefficients that are found in literature are based on the guidelines of Det Norske Veritas (2010b), British Standards Institution (1989) and Dynasim Engineering (2017), Appendix D.4. The governing drag coefficient is based on the Computational-Fluid-Dynamics model (CFD) computed by the company Dynasim Engineering in 2017. The applicability of the model is questionable, the intention of the model was to compute the possible energy generation and not to indicate the drag coefficient. The turbines are secured in place and not able to move, neglecting the influence of additional forces if rotations are present. In addition, the model is only tested on a perpendicular flow. If the flow enters under an angle, the drag force will differ consequently. The drag coefficient on the pontoons and turbines is depending on the shape of the structures, a slender streamlined structure experiences less drag than a robust structure. The estimation of the drag coefficient for the pontoons is provided in Appendix D.

The company Tidal Bridge set a requirement regarding the maximum moment that may arise from turbine induced pressures. The moment, located at the waterlevel, is 21 000 kNm/m acting along the x-axis. Figure 4.6 visualises the pressures that arise with a perpendicular current of 2 m/s. It can be seen that a significant counteracting moment will be present as a result of the turbine housing. The moments are transformed into one total drag force of 1,27 MN that acts at an arm of 7,32 m below the waterline.

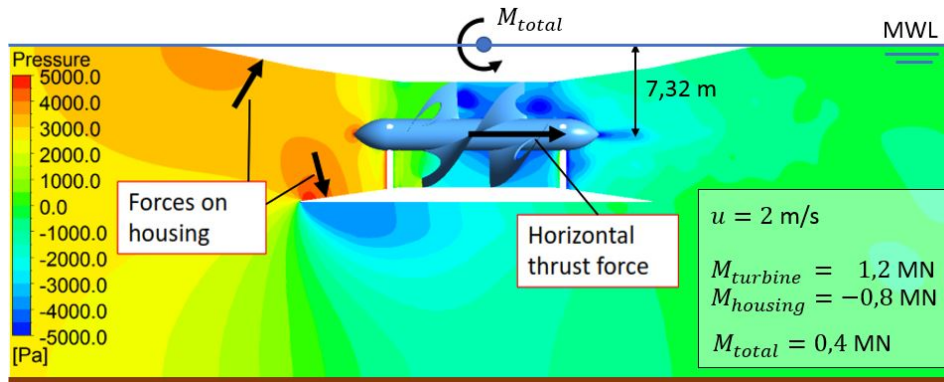


Figure 4.6: Schematic representation forces on FishFlow (inlet velocity = 2m/s) (Dynasim Engineering, 2017)

With the data of Dynasim, the drag coefficient can be iteratively calculated resulting in a drag coefficient of 2,11. This implies that the maximum moment of 21 000 kNm is reached if a flow velocity of 5,2 m/s is present. The measured maximum velocity is 7,5 m/s suggests that the the amount resistance of the FishFlow turbines should be adjusted during high flow velocities.

The current has another effect on the dynamic response, the mass of the water body that flows through the turbine stabilises the system. If the mooring system induces a rotation of the system around the x-axis, the velocity potential induces counteracting rotation forces, Figure 4.7. The forces are very complex to implement in a model as they are a function of multiple unknowns variables. For example, the flow speed through the turbine may be smaller than the flow speed in the channel as a result of the transmitted energy through turbine resistance. Next, the induced rotations by the mooring system and the flow potential will be constantly iterating and therefore δh will not be constant. Also, the water level before and after the bridge may vary due to an overall energy loss. Yet, this moment may have a significant positive effect on the stability of the system. A part of the stabilising moment is already included in the CFD model of Dynasim, the housing moment. The actual counteracting moment may increase if the system rotates. The sensitivity analysis elaborates on the effect of high moments on a rotated system.

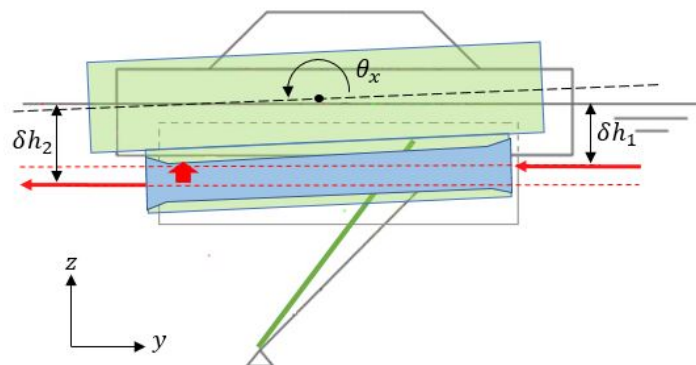


Figure 4.7: Visualisation of the stabilizing moment due to the flow potential

Summary: Chapter 4: Load inventory

In the chapter and in Appendix D the loads that are acting on the floating system are elaborated and quantified to answer subquestion 1b: "What types of loads are probable to induce significant motion?". The loads that may act on the system simultaneously are presented in Table 4.1 and in Figure 4.8.

Selfweight	F_{sw}	$22,8 \cdot 10^3$	[kN]
Buoyancy force	F_{buoy}	$7\,521 \cdot d_p$	[kN]
Maximum Turbine moment	M_t	21\,000	[kNm]
Drag force pontoons	F_D	$0,5C_D A_n \rho_w u^2$	[kN]
Wave induced pressure	f_{wave}	$0,5\rho_w g H_s$	[Pa]

Table 4.1: Overview of forces acting on a Tidal bridge element

Three 'static' traffic cases that will be analysed are:

1. Maximum rotation around the y-axis: Point forces acting on points 2 and 4.
2. Maximum rotation around the y-axis: Point forces acting on points 1 and 5.
3. Maximum rotation around the x-axis: The eccentric point load of 3 825 kN with an eccentricity of 2,60 m left of the centre axis.

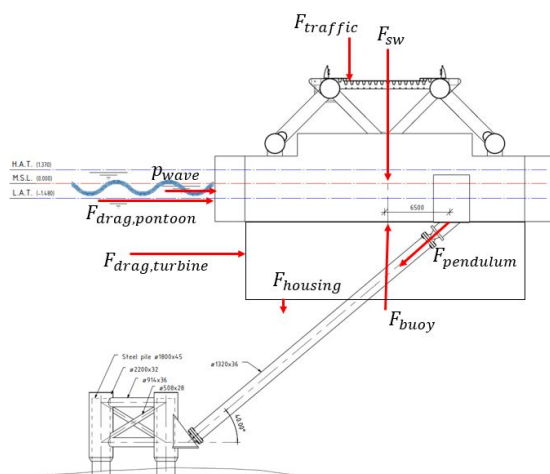


Figure 4.8: Overview of attachment point of forces

The **drag force** that is assumed for the system is based on a CFD model of the company Dynasim Engineering (2017). The drag force is proportional to a **horizontal force of $1,27 \text{ } u^2 \text{ MN/m}$ at an arm of 7,32 below the waterline**. The drag coefficient that is used for the combines pontoon and turbine system as value of $C_d = 2,11$. The requirement regarding the **maximum turbine moment of 2,1 MNm/m** is reached at a **flow velocity of 5,2 m/s**. During higher flow speeds, the amount of resistance within the turbines should be reduced. The **water body that travels through the FishFlow turbine results in a stabilising moment** around the x-axis. This counteracting moment may influence the stability significantly.

Third Order Stokes waves are present in the Strait of Larantuka. A third order Stokes wave is very complex compared to a linear wave. The difference between wave heights is only 0,017 m, hence a **linear wave** is assumed as an valid approximation of the waves.

The critical load combinations follow from the sensitivity analysis and are a combination between current, waves and traffic. In addition, **the FishFlow turbines induce a stabilising effect** that is complex to estimate and should be indicated with additional model tests.

5

Structural properties of the Tidal Bridge

This chapter elaborates on the dynamic characteristics of the bridge and answers the question 1C: "What are the dynamic properties of the Palmerah Tidal Bridge?". The realistic situation of a fully coupled bridge including all external loads is too complex to analyse. Hence, the system is simplified to a three-dimensional model in the equilibrium conditions.

5.1. Analysis type

First, the type of analysis is assessed. A division between three main analysis types is made (Bartrop, 1998):

- *Static analysis*: where known stiffness and forces indicate the unknown displacement: equation 5.1.
- *Dynamic analysis*: mass times acceleration and damping times velocity are included: equation 5.2.
- *Quasi-static analysis*: combination of static and dynamic analyses. Used when the body is accelerating essentially as a rigid body, equation 5.3 (Bartrop, 1998).

$$Kx = F \quad (5.1)$$

$$M\ddot{x} + C\dot{x} + Kx = F \quad (5.2)$$

$$Kx = F - M\ddot{x}_r - C\dot{x}_r \quad (5.3)$$

In the equations, M represents the mass matrix of the system, C the damping matrix, K the stiffness matrix and $F(x)$ the excitation force on the system, all defined in every degree of freedom. All variables are depending on the motion x , the motion is for example a wave at the frequency (ω). The subscript x_r indicates the motion of the rigid body.

Where:

$$x = a \sin(\omega t)$$

$$\dot{x} = a\omega \cos(\omega t)$$

$$\ddot{x} = -a\omega^2 \sin(\omega t)$$

Floating structures are commonly modelled with a combination of dynamic rigid body analysis and quasi-static structural analysis. First, a structural dynamics analysis is obtained to indicate the dynamic characteristics of the system. Next, the dynamic properties are implemented in the model and a quasi-static analysis determines the impact of the loads on the system. Therefore, the combination of a dynamic and quasi-static analysis is suitable to determine the behaviour of the Tidal Bridge.

The dynamic analysis can be computed in two domains:

- *Frequency domain analysis*: Linear method that creates insight in behaviour such as natural frequencies of the system. A disadvantage of the linearity is that the response is proportional to the load or the wave height. The analysis is valid if small waves are present.
- *Time domain analysis*: includes non-linearities that become important if large waves are present. This method is more complex and difficult to calculate exactly.

Prediction of the motion of structures in water, especially vessels, is extensively studied. The most common type of analysis is an analysis in the linearised frequency domain, yet this type of analyses is not time-dependent. Linear Wave Theory problems are linearly dependent on displacement, velocity and acceleration, resulting in a suitable problem to solve in the frequency domain analysis. Nevertheless, a Time Domain analysis is required in order to mimic the response of the coupled construction over time and to include second order effects. For the Tidal Bridge, both a frequency and time domain analysis are considered to find reasonable estimates of the response of the system.

Loads act in multiple time-scales with specific motions as response. For current and wave induced loads three time-scales are possible, (Det Norske Veritas, 2010b):

1. Wave frequency motion: induces largest motions on offshore structures.
2. Low frequency motion: non-linear load effects induce motion at the natural frequencies of the structure, even if the loads are not of the same frequency (slow-drift motions).
3. High frequency motion: can induce elastic motion response (spinging and whipping).

It is probable that the *Wave frequency motion* time-scale induces governing motion. The other two time-scales are dependent on non-linear effects that are not included in the infinitely stiff model analysis. In addition, low-frequency motions are corresponding to long (tidal) waves. The effect of a varying waterlevel extends the scope of the project. The opposite domain, the high frequency motion, considers very short waves that are dampened by the weight and dimensions of the bridge structure. Hence, the wave frequency motion is assumed to be governing.

5.2. Structural dynamics

The combination of a coupled system and variable loads, results in a continuously moving system that experiences motion in every six degrees of freedom. The motion can be described after an analysis in the Frequency Domain and will be subjected to a particular degree of freedom. Figure 5.1 indicates the six degrees of freedom projected on the Fixed Reference Axis (FRA) of the Tidal Bridge. It is probable that the motions of the Tidal Bridge will be most sensitive with respect to roll and heave motions induced by the incoming waves and perpendicular current.

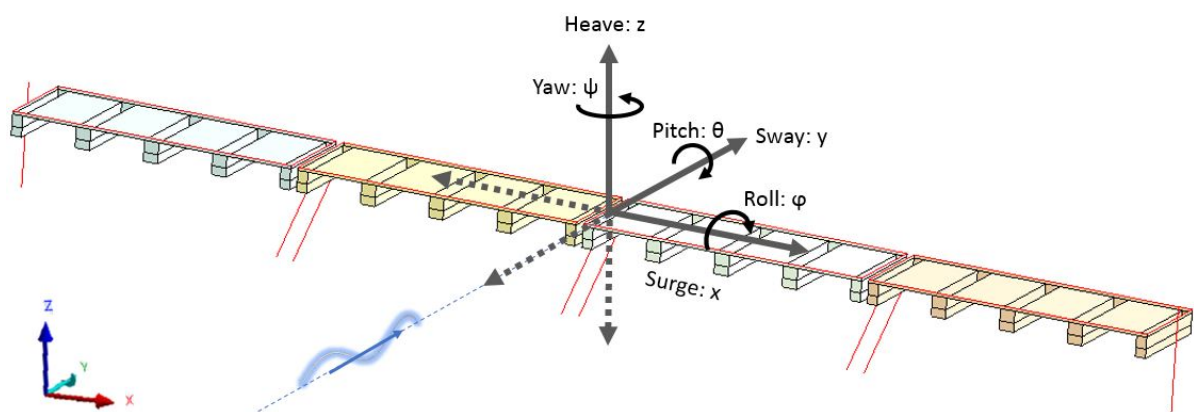


Figure 5.1: Six-degrees-of-freedom system with positive axes

Complications arise when the natural frequencies of the bridge and a force coincide and cause resonance. The phenomenon of resonance arises if an external force or vibration causes another system to oscillate at a the same frequency with an increased amplitude. It is possible to interfere with the natural frequency of a

system by applying damping, adding mass or adjusting other characteristic properties. The natural frequencies can be computed by calculating the steady state response of the bridge. A simplified example of how to calculate the natural frequency in heave direction of a buoy in water is provided in Appendix E.1.1.

The Tidal Bridge can experience motion in all six degrees of freedom. In the equilibrium position, without any external loads, the bridge floats in a straight line between the spudpole connections of the civil bridges. The self-weight of the bridge is in counterbalance with the upwards water pressure, creating a stable system. The stable equilibrium situation is used to obtain the dynamic characteristics of the system.

The dynamic response of a single degree of freedom in equilibrium mode can be described with a mass-spring-damper system. When the dynamic response due to additional loads is requested, external forces can be added to the equation. This specific type of equation is called the *Equation of Motion*.

$$m\ddot{x} + c\dot{x} + kx = f(x) \quad (5.4)$$

Where x is in the form of:

$$\begin{aligned} x &= a \sin(\omega t) \\ \dot{x} &= \frac{\delta x}{\delta t} = a\omega \cos(\omega t) \\ \ddot{x} &= \frac{\delta^2 x}{\delta^2 t} = -a\omega^2 \sin(\omega t) \end{aligned}$$

In equation 5.4, m represents the mass [kg], c the damping [kN/m²], k the stiffness [kN/m] and $f(x)$ the excitation force [kN]. All variables are depending on the motion x [m], the motion is for example a wave at the same frequency (ω). The mass, damping and stiffness are dynamic characteristics of the system and depend and differ for the particular components. To find the parameters, multiple system components are analysed in the chapter and Appendix E. The combined Equation of Motion for the total dynamic response of the Tidal Bridge can be written as Equation 5.5 (Spijkers et al., 2006).

$$[\mathbf{M} + \mathbf{M}_a(\omega)]\ddot{\mathbf{x}} + \mathbf{C}\dot{\mathbf{x}}(\omega) + \mathbf{K}\mathbf{x} = \mathbf{F}_i(\omega) + \mathbf{F}_d(\omega) \quad (5.5)$$

Where:

$$\mathbf{x} = \begin{Bmatrix} x(x, t) \\ y(x, t) \\ z(x, t) \\ \varphi(x, t) \\ \theta(x, t) \\ \psi(x, t) \end{Bmatrix} = \begin{Bmatrix} \text{Surge} \\ \text{Sway} \\ \text{Heave} \\ \text{Roll} \\ \text{Pitch} \\ \text{Yaw} \end{Bmatrix} \quad (5.6)$$

In which,

\mathbf{M}	System Mass Matrix [6x6]	[kg]
\mathbf{M}_a	System Added Mass Matrix [6x6]	[kg]
\mathbf{C}	System Damping Matrix [6x6]	[kN/m]
\mathbf{K}	System Stiffness Matrix [6x6]	[kN/m ²]
$\mathbf{x}(\omega)$	Displacement of the system	[m]
\mathbf{F}_i	Initial forcing function	
\mathbf{F}_d	Dynamic forcing function	

The answer to equation 5.5 can be found when all other structural properties are computed. The next section elaborates on the systems structural properties and characteristics.

5.3. System characteristics

The Tidal Bridge system consists of multiple separate 'individual' structural parts and components. Each element has specific structural properties that influence the stability and hence the dynamic response. Examples of this type of properties are: mass, stiffness, damping, moments of inertia and centres of gravity. An overview of all calculations is presented in Appendix E.

5.3.1. Geometry

First, the geometry of the bridge is analysed to indicate the rotation point, centre of gravity and centre of buoyancy of the bridge. First, the centre of gravities of the individual components are determined. All data is combined and the combined centre of gravity of one complete 100 m long floater is found with formula 5.7. The data that is implemented in the equation is elaborated in Appendix E.

$$CG_{total} = \frac{\sum M_i [z_i]}{\sum M_i} = \begin{Bmatrix} 0 \\ 0 \\ 3,36 \end{Bmatrix} m \quad (5.7)$$

In the equation M represents the mass of the component part [kg] and z the distance arm measured from the z -axis [m]. An overview of all important geometry points is presented in Figure 5.2. In the figure, CG_{TB} indicates the centre of gravity of the total 100 m Tidal Bridge element, CG_p is the the centre of gravity of the pontoon and CB the centre of buoyancy.

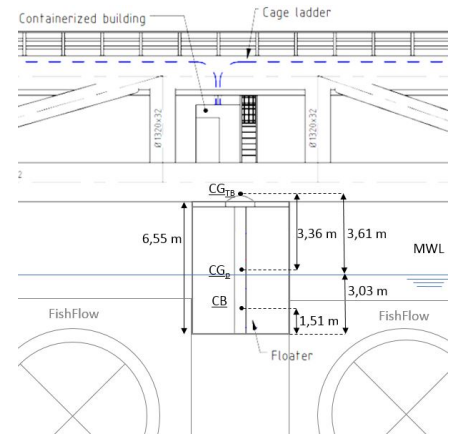


Figure 5.2: Centres of gravity Tidal Bridge, side view pontoon

Next step is to calculate the moments of inertia (I_{ij}). With the masses of the individual parts and the centre of gravity the moments of inertia are found with *MathCad* and described in Appendix E.

$$I_{TB} = \begin{Bmatrix} I_{xx} & I_{xy} & I_{xz} \\ I_{yx} & I_{yy} & I_{yz} \\ I_{zx} & I_{zy} & I_{zz} \end{Bmatrix} = \begin{Bmatrix} 2,14 \cdot 10^8 & 0 & 0 \\ 0 & 1,73 \cdot 10^9 & 0 \\ 0 & 0 & 1,76 \cdot 10^9 \end{Bmatrix} [\text{kg m}^2] \quad (5.8)$$

5.3.2. Stiffness properties

The stiffness and damping parameters of the system are more complex to indicate. Especially, as the modelling software Ansys Aqwa assumes infinitely stiff bodies that will not deform. Two different groups are analysed: the properties of the hinges and the stiffness of the system components. The second group results in the hydrostatic stiffness characteristics.

Stiffness of the connecting hinges

Four types of hinges can be distinguished in the bridge design. An illustration of the location of the hinges in the bridge is presented in Figure 5.3. The properties of all four hinge types are analysed in Appendix E and summarised in Table 5.1. The characteristics of the mainland connections are based on the present spudpole design that is analysed in the sensitivity study in Chapter 7.

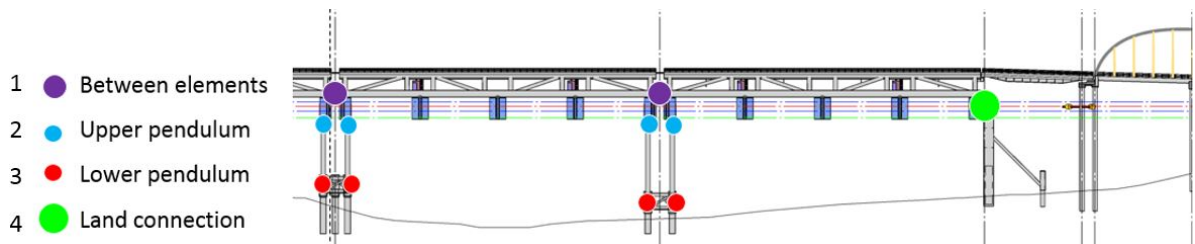


Figure 5.3: Springs of right side of Tidal Bridge (sideview)

Hinge type	Stiffness [N/m]	Damping [N/m ²]	Additional information
1 Between bodies	∞	0	Constructed as infinitely stiff frictionless hinges
2 Upper pendulum	∞	0	Constructed as infinitely stiff frictionless hinges
3 Lower pendulum	944 000	0	Grouted connection to tripod allows limits stiffness
4 Land connection	$72,5 \cdot 10^6$	0	One spudpole allows initial displacement along the x-axis

Table 5.1: Overview of variable horizontal loads

Hydrodynamic Stiffness

The equation of motion requires the input of the hydrodynamic stiffness matrix. The stiffness acting on the floating body in still water can be expressed in terms of water pressure and geometry terms. The natural frequencies of the system are calculated for the steady state response according to Gerritsma (2003) and Vos (2017). The important modes of motion and corresponding formulas are given. The input parameters and characteristics are elaborated in Appendix E.4.

$$k_{heave} = A_w \rho_w g = 7,52 \text{ MN/m} \quad (5.9)$$

$$k_{roll} = \rho_w g \nabla \overline{GM}_T = 607,7 \text{ MNm/rad} \quad (5.10)$$

$$k_{pitch} = \rho_w g \nabla \overline{GM}_L = 7 299,3 \text{ MNm/rad} \quad (5.11)$$

$$f_{heave} = \frac{1}{2\pi} \cdot \sqrt{\frac{k}{m}} = 0,287 \text{ Hz} \quad (5.12)$$

$$f_{roll} = \frac{1}{2\pi} \cdot \sqrt{\frac{k}{I_{xx}}} = 0,328 \text{ Hz} \quad (5.13)$$

$$f_{pitch} = \frac{1}{2\pi} \cdot \sqrt{\frac{k}{I_{yy}}} = 0,334 \text{ Hz} \quad (5.14)$$

5.3.3. Natural frequencies

Next, the natural frequencies can be found. It is apparent that the critical degrees of freedom with respect to induced motion are roll, heave and pitch, illustrated in Figure 5.4. Often, the natural periods of large offshore structures that are moored are typically over 100 seconds for sway, surge and yaw. Roll, pitch and heave, have generally natural periods around 20 seconds (Det Norske Veritas, 2010b). The characteristic eigenperiods of the Tidal Bridge elements have a smaller period. The critical factor that influences the decrease in eigenperiod is the amount of damping in the mooring system. The pendulums behave differently to mooring cables and influence the stability. The critical characteristic eigenfrequencies are given in Table 5.2, the table is a result of the calculations in Appendix E.

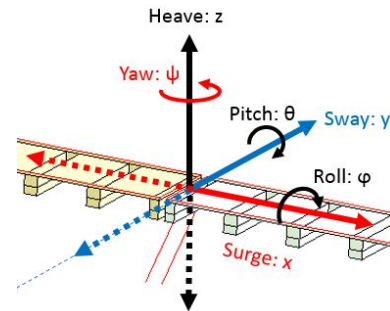


Figure 5.4: Probable limited degrees of freedom

Mode	Axis	Hydrostatic stiffness		Frequency [Hz]	Period [s]
Heave	z	k_z	7 518 758 [N/m]	0,287	3,49
Roll	x	k_φ	607 767 558 [Nm/rad]	0,268	3,73
Pitch	y	k_θ	7 299 345 191 [Nm/rad]	0,327	3,06

Table 5.2: Hydrostatics computed with Mathcad

The eigenperiods are of the same ordersize as the frequencies of the vertical motion of wind generated waves on the ocean surface. This indicates that the probability of resonance and hence large motions are realistic. Influencing the natural frequencies can be accomplished by adjusting the stiffness and damping properties. Examples are introducing cables in the mooring system or implementation of for example 'anti-roll tanks'.

5.4. Stability calculation of floater

The hydrostatic stiffnesses are used to indicate the magnitude of roll-rotation induced by the maximum tolerable drag force. One 100 metre long floater is modelled in Matrixframe according to the technical drawings, a schematic overview of the model is given in Figure 5.5. The bridge is supported with springs with the magnitudes of the hydraulic stiffnesses. The model is elaborated in Appendix E.

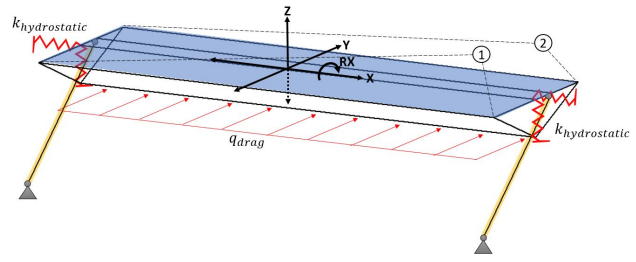


Figure 5.5: Probable limited degrees of freedom

The heave stiffness is based upon the submerged area of the pontoons but as the mass is not defined in the Matrixframe model, the magnitude of the vertical displacement is too high and not probable. When the mass is added, the structure instantaneously shifts downwards, which is not realistic as the equilibrium situation is defined in the geometry. Another inaccuracy in the Matrixframe model is that the drag force moves with the structure and displaces parallel to the floater. In reality, the drag force is at a constant water level and will not 'move' vertically. Hence, the influence of the vertical heave stiffness is checked by defining two values for the heave stiffness in the model. The second stiffness is a stiffness based upon the whole area of one floater $100 \times 34 = 3400 \text{ m}^2$, instead of the pontoon area (748 m^2). The heave stiffness is linear dependent on the area, $k_{heave} = \rho g A$, and increases with a factor 4,5. The results of the Matrixframe calculations are presented in Table 5.3, illustrated in Figure 5.6 and elaborated in Appendix E.

k_{heave} (kN/m)	q_{drag} (kN/m)	Point 1			Point 2			Displacement centre point			Rotation RX [°]
		X [m]	Y [m]	Z [m]	X [m]	Y [m]	Z [m]	dX [m]	dY [m]	dZ [m]	
3 759	351	0,0006	2,4051	-5,6824	-0,0004	2,4051	-1,7011	0,0005	2,4051	-3,6918	-6,7400
3 759	-351	-0,0006	-2,4051	5,6824	0,0004	-2,4051	1,7011	0,0005	-2,4051	3,6918	6,7400
16 666	351	0,0006	0,0954	-2,8289	-0,0004	0,0953	1,1524	0,0005	0,0954	-0,8383	-6,7400
16 666	-351	-0,0006	-0,0954	2,8289	0,0004	-0,0953	-1,1524	-0,0005	-0,0954	0,8383	6,7400

Table 5.3: Displacement of points 1 and 2 to a horizontally distributed drag force.

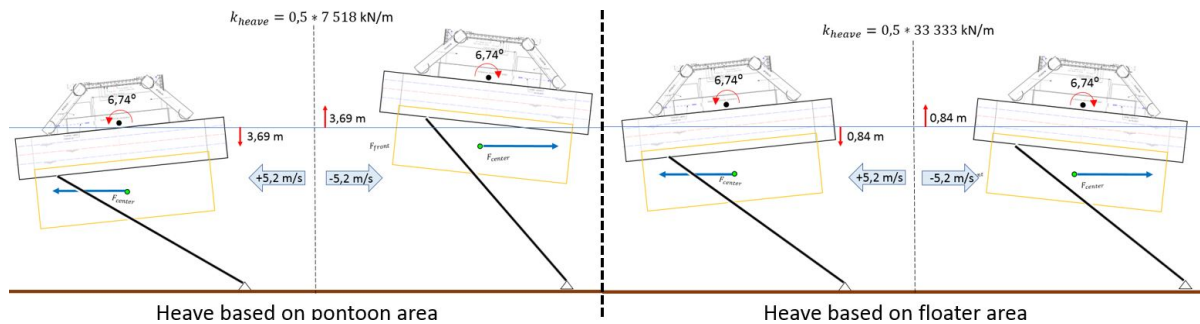


Figure 5.6: Illustration of displaced floater with computed values from Table E.6

The results of the Matrixframe stability calculation indicate that the amount of roll-rotation is not effected by an increase in heave stiffness. The rotation is primarily induced by the hydrostatic roll stiffness and solely for a small part dependent on the other stiffness and connections. The increased heave stiffness scales down the magnitude of vertical displacement and 'secures' the bridge below the water level. Another observation is that the direction of the current does not influence the rotation of the floater. The reaction of the floater with the increased heave stiffness is more probable and assumed as correct in for the indication of the dynamic response of the floater.

Summary: Chapter 5: Structural properties of the Tidal Bridge

The focus of the chapter is to indicate the dynamic characteristics of the Tidal Bridge and answer the corresponding subquestion: "What are the dynamic properties of the Palmerah Tidal Bridge?"

The Bridge can move along every six degrees of freedom, yet with a different extent. The magnitude of motion depends on the direction of the incoming loads and the geometry of the system. It is probable that **roll, heave and pitch motion will surpass the amount of motion** of the other degrees of freedom, Figure 5.7.

The dynamic response of the Tidal Bridge can be calculated by solving the **Equation of Motion in the Frequency Domain and in the Time Domain Analysis**. First, the Frequency Domain should be completed to be able to accurately solve the response during an specific time sequence. The simplified equation of motion that should solved is:

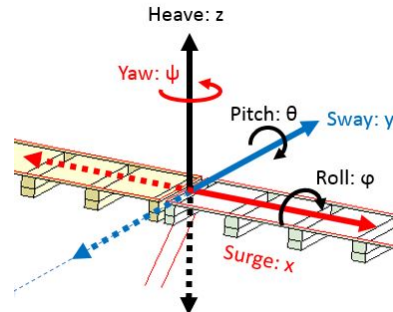


Figure 5.7: Six-degree-of-freedom system for the Tidal Bridge

$$[M + M_a(\omega)]\ddot{\mathbf{x}} + \mathbf{X}\dot{\mathbf{x}}(\omega) + \mathbf{K}\mathbf{x} = \mathbf{F}_i(\omega) + \mathbf{F}_d(\omega) \tag{5.15}$$

Where:

$$\mathbf{x} = \begin{Bmatrix} x(x, t) \\ y(x, t) \\ z(x, t) \\ \varphi(x, t) \\ \theta(x, t) \\ \psi(x, t) \end{Bmatrix} = \begin{Bmatrix} \text{Surge} \\ \text{Sway} \\ \text{Heave} \\ \text{Roll} \\ \text{Pitch} \\ \text{Yaw} \end{Bmatrix} \tag{5.16}$$

The **natural frequencies** are obtained and the eigenperiods of the most significant modes are found and given in Table 5.4. The 100 m long floating elements are most sensitive to **wind-generated ocean waves**. The eigenperiods can be influenced by adjusting the stiffness and damping.

Mode	Axis		Hydrostatic stiffness		Frequency [Hz]	Period [s]
Heave	z	k_z	7 518 758	[N/m]	0,287	3,49
Roll	x	k_φ	607 767 558	[Nm/rad]	0,268	3,73
Pitch	y	k_θ	7 299 345 191	[Nm/rad]	0,327	3,06

Table 5.4: Hydrostatics computed with Mathcad

A first indication of the magnitude of roll-rotation is calculated with the hydrostatic stiffnesses in Matrixframe. One 100 metre long floater connected to two mooring pendulums is defined in Matrixframe. The body is supported by springs with the magnitude of the hydrostatic stiffness and an increased heave stiffness. An increased value of the heave stiffness is considered to limit the vertical displacement, the value is substantiated as it is based upon the floater area. The calculations suggest a roll-rotation of 6,74 degrees induced by the maximum drag force. The rotation is of the same magnitude for a positive and negative current.

Combined with the analyses of the previous chapters the system the subquestion "What data is required to compute the likely motion of the Palmerah Tidal Bridge?" can be answered. The next stage of the research is to implement all gathered information into one model and to indicate the sensitivity of the loads to the dynamic response of the bridge.

III

Motion analysis

The third part elaborates on the theory, implementation and restrictions regarding the virtual model. The sensitivity of the floating bridge to wave, current and traffic induced pressures is analysed. Critical load combinations are subjected to the bridge and the amount of motion and acceleration is found. With the results of the sensitivity study design improvements that may increase the stability are proposed. An overview of the part is presented in Figure 5.8.

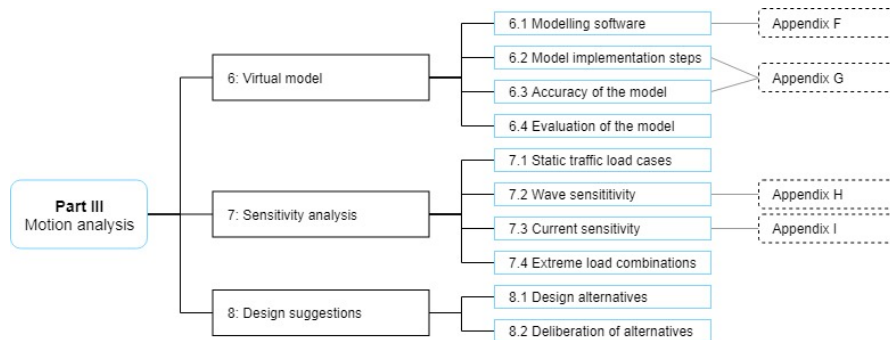


Figure 5.8: Part outline with corresponding sections

6

Virtual model of the Tidal Bridge

This chapter elaborates upon the question "How can the Tidal Bridge be implemented in a virtual model?". The modelling software is selected and the virtual bridge is defined. The accuracy of the model is discussed and the implementation of hydraulic loads is described.

6.1. Modelling software

Ansys Aqwa, a software product of *Ansys Inc.*, is recommended for hydrodynamic assessments of all types of marine and offshore structures (Ansys Inc., 2012b). The software product consists out of two coupled packages: *Ansys Aqwa Diffraction* and *Ansys Aqwa Suite*. The Aqwa software determines the effect of wind, wave and current on offshore and marine structures. A short description of the applicability of the software for respectively the first and the second package is quoted out of the 'Theory Manual of Ansys Aqwa' (Ansys Inc., 2015). Convenient features for the research are coloured within the quotation.

"Aqwa can simulate linearized hydrodynamic fluid wave loading on floating or fixed rigid bodies. This is accomplished by employing three-dimensional radiation/diffraction theory and/or Morison's equation in regular waves in the frequency domain. Aqwa can estimate the equilibrium characteristics and static and dynamic stability of coupled (by moorings and connectors) bodies under steady state environmental loads e.g. wind, wave drift and current.

Aqwa can perform frequency domain statistical analysis of the coupled or uncoupled responses of floating bodies while operating in irregular waves. The linearized drag due to Morison elements (tube,disc), wind and dynamic cables can also be simulated in Aqwa.

The real-time motion of a floating body or bodies while operating in regular or irregular waves can be simulated, in which nonlinear Froude-Krylov and hydrostatic forces are estimated under instantaneous incident wave surface. Additionally, the real-time motion of a floating body or bodies while operating in multi-directional or unidirectional irregular waves can be simulated under first- and second-order wave excitations. Wind and current loading can also be applied to the bodies, as well as external forces at each time step imported or defined by a user-written dynamic-link library. If more than one body is being studied, coupling effects between bodies can be simulated. The convolution approach is used to account for the memory effect of the radiation force."

- Ansys Inc. (2015)

The quotation indicates the suitability of the modelling software for the computation of the dynamic response of the Tidal Bridge. A floating, connected system, including mooring components and characteristics such as mass, stiffness and damping, can be exposed to multiple types of waves and current induced pressure.

Nevertheless, the software has incapacibilities and inaccuracies. Deformations in the structure are not accounted for. Aqwa considers the geometry as empty thin-walled infinitely stiff shells, while in reality all components will experience forms of deformation. In addition, Ansys Aqwa is mostly used to calculate the dynamic response to waves and the software is not specifically designed to compute accurate reactions induced by flow speeds. The drag forces are solely computed for 'tube-shaped' elements, for differently shaped elements drag forces should be defined manually. Vortex-induced vibrations induced by the flow are not implemented in the software and should be modelled as external forces on the system (Ansys Inc., 2015).

The scope of the project is limited to the computation of the motion of the Tidal Bridge to solely current and wave induced pressures. In here, the structural characteristics of the components are not part of the project. The system may be seen as an infinitely stiff system that interacts with external loads. The magnitude of motion induced by waves can be determined correctly with Ansys Aqwa. The dynamic response to high flow speeds is probably not accurate. However, additional options to implement drag forces on non tube-shaped elements are present. Another important reason that substantiates the usage of the Ansys Aqwa software is that BAM and the TU Delft are familiar with the software and a license to the software package is available from the university. Hence, the Ansys Aqwa software package is found suitable to estimate the dynamic response of the Tidal Bridge even though the chance on an inaccurate response to current induced pressures is present.

The theory behind the model software is elaborated in Appendix F. A short overview of the implemented formulas and theory in the software package is listed:

- | | |
|----------------------------------|---|
| • Wave pressures | Potential theory |
| • Fluid potential | Boundary integration approach |
| • Radiation and diffraction | Greene's function, boundary integration approach |
| • Drag on cylindrical components | Morison equation, assuming sufficiently large Reynolds number |
| • Linear waves | Linear wave theory and diffraction forces |
| • First order waves | Froude-Krylov force, wave spectra and diffraction force |
| • Second order waves | Diffraction panels with potential theory |
| • Current | Barltrop and Adams theory |

The main restrictions of the software are stated, the restrictions indicate what results are possible to compute with Ansys Aqwa. Tidal waves can not be implemented in Ansys Aqwa as the wave periods are too long. Aqwa calculates the dynamic response by iterating from the equilibrium position of the structure. During high or low tide, the equilibrium situation changes, inducing "errors".

Linear airy waves are assumed as homogeneous, incompressible and frictionless fluid in an irrotational flow. The flow is expressed by a velocity potential that satisfies the Laplace equation for the boundary conditions, Appendix F. Non-linear second order (Stokes) waves are computed by estimation of the Froude-Krylov force over the instantaneous wetted surface area. The ratio of the amplitude and the wave length indicates the order size of the Taylor polynomial used in the calculations. The Tidal Bridge is located in deep water and thus the Stokes wave order potential consists of first order components only.

Irregular sea spectra are formed on the chosen type of wave spectrum. The wave pattern is created according to linear wave theory. It is possible to define an irregular wave group that consists of multiple individual wave groups acting in multiple directions. Wave spectra that can be selected are the JONSWAP-, Pierson-Moskowitz-, Gaussian- or an User-defined-wave spectrum. Each type of spectrum requires characteristic wave input parameters.

Two types of currents can be defined: an uniform current and a current that varies in magnitude along the depth profile. Ansys Aqwa solely computes the drag force induced by the current on 'tube'-shaped elements and the implementation of the drag force on the submerged bridge areas is analysed in Appendix G.3. The wave and current interaction is complex to compute as all parameters are correlated. Therefore, Ansys Aqwa assumes a constant water depth and a constant current. If an additional wave is defined, the wave propagates on 'top' of the current.

6.2. Model implementation steps

The computer model is constructed in the software package *Ansys v.19 Academic*. The model is created in several steps. Every step is individually explained in Appendix G. In addition, the appendix discusses the validity of the model set-up. An overview of the model steps that are defined is given in Figure 6.1, the two squares indicate the two analysis types within Ansys Aqwa. The Hydrodynamic Diffraction analysis computes the hydrostatic properties in the Frequency Domain and the Hydrodynamic Response analysis determined the dynamic response over a period of time. A list is presented with an overview of the model set-up steps, the italic words indicate the additional programs used.

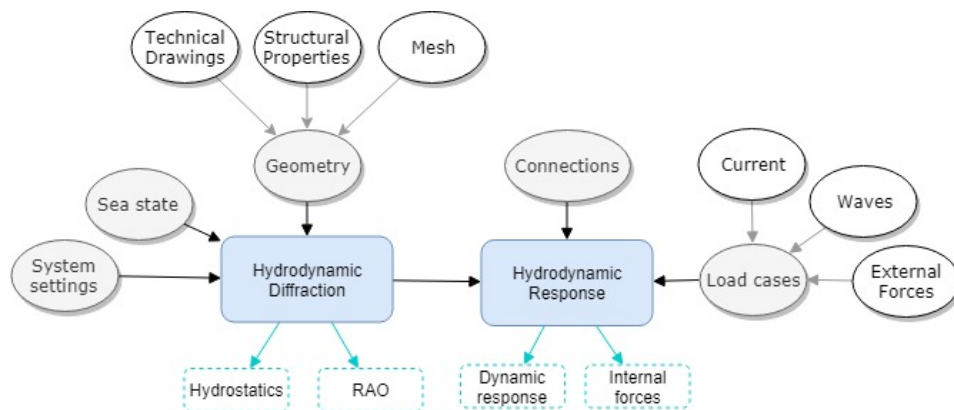


Figure 6.1: Set-up steps of the Tidal Bridge model in Ansys Aqwa

1. Create Hydrodynamic Analysis Systems
2. Attach geometry
 - Create characteristics geometry according to technical drawings in *Design Modeller*
3. Define parts behaviour
 - Implement structural properties (mass, centre of gravity, inertia moments, etc).
 - Properties are calculated with *Excel*, *MathCad*, *Matrixframe*
4. Define connection properties
 - Select hinge types, define attachment points and deactivated some degrees of freedom
5. Mesh
 - Define the panel size, accuracy settings
6. Establish Analysis Settings
 - Set-up the *Hydrodynamic Diffraction* and *Hydrodynamic Response* analysis.
 - Define timestep, load direction, frequencies, etc.
7. Applying Ocean Environment and Forces
 - Select and define characteristics of the sea state and implement the hydraulic loads (*Matlab*).
 - Create database in *Excel*.
8. Solution
 - Select results that should be computed and save and process the results (*Excel*)
9. Redefine and iterate the Analysis settings, Ocean environment and forces and Solutions.

The geometry is constructed in *Design Modeller*. The geometry consists of four identical 100 m elements that float on five pontoons. Six pendulum *tubes* and two spudpole *tubes* are defined with diameters and thicknesses according to the technical drawings. The turbine structure is not attached in the geometry as the diffracting waves will not reach the fully submerged turbines. The influence of the current can solely be computed for 'tube' shaped elements by Ansys Aqwa. If another drag force method is implemented, the force acts on the centre of gravity of the system and the submerged area is not of influence. In addition, the maximum number of bodies within the limited academic version of Ansys Aqwa is exceeded if the turbines are added. The bodies are seen as infinitely stiff empty shells without structural characteristics.

The next step, is to add the mass, centres of gravity, moments of inertia, centre of buoyancy and other characteristics. The characteristics are calculated in chapter 5 and listed in Appendix G. All connection points and fixed points are implemented.

The total system is meshed into small diffracting panels for the Hydrodynamic analyses. The mesh size and tolerances indicate the accuracy of the model, An increase in number of panels results in more accurate results, but also in an increase in computational time. The sensitivity of a high amount of panels to an increase in computational time are compared and a maximum element size of 2 m with tolerances of 0,30 m is chosen. The mesh consists of over 20 000 elements and is proportional to a maximum allowable frequency of 0,436 Hz, elaborated in Appendix G.

At the moment, the bodies are treated by Ansys Aqwa as uncoupled individual floating elements. Within the *Hydrodynamic Diffraction* analysis all four floaters are set to 'interacting floating structures'. The structures are individually floating in their equilibrium state. The *Time Response analysis* operates with the totally connected system. The structures are connected with 'Ball and Socket' hinges that rotate in every degree of freedom. The behaviour of the spudpoles, that allow vertical motion and limited horizontal motion, is expressed by setting the poles to 'free to move' and deactivate all degrees of freedom except the Z and X displacement. Limited X-displacement is realised by connecting the spudpole to a cable with certain stiffness and with an initial elongation. With these steps the base model is established and after designating the Analysis setting the validity of the model is determined. A schematic overview of the model is presented in Figure 6.2. The image shows the characteristic axis system that is implemented in Ansys Aqwa model, the z-axis is upwards directed. The axis system considers waves and currents perpendicular directed to the bridge, under an angle of 90 degrees (from the x-axis), or parallel to the y-axis.

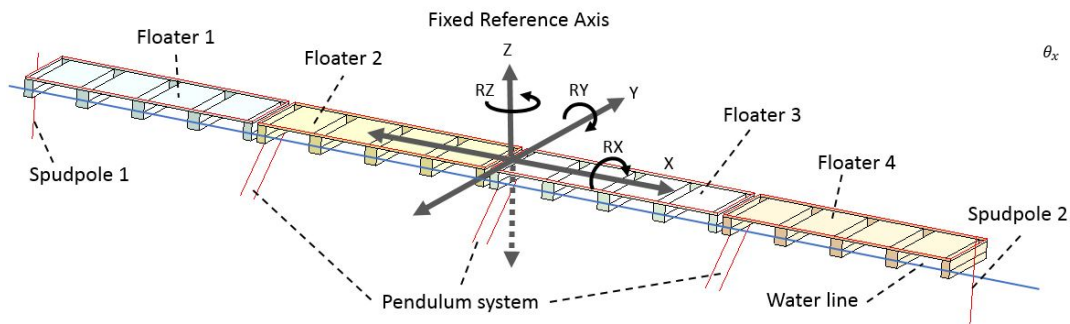


Figure 6.2: Screenshot with geometry and corresponding model characteristics and nomenclature within Ansys Aqwa

6.3. Accuracy of virtual bridge model

Ansys Aqwa is a computer software package with an extensive manual. The model runs only with correctly implemented parameters and data, a small mistake emerges in an abrupt stop of the modelrun. The section discusses the input of parameters and determines the validity of the model. A schematic simplified overview of the set-up of the geometry and corresponding names is presented in Figure 6.3.

The model is validated by defining loads on the system and comparing the results of Ansys Aqwa with the values found in the structural dynamics analysis of Chapter 5. The fundamental check is whether the hydrostatic characters of the main structures are correctly resolved. The *Hydrodynamic Diffraction* analysis computes the hydrostatic properties of every part and calculates the sensitivity of the uncoupled system to the sea spectrum with Response Amplitude Operators (RAO). The RAO shows which combination of wave characteristics (frequency, direction and phase) will probably induce the highest amount of motion.

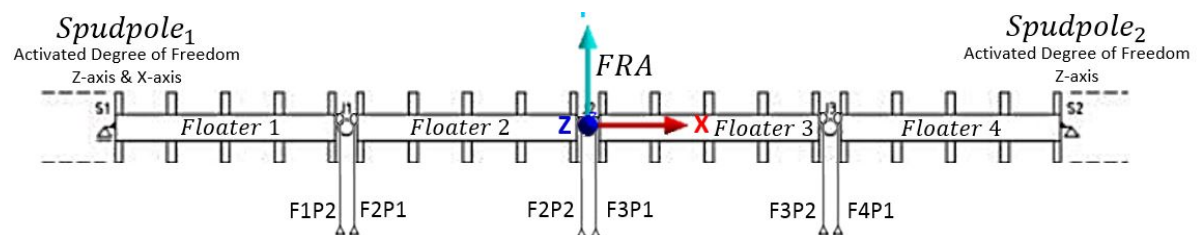


Figure 6.3: Schematic overview of the Tidal Bridge and Ansys Aqwa axis

6.3.1. Hydrostatics of 'floater'

The first check is to determine whether the geometry and structural properties are correctly implemented. Ansys Aqwa bases its computations on the hydrostatics of the floating bodies. Examples of hydrostatic properties are the natural frequencies, the centres of gravity, displaced volumes. In this analysis, the floaters are considered as freely floating bodies in still water in the Frequency Domain. The output of the hydrostatic analysis computed by Aqwa is compared to the calculated values from section E in Table 6.1. The difference between both values is presented as a percentage. All percentages are below 3%, suggesting that the Aqwa geometry model is an accurate approximation of the floating Tidal Bridge bodies. The highest amount of inequality between the calculated and the computed hydrostatics is for the rotation around the x-axis. The difference can be explained by the selected setting that results in 'interacting structure groups'. The influence of diffracted waves between the structures is included in the Hydrostatics calculation, while the calculated structural properties are solely for one individual floater.

			Ansys Aqwa	Calculations	Difference
Centre of Gravity Position	X	(from FRA)	50	50	0,00%
	Y		0	0	0,00%
	Z		3,605	3,605	0,00%
Hydrostatic stiffness	Heave (Z)	[Nm/m]	7 518 763	7 518 758	0,00%
	Roll (RX)	[Nm/rad]	607 664 000	607 767 558	0,02%
	Pitch (RY)	[Nm/rad]	7 129 240 000	7 299 345 191	2,33%
Displaced volume	X-Y-Z plane	[m ³]	2 266,4	2 266,4	0,00%
Centre of Buoyancy	Z		-1,515	-1,52	0,33%
Cut water plane	X-Y plane	[m ²]	748	748	0,00%
Second moments of area	X	[m ⁴]	72 057,3	72 057	0,00%
	Y	[m ⁴]	720 853	737 765	2,29%

Table 6.1: Structural characteristics Aqwa Hydrostatic versus calculations for a 100 meter long floater

6.3.2. Sea spectrum

An accurate indication of the magnitudes of the likely motion requires a wide variety of combinations of wave characteristics. A comparison between 35 directions and 50 possible wave frequencies is defined, resulting in 1 750 possible wave combination. The expected response of the floating structure to a certain sea state, the Response Amplitude Operator (RAO), is computed for every combination. An example of one of the 1 750 combinations is the likely response of the system to an incoming wave with an angle of 80 degrees with a frequency of 0,16 Hz. The range of incoming directions varies between 0 - 350 degrees, computed for every 10 degrees (total 25 directions). If a wave enters in between two directions, for example 83 degrees, Ansys Aqwa iterates the likely response linearly between the known values. A total of 50 possible frequencies is defined. The range of frequencies is determined by the mesh size and linearly distributed between: 0,016 and 0,44 Hz. An increase in frequency results in a decrease in wave length and period. Small period waves will have very limited effect on the dynamic response of the bridge. Therefore, the maximum frequency limit of 0,44 Hz will not influence the research substantially. The concept is illustrated in Figure 6.4 and elaborated in Appendix G. The figure suggests that a significant response for a free floating body will be induced by a wave with a wave length proportional to the width of the bridge, being 34 m.

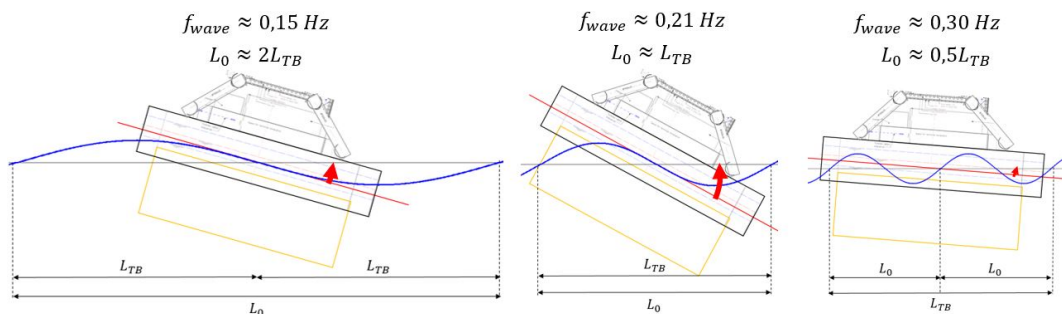


Figure 6.4: Influence of motion induced by waves with respect to the wave length

The RAO for the rotation around the x-axis confirms the suggestion. High motion peaks are visible at a frequency of 0,213 Hz for a perpendicular directed wave, RAO-plot 6.5 which is further elaborated in Appendix G.2. The magnitude of the peak value is 16,23°/m, implying that waves with a wave height of 1 m and a frequency of 0,213 Hz directed perpendicular to the bridge will induce a rotation around the x-axis of 16,23°. The induced rotation exceeds the estimated serviceability limits heavily. However, as stated before, the floater is considered as freely floating on the water surface, not connected to any other element. The likely motion of the connected system is less severe and below the computed RAO value. The influence of the coupled system to the RAO's is discussed in the sensitivity analysis in Chapter 7. A scale model or other data to verify the magnitude of motion is absent, hence the validity of the amount of rotation is not substantiated. Ansys Aqwa is a software package that is globally used by many companies and hence it is assumed that the theory behind the software is correctly implemented.

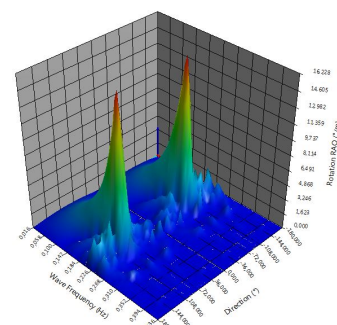


Figure 6.5: Response Amplitude Operator for individual floater with respect to the rotations around the x-axis

The second type of analysis, the *Hydrodynamic Response* is acting in the Time Domain and uses the results of the previous analysis in the Frequency Domain. The sea spectrum is defined over a period of time for irregular waves distributed in according to a JONSWAP wave spectrum. The JONSWAP wave spectrum is a one dimensional frequency sea spectrum often used for young sea states that are generated by winds (Holthuijsen, 2007). If a fully-developed sea state is present, the Pierson-Moskowitz type spectrum is more accurate. The wave characteristics are based on hourly wind data that register the maximum wind speeds that occur every hour. No data is available on the duration of the particular wind gust. Probably, the wind gust will be present during a couple of minutes, suggesting a young sea state. In the analysis an irregular wave is shaped according to the JONSWAP wave spectrum with a duration of one hour. One hour is considered as a conservative duration for the wind wave generation, but a reasonable duration for the development of a JONSWAP wave spectrum. Appendix G.2 shows the wave surface elevation for a wave with the 100 year maximum wave height conditions. The ratio between the significant and the maximum wave height within the one hour wave distribution is approximately 1:2,12 (2,26 : 5,01). A reasonable value according to the distribution of wave heights elaborated in Chapter 4.

6.3.3. Current implementation

A current with an uniform velocity and direction is defined in Ansys Aqwa. Unfortunately, the induced current pressures are solely computed for 'tube' shaped structures with the Morison equation. The tube-shaped elements correspond with the pendulum system and the spudpoles. The main submerged bridge parts are not included in the drag force calculations and Ansys Aqwa let the current flow 'through' the submerged bridge parts. The submerged volume of the floaters and attached turbines is significantly larger than the area of the pendulum and spudpoles. Indicating that the main drag force will be present on the pontoons and the turbines. Three methods are compared to simulate the drag force that is present on the bodies. The methods are elaborated in Appendix G.3 and shortly discussed in the section. The following drag force implementation methods are analysed:

1. Current Force Coefficient Matrix
2. Structure Force Matrix
3. Horizontal Point Forces

The maximum turbine moment around the x-axis is set to 21 MNm/m by the company Tidal Bridge. According to the data and CFD-model of Dynasim, the maximum moment is reached with a current velocity of 5,2 m/s. The scope of the research recognizes the maximum moment as an outer limit. If higher current velocities are present, the magnitude of turbine resistance should be lowered. The Ansys Aqwa model is tested for a maximum current velocity of 5,2 m/s. The drag force that is generated by the current is complex to estimate exactly. The CFD-model is created to check the possible electricity generation of the turbine, is assumed as an accurate estimation of the perpendicular drag force. The influence of the current drag force that arises if the current is aimed under an angle is unknown. The drag force and moment are exponentially dependent on the current magnitude, the relation is presented in Figure 6.6.

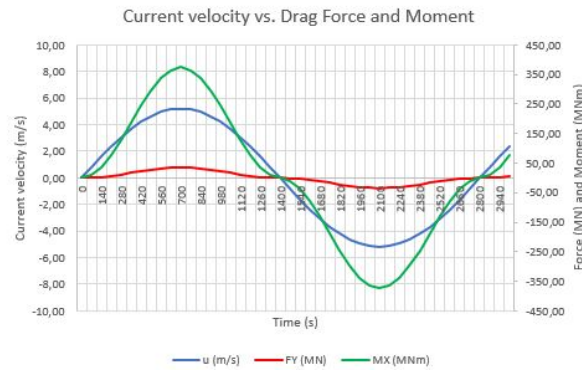


Figure 6.6: Current induced drag force [kN] and moment [kNm] for a perpendicular flow acting on one 100 m long floater

Current Force Coefficient Matrix

The *Current Force Coefficient Matrix* is the only method that computes the drag force according to a defined current velocity and direction. A matrix is implemented with the drag force per unit velocity squared for every degree of freedom over a direction range of 360 degrees, Figure 6.7 and elaborated in Appendix G.3. The drag force that is computed by the matrix is acting on the centre of gravity of the structure and is simplified as a point load. Solely one force is present on one structure, hence the drag force of the combined floater-pontoon system over a length of 100 meters is defined. Ansys Aqwa considers a rotated axis system indicated in Figure 6.8, the drag force that acts perpendicular to the bridge deck is thus the drag force in the Y-direction (F_y), present at an angle of 90 degrees.

$$\begin{array}{c}
 \text{Current Force Coefficient Matrix} \\
 \text{Direction } (^\circ) \quad \begin{array}{c} \text{Force} * u^2 \left(\frac{kN}{m/s^2} \right) \\ \text{Moment} * u^2 \left(\frac{kNm}{m/s^2} \right) \end{array} \\
 \left[\begin{array}{cccccc}
 0^\circ & F_{x,0} & F_{y,0} & F_{z,0} & M_{x,0} & M_{y,0} & M_{z,0} \\
 \vdots & \vdots & \vdots & \vdots & \vdots & \vdots & \vdots \\
 360^\circ & F_{x,360} & F_{y,360} & F_{z,360} & M_{x,360} & M_{y,360} & M_{z,360}
 \end{array} \right]
 \end{array}$$

Figure 6.7: Overview of the implementation matrix of the *Current Force Coefficient Matrix* in Ansys Aqwa

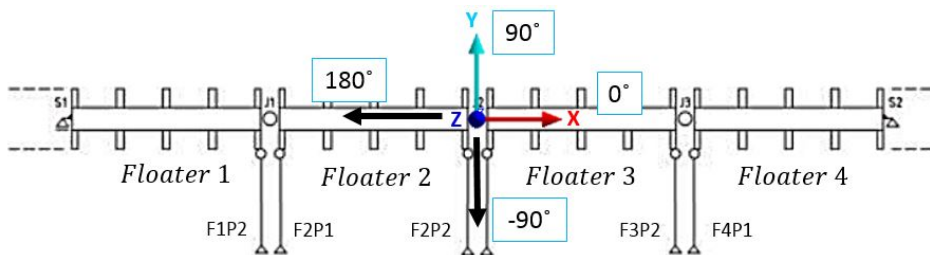


Figure 6.8: Rotated axis system Ansys Aqwa and nomenclature

The model is exposed to a current velocity of 5,2 m/s for a duration of 400 seconds. At $t = 0$ an impulse load is released on the centre of gravity of the system, resulting oscillatory motion that dampens out over time. In reality, the current velocity changes gradually and an impulse reaction is not realistic. The dampened response suggests that the system will rotate approximately 6 degrees around the x-axis. A disadvantage of the method is that only one current velocity can be defined at a time and that the velocity acts instantaneously on the elements. The impulse reaction induces extreme displacements that result in an 'abortion of the solve'. An advantage is the possibility to direct a current along a range of 360 degrees on the horizontal plane. In addition, the influence of the drag force on both the large submerged structures and the mooring system (Morison equation for tube-shaped elements) is combined.

Structure Force Matrix

Second method considered is the *Structure Force Matrix*, as the name suggests, an external force is defined that act on the centre of gravity of a specific structure. The matrix indicates forces and moments that act on the structure at a specific timestep. In between timesteps the force is iterated linearly, see Figure 6.9. The total drag force of a 100 m long element is defined in X, Y and Z direction and the moment is defined accordingly. The main advantage of the method is the dependency on time. The impulse effect that is present with the Current Force Coefficient Matrix is avoided by initiating the run at a current velocity of zero. The current is defined in the form of a sinus function with a maximum amplitude of 5,2 m/s, the corresponding input matrix is analysed in Appendix G.3.

$$\begin{array}{c}
 \text{Structure Force Matrix} \\
 \begin{array}{c}
 \text{Time (s)} \\
 \begin{array}{c}
 \text{Force (kN)} \\
 \text{Moment (kNm)}
 \end{array}
 \end{array}
 \end{array}
 \begin{bmatrix}
 0 & F_{x,0} & F_{y,0} & F_{z,0} & M_{x,0} & M_{y,0} & M_{z,0} \\
 \vdots & \vdots & \vdots & \vdots & \vdots & \vdots & \vdots \\
 t_{max} & F_{x,t_{max}} & F_{y,t_{max}} & F_{z,t_{max}} & M_{x,t_{max}} & M_{y,t_{max}} & M_{z,t_{max}}
 \end{bmatrix}
 \end{array}$$

Figure 6.9: Overview of the implementation matrix of the *Structure Force Matrix*

A problem originates if Ansys Aqwa tries to solve the response of the structure to the force matrix. A negative current velocity induces more extreme rotations and tries to 'flip' the system to the other side. The illustration in Figure 6.10 shows how the system may rotate concerning infinitely stiff pendulums. One spudpole allows motion along the x-axis and allows the system to 'flip' to the other side. Of course, this is not realistic and the displacement of the spudpole is restricted with a cable that acts as a spring. Appendix G.3 analyses the properties of the spudpoles and the rotational effect induced by the negative current velocity. The extreme response is present in every drag implementation method.

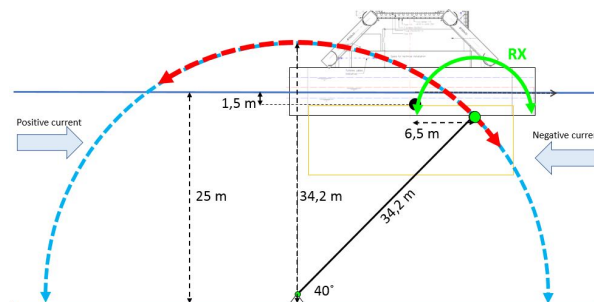


Figure 6.10: Maximum rotation radius of pendulum system

With the inclusion of a cable, Ansys Aqwa is able to finish the run. The response of the system with an additional cable is presented in the plot in Figure 6.12. It is clear that extreme rotations arise if a negative current is present. The rotations are compared to a kite in the air, the coupled floaters will start to 'fly' and catch 'wind' like a kite, see Figure 6.11 and elaborated in the Appendix F. The response is not realistic, the flow potential and mass of the water body through the turbines will have a stabilising effect that secures the system underneath the waterline. The shape of the FishFlow turbine that induces the counteracting effect on the rotation is illustrated in Figure 6.13. The magnitude of the stabilising effect and the sensitivity to rotations of the turbines is unknown and should be determined by model tests or scale tests in future research.

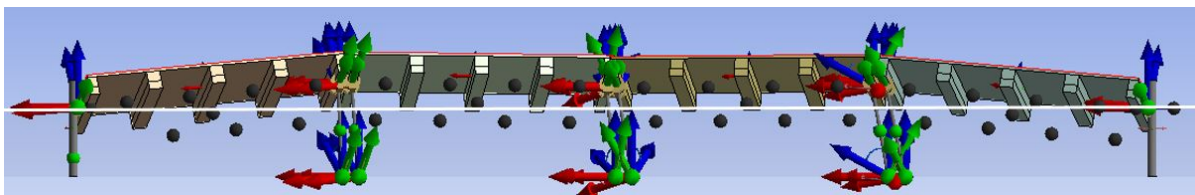


Figure 6.11: Front view of the system at a *negative* flow speed, white line indicates the waterline.

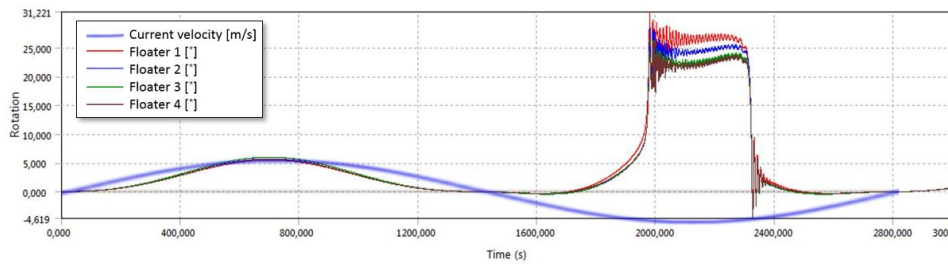


Figure 6.12: Rotation around the X-axis induced by a current velocity of + or - 5,2 m/s

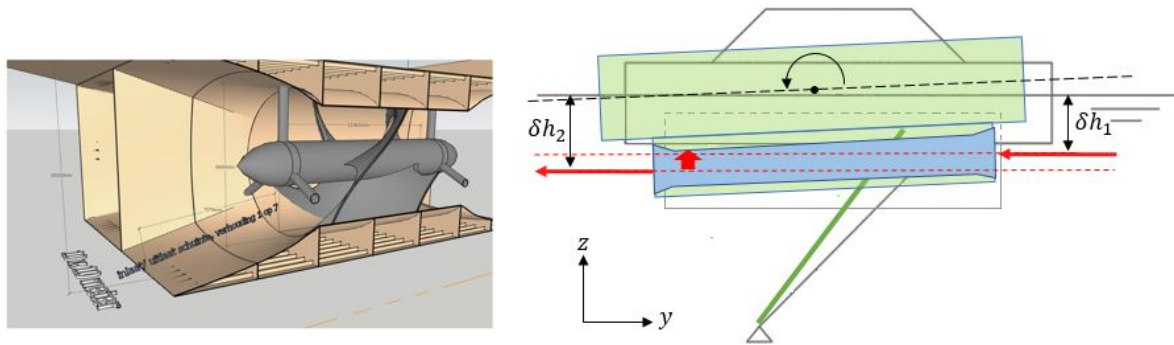


Figure 6.13: Visualisation of the water tunnel through the turbine housing of the FishFlow turbine

The extreme response to a negative current velocity arises for each of the drag implementation methods. This confirms that restriction of displacement along the x-axis is obligatory. The sensitivity analysis elaborates on the best fitting cable type with respect to the induced motion and external forces that are present. The displacement of the spudpole and the elongation of the cables are converted to realistic values and the validity of the system is discussed. The maximum rotation that arises for the *Structure Force Matrix* in a *positive current velocity* is a rotation of 6,00°.

Horizontal Point Forces

Last method to simulate the drag is to apply external point forces on the structure. Point forces are defined at a specific point attached to a structure. If the drag force is converted to a single point force, the force acts at an arm of 7,32 m below the fixed reference axis. A point force is defined between every two pontoons, resulting in four point forces for one 100 m long element. The magnitude of the force is determined for a current velocity of 5,2 m/s for a quarter of the element, $F_{point\ force} = 8\ 558\ kN$. The force acts on the centre of gravity of the structure at a specific arm, the arm and direction of the force for a rotated system may change according to the settings implemented for the force. The force can set to *Constant direction of Force* or *Force moves with structure*. The influence of the both settings is presented in Figure 6.14 and elaborated in Appendix G.3. In addition, the attachment point of the drag force is discussed. The first and highest pressure is present at the front of the turbine, but the combined action point of the water body floating through the turbine is present at approximately the middle of the turbine.

The system is checked for all possible combinations of point forces: applied at the centre or front, a force that is constantly horizontal directed or a force that moves with the structure, or even a combination. The results are discussed in Appendix G.3, the current application at the centre of the turbine results in rotations around the x-axis of approximately 6,06°. If the point force is applied to the front of the turbine, a significant increase in rotation is distinguished. In addition, the point force acts as an impulse load as well. High oscillations arise in the beginning of the time response and dampen out over time.

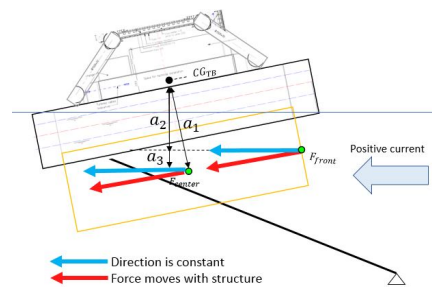


Figure 6.14: Application possibilities and selection options for the Point Forces (not to scale)

Conclusion of the current implementation method

Only one method is considered to indicate the dynamic response due to current induced pressures. An inaccuracy in all methods is the extreme response of the bridge in a negative current. Yet, if a stiff cable is defined, the magnitude of motion is limited and proportional to the rotation calculated in the stability calculation in Chapter 5. This magnitude of roll-rotation is approximately equivalent for every implementation method, between 6 and 7 degrees. Substantiated validation or calibration of the magnitude of rotation is not possible as no actual data or scale model is present.

Every method allows implementation of an oblique drag force. With the *Current Force Coefficients* the current direction can be changed easily. The other two methods require a time-consuming manual input: the drag force is divided into X, Y and Z components. On the other hand, the absence of knowledge on the drag coefficients, especially under an oblique angle, implies non-realistic results. At the moment, the assumptions for the oblique drag values are based upon rescaling a graph of the British Standard of pontoons. The method is not scientific or substantiated in an appropriate manner. Due to the inaccurate estimated values, the research is focused on a perpendicular current direction specifically.

An inaccuracy arises in the time response analysis of methods 1 and 3. In both methods the *current* or *point force* is considered as an instantaneous impulse load at $t=0$ s. This induces an oscillatory response of the system that dampens out over time. The current is varying gradually and the oscillating impulse effect is not realistic. With the *Structure Force Matrix* the force is applied gradual over a period of time, preventing the impulse effects. Therefore, the best suitable method that is used is the *Structure Force Matrix*.

6.3.4. Simulation of mainland connection

A mechanism is created by allowing slight displacement from the mainland connections (the spudpoles). Initially, the x-displacement for one spudpole was defined as unlimited, resulting in the flipping of the floaters and an abrupt abortion of the solve in Ansys Aqwa. In reality the spudpole allows some vertical displacement and limited horizontal displacement (x-direction). This is visualised in Figure 6.15, the green line indicates a possible displacement of the bridge deck and the required x-displacement of the spudpole is denoted with δx .

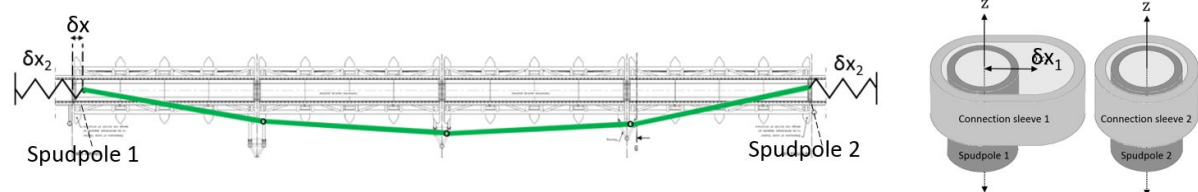


Figure 6.15: Spudpole that allows movement along the x-axis and the actual limited displacement.

Figure left: topview of possible displacement of bridge deck. Figure right: topview of spudpole connections to floaters.

The allowable x-displacement consists of two types of induced displacements: δx_1 and δx_2 . The connection between the spudpole and the floater is not designed yet. The idea is to allow limited initial displacement by creating a 'sleeve' between the spudpole and the connection.

Next to the displacement, a second type of displacement is induced by the bending of the spudpoles. The general outline of the spudpoles is designed in technical drawings, Appendix G.3.3. The spudpole itself is designed as a 25 m long steel pipe with a diameter of 3 m and a thickness of 5 cm. The spudpole has a characteristic bending stiffness that is calculated with *Matrixframe* as 72,55 MN/m. The calculation and *Matrixframe* model is elaborated in Appendix G.3.3. The bending of the spudpoles is simulated in Ansys Aqwa by defining a *linear elastic cable* between a *Fixed Point* and the 'infinitely stiff' spudpole. The stiffness of the cable is proportional to the amount of bending of the actual spudpole and the second order displacement δx_2 . The effect of adjusted spudpole properties is analysed in the sensitivity analysis in Chapter 7.

The maximum rotations that arise in one current cycle with the present spudpole design are $5,96^\circ$ for a positive current velocity and $19,68^\circ$ for a negative current velocity. The system is not accurate for negative flow speeds as the bridge deck is levitated above the water level and 'flies' between the spudpoles, like a kite in the air. The stabilising effect of the water body that flows through the turbine counteracts the upwards effect in reality and secures the bridge at the waterline. Unfortunately, the characteristics of the FishFlow model are unknown and the magnitude of the effect can not be implemented or calibrated.

6.4. Evaluation of the Ansys Aqwa Tidal Bridge model

The dynamic response is computed with a virtual model and is an approximation of the reality, but with an error range. Model validation is required in order to determine the size of the error. In general, a virtual model is compared to scale model tests, other computer software models, many structural and mechanical calculations, and consultations of many engineers and companies. The Tidal Bridge project is still in the pre-feasibility stage and such models and calculations are not conducted yet. Hence, the virtual model can not be calibrated and the error-order size can not be computed.

The main uncertainty is the stabilising effect that is induced by the water body that flows through the turbine at a certain flow speed. The pressures induced by the flow potential are dependent on many variables: the rotation of the turbines, the magnitude of the flow through the turbine housing, the angle of the current and the resistance of the turbines. The stabilising effect of the turbine housing is partly included for a perpendicular current. The drag force is based on the CFD-model computed by Dynasim Engineering to estimate the maximum power generation of the FishFlow turbines. In the model, the turbine is secured in place, not able to move in any degree of freedom. A perpendicular current indicates the relation between flow speed, drag force and pressure distribution, Figure 6.16. In the figure, the moment that is induced by the housing of the turbine is large, approximately 2/3 of the moment induced by the turbines. The turbine is secured in place and the induced rotation is not checked. Therefore, no data is present regarding the pressure distributions of a displaced and rotated system. The counteracting moment induced by the housing is implemented in the drag force calculations. The stabilising effect of the water body through the turbine if the turbine is rotated is not implemented.

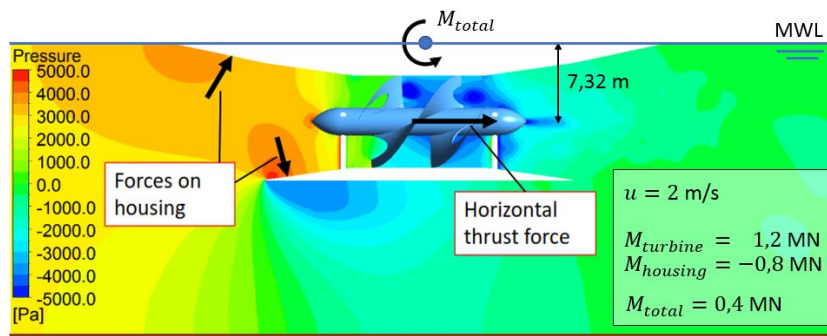


Figure 6.16: Illustration of the CFD-model that indicates the FishFlow pressure distribution with a flow speed of 2 m/s (Dynasim Engineering, 2017)

The Ansys Aqwa model indicates that the rotation around the x-axis will induce the highest rotations and is thus the critical degree of freedom in combination with the displacement in Z-direction that results in 'flying' of the bridge deck above the water level. The unrealistic response is compared to the behaviour of a kite in the air, the floaters turn towards the 'wind' side and will 'fly' in the air. One of the reasons for the model inaccuracy is the application point of the drag forces at the centre of gravity of the body. If the body moves, the force moves accordingly. In reality, the drag force is present solely below the water level and never located 'in the air'.

The likely amount of motion induced by the waves is assumed as correctly implemented. The wave induced motion is extreme if the current approaches zero. The water particles within a wave have no forward speed, indicating the absence of an additional drag force. Waves diffract on the structure parts located around the water level, hence the fully submerged turbines are not included in the wave diffraction analysis. The stabilising effect of the water body through the turbine is absent without a flow speed. This suggests that the previous model inaccuracies are not valid for the likely response of the Tidal Bridge induced by waves.

Summary: Chapter 6: Virtual model of the Tidal Bridge

The chapter is dedicated to the virtual model of the Palmerah Tidal Bridge. The software package that is used to determine the response to current and wave induced pressures is *Ansys Aqwa*. The software is widely used by many companies to compute the motion of offshore and marine structures. The theory behind the Ansys Aqwa software is applicable for the project. Limitations are present in the Ansys Aqwa software regarding the implementation of the tidal current. Nonetheless, the tidal current can be defined manually as an external force. In total, the software package is considered to compute the dynamic response for the Tidal Bridge model.

The validity of the Tidal Bridge model is checked by discussing the input data and set-up properties of the model. After implementation of the geometry and the structural characteristics of the Tidal Bridge, the hydrostatic properties are compared. The characteristic properties, as for example the natural frequencies of the system, are nearly identical when compared to the calculated structural properties and the Hydrostatic properties computed by Ansys Aqwa. Therefore, it is stated that the **geometry is correctly implemented** in the Ansys Aqwa software. The geometry, including the characteristic rotated axis system of Ansys, is presented in Figure 6.17.

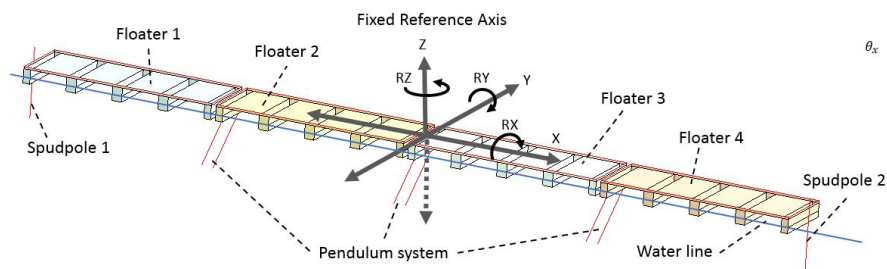


Figure 6.17: Geometry of the Ansys Aqwa model including rotated axis system and nomenclature.

First the **implementation of waves** is elaborated for the *Hydrodynamic Diffraction* analysis in the **Frequency Domain**. In the analysis, the individual structures are considered as freely floating structures not connected to one another. The purpose of the frequency domain analysis is to indicate the likely response of an individual floating element to a certain sea state. The **Response Amplitude Operators** (RAO) define the likely response of the floater to a 1 m wave with specific frequency and direction. The input data of the RAO's consists of 35 possible incoming wave directions (every 10 degrees) combined with 50 possible wave frequencies linearly distributed between 0,016 and 0,44 Hz. The RAO for the likely rotation around the x-axis indicates that **the peak values correspond with the assumed maximum rotation frequency and direction** (Figure 6.18).

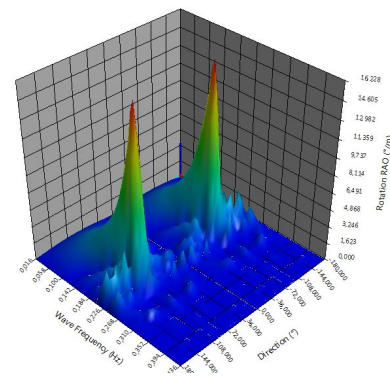


Figure 6.18: Response Amplitude Operator for the rotation around the x-axis

The analysis in the **Time Domain**, the *Hydrodynamic Response Analysis*, requires definition of a wave spectrum. The wave surface elevation for an **irregular wave** during the desired time response computation period is computed according to a **JONSWAP wave spectrum distribution**. The JONSWAP wave spectrum is often used to describe a young sea state with wind generated waves. The duration of the analysis is set to 3 600 seconds (one hour) as the wave data is computed on hourly wind data. The maximum wind speeds during one hour will not be present during the whole hour but only a fraction of the time. Within the 3 600 seconds, the ratio between the significant and maximum wave height is approximately 1:2,12. In addition, the effect of the shape of a **second order Stokes wave**, a steeper and narrower crest, is checked by defining a **regular wave** with a constant frequency and wave height.

Summary: Chapter 6: Virtual model of the Tidal Bridge

Secondly, the implementation method for the **current induced pressures** is elaborated. The **drag force 'tube'-shaped elements are automatically computed according to the Morison equation** for defined current magnitudes. The combined **turbine-pontoon structure** experiences major drag forces that should be defined manually. Three implementation methods are compared and discussed: The Current Force Coefficient Matrix, The Structure Force Matrix and Horizontal Point Forces. The best suiting implementation method is the **Structure Force Matrix**. The method allows time-dependent varying forces, hence the tidal current cycle can be analysed, as seen in Figure 6.19. The other two methods consider the current forces as constant instantaneously loads, that induce high oscillations that dampen over time until the equilibrium state is reached.

$$\begin{array}{c}
 \text{Structure Force Matrix} \\
 \begin{array}{c}
 \text{Time (s)} \quad \begin{array}{c} \text{Force (kN)} \\ \text{Moment (kNm)} \end{array} \\
 \left[\begin{array}{ccccccc}
 0 & F_{x,0} & F_{y,0} & F_{z,0} & M_{x,0} & M_{y,0} & M_{z,0} \\
 \vdots & \vdots & \vdots & \vdots & \vdots & \vdots & \vdots \\
 t_{max} & F_{x,t_{max}} & F_{y,t_{max}} & F_{z,t_{max}} & M_{x,t_{max}} & M_{y,t_{max}} & M_{z,t_{max}}
 \end{array} \right]
 \end{array}
 \end{array}$$

Figure 6.19: Input format for the *Structure Force Matrix*, the method that is used to implement the drag force

The **negative current velocities induce very unlikely behaviour of the system**. The combination of the pendulum and the force that acts at the centre of gravity of the system (instead of a constant depth), levitate the bridge above the water level and let the bridge **'fly like a kite'**, Figure 6.20. **In reality the water body that flows through the turbines secures the turbine beneath the water level.**

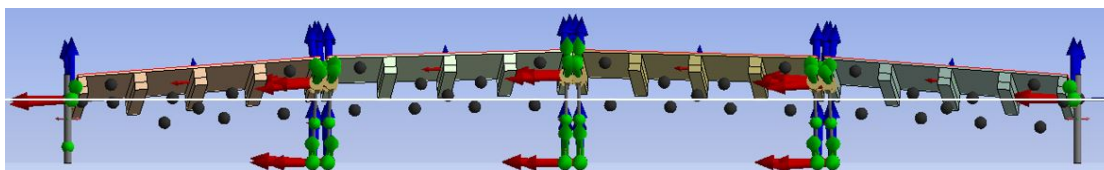


Figure 6.20: Screenshot of maximum bridge displacement, white line indicates water level

The bridge is able to behave as a mechanism through the properties of the **spudpoles**. Next to vertical motion, limited horizontal motion is present. **The horizontal motion consists of two components: initial motion possible from the connection sleeve between the spudpole and the floater and second order motion due to the bending of the steel spudpole frame.** The bending stiffness of the spudpoles is calculated in the software *Matrixframe* with the technical drawings of the spudpole. With the results of the *Matrixframe* computation, the stiffness of 72,55 MN/m is found. Ansys Aqwa considers all bodies as infinitely stiff and therefore the bending is defined in Ansys Aqwa with a **cable**. For both spudpoles a cable is defined with characteristic properties. The sensitivity study elaborates on the dynamic response for an increase in cable stiffness and a range of initial displacements along the x-axis.

In the end the subquestion that is elaborated in the Chapter: *"How can the Tidal Bridge be implemented in a virtual model?"* is answered. The modelling software **Ansys Aqwa is partly suitable** for an estimation of the likely motion of the Tidal Bridge. The Ansys Aqwa model computes a reasonable approximation of the induced motion with respect to wave induced pressures. **The validity concerning the likely response induced by a certain (negative) current velocity is questionable.** The influence of the spudpole properties on the response will discuss whether the response of the Tidal Bridge is indicated for a negative current velocity. The absence of knowledge of the response of the system eliminates the possibility to calibrate the model or to indicate the error order size.

Sensitivity analysis

The scope of the research is set to wave and current induced pressures on the Tidal Bridge structure *after* construction. Failure during construction, transport or assembling stage of the project is not considered. In addition, the structural properties of the construction materials and components are assumed as infinitely strong and stiff. The failure of a connection or the amount of buckling of a pendulum is not calculated. In the sensitivity analysis, the influence of multiple individual load cases is analysed. With this information the most extreme load combinations that may occur simultaneously are found. The load combinations can exist of the waves, currents and static traffic forces.

The sensitivity analysis is conducted in order to find the vulnerable elements of the Tidal Bridge announced in subquestion 3b: "*What is the dynamic response of the Tidal Bridge and what loads induce governing motion?*". First, the influence of traffic loads is analysed, followed with the determination of the critical sea spectrum and the likely motion induced by current pressures.

7.1. Static traffic load cases

Three traffic cases are considered in the sensitivity analysis, the traffic cases are elaborated in Chapter 4. The influence of the point loads is checked on the equilibrium situation, when the coupled bridge is floating in water without wave or current loads. The first two cases are based upon a traffic jam that will be present on parts of the bridge, illustrated in Figure 7.2 with the red and blue load combinations. Case 1 and 2 induce a slope on the bridge deck corresponding to a rotation around the y-axis, Figure 7.1. The third critical traffic case is when solely one side of the road is occupied with vehicles. The bridge will tilt to the side at which the traffic is located and induce rotation around the x-axis, case 3.

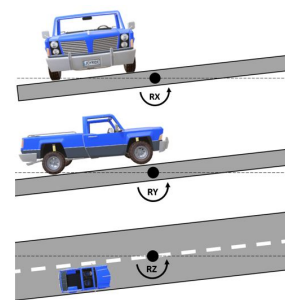


Figure 7.1: Illustration of the rotational axis with respect to the driving comfort of a vehicle

- Case 1 Maximum rotation around the y-axis: Point forces of 5 700 kN acting at points 2 and 4, *red* traffic distribution in the figure.
- Case 2 Maximum rotation around the y-axis: Point forces of 2 705 kN acting on points 1 and 5, *blue* traffic distribution in the figure.
- Case 3 Maximum rotation around the x-axis: The eccentric point load, 3 825 kN, (equation D.4) with an eccentricity of 2,60 m acting in the middle of each floater.

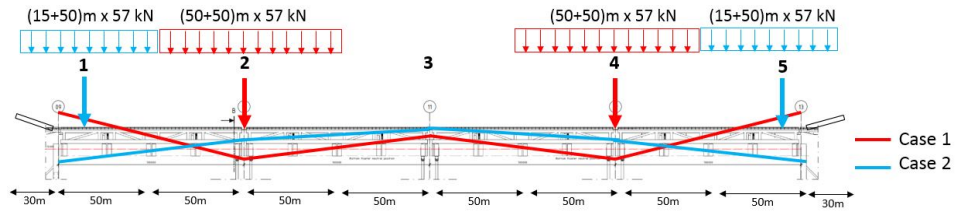


Figure 7.2: Traffic attachment points (not to scale)

The response of the bridge with respect to the traffic cases is presented in Figures 7.3 to 7.6. The measure points are located at the centre of gravity of the floaters, in the middle of a 100 m long element. The first plot in Figure 7.3 indicates the rotation around the x-axis. Immediately it is seen that the governing rotation is at the third load case with the eccentric point load. The peak value is a rotation of approximately 1 degree, which is still within the estimated serviceability limits, Table 7.1.

	Z-displ. [m]	Rot. x-axis [°]	Rot. y-axis [°]	Rot. z-axis [°]
Serviceability limits	-	2,52	2,01	3,44
Case 1	0,44	0,06	1,12	0,91
Case 2	0,46	0,10	0,73	0,11
Case 3	0,56	1,00	0,07	0,16

Table 7.1: Maximum rotations induced by traffic load cases

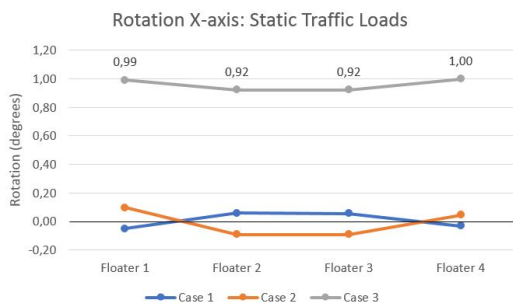


Figure 7.3: Rotations around X-axis induced by traffic load cases

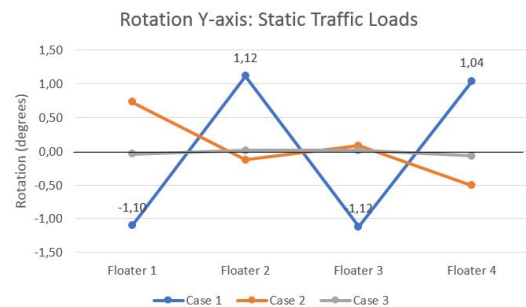


Figure 7.4: Rotations around Y-axis induced by traffic load cases

The rotation around the y-axis is indicated in the second plot, Figure 7.4. The conducted rotations correspond with the probable rotations that are illustrated in Figure 7.2. The rotation around the y-axis for the first traffic load case is governing with peak values of 1,12 degrees for the centre pontoons. The angle of the rotation between the two floaters is the sum of two adjacent values, equivalent with $1,12+1,12=2,24^\circ$. The rotation around the z-axis (Figure 7.5) is induced by the pendulum system as a result of the increase in draught and is related to the vertical displacement (Figure 7.6). The displacement is measured from the centre point of the floaters, which explains why the shape of the graph is not corresponding to the illustrated z-displacement.

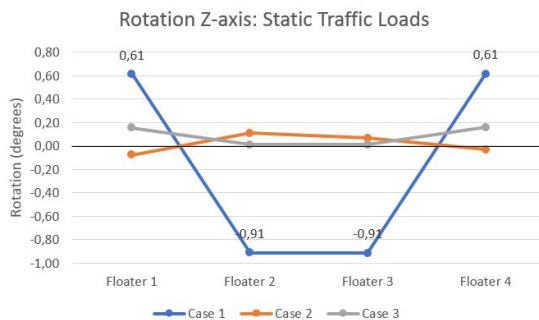


Figure 7.5: Rotations around Z-axis induced by traffic load cases

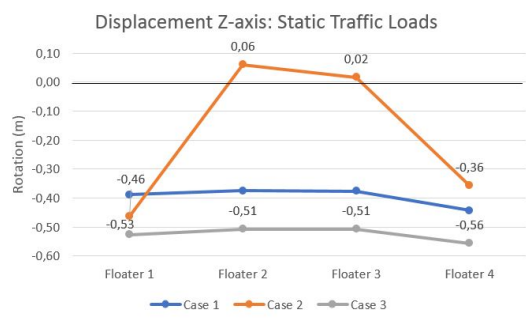


Figure 7.6: Displacement along Z-axis induced by traffic load cases

The governing extreme traffic load case depends on the combination of loads. When high roll rotation is present, then the eccentric traffic distribution is governing. The other two rotational degrees of freedom suggest high motion for the first traffic load case. The second load case is extreme with respect to the vertical displacement. Depending on the foundings in the sensitivity studies, the extreme load case is determined.

7.2. Wave sensitivity

The system is checked for the likely response to a variety of waves. First, the likely behaviour of the floaters is analysed in the Frequency Domain with Response Amplitude Operators (RAO). And secondly, the coupled system is subjected to a wave spectrum over a certain period in time. The most critical wave properties are indicated and suggestions that may improve the stability of the system will form the conclusion. The chapter is supported with additional graphs, calculations and information in Appendix G.2. The degrees of freedom over which the system will move are illustrated in the Tidal Bridge axis system in Figure 7.7.

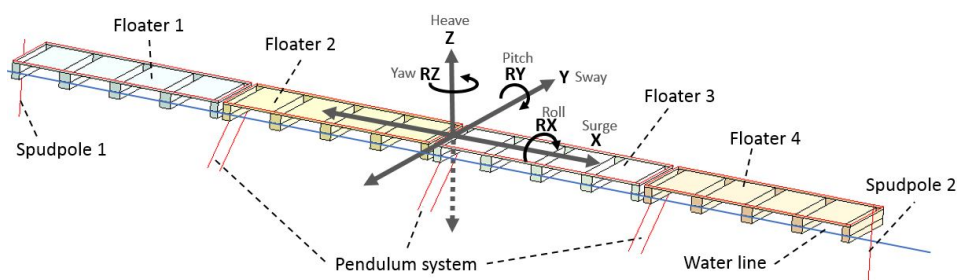


Figure 7.7: Geometry, nomenclature and axis system Ansys Aqwa

7.2.1. Response amplitude operators of individual floaters

The hydrostatics of the likely behaviour of a single floating structure of 100 m indicate what force magnitude induces what rotations or displacements. The governing degrees of freedom are the vertical heave displacement, the roll rotation and the pitch rotation. The natural frequencies in the governing degrees of freedom are listed and calculated in Chapter 5. The frequencies are equal to the hydrostatic properties computed by Ansys Aqwa. The hydrostatic stiffness is listed.

- Heave: 7,52 MN/m
- Roll: 10,61 MNm/°
- Pitch: 124,43 MNm/°

The hydrostatic properties are calculated for the equilibrium position of an individual body that is freely floating in water, no additional loads or forces are present. The characteristic values of the hydrostatic stiffness suggest that heave and roll will likely induce a higher magnitude of motion than pitch. The waves are governing in Y-direction, perpendicular to the bridge axis, resulting in roll rotation and vertical displacement.

The likely motion of the freely floating Tidal Bridge floaters to a certain sea state is analysed with *Response Amplitude Operators* (RAO) in the Ansys Aqwa Hydrodynamic Diffraction model. The RAO indicates a ratio between the wave amplitude and the reaction amplitude of the structure, equation 7.1 (British Standards Institution, 1989). A variety of regular waves is exposed to the floaters and the likely response is presented in a three-dimensional plot. The sea spectrum consists of 1 750 wave combinations, 50 frequencies and 35 directions, elaborated in Chapter 6. The RAO's for the three governing degrees of freedom are presented in Figures 7.8 to 7.10, all RAO's are elaborated and discussed in Appendix H.2. The likely motion of the uncoupled floating structure indicates the motional sensitivity to a certain regular wave.

$$RAO = \frac{\text{amplitude of motion of structure}}{\text{amplitude of wave motion}} \quad (7.1)$$

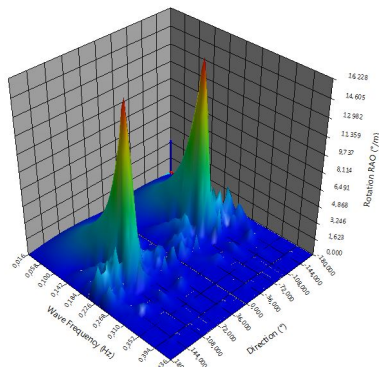


Figure 7.8: RAO for the rotations around the x-axis

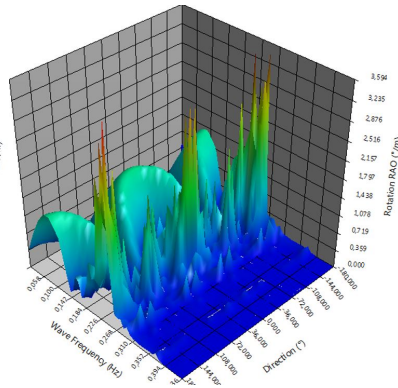


Figure 7.9: RAO for the rotations around the y-axis

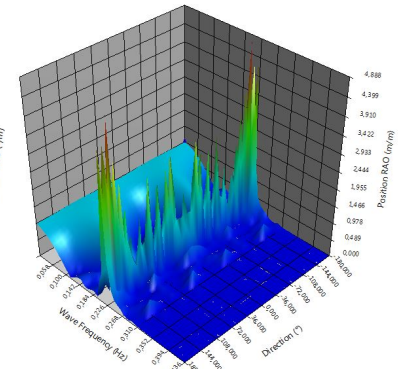


Figure 7.10: RAO for the displacement along the z-axis

The peak values and corresponding properties of the RAO's of the freely floating floaters in all degrees of freedom are given in Table 7.11. The magnitude of motion is significantly higher for the rotation around the x-axis than for the other degrees of freedom. In addition, peaks are distinguished at low frequencies or frequencies in the range of the natural frequency of the bridge. The likely motion for high frequencies (small period) waves is limited due to the short wave lengths.

	Directions [°]	Frequencies [Hz]	Value RAO	
X	180, 0, -180	0,016	6,076	[m/m]
Y	90,-90	0,016	6,262	[m/m]
Z	160, -160	0,222	4,888	[m/m]
RX	90, -90	0,213	16,228	[° / m]
RY	160, 0, -160	0,230	3,594	[° / m]
RZ	100, -100	0,255	1,553	[° / m]

Figure 7.11: Peak values of the RAO with respect to motion or rotation

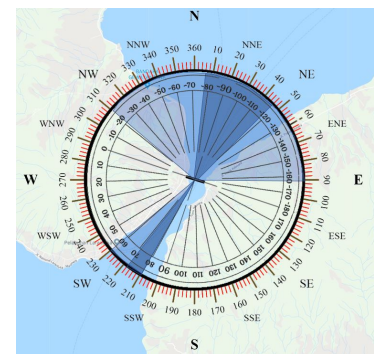


Figure 7.12: Rotated axis system Ansys Aqwa versus topography angle and governing wave directions

According to the estimated wave properties in Chapter 3, the smallest wave frequency that may be present within 100 years in the Strait of Larantuka is 0,14 Hz. Waves may enter with an maximum angle of 45 degrees perpendicular to the bridge deck. The axis system in Ansys Aqwa is rotated, Figure 7.13, and corresponding to the inner direction rose in Figure 7.12. The bridge has a symmetrical design and the likely motion is identical along the symmetry-axis. For example, waves are directed perpendicular to the bridge at 90°, if the waves vary with an angle of 10°, being 80° or 100°, the induced motion is equivalent. Concerning the information, the likely motion for five direction couples is computed and presented in Table 7.2.

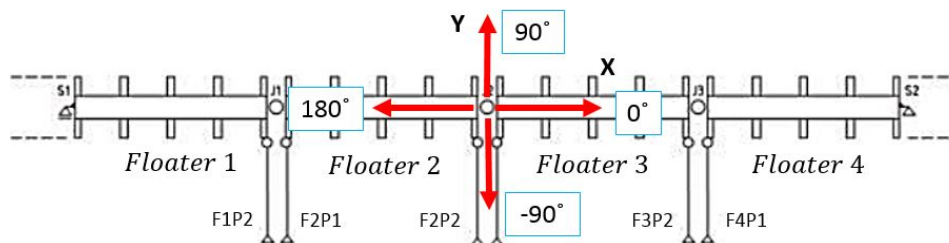


Figure 7.13: Schematic overview of directions in Ansys Aqwa

Direction	X [m/m]	f_{peak} [Hz]	Y [m/m]	f_{peak} [Hz]	Z [m/m]	f_{peak} [Hz]	RX [°/m]	f_{peak} [Hz]	RY [°/m]	f_{peak} [Hz]	RZ [°/m]	f_{peak} [Hz]
90°	0,23	0,25	0,58	0,14	1,13	0,22	16,23	0,21	2,08	0,25	0,58	0,25
80 & 100°	0,16	0,22	0,53	0,14	2,85	0,22	11,17	0,21	1,37	0,22	0,54	0,25
70 & 110°	0,10	0,14	0,38	0,14	0,61	0,22	2,97	0,15	0,96	0,15	0,62	0,14
60 & 120°	0,18	0,37	0,21	0,14	2,58	0,22	2,04	0,20	1,54	0,22	0,71	0,14
50 & 130°	0,18	0,28	0,07	0,14	0,96	0,22	1,62	0,19	1,57	0,21	0,63	0,14

Table 7.2: Maximum motion response for Range of direction in between 0,14 - 0,43 Hz. Highest value of direction couple is provided.

The governing motion values per degree of freedom are coloured and are primarily present at the direction of 90°. The Response Amplitude Operator for the direction of 90° and for every degree of freedom is plotted in Figure 7.14, a zoomed version is presented in Figure 7.15. Appendix H.2 shows and elaborates on the RAO's for each direction couple. The left vertical axis corresponds to the displacement in [m/m] and the right vertical axis with rotation in [°/m]. It is clear in the plot that Y-displacement and rotation around the x-axis are governing. The majority of peak values is in the frequency range of 0,21 to 0,27 Hz, proportional to a wave length that is in the order of the width of the bridge (34 m).

The relation between a perpendicular wave and an oblique wave is presented for the two governing rotational RAO's degrees of freedom in Figures 7.16 and 7.17. The magnitude of motion decreases significantly for oblique waves. Further, the peak frequencies of both degrees of freedom tend to shift towards lower frequencies.

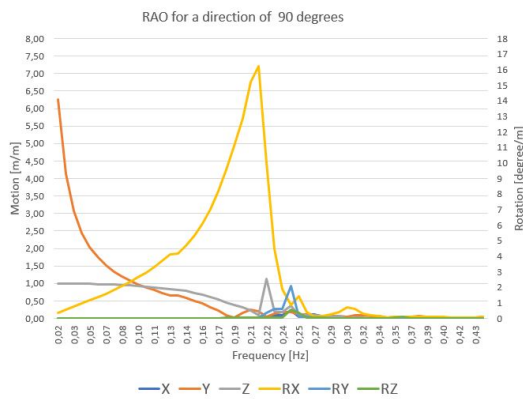


Figure 7.14: RAO for direction of 90° in six degrees of freedom

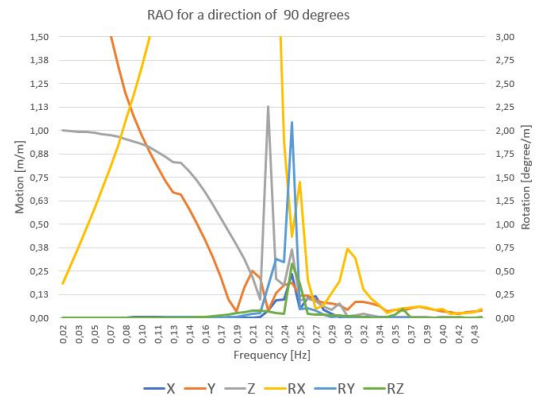


Figure 7.15: RAO for direction of 90°. Rescaled vertical axis.

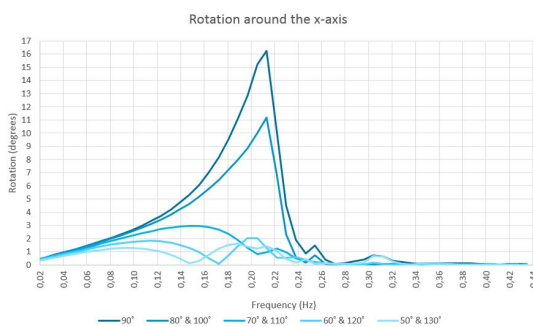


Figure 7.16: RAO: Rotation around the x-axis for sequence of incoming flow angles

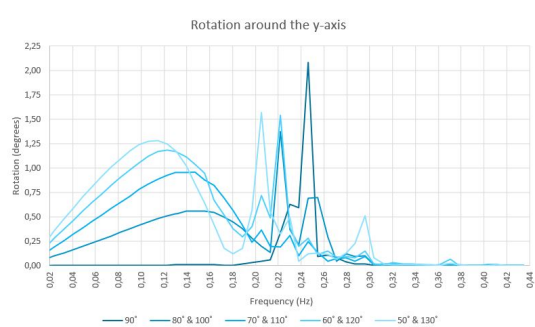


Figure 7.17: RAO: Rotation around the y-axis for sequence of incoming flow angles

The RAO-based response of the freely floating floaters alters compared to the actual likely response of the connected bridge system. The mooring system retains the bridge at a specific position and motion is restricted by hinges. The behaviour of all structures is correlated instead of solely depending on its own floating characteristics. The RAO-plots suggest that the critical waves are perpendicular directed in a frequency range of 0,21 to 0,27 Hz.

The likely motion of the coupled system is determined in the *Time Response Analysis*. The amount of damping that is induced by the mooring system is compared to the RAO situation that is based on freely floating floaters. First, the effect is checked for a second order Stokes wave with a wave height of 1 m and a frequency of 0,21 Hz. The mooring system manipulates the RAO-based motion and dampens the magnitude of motion with a factor 2,5 for the rotation around the x-axis, Figure 7.18.

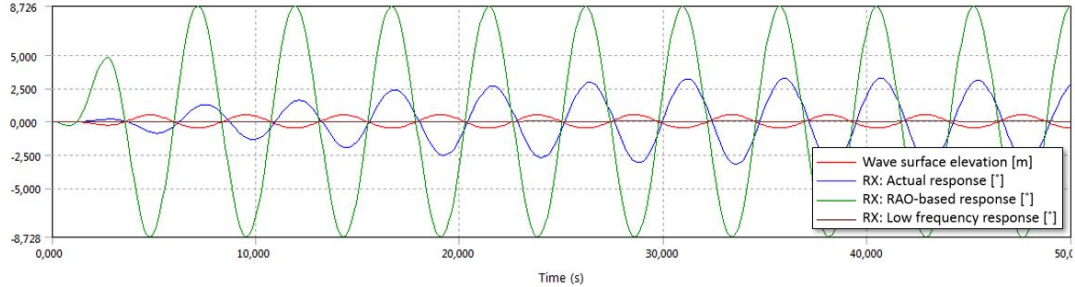


Figure 7.18: Relation between wave surface elevation and rotation around the x-axis
(Freely floating RAO-based response of individual floater vs. response of the fully connected bridge)

Displacement of the bridge will not cause sincere discomfort, but accelerations of the deck do. Hence, the maximum accelerations that are induced by the Stokes waves are calculated and compared to the estimated serviceability limits of Chapter 3 in Table 7.3. According to the estimated serviceability limits and the model outcome, three limits are exceeded. The exceedance of the vertical displacement (heave) will not have large negative effect on the decrease of comfort when driving over the bridge. Nonetheless, the acceleration along the z-axis and the rotation around the x-axis will effect driving comfort significantly. In reality, a *regular* wave will not develop in the sea. Irregular wave groups pass by the bridge and generate an irregular dynamic bridge response. Hence, the effect on the actual response for *irregular* waves with critical frequencies and directions is analysed.

	Surge		Sway		Heave		Roll		Pitch		Yaw	
	Along x-axis [m]	[m/s ²]	Along y-axis [m]	[m/s ²]	Along z-axis [m]	[m/s ²]	Around x-axis [rad]	[rad/s ²]	Around y-axis [rad]	[rad/s ²]	Around z-axis [rad]	[rad/s ²]
Tidal Bridge (rad)	-	0,5	0,5	0,5	0,5	0,7	0,044	0,107	0,035	0,07	0,06	0,05
(degrees)	-	0,5	0,5	0,5	0,5	0,7	2,521	6,131	2,005	4,01	3,44	2,86
Response minima	-0,032	-0,078	-0,198	-0,343	-0,780	-1,159	-3,268	-5,577	-0,566	-1,065	-0,073	-0,119
Response maxima	0,048	0,057	0,188	0,315	0,629	1,253	3,297	5,941	0,692	1,056	0,089	0,183

Table 7.3: Overview of estimated serviceability limits Tidal Bridge and the actual displacement that arises if a 1 meter wave perpendicular to the bridge deck is present

7.2.2. Irregular waves

An irregular wave group represents a better estimation of the actual sea spectrum. 28 Combinations of wave properties are defined in the Ansys Aqwa Hydrodynamic Response analysis. All waves have significant wave heights of 1 m and the surface elevation is computed according to a JONSWAP wave spectrum. The varying properties are the direction and the wave frequency. An overview of the implemented frequencies and directions is given in Table 7.4. The nomenclature used in the report and an illustration of the incoming directions is presented in Figure 7.19.

RAO frequencies (f)	0,14, 0,21, 0,22 and 0,25 Hz
Natural frequencies (f_n)	0,287 (Z), 0,268 (RX), 0,327 (RY)
Direction (α)	90, -90, 100 and -100°

Table 7.4: Input parameters for the irregular JONSWAP distributed waves

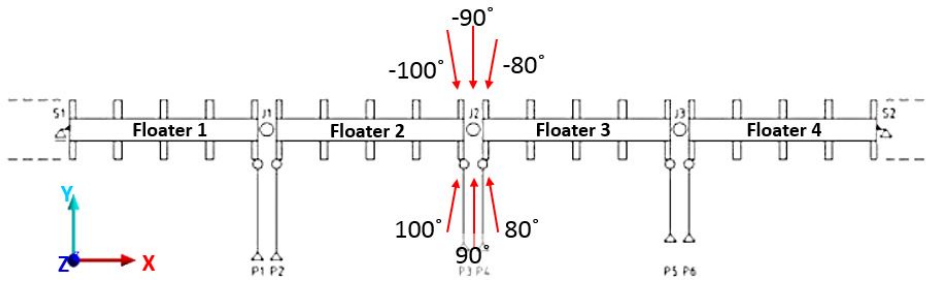


Figure 7.19: Overview of the implemented wave parameters in Ansys Aqwa

The maximum rotations that arise in the response of the fully connected system are plotted for every floater and compared with the RAO-estimated response of freely floating individual floaters in Appendix H.3. The plot for the rotation around the x-axis for the actual coupled system response and the individual RAO-based response is given in Figure 7.20. First observation, is the shift of the peak values to low wave frequencies instead of the natural frequencies of the freely floating system. This suggests that the natural frequencies of the floaters are influenced by the mooring system, a favourable adjustment as low frequency waves do not arise often. According to the wave analysis, the smallest wave frequency that arises within 100 years is 0,14 Hz.

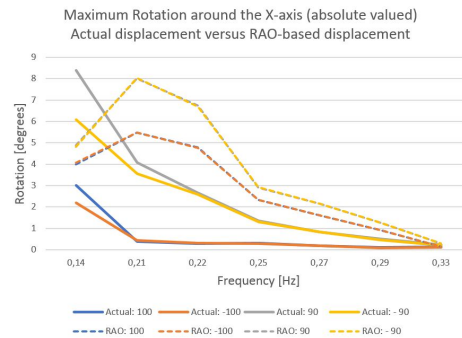


Figure 7.20: Rotation around the X-axis. Actual rotation of the fully coupled system versus individual freely floating RAO-based rotation of the floaters

Second observation is the identical behaviour of floater couples 1 & 4 and the centre two pontoons 2 & 3 as a result of symmetry. The rotation per frequency and direction is plotted per floater couple and visualised in Figures 7.21 to 7.23. The figures indicate that the response of the system is equivalent for the positive and negative wave directions, this is contrary with the actual motion computation. The rotations around the x-axis are 2,5° smaller for a *negative* wave direction. The likely rotation for an oblique wave of 100° is minor to the perpendicularly directed waves.

The sensitivity with respect to the rotations is checked for every parameter in Appendix H, an overview is presented in Table 7.24. The plots clearly demonstrate that low frequencies induce higher rotations than high frequencies. The magnitude of the rotation around the x-axis is four times the rotation around the y-axis and the impact of the type of rotation induces high discomfort and is governing, Figure 7.25. The findings are summarised into the conclusion that the dynamic response of the *Palmerah Tidal Bridge* is most sensitive for low frequency waves directed positively perpendicular to the bridge deck.

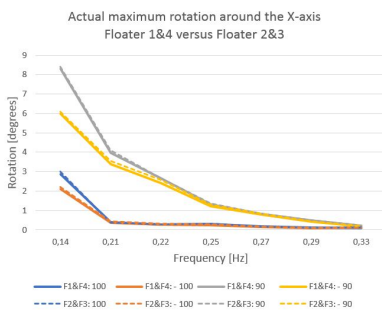


Figure 7.21: Rotation around the X-axis Actual rotation Floater 1 and Floater 4 versus Floater 2 and Floater 3

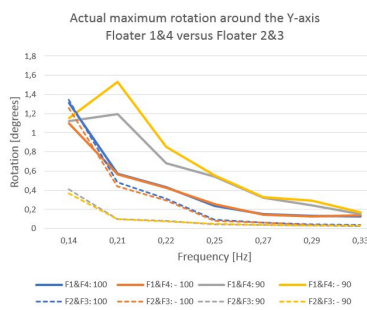


Figure 7.22: Rotation around the Y-axis Actual rotation Floater 1 and Floater 4 versus Floater 2 and Floater 3

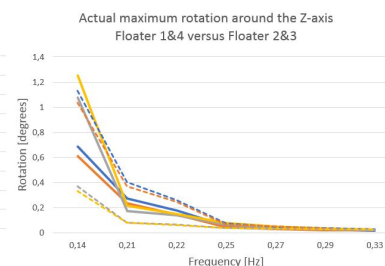


Figure 7.23: Rotation around the Z-axis Actual rotation Floater 1 and Floater 4 versus Floater 2 and Floater 3

		RX	RY	RZ
Natural frequency [Hz]		0,268	0,327	0,287 (heave)
Rotational peak value		8,31°	2,19°	1,13°
Floater couple	F1&F4 / F2&F3	-	F1&F4	-
Angle [°]	90/100	90	90	-
Direction	positive/negative	positive	negative	-
Frequency [Hz]	0,14/0,21/0,22/0,25	0,14	0,14 / 0,21	0,14

Figure 7.24: Most sensitive parameters with respect to rotation

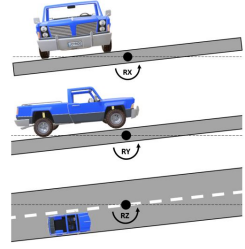


Figure 7.25: Repost of the illustration of rotation around every axis (RX, RY, RZ)

7.2.3. Time response analysis for the governing waves

The previous analysis indicated the motional sensitivity to certain wave properties with 1 meter high waves. The motion of the Tidal Bridge for the estimated 1, 50 and 100 year extreme waves is computed in two ways. The first analysis is subjected to *irregular* waves based upon the *significant* wave height and formed according to a *JONSWAP shaped wave spectrum* with a duration of one hour. The wave records are based upon maximum wind velocities during one hour, hence the duration of one hour is chosen. The duration is conservative, as the maximum wind velocity measured will not persist a complete hour. Within one hour, the ratio significant wave height to maximum wave height for the wave surface elevation of the JONSWAP spectrum is approximately $2, 2H_s = H_{max}$, corresponding with previous information. The second analysis is to indicate the sensitivity to the wave slope of a *Second Order Stokes wave*, a wave slope with a steep narrow crest and wide flat troughs. The *maximum* wave height is implemented for a *regular* Stokes wave. An overview of the governing wave properties for both types of analyses is given in Table 7.5. The exact implementation data of both analyses is elaborated in Appendix D.3.

	JONSWAP wave spectrum			Second order Stokes wave		
	Direction	H_s [m]	f [Hz]	Direction	H_{max} [m]	f [Hz]
5 % Downtime	90°	0,742	0,23	90°	1,47	0,23
1 year	90°	1,473	0,16	90°	2,95	0,16
50 years	90°	2,147	0,14	90°	4,29	0,14
100 years	90°	2,256	0,14	90°	4,51	0,14

Table 7.5: Input parameters for maximum wave response at particular time period.

The maximum values within the analysis are presented with the estimated serviceability limits for the Tidal Bridge in Table 7.6. The data values are coloured if the estimated serviceability limits are exceeded.

	Surge		Sway		Heave		Roll		Pitch		Yaw	
	Along x-axis [m]	[m/s ²]	Along y-axis [m]	[m/s ²]	Along z-axis [m]	[m/s ²]	Around x-axis [°]	[°/s ²]	Around y-axis [°]	[°/s ²]	Around z-axis [°]	[°/s ²]
Serviceability limits	-	0,5	-	0,5	-	0,7	2,52	6,13	2,01	4,01	3,44	2,86
Irregular JONSWAP wave spectrum Analysis (H_s)												
Downtime of 5%	0,04	0,22	1,99	0,27	0,69	1,35	2,56	5,39	1,26	2,65	0,17	0,34
1 year	0,05	0,22	4,01	1,33	1,26	1,51	10,69	11,03	1,68	2,39	1,20	1,24
50 years	0,05	0,57	7,06	3,34	2,68	3,01	24,35	23,63	3,17	3,18	3,68	3,44
100 years	0,06	0,42	7,46	3,57	2,60	3,24	25,90	25,16	2,89	3,02	3,64	3,64
Regular Second Order Stokes Analysis (H_{max})												
Downtime of 5%	0,02	0,08	3,47	0,12	0,54	1,08	1,69	2,82	0,54	1,13	0,07	0,16
1 year	0,07	0,23	5,26	1,84	1,89	2,13	15,69	12,45	2,03	2,48	1,82	1,76
50 years	0,10	0,76	6,71	3,96	4,05	5,07	27,70	23,25	3,71	4,93	4,29	4,26
100 years	0,10	1,15	7,07	3,90	4,61	6,83	29,00	25,15	4,83	7,54	4,65	4,63

Table 7.6: Overview of estimated serviceability limits of the Tidal Bridge and the maximum dynamic response with respect to waves.

First thing that strikes is the amount of coloured values in Table 7.6. The exceedance of the serviceability limits is not extraordinary. A bridge downtime of 5% is desired, indicating that indeed during 5% of the time the serviceability limits are exceeded and that the bridge is closed for traffic. Even though the serviceability limits are conservative, the desired downtime of 5 % seems realistic considering the maximum rotation. Solely heave acceleration is exceeded significantly, roll rotation is of a reasonable amount. Heave acceleration exceeds the tolerable limits, but it is plausible that the accelerations will be damped by the stabilising effect of the flow through the turbines.

The highest rotation that is present within 100 years is 29 degrees and arises around the x-axis. A visualisation of the rotation is presented in Figure 7.26. During these conditions, the bridge should be closed definitely. The amount of motion for the floater couple 1 & 4 and the couple 2 & 3 are plotted for both analysis types in Figures 7.27 and 7.28.

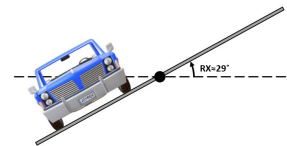


Figure 7.26: Visualisation of the maximum rotation around the x-axis

An increase in magnitude of motion for the regular Stokes wave is seen for nearly every degree of freedom. Especially, the shift of +5° for the roll-rotation is considerably large. The upwards shift is explained by the difference in shape of the Stokes wave slope: higher crest heights and smaller trough depths.

The floater couples behave individually as a result of the junctures with the pendulum system and/or a spudpole. The motion of the middle two floaters is governing for all degrees of freedom. An explanation is that the floaters are connected to a dynamic pendulum that allows motional freedom in all directions.

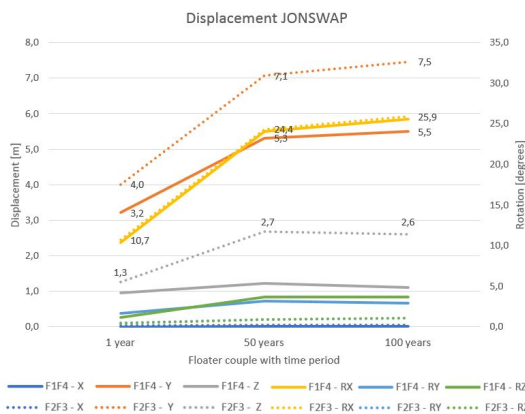


Figure 7.27: Magnitude of motion for JONSWAP wave spectrum
Significant wave characteristic with respect to return period

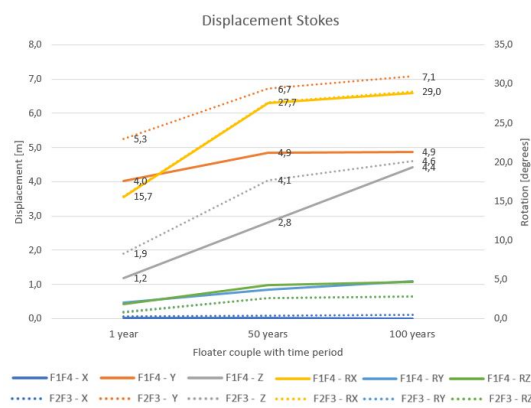


Figure 7.28: Magnitude of motion for Stokes waves
Maximum wave characteristic with respect to return period

In addition, the displacement in Z- and Y-direction is severe. An explanation is the forced motion as a result of the pendulum. High forces arise in the pendulum system, the forces try to find the route with the smallest amount of resistance. The possible route is along the red line in Figure 7.29 and rotations around the green hinge. The extreme displacement is in all probability an inaccuracy in the virtual computer model. The bridge is lifted above the water line along the radius of the pendulum. Hence the extreme displacements are set aside.

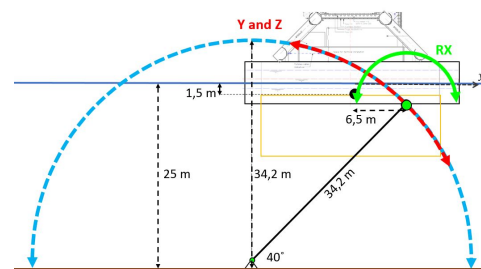


Figure 7.29: Pendulum radius with characteristic dimensions

Elaborating on Figure 7.29, the combination of rotation and displacement that may 'flip' the system to the other side is determined. If the centre of gravity of the floater moves past the highest point of the pendulum circle the whole structure might flip. The length of the pendulum is 34,2 m and the water depth in equilibrium position is 25 m. The centre of buoyancy of the floater is located 1,51 m below MWL. The distance between the pendulum and the midpoint of the bridge is 6,5 m. The maximum rotation around the x axis is 29 degrees within 100 years, the rotation is proportional to a z-displacement of the centre of buoyancy of: $\sin(29) \cdot 6,5 = 3,15$ m. Without a current drag force, an increase in waterlevel of $34,2 - (25 - 1,5) - 3,15 = 7,55$ m can flip the system. The maximum wave height in 100 years is estimated as 4,51 m, suggesting that the system is not flipped by waves only.

The serviceability limits for the tolerable *acceleration* are exceeded likewise, illustrated in Figures 7.31 and 7.32. Immediately, the increase in Z-displacement is noticed for the Stokes Analysis. An explanation might be the constant wave with frequency of 0,14 Hz in combination with the natural heave frequency of 0,287 Hz. The wave frequency is approximately 2 times the natural frequency, acting on the second natural frequency mode of the bridge, Figure 7.30. The resonance effect explains the increase in heave acceleration for a wave with a frequency of 0,14 Hz.

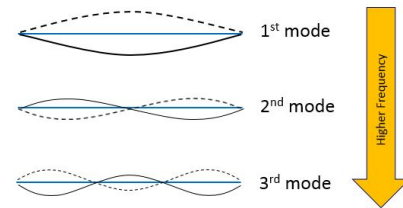


Figure 7.30: Visualisation of frequency modes (Siemens, 2018)

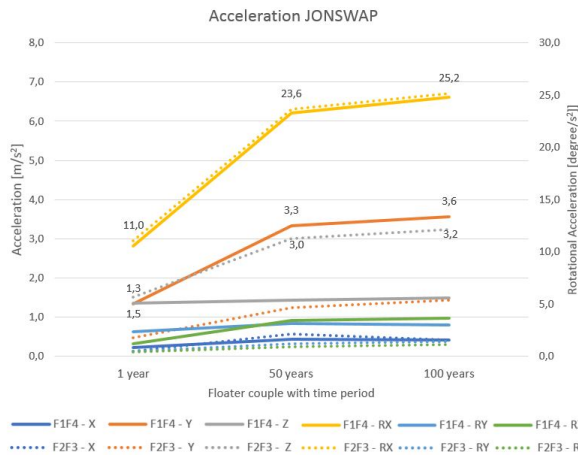


Figure 7.31: Dynamic response acceleration JONSWAP spectrum Significant wave characteristic with respect to return period

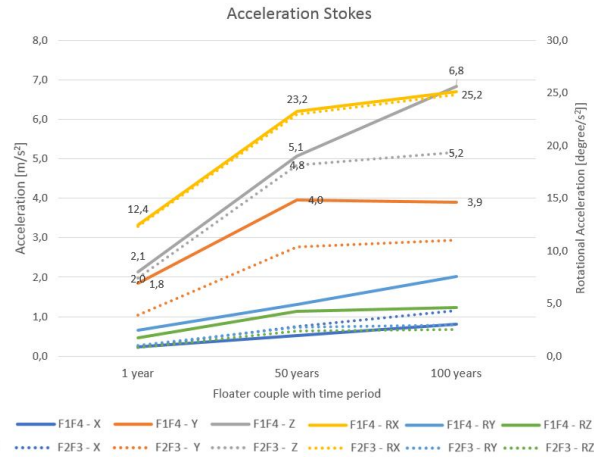


Figure 7.32: Dynamic response acceleration for Stokes wave Maximum wave characteristic with respect to return period

The wave surface elevation of the *regular* Stokes wave and the acceleration along the Z-axis are plotted in Figure 7.33. A few clear peaks are distinguished, the peaks appear at the moments where the periods of the wave and the second natural period of the bridge coincide. Fortunately, a regular wave spectrum is extremely unlikely and the resonance vertical displacement of the floaters is thus not probable. An irregular wave spectrum result in a non-linear dampening effect and prevents acceleration of the system in the resonance area.

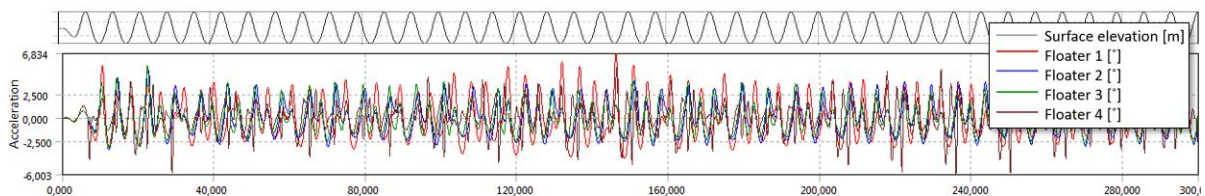


Figure 7.33: Acceleration along the z-axis with respect to every floater. Wave surface elevation is presented at the top of the plot

The acceleration plots suggest that again the most critical degrees of freedom are the rotation around the x-axis (roll) and the displacement along the y-axis (sway), Figure 7.34. The acceleration peak values of $25^\circ/s^2$ exceed the estimated limits approximately five times and are way beyond any tolerable motion limits. A real life example where the acceleration limit is exceeded five times the gravitational acceleration is in roller coasters and bungee jump attractions. The maximum limit in the attractions may not exceed five times the gravitational acceleration $5g$. It can be concluded that an increase in stabilisation with respect to this degrees of freedom is desired and required.

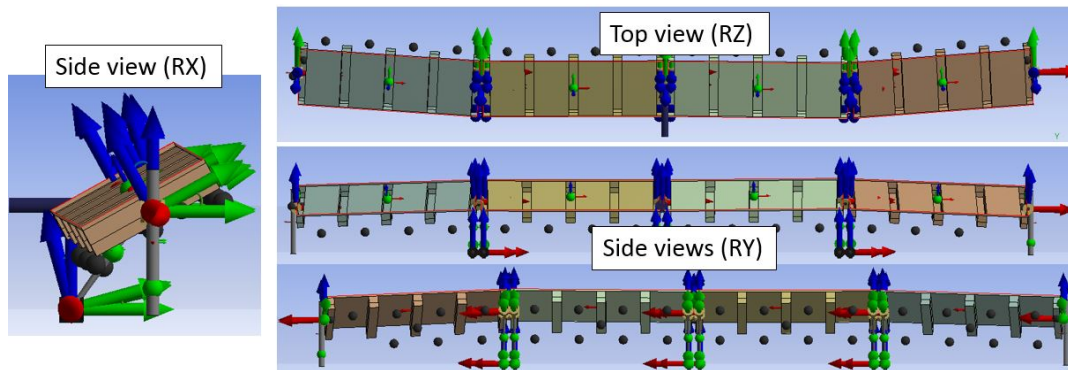


Figure 7.34: Screenshot at time of maximum rotation around the x-axis. Regular Stokes wave with return period of once every 100 years.

The sensitivity for a positive (+90°) or negative (-90°) wave propagation direction is analysed in Figures 7.35 and 7.36. According to the wave data, the maximum wave heights differ considerably. Waves coming from the north-east (*negative*) are twice the size of the south-western (*positive*) waves. The sensitivity study is computed for the maximum wave properties for a specific return period acting in both direction.

The displacement plot, Figure 7.35, shows that the sensitivity per wave direction differs per degree of freedom. However, the governing roll-rotation is $7,5^\circ$ larger at a *positive* current direction. The high displacement in y- and z- direction for the *negative* current is again a result of the inaccuracy of the virtual model.

The acceleration plot, Figure 7.36, clearly demonstrates an even larger difference for the rotational accelerations: $25,2^\circ/s^2$ versus $16,2^\circ/s^2$. The high acceleration along the z-axis are neglected as resonance at the second frequency mode of the bridge will not occur during a realistic sea state (elaborated in previous paragraph).

The Tidal bridge is most sensitive to waves around the frequency of 0,14 Hz directed perpendicular to the bridge deck and coming from the north-east. The maximum rotation induced for an irregular wave spectrum with a return period of once every 100 years has maximum values of 26 degrees. The influence of the wave slope of a Stokes wave increases the magnitude of rotation slightly.

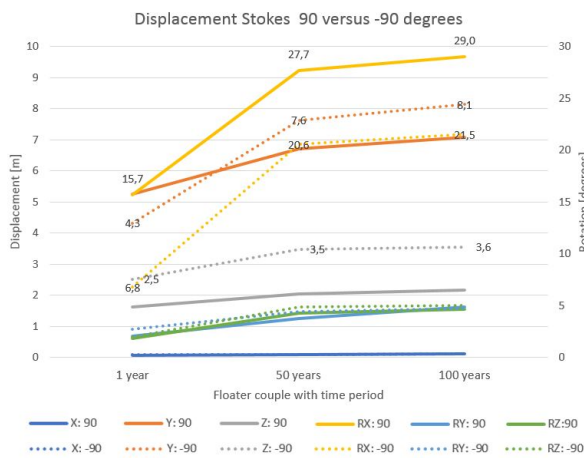


Figure 7.35: Displacement for Stokes waves Variation in direction +90° versus -90°

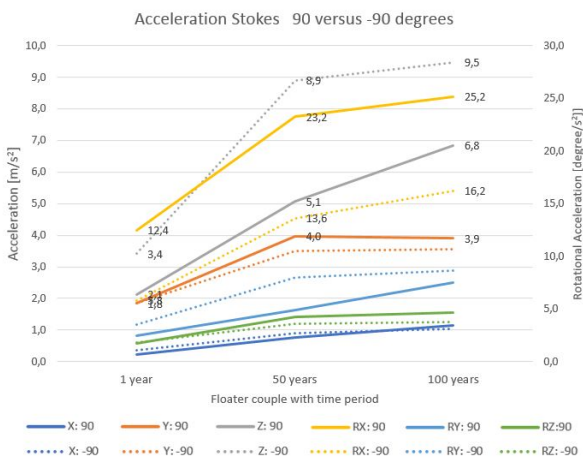


Figure 7.36: Acceleration for Stokes waves Variation in direction +90° versus -90°

7.3. Current sensitivity

The sensitivity for the dynamic response of the Tidal Bridge to specific flow speeds is checked in a different manner. The scope of the project states that the maximum turbine moment around the x-axis is 2,10 MNm/m and that the moment may not be exceeded by the turbine suppliers. With a (perpendicular) drag coefficient (Chapter 4) the moment is reached at a flow speed of 5,2 m/s.

The lack of data and knowledge about the drag coefficients of the combined FishFlow-pontoon system, concludes that it is solely possible to check the drag force for a perpendicularly directed flow speed for the combined FishFlow-pontoon system. In addition, the tidal range can not be implemented in Ansys Aqwa. Therefore, the sensitivity study considers exclusively one current cycle with peak flow speeds of 5,2 m/s. The relation between the flow speed, the drag force (red line) and the maximum moment *around the centre of gravity* (green line) is presented in Figure 7.37 along with the flow velocity (blue line). The distance between the centre of gravity of the pontoon and the application point of the drag force is higher than the distance between the x-axis and the application point, explaining a maximum moment value of 370 MNm/100m.

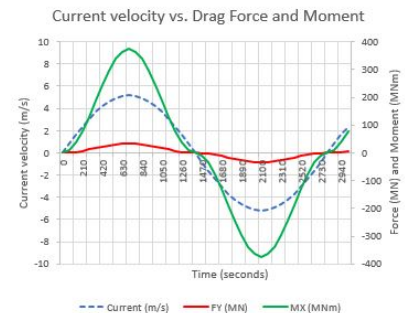


Figure 7.37: Maximum current velocity with corresponding drag force (MN) and rotational x-moment (MNm) with respect to a 100 m long floater

Instead of a varying load, the influence of different spudpole characteristics are analysed. The Tidal Bridge is able to move as a result of the displacement that is allowed by the spudpoles, Figure 7.38. In the situation with infinitely stiff poles and bodies, the system would not have been able to move. The properties of the spudpoles that are checked on sensitivity are divided into two sections: the allowable bending of the pole (δx_2) and the magnitude of the initial displacement (δx_1), both illustrated in Figure 7.39. No restriction of δx results in flipping over of the floater to the other side of the pendulum and failure of the conceptual design, elaborated in Appendix G.3.

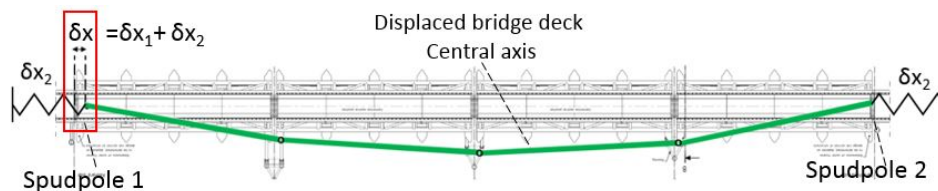


Figure 7.38: Necessary displacement needed to create a mechanism. Topview. Green line indicates the location of the displaced floaters.

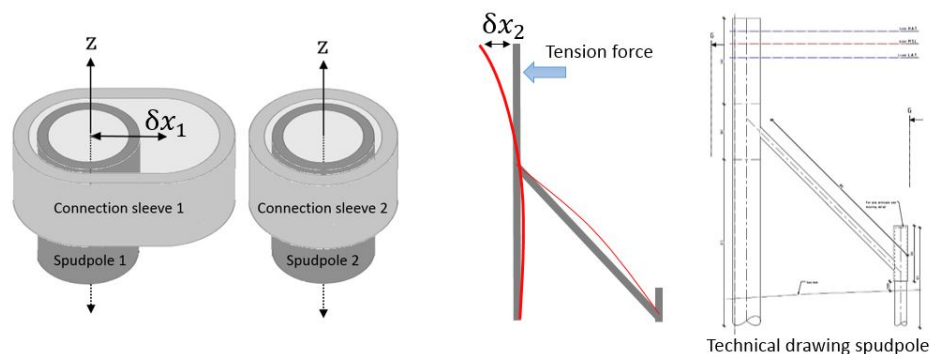


Figure 7.39: Illustration of the two 'variable' displacement properties of the spudpole.

First, the bending of the spudpole is analysed by defining a *linear elastic cable* between the spudpole and an 'imaginary fixed point'. The stiffness of the cable is proportional to the bending stiffness of the spudpole. An indication of the stiffness is determined by implementing the present spudpole design in *Matrixframe* and applying a (drag) force. The magnitude of bending of the spudpole is proportional to the stiffness of a cable: $k = F/x$, being 72,55 MN/m. The bending of spudpoles is present at both sides of the bridge and thus a cable is defined at both bridge ends. If the bridge is subjected to one tidal cycle that reaches a maximum and minimum flow speed of +/- 5,2 m/s, high rotations arise for the negative flow speed (elaborated in Appendix G.3). In addition, a remarkable result is that the roll-rotation is turned to the same side for a positive and negative current. The rotations found by Ansys Aqwa are contrary to the forecasted stability calculation computed in Chapter 5, the difference is illustrated in Figure 7.41. With restricted motion possibilities, another extraordinary unfavourable result is revealed. The spudpole stiffness combined with the pendulum system results in significant vertical displacement. The vertical displacement is not realistic as the bridge is located above the waterline, Figure 7.40. Ansys Aqwa includes the mass of the structure in the stability calculation, but the drag force moves with structure and induces the vertical displacement.

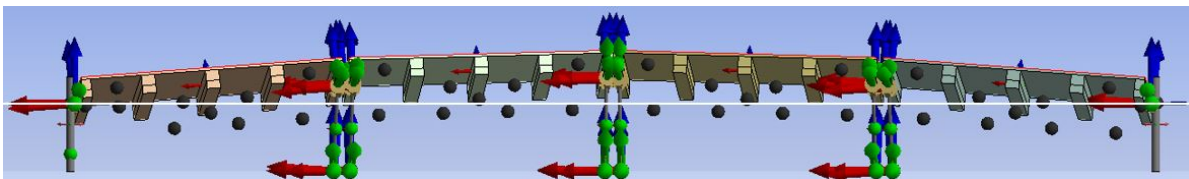


Figure 7.40: Screenshot of displaced Tidal Bridge. Middle two pontoons are located above the water line. Water line is presented as the white horizontal line

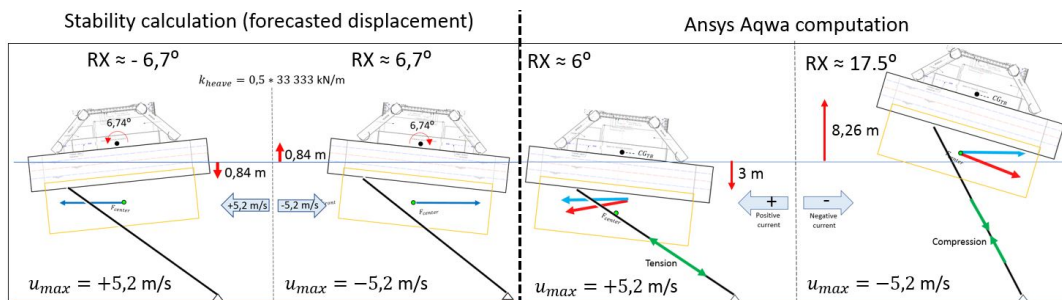


Figure 7.41: Forecasted displacement versus Displacement computed by Ansys Aqwa. Both seen with respect to the middle two floaters

7.3.1. Spudpole bending stiffness

The stiffness of the spudpole is adjusted by changes in the design. Examples are an increasing length of the supporting beams, change in attachment point or an increase of the thickness or the diameter of the poles, Figure 7.42. First, the sensitivity of the stiffness to an increased cable stiffness is analysed. Secondly, the spud construction is redesigned. The response of the system to five different magnitudes of cable stiffness are computed and compared: 73, 85, 100, 120 and 150 MN/m.

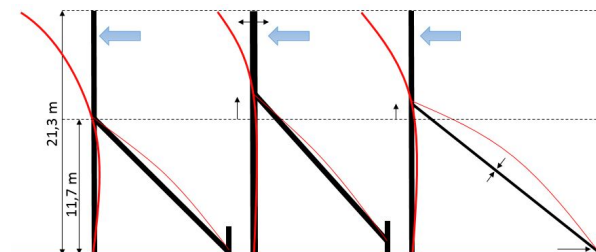


Figure 7.42: Bending of spudpole with different designs. Variable parameters might be: increase/decrease in length, diameter, thickness or material. (not drawn to scale)

Figure 7.43 and 7.44 show the rotational peak values for floater couple 1 & 4 and floater couple 2 & 3 for a *positive* and *negative* current velocity. The negligible damping effect for and increased stiffness in the positive flow speeds is contradictory to the significant decrease in rotations by a negative current. It is clear that with an increase in stiffness, the magnitude of rotation decreases significantly. The cable stiffness of 150 MN/m even suggests that the magnitude of rotation for the negative flow is smaller than for a positive flow. The relation between the roll-rotation for one flow cycle to a specific cable stiffness is showed in Figure 7.45. Figure 7.45 shows the inaccurate rotational peak present at negative flow speeds. At a certain cable stiffness the rotations around the positive axis are governing and additional damping of the rotations in negative current speeds is not longer effective.

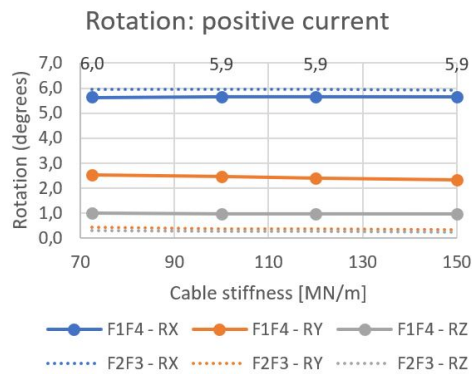


Figure 7.43: Maximum rotation of floaters during a *positive* current velocity of maximum 5,2 m/s versus cable stiffness

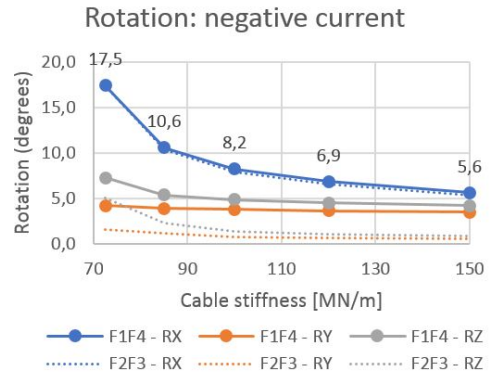


Figure 7.44: Maximum rotation of floaters during a *negative* current velocity of maximum 5,2 m/s versus cable stiffness

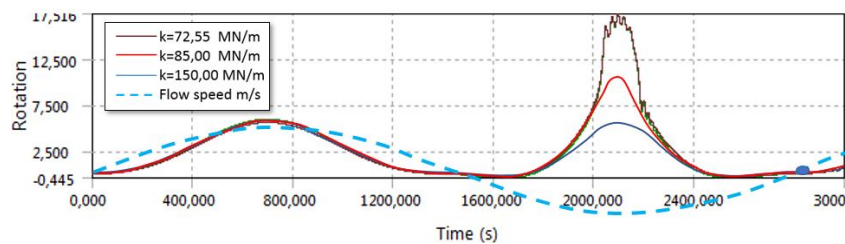


Figure 7.45: Rotation around the x-axis for total tidal cycle with three cable stiffness types

Next, the vertical displacement is analysed. The maximum allowable Z-displacement is based on the pontoon dimensions and indicated in Figure 7.46. The bridge deck level is located above the top of the pontoon and is not flooded if the draught of the pontoon increases. An increase in draught corresponds to an increase in drag force. The area that faces the flow increases significantly if the steel frame of the bridge construction is reached. Hence, a positive displacement of maximum 3,5 m is considered. The limit value regarding upwards displacement is assumed as 3,03 m, resembling the bottom depth of the pontoon. The sensitivity of a certain cable stiffness to the maximum vertical displacement is presented in Figures 7.47 and 7.48, the limit values are marked with a red dashed line.

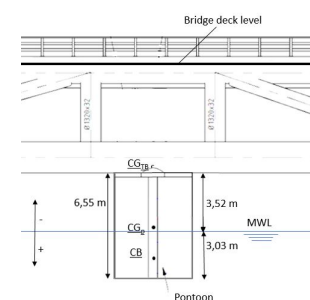


Figure 7.46: Allowable amount of Z-displacement pontoons

During a *positive* current, the limit value is not exceeded and the effect of an increase in cable stiffness is once more small, figure 7.47. The *negative* current plot implies that both floaters are located above the water line. An increase in cable stiffness reduces the amount of Z-displacement slightly, just enough to prevent the two outer floaters from 'flying' above the waterline. The centre pontoons are located above the water level in all inspected stiffness values, visualised in Figure 7.49. As stated before, the real response probably secures the system below the water level by the flow potential of the water body through the turbines.

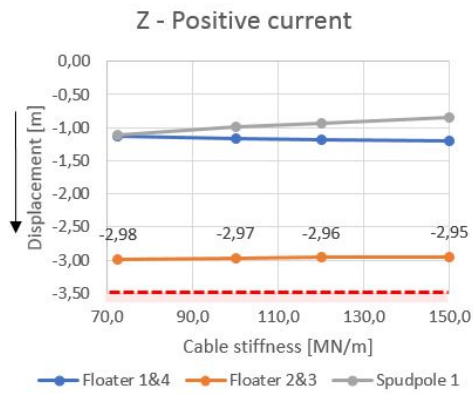


Figure 7.47: Maximum Z-displacement floaters, positive current velocity. Above the red line the pontoon is fully submerged.

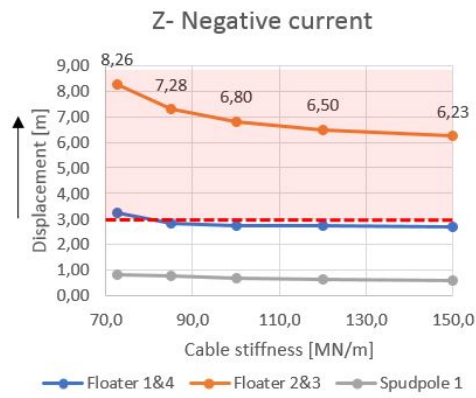


Figure 7.48: Maximum Z-displacement of floaters, negative current velocity. Below the red line the pontoon is above the water line

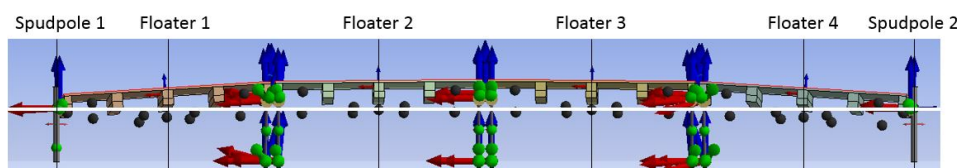


Figure 7.49: Displaced situation during maximum negative flow speed for cable stiffness of 150 MN/m. White line represents waterline. Vertical black lines indicate measure points at centres of gravity of system.

At last, the magnitude of the displacement of the spudpoles along the x-axis is analysed. The displacement is proportional to the elongation of the cable and to the distance δx_2 . High displacement induces extreme bending in the spudpole and probable failure of the spudpole. Repeatedly, no significant decrease of displacement is measured for an increasing stiffness in the positive current direction and severe reduction is visible during negative flow speed, Figure 7.50. The original spudpole design bends approximately 1,51 m horizontally twice a day, implying a serious fatigue failure probability. Fatigue is out of the scope of the report, but a substantial decreased amount of bending is considered as essential.

The bending of the spudpole (or elongation of the cable) is related to a tension force that should be received by the spudpole. The tension force in Figure 7.51 indicates a linear relation between force and stiffness after a stiffness of 100 MN/m. A lower limit is present at negative flow speeds for a cable stiffness of 100 MN/m. Higher or lower cable stiffnesses result in increased tension forces. Especially, values below a stiffness of 100 MN/m show undesirable effects. The cable stiffness of 100 MN/m is therefore considered as the lower stiffness limit. The upper limit of stiffness is based upon the governing rotation that will originate. The maximum roll rotation during positive flow speed is $5,9^\circ$, the minimum stiffness that induces the same or rotation during negative flow speeds results in a desired bending stiffness of > 145 MN/m.

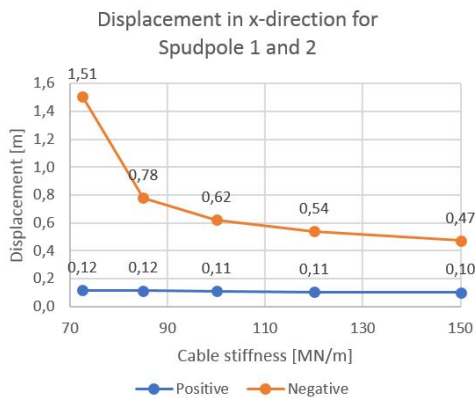


Figure 7.50: Displacement spudpoles along x-axis. Representing the elongation of the cable.

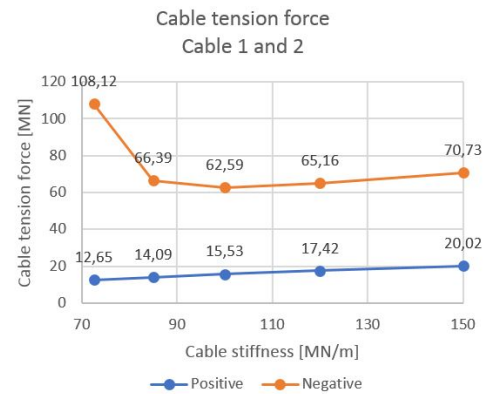


Figure 7.51: Tension force within cables for positive and negative current velocity

7.3.2. Spudpole 'connection' sleeve

The present design study of the spudpoles states that a limited initial displacement possibility is desired for one spudpole, δx_1 in Figure 7.52. The main reason for the initial displacement is that the system should be able to adapt easily to the daily tidal range. The minimum displacement caused by the tidal range is estimated in Appendix E.3.4 as 12 cm. The value is based upon the maxima of the water levels (HAT and LAT) where the system floats parallel to the water surface level. The displacement in x-direction is based on the reaction of the pendulum to low and high water levels. The influence of a change in water level is not analysed in the research.

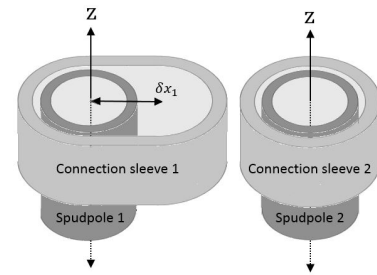


Figure 7.52: Illustration of the initial x-displacement of spudpole 1

When the model is run for solely the positive current direction, the maximum displacement of the spudpole is 0,353 m, Appendix G.3. The displacement is seen as a second reasonable value of the displacement δx_1 . The sensitivity to initial displacement is checked for four distances, respectively 0, 0,12, 0,35 and 0,50 metres. The results of the sensitivity study to *negative* flow speed are presented in plots 7.53 to 7.56. The plots imply that the magnitude of rotation increases almost linearly with an increase in size of δx_1 . The distribution between the analysed lines remains constant but the distance between the maximum and minimum value converges. An increase in the size of δx_1 is proportional to an increase in rotation for a certain stiffness.

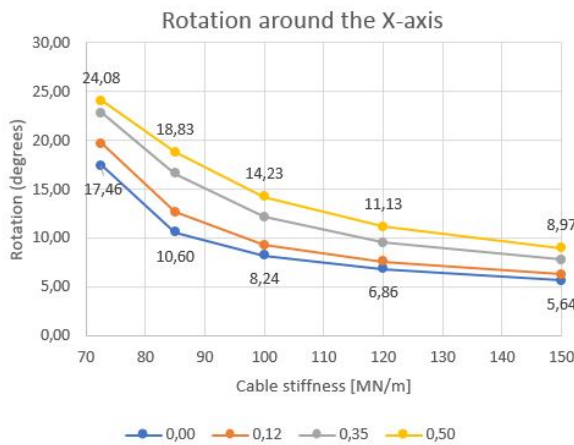


Figure 7.53: Rotation around the x-axis for different distances of δx_1

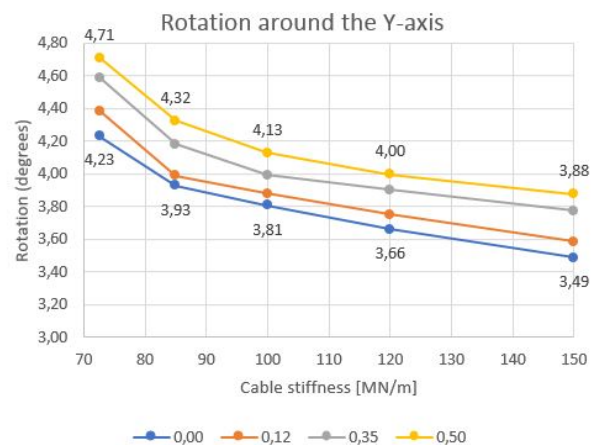


Figure 7.54: Rotation around the y-axis for different distances of δx_1

The vertical displacement for each type of structure with limit values is computed in Figure 7.56. The two middle floaters are again located above the waterline for all stiffnesses. As stated before, this is an inaccuracy in the computer model and the probable displacement will be less severe. The vertical displacement of the outer floaters converges with increased stiffnesses. The most favourable likely motion of the bridge is with the smallest possible δx_1 . The minimum distance to adapt smoothly to the tidal range is 0,12 m. Hence, the distance is governing for the maximum initial displacement that is possible within the spudpole 'connection sleeve'.

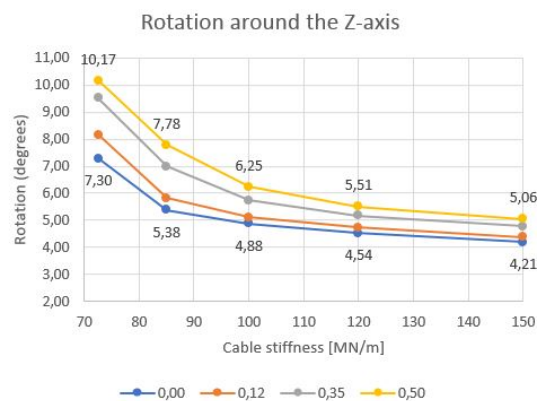


Figure 7.55: Rotation around the x-axis for different distances of δx_1

A quick check is conducted to check whether the initial displacement δx_1 influences the rotation around the x-axis for a *positive* flow speed and a cable stiffness of 150MN/m. The difference of an initial displacement of 0,12 m is a slight increase in rotation of 0,02 degrees (peak values change from 5,93° to 5,95°). The increase for the *negative* current is 0,66 degrees (5,64° to 6,30°), compared to the situation that does not allow initial displacement.

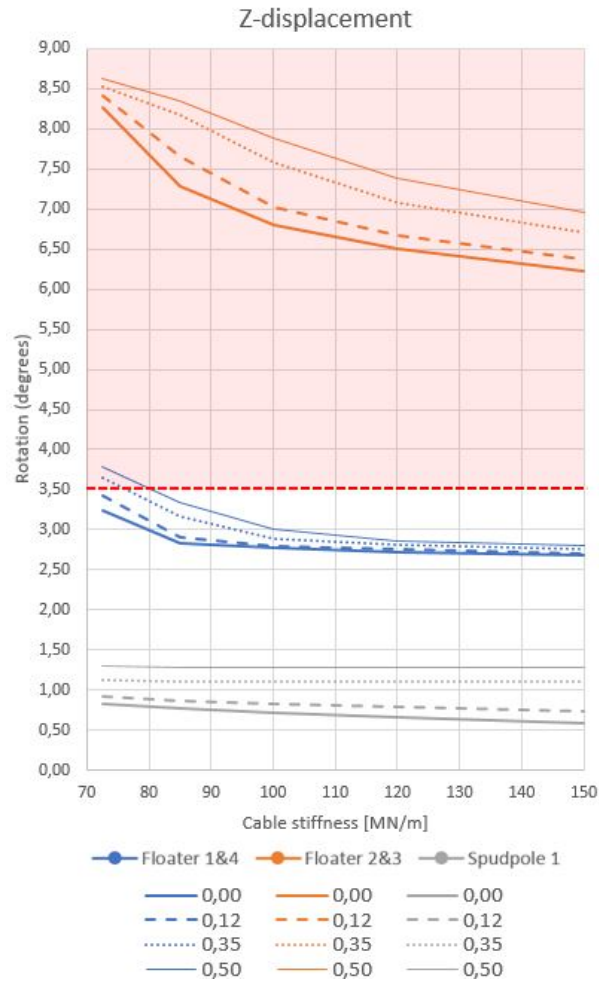


Figure 7.56: Vertical displacement along the z-axis for different distances of δx_1 and a *negative* flow speed

7.3.3. Improved spudpole design

The sensitivity study regarding the bending stiffness of the spudpole resulted in a desired stiffness of at least 145 MN/m. A small iterative study is conducted in Appendix G.3 to check whether the stiffness can be achieved easily. A renewed spud design is proposed that approaches a stiffness of 160 MN/m. The adjustments of the design are a shift of the application point of the supporting beams of 2 m and an increase in supporting beam thickness from 30 mm to 50 mm, illustrated in Figure 7.57 and elaborated in Appendix G.3.

The force distribution of the maximum negative drag force in the mooring system with a spudpole with bending stiffness of 160 MN/m and an initial displacement of 0,12 m at one side is determined and visualised in Figure 7.58.

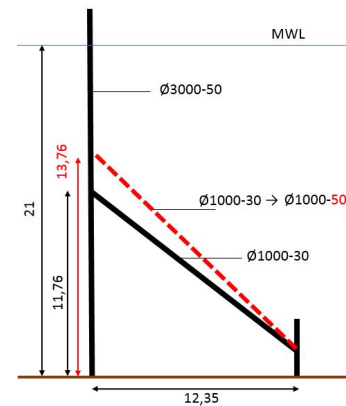


Figure 7.57: Improved spudpole design

The mooring system needs to transfer high forces, especially the spudpoles and the outer pendulums. The forces in the pendulum switch continuously between tension and compression. It is strongly recommended to check all possible failure mechanisms that may occur through the high forces, pressures and fatigue loading.

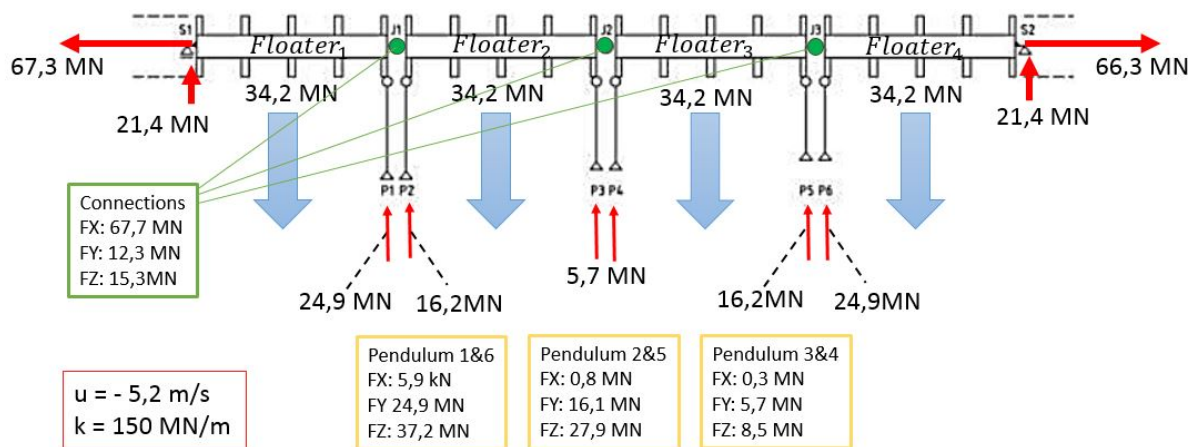


Figure 7.58: Force distribution for a *negative* maximum flow speed and spudpole with stiffness of 150 MN/m and initial displacement of 0,12 m.

7.4. Response to extreme load combinations

Combining the information regarding the sensitivity of the Tidal Bridge to waves and current induced pressures the most critical load scenario is checked. The peak values in the total cycle are given in Table 7.7. The maximum current velocity is based on the maximum allowable horizontal moment induced by the turbines. The resistance of the turbines can be adjusted to meet this moment regarding the flow speed. Therefore, the maximum moment is assumed to be governing as an indication of the current velocity. The tidal cycle is scaled to reach the requested velocity, in reality the turbine resistance represents the scaling effect that induces an increased drag force.

- Waves with significant wave heights that arise 5% of the time implemented in irregular JONSWAP wave spectrum:
 - South-western waves: $H_s = 0,33$ m and $f = 0,38$ Hz
 - North-eastern waves: $H_s = 0,80$ m and $f = 0,22$ Hz
- One full tidal cycle with the original spudpole design:
 - Tolerable initial elongation: $\delta x_1 = 0,12$ m
 - Spudpole stiffness: $k = 72,55$ MN/m
- A maximum moment around the x-axis of 2,1 MNm/m induced by drag forces
 - Current of minimum 5,2 m/s and maximum 3,7 m/s

		Surge		Sway		Heave		Roll		Pitch		Yaw	
		Along x-axis		Along y-axis		Along z-axis		Around x-axis		Around y-axis		Around z-axis	
		[m]	[m/s ²]	[m]	[m/s ²]	[m]	[m/s ²]	[°]	[°/s ²]	[°]	[°/s ²]	[°]	[°/s ²]
Serviceability limits		-	0,50	-	0,50	3,00	0,70	2,52	6,13	2,01	4,01	3,44	2,86
Waves	Current												
from SW	No	0,13	0,01	3,51	0,08	0,06	0,07	0,12	0,25	0,10	0,08	0,03	0,04
from NE	No	0,14	0,09	3,36	0,28	0,49	0,83	1,70	2,96	0,41	0,61	0,11	0,16
No	Yes	0,15	0,02	20,27	0,15	8,41	0,05	19,68	0,28	4,38	0,09	8,16	0,10
from SW	Yes	0,15	0,02	20,25	0,17	8,42	0,40	19,65	0,57	4,44	0,54	8,16	0,20
from NE	Yes	0,17	0,37	20,47	0,32	8,53	0,78	20,49	2,87	4,44	0,90	8,26	0,33

Table 7.7: Overview of estimated serviceability limits of the Tidal Bridge and the maximum dynamic response with respect to waves.

In the situation with waves only, the peak values displayed in Table 7.7 are almost all within the tolerable serviceability range. Solely the heave acceleration limit is exceeded if severe north-eastern directed waves are present. The moment that a current is present, the peak values increase significantly. The current is the governing motion component and the waves fluctuate around the 'current-induced-motionline'. The wave fluctuation is not constant due to the irregular wave spectrum. The extreme peak at the negative flow speed is an inaccuracy in the Ansys Aqwa model. Additional research is obligatory to indicate the actual order of magnitude of the rotation.

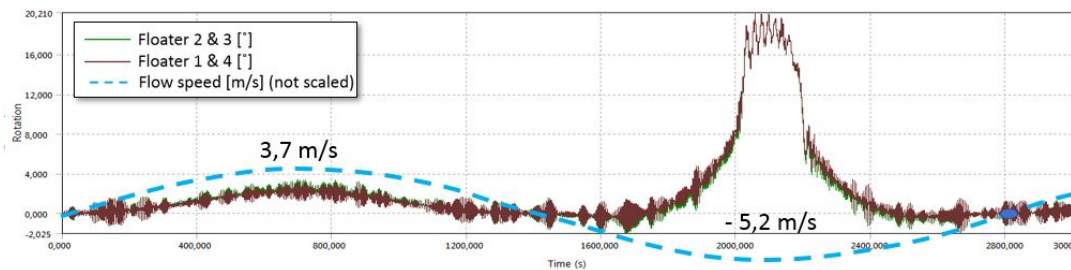


Figure 7.59: Most extreme scenario, maximum drag force and maximum wave height for original spudpole design

In the computation of the motion of the original Palmerah Tidal Bridge design to the determined hydraulic loads, solely one of the *acceleration limits* is exceeded. Nonetheless, accelerations are continuously present which has a negative effect on the comfort of driving. The unfavourable effect of the continuous motion increases with an increase in exposure time to the motion. If traffic drives at a speed limit of 20 km/h and the floating bridge part has a length of 400 m, a car will be exposed to accelerations during 72 seconds ($x = v \cdot t$). A person walking over the bridge will need approximately 5 minutes to cross the bridge. The effect of the accelerations during these exposure times should be checked in a later stage.

The relation between the roll-rotation and the flow speed and wave height is elaborated according to Figures 7.60 and 7.61. The first figure indicates the roll-response for an improved spudpole design, with $k = 150$ MN/m and flow speeds of + and - 5,2 m/s.

Conclusions are drawn from the relation between the waves and current. First, wave induced motions are governing at flow speeds around zero. The decrease of drag forces results in a more dynamic system that reacts heavier to waves. Next observation is that the positive flow speeds dampen the wave motion more than negative flow speeds. This is explained by the increase in draught of the pontoons during positive flow velocities. The Ansys Aqwa model is inaccurate for negative flow velocities as the system is located above the waterline. The draught of the pontoons decreases and as a result the response to waves is more severe for negative flow speeds. Third remark is that the bridge is constantly in motion, even though acceleration limits are not exceeded, driving over the bridge will cause a great deal of discomfort. The animation computed by Ansys Aqwa confirms this conclusion, although the duration of the tidal cycle is set to 3 600 seconds and not to 12 hours, the wave-induced response is the critical component that results in constant accelerations.

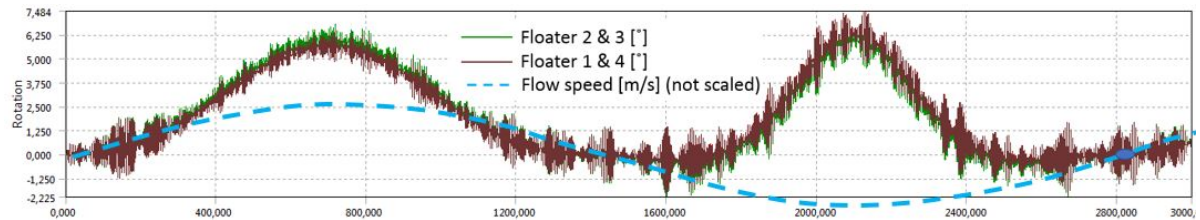


Figure 7.60: Roll rotation around the x-axis with improved spudpole design ($k = 150$ MN/m). North-Eastern wave and maximum flow speeds of + and - 5,2 m/s

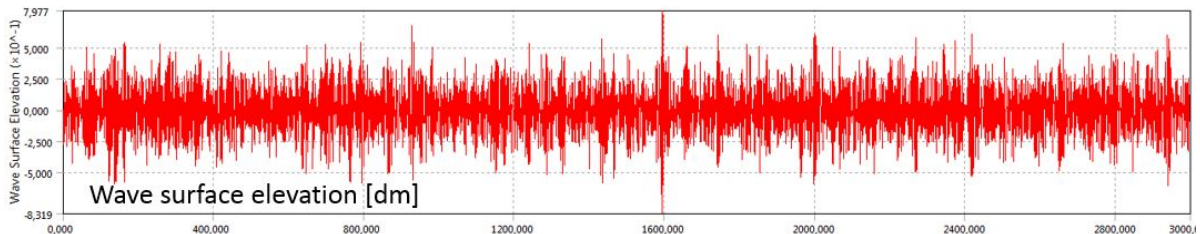


Figure 7.61: Water level elevation of north-eastern wave over 3 000 seconds

Summary: Chapter 7: Sensitivity analysis

The task of the chapter was to find an answer to the question: "What is the dynamic response of the Tidal Bridge and what loads induce governing motion?". The answer is found by determining the dynamic response of the Tidal Bridge to various load combinations.

First, a small study on extreme static traffic distributions was conducted. The study showed that the governing traffic distribution is dependent on the requested critical degree of freedom. For example, an **eccentric traffic** load distribution results in **roll-rotation of 1 degree** and traffic jams at the centre hinges induce a pitch rotation of 1,12 degrees.

Secondly, the **Response Amplitude Operators (RAO)** of the individual uncoupled freely floating floaters are analysed in the **Frequency Domain** to find the critical sea state for the governing likely motion of the floater. The RAO's imply that the **motion peaks** are present with wave frequencies in the same order size as the natural frequencies of the bridge, **in the range of 0,21 till 0,27 Hz**. An overview of the RAO-based peak values for the perpendicularly directed waves is given in Table 7.8. The RAO-based response implies that the **rotation around the x-axis is governing**. In addition, perpendicular directed waves induce higher motion than oblique waves indicated in Figure 7.63.

Direction	X [m/m]	f_{peak} [Hz]	Y [m/m]	f_{peak} [Hz]	Z [m/m]	f_{peak} [Hz]	RX [°/m]	f_{peak} [Hz]	RY [°/m]	f_{peak} [Hz]	RZ [°/m]	f_{peak} [Hz]
90°	0,23	0,25	0,58	0,14	1,13	0,22	16,23	0,21	2,08	0,25	0,58	0,25

Table 7.8: Maximum motion response based on the RAO of an individual uncoupled freely floating floater for a perpendicular directed waves in a frequency range of 0,02 to 0,44 Hz.

The RAO-based response considers the response of individual uncoupled freely floating structures. When coupled as one total mechanism the response of the full Tidal Bridge is computed. The dynamic response of the total coupled system is analysed in the **Time Domain**. The magnitude of motion of the **coupled bridge system is approximately 2,5 times smaller than the RAO-based response of the individual uncoupled floaters**. In addition, a **shift towards lower frequencies** is seen for the rotation around the x-axis, Figure 7.62. The shift is favourable as low frequency waves are more scarce. A wave with a frequency of 0,14 Hz will arise once every 100 years. In conclusion, the floating part of the Tidal Bridge is **most sensitive to positive perpendicular waves with low frequencies**.

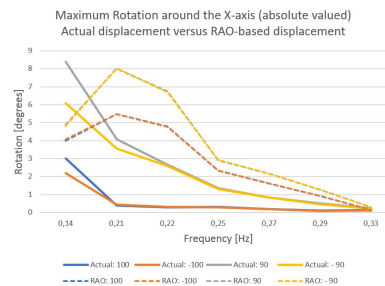


Figure 7.62: Rotation around the X-axis Individual freely floating RAO response of floater versus actual response of the connected bridge

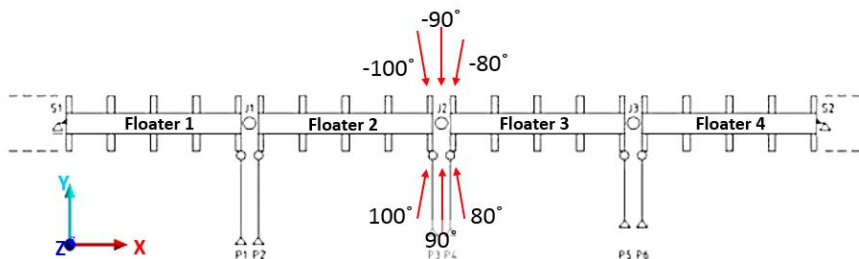


Figure 7.63: Overview of the implemented wave parameters in Ansys Aqwa

Summary: Chapter 7: Sensitivity analysis

The governing wave combination with return period of 5%, 1 year, 50 years and 100 years are implemented in the Ansys Aqwa model to determine the maximum dynamic response. The influence on the amount of motion for two types of wave analysis is checked: an **irregular** wave distributed according to the JONSWAP wave spectrum and a **regular** second order Stokes wave. Comparing the maximum motion and acceleration values to the estimated serviceability limits shows that for every scenario some limits are exceeded, the peak values are given in Table 7.9.

	Surge		Sway		Heave		Roll		Pitch		Yaw	
	Along x-axis [m]	[m/s ²]	Along y-axis [m]	[m/s ²]	Along z-axis [m]	[m/s ²]	Around x-axis [°]	[°/s ²]	Around y-axis [°]	[°/s ²]	Around z-axis [°]	[°/s ²]
Serviceability limits	-	0,5	-	0,5	-	0,7	2,52	6,13	2,01	4,01	3,44	2,86
Irregular JONSWAP wave spectrum Analysis (H_s)												
Downtime of 5%	0,04	0,22	1,99	0,27	0,69	1,35	2,56	5,39	1,26	2,65	0,17	0,34
1 year	0,05	0,22	4,01	1,33	1,26	1,51	10,69	11,03	1,68	2,39	1,20	1,24
50 years	0,05	0,57	7,06	3,34	2,68	3,01	24,35	23,63	3,17	3,18	3,68	3,44
100 years	0,06	0,42	7,46	3,57	2,60	3,24	25,90	25,16	2,89	3,02	3,64	3,64
Regular Second Order Stokes Analysis (H_{max})												
Downtime of 5%	0,02	0,08	3,47	0,12	0,54	1,08	1,69	2,82	0,54	1,13	0,07	0,16
1 year	0,07	0,23	5,26	1,84	1,89	2,13	15,69	12,45	2,03	2,48	1,82	1,76
50 years	0,10	0,76	6,71	3,96	4,05	5,07	27,70	23,25	3,71	4,93	4,29	4,26
100 years	0,10	1,15	7,07	3,90	4,61	6,83	29,00	25,15	4,83	7,54	4,65	4,63

Table 7.9: Overview of estimated serviceability limits of the Tidal Bridge and the maximum dynamic response with respect to waves.

The Tidal bridge is most sensitive to waves with **frequencies of 0,14 Hz directed perpendicular (+90)** to the bridge deck and coming **from the north-east**. The desired **downtime of 5% seems a realistic requirement** with respect to wave-induced pressures. The limits for heave acceleration and roll rotation are exceeded, however it is probable that design improvements stabilise the system. The maximum rotation induced for an irregular wave spectrum with a wave height with a return period once every 100 years is 26 degrees. The influence of the **wave slope of a Stokes wave increases the magnitude of rotation slightly**.

The dynamic response induced by the **flow speeds** is checked for solely a perpendicular directed current. The sensitivity of the system with **two variable spudpole properties** is analysed for a maximum positive and negative flow speed of 5,2 m/s. The variable spudpole characteristics are the initial displacement that is desired to adapt smoothly to the tidal range (δx_1) and the amount of bending that is present (δx_2), Figure 7.64. The findings resulted in a **proposed spudpole design with an initial displacement possibility of $\delta x_1 = 0,12$ m and a bending stiffness of $k=150$ MN/m** (the stiffness is related to δx_2).

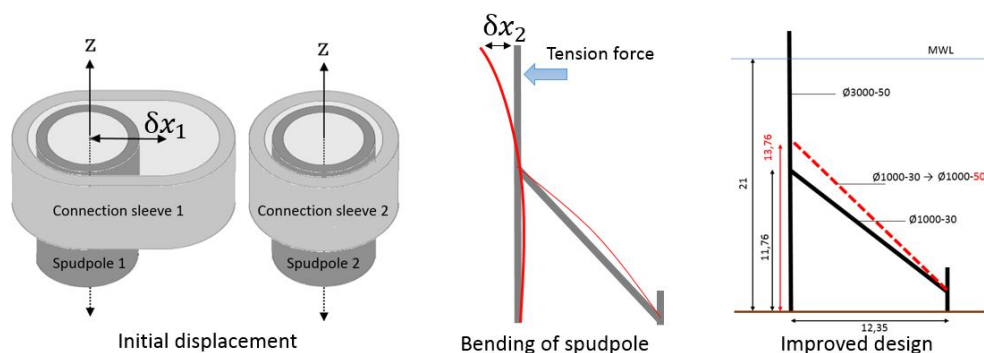


Figure 7.64: Illustration of possible displacement along x-axis for both variable spudpole characteristics: δx_1 and δx_2

Summary: Chapter 7: Sensitivity analysis

The sensitivity analysis indicated that the **Ansys Aqwa model is inaccurate**. In negative flow velocities the bridge moves upwards and is located above the waterline, analogous to a kite. The water body that flows through the FishFlow turbine stabilises the system by securing the bridge below the waterline and reducing the rotations around the x-axis. An estimation of the magnitude of the counteracting effect of the FishFlow turbines is absent and can be best estimated with scale-model tests. The inaccuracy of the model is visualised in Figures 7.65 and 7.66.

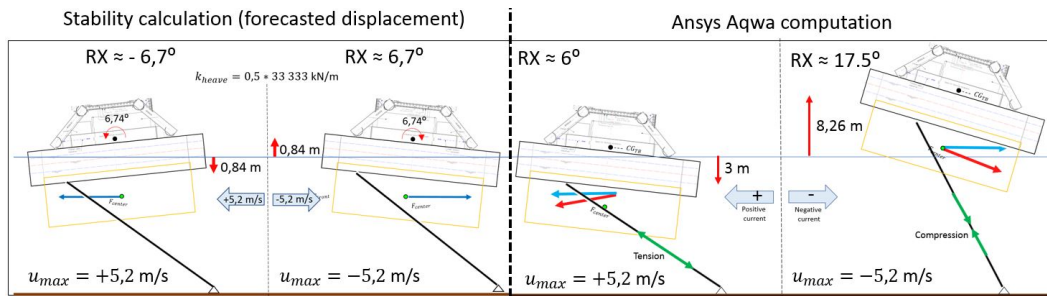


Figure 7.65: Forecasted displacement versus displacement computed by Ansys Aqwa. Both seen with respect to the middle two floaters

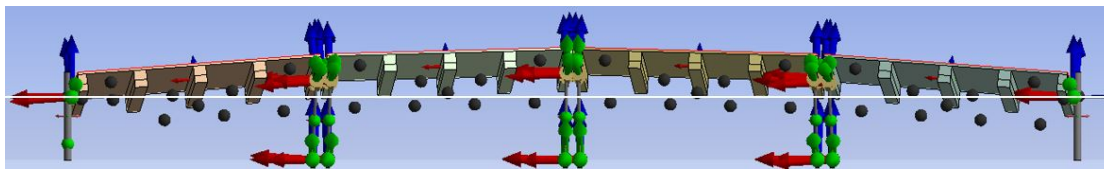


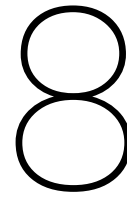
Figure 7.66: Screenshot of displaced Tidal Bridge. Middle two pontoons are located above the water line. Water line is presented as the white horizontal line

The dynamic response of the **critical wave properties** that arise during 5% of the lifetime of the bridge are **combined with the tidal current** and original spudpole design and presented in Table 7.10. The dynamic response to the situation with solely waves, solely current and combination of the two is computed. It became clear that the current induces the major motion and that wave fluctuate around the 'current induced motion-line'. The maximum accelerations exceed serviceability limits only if north-eastern waves are present, but the **magnitude of motion is exceeded severely and not tolerable for traffic**.

The combined response indicates that motion induced by waves is governing if the flow speed approaches zero. In addition, an increased draught of the pontoons results in dampening of the wave induced motions. The bridge deck is **constantly in motion** due to the waves, driving over the bridge will cause sincere discomfort. Hence, the stability of the system should be improved.

	Surge		Sway		Heave		Roll		Pitch		Yaw		
	Along x-axis [m]	[m/s ²]	Along y-axis [m]	[m/s ²]	Along z-axis [m]	[m/s ²]	Around x-axis [°]	[°/s ²]	Around y-axis [°]	[°/s ²]	Around z-axis [°]	[°/s ²]	
Serviceability limits	-	0,50	-	0,50	3,00	0,70	2,52	6,13	2,01	4,01	3,44	2,86	
Waves													
from SW	No	0,13	0,01	3,51	0,08	0,06	0,07	0,12	0,25	0,10	0,08	0,03	0,04
from NE	No	0,14	0,09	3,36	0,28	0,49	0,83	1,70	2,96	0,41	0,61	0,11	0,16
No	Yes	0,15	0,02	20,27	0,15	8,41	0,05	19,68	0,28	4,38	0,09	8,16	0,10
from SW	Yes	0,15	0,02	20,25	0,17	8,42	0,40	19,65	0,57	4,44	0,54	8,16	0,20
from NE	Yes	0,17	0,37	20,47	0,32	8,53	0,78	20,49	2,87	4,44	0,90	8,26	0,33

Table 7.10: Overview of estimated serviceability limits of the Tidal Bridge and the maximum dynamic response.



Design suggestions

This chapter suggests design changes and estimates whether the influence of the alternative designs may be more efficient than the current design of the Tidal Bridge. In the end of the chapter subquestion 3c: "What are design suggestions that improve the stability of the bridge?" is answered.

8.1. Possible design alternatives

The sensitivity study indicated the dynamic response to the current design of the Tidal Bridge. The results suggested the sensitivity of the bridge to certain loadings and structural properties. According to the results design suggestions are proposed and shortly elaborated. An overview of suggested possible alternatives that may improve the stability of the bridge is given. All items are shortly elaborated and for some alternatives a quick check of the 'new' dynamic response is computed.

1. Implementation of improved spudpole design.
2. Rotation of the bridge design with 180 degrees.
3. Initial tilt of the bridge with ballast.
4. Increase of mass.
5. Limitation of vertical displacement with cables.
6. Adjusting the mooring pendulum angle.
7. Applying hydraulic springs in pendulum system.

8.1.1. Improved spudpole design

The present spudpole design experiences 1,5 m of horizontal bending and is very likely to collapse as a result of fatigue or structural failure. An improved design of the spudpole is proposed according to the data in chapter 7. The improved design will limit the maximum horizontal displacement to 0,47 m and reduces the maximum rotation from 17,5 ° to 5,9 °. Both suggest a stabilising effect of almost 70%. The spud design can be adjusted in many ways, one manner is to increase the thickness of the supporting beams from 30 mm to 50 mm and to move the connection point of the beams 2 m upwards, illustrated in Figure 8.1. With the adjustments the bending stiffness is increased from 72,5 to 160 MN/m.

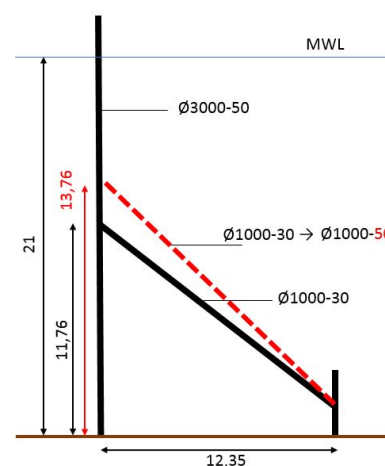


Figure 8.1: Improved spudpole design

8.1.2. Rotation of Tidal Bridge design

Second suggestion is based on the facts that the Tidal Bridge will experience less likely motion for a *negative* directed wave and the fact that the estimated wave heights of south-western *positive* waves are half the size, Table 8.1 and directions illustrated in Figure 8.2. Implying that a turn of 180 degrees is favourable.

Direction [°]	Aqwa axis[°]	H_s [m]	H_{max} [m]	T_p [s]	L [m]	f [Hz]
0-20	-78	0,74	1,47	4,30	28,86	0,23
20-40	-102	0,80	1,61	4,49	31,49	0,22
200-220	78	0,10	0,20	1,14	2,02	0,88
220-240	58	0,33	0,67	2,66	11,01	0,38

Table 8.1: Governing waves with an occurrence probability of 5%

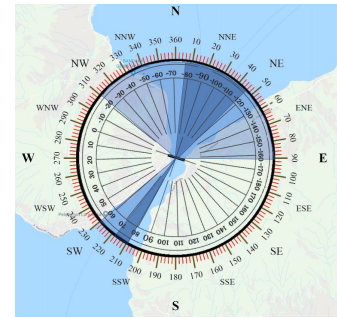


Figure 8.2: Ansys axis system and governing wave directions

From the flow speed perspective, a full rotation is a logical change as well. The bridge reacts more extreme to a *negative* directed current magnitude. According to the flow survey, the negative current velocity is of a higher magnitude than the positive current velocity peaks, Figure 8.3.

- Maximum north-eastern current = - 5,2 m/s
- Maximum south-western current = 3,7 m/s

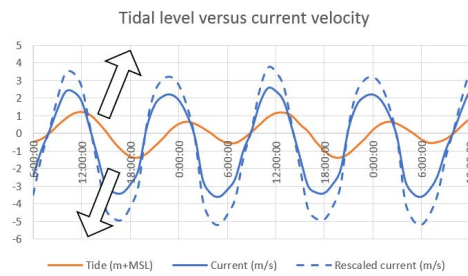


Figure 8.3: Relation between Tidal Range, average current velocity and rescaled maximum current velocity (Aquatera (2017)). Arrows indicate the direction of the current

The reduced displacement for a negatively directed waves is presented in the plot of the sensitivity study that indicates the magnitude of motion for each degree of freedom for the maximum return periods, Figure 8.4. Combined with decreased wave heights, the induced rotations are reduced. The design suggestion is presented in Figure 8.5. Full rotation of the bridge design results in a decrease in magnitude of the critical loads. The maximum flow speed that approaches the most sensitive side is approximately 3,7 m/s instead of 5,2 m/s. In addition, the highest waves are subjected to the favourable side and are half the size.

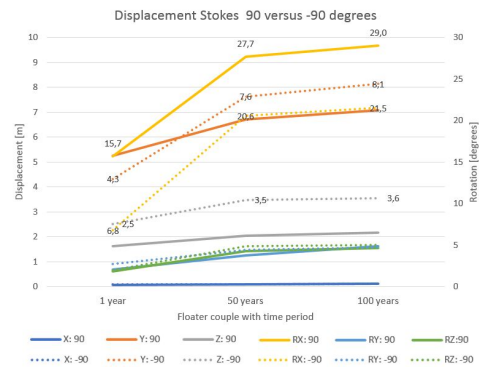


Figure 8.4: Influence on displacement of positive versus negative wave direction (Repost of sensitivity study)

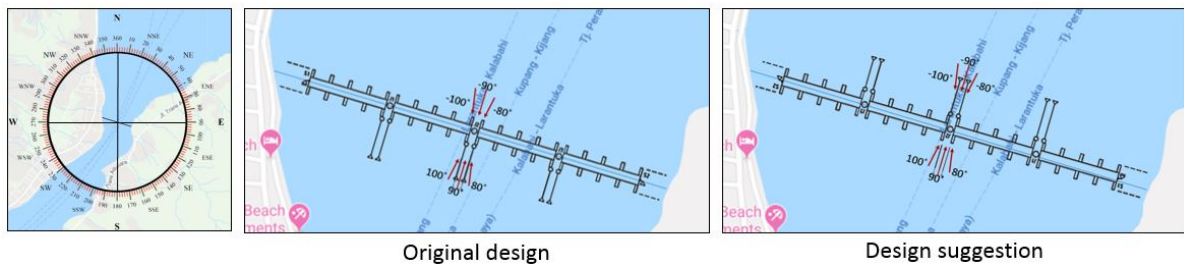


Figure 8.5: Proposed design suggestion with respect to the maximum current velocity peaks

The impact of the design change is checked by switching the sign of the hydraulic loads. Table 8.2 illustrates the switch of the hydraulic loads that arise from the 'same' direction. The effect of the rotated design is checked for three scenarios: solely current velocities, a current with the governing south-western waves and a current with governing north-eastern waves. The waves are defined as irregular waves distributed according to the JONSWAP wave spectrum. The maximum motions and accelerations are presented in Table 8.3. With the adjusted design the serviceability limits are still exceeded for roll and pitch rotation.

	Aqwa axis direction		Maximum flow speed	H_s [m]	Frequency
Original	<i>Negative</i>	from north-east	5,2 m/s	0,80 m	0,22 Hz
	<i>Positive</i>	from south-west	3,7 m/s	0,33 m	0,38 Hz
Design suggestion	<i>Positive</i>	from north-east	5,2 m/s	0,80 m	0,22 Hz
	<i>Negative</i>	from south-west	3,7 m/s	0,33 m	0,38 Hz

Table 8.2: Implementation data to check influence on rotation of bridge design.

		Surge		Sway		Heave		Roll		Pitch		Yaw	
		Along x-axis		Along y-axis		Along z-axis		Around x-axis		Around y-axis		Around z-axis	
		[m]	[m/s ²]	[m]	[m/s ²]	[m]	[m/s ²]	[°]	[°/s ²]	[°]	[°/s ²]	[°]	[°/s ²]
Serviceability limits													
Original design	Solely current	0,15	0,02	20,27	0,15	8,41	0,05	19,68	0,28	4,38	0,09	8,16	0,10
	Waves from SW	0,15	0,02	20,25	0,17	8,42	0,40	19,65	0,57	4,44	0,54	8,16	0,20
	Waves from NE	0,17	0,37	20,47	0,32	8,53	0,78	20,49	2,87	4,44	0,90	8,26	0,33
Improved spudpole	Solely current	0,14	0,04	8,89	0,01	6,38	0,05	6,30	0,04	3,59	0,09	4,39	0,01
	Waves from SW	0,14	0,04	8,89	0,03	6,38	0,11	6,30	0,11	3,60	0,17	4,39	0,05
	Waves from NE	0,16	0,51	9,10	0,32	6,60	0,78	7,90	2,86	3,68	0,82	4,48	0,21
Rotated + new spudpole design	Solely current	0,14	0,15	2,36	0,01	2,97	0,07	5,95	0,04	2,46	0,12	1,66	0,02
	Waves from SW	0,15	0,25	2,37	0,04	2,97	0,13	5,97	0,12	2,48	0,21	1,66	0,04
	Waves from NE	0,19	0,71	2,49	0,36	3,32	0,79	6,84	3,46	2,64	0,77	1,71	0,30

Table 8.3: Overview of estimated serviceability limits of the Tidal Bridge and the maximum dynamic response with respect with original versus rotated design.

The change in magnitude of motion is compared to the original design and presented in Table 8.4. For five of the six degrees of freedom the improved design is favourable, solely the magnitude of surge increases with 910%. The magnitudes of the surge motions and accelerations are still of a reasonable magnitude and not extraordinary high. Almost every degree of freedom shows significant decrease in motion. In addition, the increased values are mostly still within the serviceability limit range and the increases magnitude is not disastrous. The governing degree of freedom, the roll rotation, reduces with 70%, but is still exceeding the serviceability limit. The favourable increase in stability and the relatively simple design change of rotating the design 180° substantiate a suitable design proposal.

		Surge		Sway		Heave		Roll		Pitch		Yaw	
		Along x-axis		Along y-axis		Along z-axis		Around x-axis		Around y-axis		Around z-axis	
		[m]	[m/s ²]	[m]	[m/s ²]	[m]	[m/s ²]	[°]	[°/s ²]	[°]	[°/s ²]	[°]	[°/s ²]
Difference compared to original design													
Improved spudpole	Solely current	0,00	-0,02	11,38	0,14	2,03	0,00	13,38	0,24	0,80	0,00	3,77	0,09
	Waves from SW	0,00	-0,02	11,36	0,14	2,04	0,29	13,35	0,46	0,84	0,37	3,77	0,16
	Waves from NE	0,01	-0,13	11,37	0,00	1,92	0,00	12,58	0,01	0,76	0,08	3,78	0,12
Rotated design (& new spudpole)	Solely current	0,00	-0,12	17,91	0,13	5,44	-0,02	13,73	0,24	1,92	-0,04	6,50	0,08
	Waves from SW	0,00	-0,22	17,88	0,14	5,44	0,27	13,68	0,46	1,96	0,33	6,50	0,16
	Waves from NE	-0,02	-0,33	17,98	-0,04	5,21	-0,01	13,65	-0,59	1,80	0,13	6,55	0,03
Optimisation with respect to original [%]													
Improved spudpole	Solely current	2%	-82%	56%	96%	24%	0%	68%	85%	18%	0%	46%	87%
	Waves from SW	1%	-66%	56%	82%	24%	73%	68%	80%	19%	68%	46%	77%
	Waves from NE	8%	-36%	56%	-1%	23%	0%	61%	0%	17%	9%	46%	36%
Rotated design (& new spudpole)	Solely current	1%	-520%	88%	90%	65%	-36%	70%	85%	44%	-40%	80%	80%
	Waves from SW	-1%	-910%	88%	79%	65%	67%	70%	79%	44%	60%	80%	81%
	Waves from NE	-9%	-89%	88%	-13%	61%	-1%	67%	-21%	41%	14%	79%	10%

Table 8.4: Difference and percentage of optimisation between the original design, the improved spudpole design and the rotated design (including new spudpole design)

8.1.3. Initial deck tilting

Waves and current loads both induce rotation to the same side, implying that adding mass to one side of the floater may reduce the amount of motion, Figure 8.6. A disadvantage may be that the bridge is tilted in equilibrium position, if no current or waves are present. Nonetheless, a small amount of tilt in the bridge deck is desired for the drainage of rainwater. The governing roll-rotation that may be present during 5% of the time is estimated as maximum 7,5 degrees and minimum -2,2 degrees. The centre line on which the structure rotates is at $7,7 - (7,7 + 2,2) / 2 = 2,75$ degrees. Shifting the centre rotation line to zero suggests adding a certain amount of ballast to one side that induces an rotation in equilibrium situation of 2,75 degrees. It should be determined whether an initial deck rotation of 2,75 degrees will induce more discomfort than occasional peak rotations of 7,7 degrees. Another option to induce the same effect is to design the bridge deck with a tilted road of 2,75 degrees. In that case additional ballast is excessive. Tilting of the FishFlow turbines will not be effective as the current switches direction and a counteracting effect will be present.

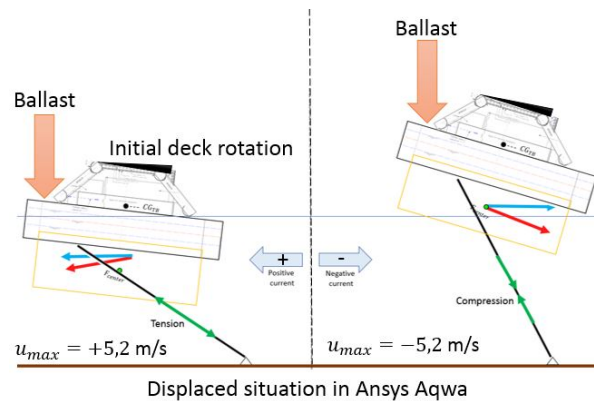


Figure 8.6: Ballast force or initial deck tilting that might counteracting rotation.

8.1.4. Increase in mass

If the mass of the structure increases, the maximum likely motion based on the RAO's of the individual unconnected floaters may shift towards lower frequencies, Figure 8.7. Implying that the floaters will be less effected by short waves (high frequency waves). Currently, the smallest wave frequency estimated in the Strait of Larantuka is 0,14 Hz, the frequency occurs once every 100 years.

If the likely motion of the floaters is shifted towards the lower frequency domain, the peak response values will decrease. A first shift to a lower frequency domain is created by the pendulum system and elaborated in Chapter 7. The RAO-based response of a freely floating floater is decreased with a factor 2,5 compared to the actual displacement, Figure 8.8. The increase of mass may increase the factor even more. A disadvantage of increasing the mass of the structure is an increased draught. An increase in draught results in an increase of the submerged area and hence an increased drag force. All mooring structures need to transfer even higher loads and failure mechanisms should be thoroughly analysed.

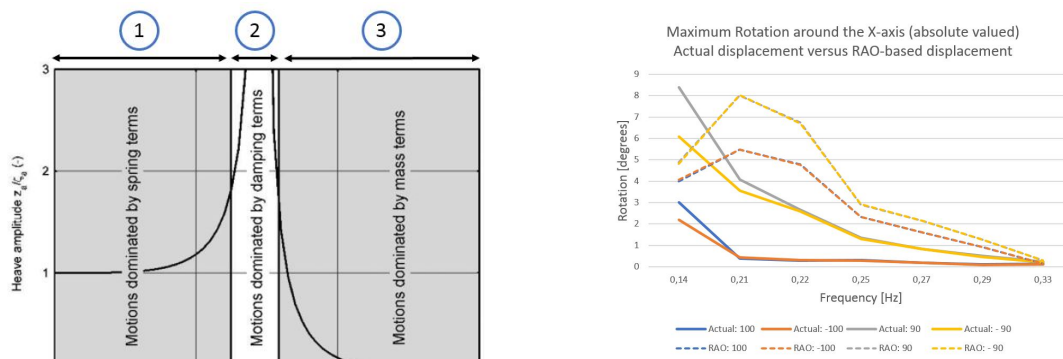


Figure 8.7: Response Amplitude Operator sections

Figure 8.8: Shift to lower frequencies induced by mooring system RAO-based response of individual uncoupled freely floating floater versus the actual response of the coupled bridge

8.1.5. Limit vertical displacement

One of the observations is the extreme vertical displacement of the bridge, what indicates that the Ansys Aqwa model is inaccurate. The upwards shift is induced by the forced motion of the pendulum system, the drag force act at a constant distance measured from the centre of gravity of the structure. If the structure moves vertically, the application point of the drag force moves collectively. In reality, the drag force is located under the water line for all conditions.

The design improvement assumes that the Ansys Aqwa predicts a correct dynamic response or that the vertical motion effect induced by the pendulum will be present and of a smaller magnitude. In that case, it may be advantageous to limit the possible vertical displacement by cables and possible an additional mass, Figure 8.9. The cable length should allow some motion, for example the combined motion induced by the tides and the pendulum. Cables should be implemented at both sides of the floater to counterbalance rotations that may be induced by the other cable. The restriction of the heave-displacement may result in a favourable decrease in likely motion for all degrees of freedom. The extreme displacements and rotations of the coupled system are damped.

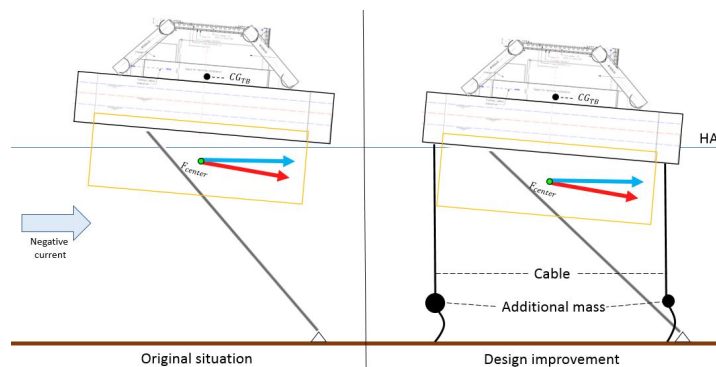


Figure 8.9: Example of design that restricts vertical displacement

In reality, the stabilising effect of the FishFlow turbines should be determined. It is probable that the stabilising effect already secures the pontoons underneath the waterline and limitation of vertical displacement is not desired. Hence, it is strongly suggested to test the FishFlow turbines and conduct the hydraulic properties and implement the data in an accurate model.

8.1.6. Adjust pendulum angle

The pendulum system rotates and as a result, the force distribution varies continuously. During low water level the angle between the pendulum and the seabed approaches 36° and at high water level this becomes 44° . A steep angle may result in a decrease in vertical pressures and fewer roll-rotations induced by the current, Figure 8.10. The influence of rotations induced by waves will not be affected with an increase in angle steepness as the rotation point of the pendulum does not change.

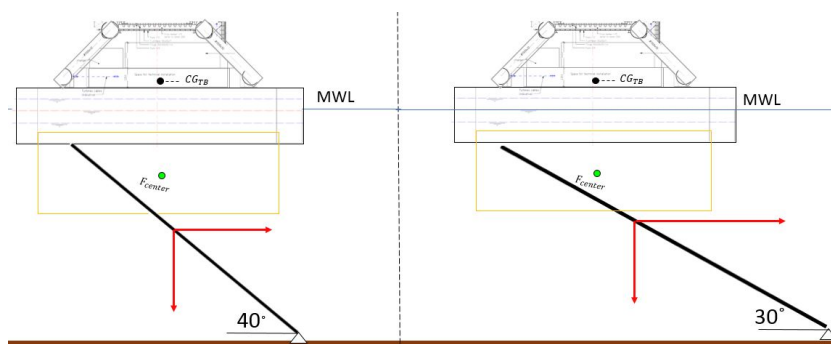


Figure 8.10: Narrow angle and elongation of pendulum change may influence force distribution

The change in water level due to the tidal range fluctuates the pendulum angle. The relation between the current velocity and the tidal water level is checked, low water level is mainly present at negative current velocities, Figure 8.11. The effect of the tidal range is assumed to be in favour for the original design, high motion arised at *negative* flow speeds and a decrease of motion is probable for a steeper pendulum angle, which occurs at low water. The design suggestion that rotates the bridge 180 degrees may result in less benefits to the stability as the governing flow speed direction is switched from negative to positive. The effect of an increased pendulum angle to the stability of the system is assumed to be relatively small.

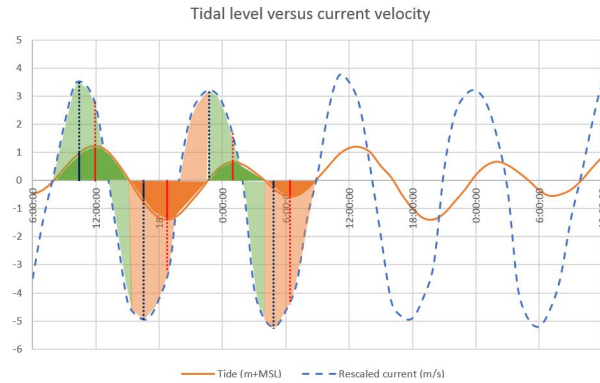


Figure 8.11: Current velocity during respectively high tide and low tide. Peak values lines are displayed for simplifying the interpretation of the graph.

8.1.7. Use of hydraulic springs

The Aqwa model indicated that the bridge will be constantly in motion by the waves. The reaction of the floating structure to the motion induced by the pendulum system is an instantaneously reaction that emerges suddenly. The result is a very abrupt motion change and anything except a gradual transition between rotations. The rapid motion change can be reduced by embedding dampening components in the pendulum. An example is the use of piston gas spring pendulum, illustrated in Figures 8.12 and 8.13. It is probable that the motion induced by waves reduces significantly with the use of hydraulic springs. Nonetheless, disadvantages of the use of hydraulic spring are present at high flow speeds. It is probable that the springs will be fully compressed or extended in severe current velocities and that the dampening effect is overruled by the severe drag forces. In addition, the springs should be able to transfer very high pressures without collapsing. Frequent maintenance checks should be performed to indicate early signs of failure. Total failure of the hydraulic spring will result in a total collapse of the bridge, which is a catastrophic event.

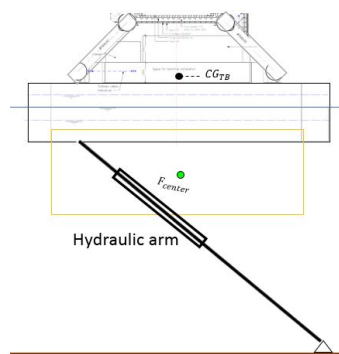


Figure 8.12: Implementation of hydraulics spring pendulum system

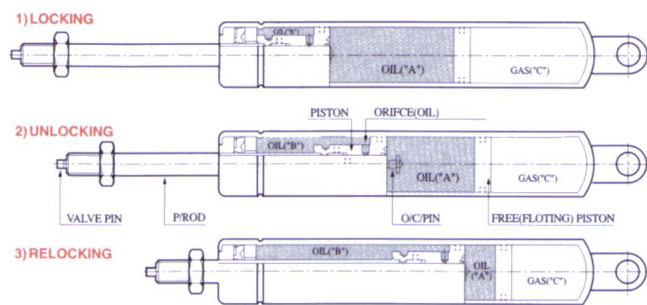


Figure 8.13: Example of a piston gas spring pendulum (Lucid Int., 2019)

It may also be effective to design hydraulic springs at the centre two pendulums. The forces present in the two pendulums are significantly smaller than the forces in the other pendulums, Figure 8.14. The combined bridge motion will presumably reduces as well.

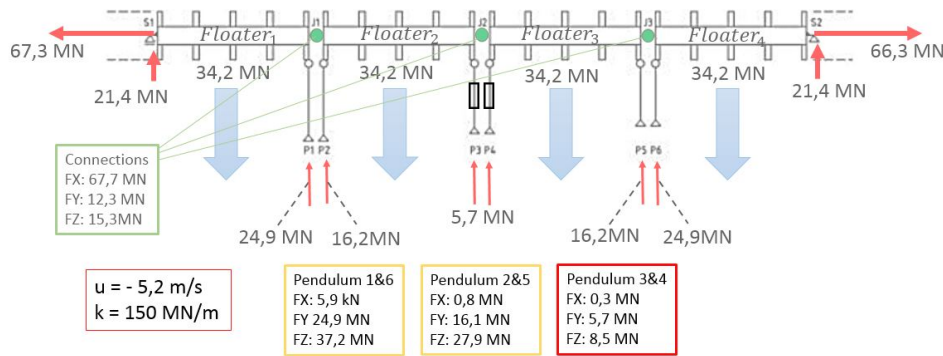


Figure 8.14: Force distribution in Tidal Bridge for negative current of 5,2 m/s. Hydraulic springs solely applied at the two centre pendulums.

8.2. Deliberation of alternatives

The proposed design suggestions are just a few of the possibilities to increase the stability of the present Tidal Bridge design. The most favourable combination of design improvements should be determined by testing all combinations of scenarios. Additional research and analyses are obligatory and strongly recommended for the second phase of the feasibility design of the Tidal Bridge. A first estimation of the effectiveness of the design improvements is considered in the paragraph. The design improvements are scored and an overview is presented in Table 8.5. The computation and interpretation of the scores are elaborated shortly.

		Waves	Current	
1	Improved spudpole design	0/+	+++	Verified
2	Rotated of 180 degrees	+	++	Verified
3	Initial tilt of structure	0	++	Uncertain
4	Increase of mass	+	-	Uncertain
5	Limitation of vertical displacement	+	-/+	Uncertain
6	Change in pendulum angle	0	0/+	Uncertain
7	Hydraulic spring in pendulum	++	0	Uncertain

Table 8.5: Probable efficiency of design suggestions. + indicates probable increase in stability, - means negative effect, 0 is no effect.

The improved spudpole design and the complete rotation of the bridge design are verified in Ansys Aqwa. The combination of the two improvements results in 70% of increased stability compared to the original design. The decrease in magnitude of motion and acceleration for the most severe scenario with a current and north-western waves is presented in Figures 8.15 and 8.16. The figures indicate the serviceability limits, an assumption of the magnitudes of displacement of the serviceability limits in X, Y and Z-direction is based upon the tidal range and the spudpole displacement and plotted as a dashed line. Serviceability limits are exceeded for roll and pitch motion and for surge and heave acceleration. However, the combination of the two proposed design suggestions seems effective. The inaccuracy in the Aqwa model should be solved to indicate the exact percentage of improvements.

		Surge		Sway		Heave		Roll		Pitch		Yaw	
		Along x-axis	Along y-axis	Along x-axis	Along y-axis	Along z-axis	Along z-axis	Around x-axis	Around x-axis	Around y-axis	Around y-axis	Around z-axis	Around z-axis
		[m]	[m/s ²]	[m]	[m/s ²]	[m]	[m/s ²]	[°]	[°/s ²]	[°]	[°/s ²]	[°]	[°/s ²]
Serviceability limits		-	0,50	-	0,50	3,00	0,70	2,52	6,13	2,01	4,01	3,44	2,86
Original design	Wave from NE	0,17	0,37	20,47	0,32	8,53	0,78	20,49	2,87	4,44	0,90	8,26	0,33
Improved spudpole	Wave from NE	0,16	0,51	9,10	0,32	6,60	0,78	7,90	2,86	3,68	0,82	4,48	0,21
Rotation & spudpole	Wave from NE	0,19	0,71	2,49	0,36	3,32	0,79	6,84	3,46	2,64	0,77	1,71	0,30
Optimatisation with respect to original design [%]													
Improved spudpole	Wave from NE	8%	-36%	56%	-1%	23%	0%	61%	0%	17%	9%	46%	36%
Rotation & spudpole	Wave from NE	-9%	-89%	88%	-13%	61%	-1%	67%	-21%	41%	14%	79%	10%

Table 8.6: Overview of estimated serviceability limits of the Tidal Bridge and the maximum dynamic response with respect governing waves and current.

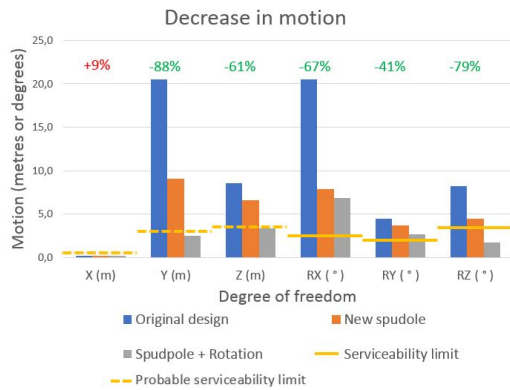


Figure 8.15: Bar diagram illustrating the decrease in motion to two design improvements

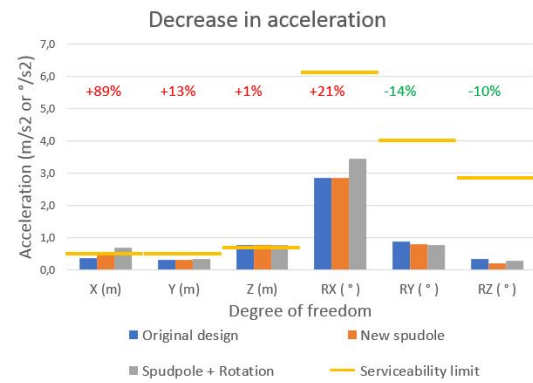


Figure 8.16: Bar diagram illustrating the decrease in acceleration to two design improvements

The other design suggestions are not verified in Ansys Aqwa, however the efficiency is estimated based on logic and assumptions. The third suggestion, the tilting of the system, may halve the roll-rotations induced by the current, but will not be effective for wave rotations as the wave induced motions fluctuate around the 'current-induced-rotation-line'. A disadvantage of initial tilting is that in the equilibrium position, if the current approaches zero, the deck is tilted and may result in unnecessary discomfort. In addition, the stability calculation indicated that the bridge will rotate to both sides, not solely a positive rotation as the Ansys Aqwa model indicates.

The increase of the mass of the bridge may shift the motion peak of the floaters towards lower frequency waves. The frequency shift results in dampening of the wave-induced motion for the estimated wave spectrum. The exact wave spectrum is unknown and therefore, the measure should be analysed again if the wave states are established. The mass increases the draught of the pontoons and thus the submerged area. The drag forces increase and the increase in force should be considered in the design of the mooring components. In addition, higher forces cause an increase in rotation and the measure may be counter-effective.

Fifth measure is limiting the vertical displacement with cables. The measure is only beneficial if indeed extreme vertical motion will be present. Currently, the induced vertical motion is assumed to be a result of an inaccuracy in the Ansys Aqwa model. The expected behaviour will be less severe as a result of the stabilising effect of the water body in the turbines. Next to the inaccurate computed vertical displacement, construction of cables in the volcanic subsoil and in high flow speeds is complex and expensive. The effect of this counteracting measure is doubtful.

The variation in the pendulum angle results in a different force distribution and preventing the 'flipping' of the system. The effect on stability will not be significant, wave induced rotations will not have any effect and the suspected effect on current induced pressures is small.

At last, the implementation of a hydraulic springs that dampen the wave induced rotations is proposed. The idea of dampening the wave induced rotations seems very beneficial. However, the execution may be questionable. The springs should be able to transfer very high forces and maintenance is complex due to the high flow speeds. In addition, the springs will be fully compressed or extended in maximum flow speeds and the counteracting measure will not be as efficient as it will be if the flow speed approaches zero. Nevertheless, it is probable that the probability of fatigue failure of all structural components will decline heavily. The continuous abrupt motion variations may disappear and the overall stability of the bridge might increase genuinely. Therefore, it is suggested to analyse and verify whether implementation of hydraulic springs will be technical feasible.

Combining all information and the scores in the table, it is recommended to implement the *improved spudpole design* and the *180 degree rotation* in the next stage of the Tidal Bridge development study. In addition, investigation on the technical feasibility and implementation options of *hydraulic springs* is endorsed. At last, it is suggested to conduct additional research on the stabilising FishFlow effect and vertical displacement. If the research confirms the vertical displacement, the increase of mass or restriction of vertical displacement by cables may be effective.

Summary: Chapter 7: Sensitivity analysis

The chapter is based on the question of which stabilising measures may influence the dynamic response of the Tidal Bridge: "What are design suggestions that improve the stability of the bridge?" A total of seven alternatives are proposed that may increase the stability of the Tidal Bridge. An illustration of the seven design improvements is presented in Figure 8.17. The alternatives are scored in Table 8.7. The effect of the first two alternatives is checked in the Ansys Aqwa model and significant decrease of motion is confirmed. The effectiveness of the other five alternatives is discussed and elaborated.

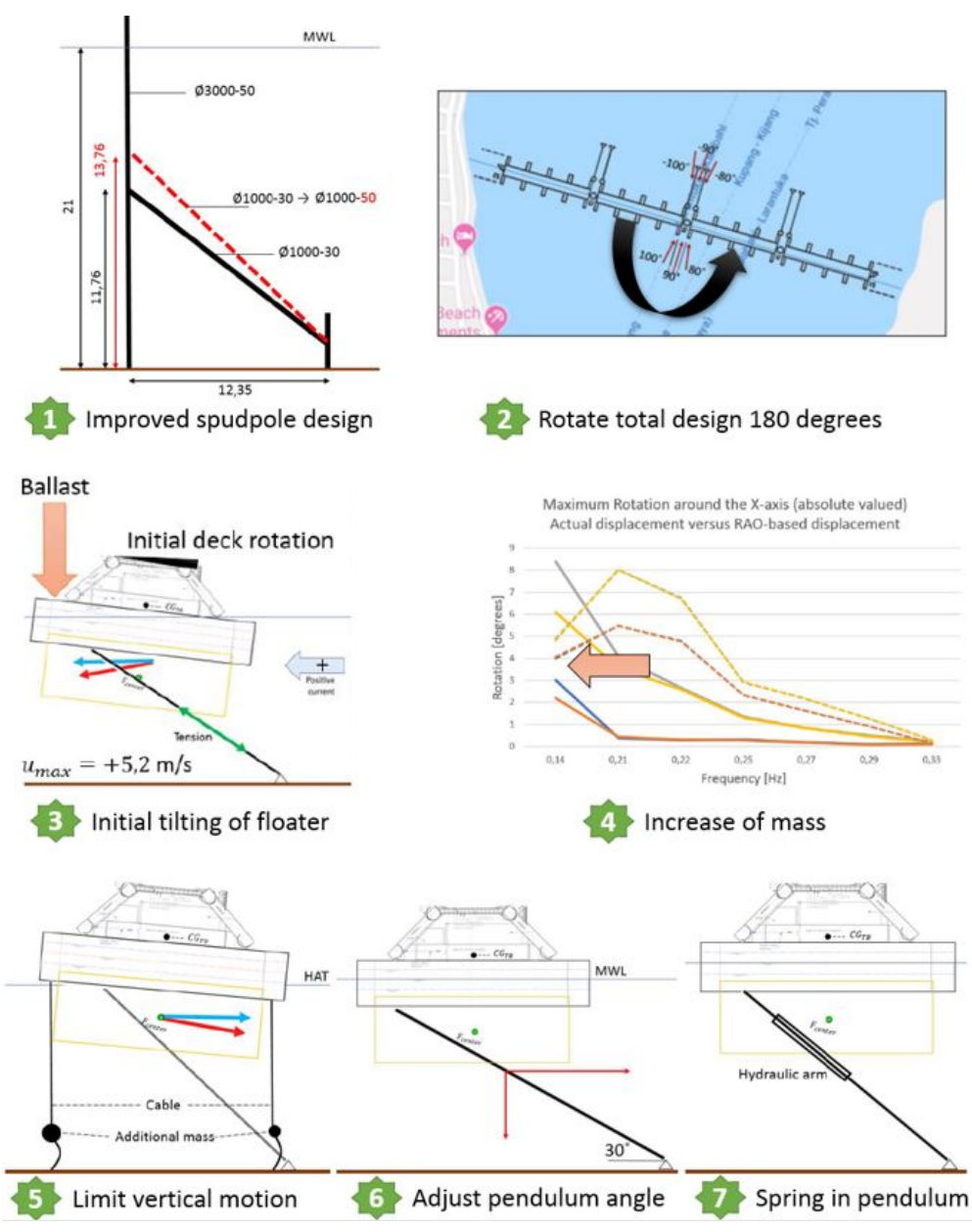


Figure 8.17: Illustration of proposed alternatives that may increase stability

Summary: Chapter 8: Design suggestions

		Waves	Current	
1	Improved spudpole design	0/+	+++	Verified: 66%
2	Rotated of 180 degrees	+	++	Verified: max 73%
3	Initial tilt of structure	0	++	Uncertain
4	Increase of mass	+	-	Uncertain
5	Limitation of vertical displacement	+	-/+	Uncertain
6	Steeper pendulum angle	0	0/+	Uncertain
7	Hydraulic spring in pendulum	++	0	Uncertain

Table 8.7: Overview of design suggestions and probable efficiency.
+ indicates probable increase in stability, - means negative effect, 0 is not effected.

It is recommended to implement the **improved spudpole design** and the **180 degree rotation** in the next stage of the Tidal Bridge development study. The combined effect of both alternatives may result in a **total decrease of roll-rotation for current induced pressures of 70%**, from 19,68° to 5,95°. The change in design results in beneficial effects with respect to motion for almost every degree of freedom, Figure 8.18. Nonetheless, **the serviceability limits are still exceeded** for waves present during of 5% of the time. The effect on accelerations is not beneficial, Figure 8.16, yet the peak values are still in the range of, or lower than, the serviceability limits. Therefore, the combination of the improved spudpole design and the rotated bridge is considered as effective.

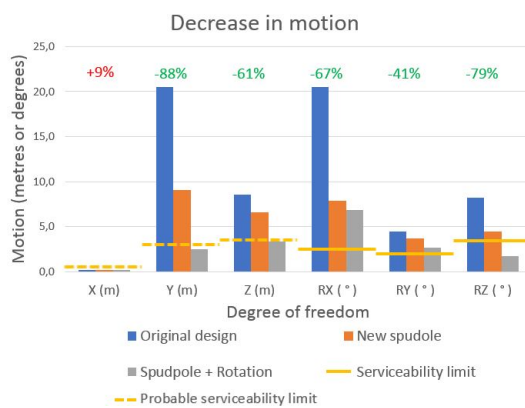


Figure 8.18: Bar diagram illustrating the decrease in *motion* to two design improvements

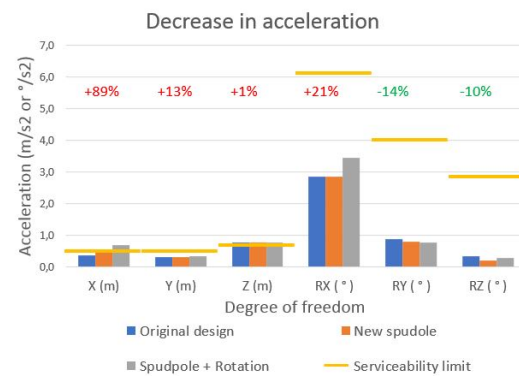


Figure 8.19: Bar diagram illustrating the decrease in *acceleration* to two design improvements

In addition, investigation on the technical feasibility and implementation options of **hydraulic springs** is endorsed as the **dampening effect on waves** is profitable. At last, it is suggested to conduct additional research on the stabilising FishFlow effect and vertical displacement. If the research confirms the vertical displacement, the increase of mass or restriction of the vertical displacement by cables may be effective.

IV

Outcome of the research

The fourth part combines all previous gathered information into one final conclusion to the research question. The report content is discussed and recommendations are stated.

9

Conclusions and recommendations

This chapter summarises the important observations and results to answer the research question. The content of the report is discussed and recommendations on future research are stated for future design studies or to substantiate assumptions. The project questions are answered and a summary of the research is formed.

9.1. Answers to project questions

The project questions are stated and the answers on the questions are given in this section. The conclusion of the research is based on the results of the subquestions and this is discussed.

Is the dynamic response of the present design of the Palmerah Tidal Bridge induced by waves and currents of an acceptable magnitude regarding traffic serviceability?

1. *What data is required to compute the likely motion of the Palmerah Tidal Bridge?*
 - (a) What are the governing hydraulic conditions at the project location?
 - (b) What types of loads are probable to induce significant motion?
 - (c) What are the dynamic properties of the Palmerah Tidal Bridge?
2. *Is the Palmerah Tidal Bridge stable enough to allow traffic safely across the bridge?*
 - (a) How can the Tidal Bridge be implemented in a virtual model?
 - (b) What is the dynamic response of the Tidal Bridge and what loads induce governing motion?
 - (c) What are design suggestions that improve the stability of the bridge?

9.1.1. Subquestion 1

The first subquestion is focussed on the data analysis and is split in three sections: the project specific conditions, the governing loads and the dynamic bridge properties. The data found is implemented in the virtual model.

IA: Project specific conditions

Serviceability limits are estimated to indicate the tolerable motion of the bridge deck for safe traffic passage. The limits are presented in Table 9.1. The limits are based upon four reference cases: two floating highway bridges in Norway, a study of the University of Singapore and upon limits stated in guidelines. None of the reference cases is equivalent to the Tidal Bridge as the majority of the bridges function as a highway and the Tidal Bridge is designed as a very dynamic bridge.

	Surge		Sway		Heave		Roll		Pitch		Yaw	
	Along x-axis		Along y-axis		Along z-axis		Around x-axis		Around y-axis		Around z-axis	
	[m]	[m/s ²]	[m]	[m/s ²]	[m]	[m/s ²]	[°]	[°/s ²]	[°]	[°/s ²]	[°]	[°/s ²]
Tidal Bridge	-	0,50	-	0,50	3,00	0,70	2,52	6,13	2,01	4,01	3,44	2,86

Table 9.1: Overview of all serviceability limits of floating bridges

Next, the conditions in the Strait of Larantuka are analysed. The project is located at the equator, nearby the intersection point of four tectonic plates. Fortunately, all adjacent volcanoes are dormant. The volcanic seabed is located at an average depth of 25 m below MSL. Hydraulic data is limited and the sea state is determined with maximum hourly wind data that is extrapolated according to various probability distributions. The governing significant wave heights are calculated according to the Young and Verhagen equations for the desired downtime of 5%, and return periods once every 1 year, 50 years and 100 years. The significant wave height of a wave that arises 5% of the time is $H_s = 0,80$ m with a frequency of 0,22 Hz. The maximum wave that originates once every 100 years has a significant wave height of 2,26 m and a frequency of 0,15 Hz. The semi-diurnal tide with a tidal range of 3 m results in flow speeds up to 5,2 m/s. The considered maximum current velocity is directed from the north-east and has a magnitude of 5,2 m/s.

IB: Governing loads

The bridge has a weight of 22,8 MN which is in balance with the upwards water pressure. The draught that results in the balance of forces is approximately 3 m. Next to the mass of the bridge, the distribution of extreme traffic results in pitch and roll motions. The governing loads on the structure are the wave and current induced pressures. The applicable wave theory is the third order Stokes wave theory, but as the sea spectrum is uncertain, the main loads are determined by the linear wave theory.

The flow velocities induce significant drag forces on the submerged parts of the bridge. The drag coefficient of the combined turbine-pontoon structure is estimated according to the force distribution of a CFD-model, resulting in a drag force for the combined pontoon-turbine structure of $C_d = 2,11$. The maximum moment allowed around the x-axis is 2,1 MNm/m and arises at a flow velocity of 5,2 m/s. The absence of possible validation, verification or calibration of the drag forces results in uncertainty and inaccuracy of the dynamic response as a result of current induced pressures. Therefore, solely the dynamic response of a perpendicularly directed current is studied. In addition, the water body that flows through the turbine tubes will probably stabilise the likely motion. The magnitude of the stabilising effect is too complex to estimate without scale-model tests.

IC: Dynamic properties

The structural dynamics theory is considered to indicate the governing frequencies of the system which may result in an extreme likely motion, namely the natural frequencies. The bridge may move in all six degrees of freedom and the dynamic response is calculated in the frequency domain and the time domain. The natural frequencies and hydrostatic stiffnesses of the 100 m long freely floating structures are calculated for the three main degrees of freedom for offshore structures: heave, roll and pitch. An overview of the structural properties is presented in Table 9.2.

Mode	Axis		Hydrostatic stiffness		Frequency [Hz]	Period [s]
Heave	z	k_z	7 518 758	[N/m]	0,287	3,49
Roll	x	k_φ	607 767 558	[Nm/rad]	0,268	3,73
Pitch	y	k_θ	7 299 345 191	[Nm/rad]	0,327	3,06

Table 9.2: Main structural properties of the freely floating Tidal Bridge floaters

The hydrostatic stiffnesses are used for a first indication of the magnitude of rotation induced by the drag force. One 100 metre long floater is connected to two mooring pendulums and subjected to the maximum drag force. The first indication of the roll-rotation induced by current pressures is found to be $6,74^\circ$. The direction of the rotation varies with the current direction, but remains to have the same magnitude. The rotation is visualised in Figure 9.1.

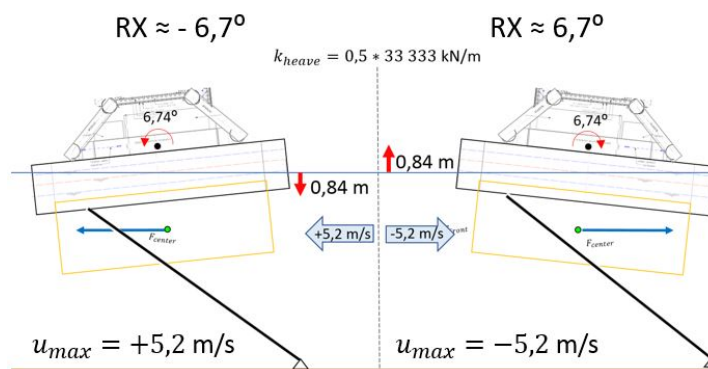


Figure 9.1: First indication of the rotation induced by the drag force, based upon the hydrostatic stiffness.

9.1.2. Subquestion 2

The second subquestion considers the motion analysis. The analysis is divided into three separate studies: the model set-up study, the sensitivity study and the study on stability improving measures. The main results of the three sub-studies form the answer to the second subquestion.

2A: Model set-up

The software package Ansys Aqwa is found to be applicable to estimate the likely response of the Palmerah Tidal Bridge to *wave* induced pressures. The Ansys Aqwa software is less accurate to estimate the response of structures to *current* velocities. The virtual bridge model is created by the use of various (sub)programs and elaborated in Appendix G. The hydrostatic properties computed by Aqwa correspond to the structural properties stated in Table 9.2. The sea state is defined according to a matrix with 50 frequencies acting in 35 directions and is present in the Frequency Domain. The likely motion of a freely floating floater to the wave spectrum is computed with Response Amplitude Operators. The RAO-plot is examined and the computation of the likely response of a *single* floater to waves is verified. The 'actual' response of all *fully coupled* bridge components is computed in the Time Domain. The total bridge is subjected to *irregular* waves distributed according to a JONSWAP wave spectrum and to *regular* second order Stokes waves.

Ansys Aqwa has limitations regarding the implementation of current induced forces. Hence, the drag force is defined manually. The best suitable implementation option is selected out of three possibilities: the current force coefficient matrix, the structure force matrix and horizontal point forces. The most suitable drag force implementation method is the Structure Force Matrix as this is the only method in which a force is defined over a period of time. The other two methods consider an instantaneous load that induces severe oscillations. None of the methods indicate an accurate approximation of the dynamic response during *negative* flow velocities. In all drag force computation methods, the two centre floaters are located above the water level, visualised in Figure 9.2. In reality this effect is prevented by the turbines. The water that flows through the turbines 'secures' the floaters below the waterline. The stabilising effect of the turbines is unknown, hence the Ansys Aqwa model can not be calibrated. The dynamic response as a result of a *positive* current is approximately 6° , the same magnitude as indicated by the stability calculations. It is assumed that the response during a *positive* current velocity is resembles the probable response.

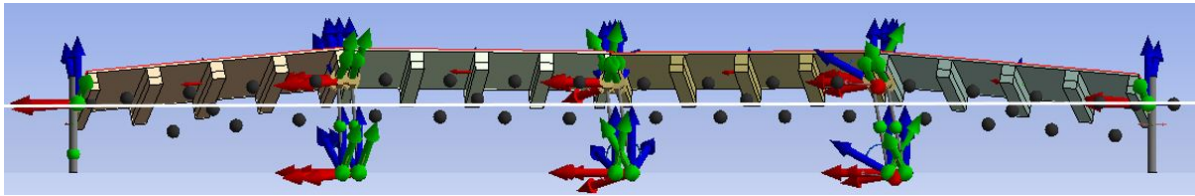


Figure 9.2: Front view of the system at a *negative* flow speed, white line indicates the waterline. (The arrows represent the internal axis of each component.)

The mainland connections (the spudpoles) allow vertical displacement and limited horizontal displacement. Ansys Aqwa considers every structure as an infinitely stiff body and does not consider horizontal displacement as a result of bending of the spudpoles. The behaviour of the spud constructions is mimicked by defining cables with certain stiffnesses and initial elongations. An overview of the virtual bridge model including nomenclature and the characteristic Ansys Aqwa axis system is presented in Figure 9.3.

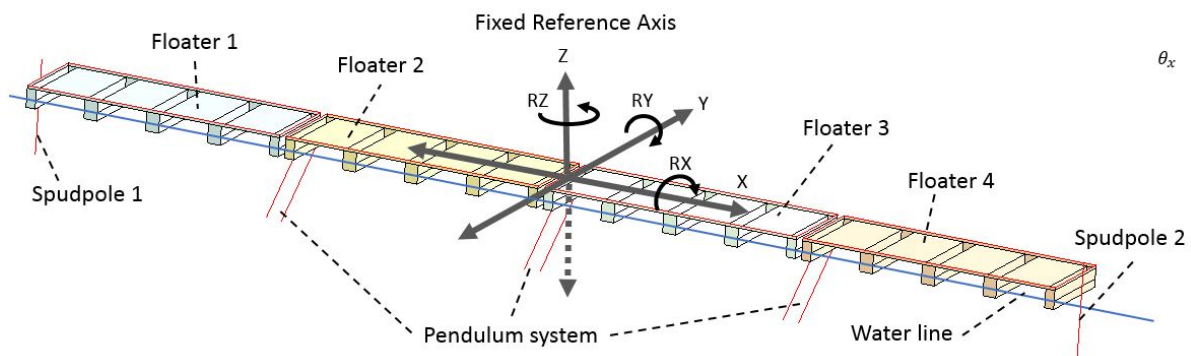


Figure 9.3: Geometry of the Ansys Aqwa model, including rotated axis system and nomenclature.

2B: Sensitivity Study

The sensitivity study shortly elaborated on rotations induced by static traffic loads. The maximum roll-rotation induced by traffic is approximately 1,00 degree and the amount of pitch rotation 1,12 degrees. Secondly, the sensitivity of the behaviour of the bridge to different wave combinations is found. The likely motion of the bridge to a full sea state is computed with Response Amplitude Operators (RAO) for every degree of freedom in the Frequency Domain. The RAO's are based upon *uncoupled individual* freely floating 'floaters' which are not connected to the mooring system. The peak values of the likely motion are primarily in the range of the natural frequencies of the bridge, between 0,21 and 0,27 Hz. The RAO's imply that the governing motional directions are roll-rotation and vertical heave displacement.

The likely response of the fully *coupled* bridge system is calculated in the time domain. The magnitude of motion for the coupled system is 2,5 times smaller than the RAO-based response. This decrease of motion is favourable. The reduction of motion is a result of the restricted freedom as a result of the mooring system. In addition, motion peaks are visible at lower frequency, implying a shift of the natural frequencies towards lower values. The bridge is subjected to *irregular* and *regular* waves during a period of one hour. The *irregular* waves are shaped according to a JONSWAP wave spectrum distribution and the *regular* waves have a shape proportional to a second order Stokes wave. The extreme displacement, rotations and accelerations are found for the governing waves. The motion of the bridge is maximum for low frequency waves ($\approx 0,14$ Hz) perpendicular ($+90^\circ$) directed to the bridge deck. The shape of a Stokes wave increases the likely motion. The response peaks that as a result of waves that will be present during 5% and once a year are presented in Table 9.3. The estimated serviceability limits are already exceeded for wave induced rotations only.

	Surge		Sway		Heave		Roll		Pitch		Yaw	
	Along x-axis [m]	[m/s ²]	Along y-axis [m]	[m/s ²]	Along z-axis [m]	[m/s ²]	Around x-axis [°]	[°/s ²]	Around y-axis [°]	[°/s ²]	Around z-axis [°]	[°/s ²]
Serviceability limits	-	0,5	-	0,5	-	0,7	2,52	6,13	2,01	4,01	3,44	2,86
Wave properties	Irregular JONSWAP wave spectrum Analysis (H_s)											
Downtime of 5%	0,04	0,22	1,99	0,27	0,69	1,35	2,56	5,39	1,26	2,65	0,17	0,34
1 year	0,05	0,22	4,01	1,33	1,26	1,51	10,69	11,03	1,68	2,39	1,20	1,24
Wave properties	Regular Second Order Stokes Analysis (H_{max})											
Downtime of 5%	0,02	0,08	3,47	0,12	0,54	1,08	1,69	2,82	0,54	1,13	0,07	0,16
1 year	0,07	0,23	5,26	1,84	1,89	2,13	15,69	12,45	2,03	2,48	1,82	1,76

Table 9.3: Overview of estimated serviceability limits of the Tidal Bridge and the maximum dynamic response with respect to waves.

Next, the dynamic response induced by the flow velocity is found. The tidal cycle is shaped according to a sine-function with an amplitude of 5,2 m/s in the Ansys Aqwa model. The duration of the tidal cycle is shortened as the current forces will not induce extreme accelerations, but solely a gradual change in rotation of the floater. An increased time-duration will not have effect on the magnitude of motion induced by the current. The tidal range is not defined in Ansys Aqwa, as a change in water level can not be implemented.

The sensitivity to current induced pressures is analysed by varying the properties of the spud construction. An increase in bending stiffness of the spudpole results in severe decrease of motion and accelerations. The 'connection sleeve' of one of the spudpoles allows initial 'frictionless' displacement to adapt smoothly to the tidal range. An increase in initial distance is linearly proportional to an increase in motion. The model inaccuracy during negative drag forces indicates that the middle two floaters are still located above the waterline with the improved spudpole design. The relation between the roll-rotation to an increased bending stiffness (k) is presented in Figure 9.4. The first peak is of the same magnitude as the rotation calculated in the stability analysis. The second rotation peak in the figure indicates the model inaccuracy.

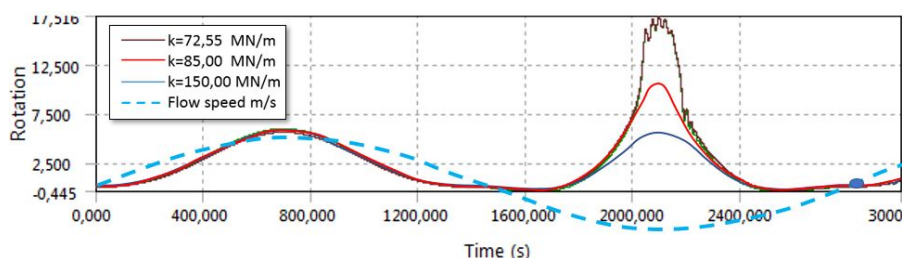


Figure 9.4: Rotation around the x-axis for total tidal cycle with three magnitudes of bending stiffnesses

The dynamic response to the combination of wave and current induced pressures is determined and the results are presented in Table 9.4. The table indicates that the main rotations are induced by the current velocity and that the accelerations are a result of the response of the system to waves. The serviceability limits are exceeded in every scenario, implying that the present Tidal Bridge design is not feasible with respect to safe traffic passage.

	Surge		Sway		Heave		Roll		Pitch		Yaw		
	Along x-axis [m]	[m/s ²]	Along y-axis [m]	[m/s ²]	Along z-axis [m]	[m/s ²]	Around x-axis [°]	[°/s ²]	Around y-axis [°]	[°/s ²]	Around z-axis [°]	[°/s ²]	
Serviceability limits	-	0,50	-	0,50	3,00	0,70	2,52	6,13	2,01	4,01	3,44	2,86	
Waves	Current												
from SW	No	0,13	0,01	3,51	0,08	0,06	0,07	0,12	0,25	0,10	0,08	0,03	0,04
from NE	No	0,14	0,09	3,36	0,28	0,49	0,83	1,70	2,96	0,41	0,61	0,11	0,16
No	Yes	0,15	0,02	20,27	0,15	8,41	0,05	19,68	0,28	4,38	0,09	8,16	0,10
from SW	Yes	0,15	0,02	20,25	0,17	8,42	0,40	19,65	0,57	4,44	0,54	8,16	0,20
from NE	Yes	0,17	0,37	20,47	0,32	8,53	0,78	20,49	2,87	4,44	0,90	8,26	0,33

Table 9.4: Overview of estimated serviceability limits of the Tidal Bridge and the maximum dynamic response with respect to waves.

2C: Design Improvements

The sensitivity study implied the critical factors in the Tidal Bridge design. With the information seven design suggestions that may improve stability are proposed and elaborated. The alternatives are scored regarding the probable effectiveness. These scores are given in Table 8.7.

		Waves	Current	
1	Improved spudpole design	0/+	+++	Verified: 66%
2	Rotated of 180 degrees	+	++	Verified: max 73%
3	Initial tilt of structure	0	++	Uncertain
4	Increase of mass	+	-	Uncertain
5	Limitation of vertical displacement	+	-/+	Uncertain
6	Steeper pendulum angle	0	0/+	Uncertain
7	Hydraulic spring in pendulum	++	0	Uncertain

Table 9.5: Overview of design suggestions and probable efficiency.
+ indicates probable increase in stability, - means negative effect, 0 is not effected.

Two promising alternatives are implemented in an Ansys Aqwa model to substantiate the stabilising effect: the improved spudpole design and a complete rotation of the design, illustrated in Figure 9.5. The combined effect of the two alternatives may result in a total decrease of roll-rotation for current induced pressures of 66%, from $17,5^\circ$ to $5,95^\circ$. If waves are present, an additional decrease of 13% in the dynamic response may originate. Nevertheless, the serviceability limits for roll- and pitch rotation are still exceeded with the design improvements. A substantiated answer to subquestion 2: *"Is the Palmerah Tidal Bridge stable enough to allow traffic safely across the bridge?"* is given. The Palmerah Tidal Bridge is not stable enough to allow traffic across the bridge during a desired downtime of 5%. The serviceability limits are exceeded and continuous motion is present as a result of waves. Dampening of the wave-induced motion is endorsed and may be possible by including hydraulic springs in the pendulum mooring design. At last, additional research on the stabilising turbine effect is obligatory. If the research confirms the extreme vertical displacement, the increase of mass or restriction of vertical displacement by cables may be an effective stabilising measure.

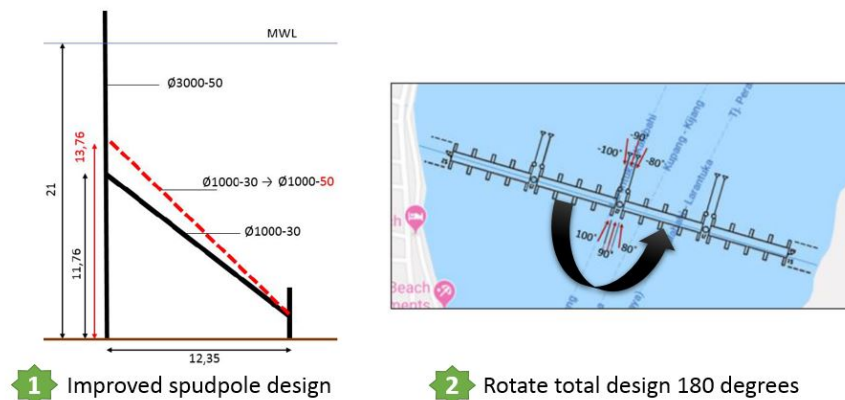


Figure 9.5: Confirmed design improvements: improved spudpole design and rotation of the total design

9.1.3. Conclusion to research question

The aim of this thesis was to answer the question: "Is the dynamic response of the present design of the Palmerah Tidal Bridge induced by waves and currents of an acceptable magnitude regarding traffic serviceability?". The dynamic response of the present design of the Palmerah Bridge will experience severe motions and accelerations as a result of wave and current induced pressures. The motion magnitudes exceed the estimated serviceability limits significantly and the dynamic response is not acceptable for traffic. Especially, the constant accelerations, induced by waves, cause severe discomfort for traffic. The current velocity results in drag forces that induce gradual rotations and limited accelerations. The waves fluctuate around the rotations induced by the current velocities, the plot of the roll-rotation due to flow speeds of + and - 5,2 m/s and north-eastern waves is presented in Figure 9.6.

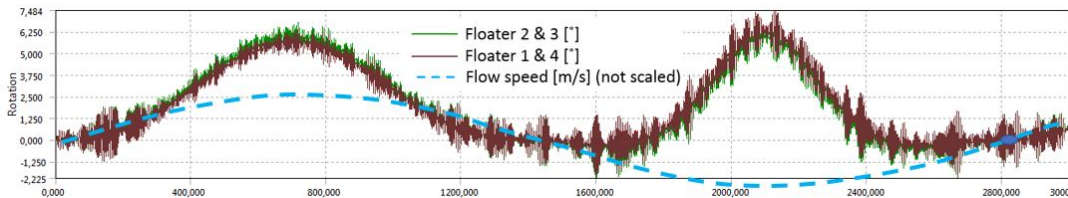


Figure 9.6: Roll rotation around the x-axis with improved spudpole design ($k = 150\text{MN/m}$). North-eastern wave and maximum flow speeds of + and - 5,2 m/s

The modelling software Ansys Aqwa is accurate to indicate wave-induced motion, but the software has limitations regarding the computation of current induced motion. The drag forces are implemented manually and act at the centre of gravity of the structure. The governing inaccuracy is that the force moves with the structure in the model. If the structure moves vertically, the 'drag force' moves accordingly. Due to this inaccuracy, the centre two floaters are located above the waterline during *negative* flow speeds, visualised in Figure 9.7. The stability calculation indicates a more probable response. Both responses are illustrated in Figure 9.8. The magnitude of roll-rotation for the stability check and the *positive* flow speed in the Ansys Aqwa model is proportional and suggests a reasonable approximation of the actual dynamic response. The model can not be calibrated as knowledge is absent about the likely motion of the Tidal Bridge.

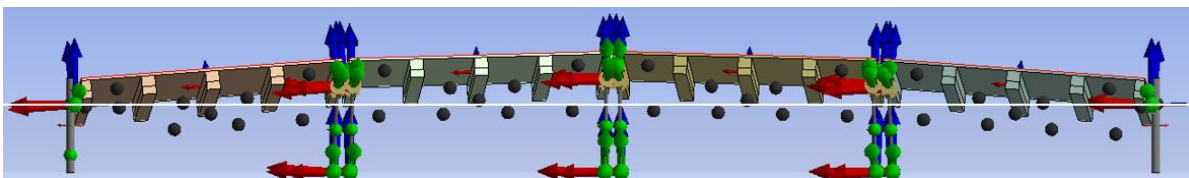


Figure 9.7: Screenshot of displaced Tidal Bridge. Middle two pontoons are located above the water line. Water line is presented as the white horizontal line

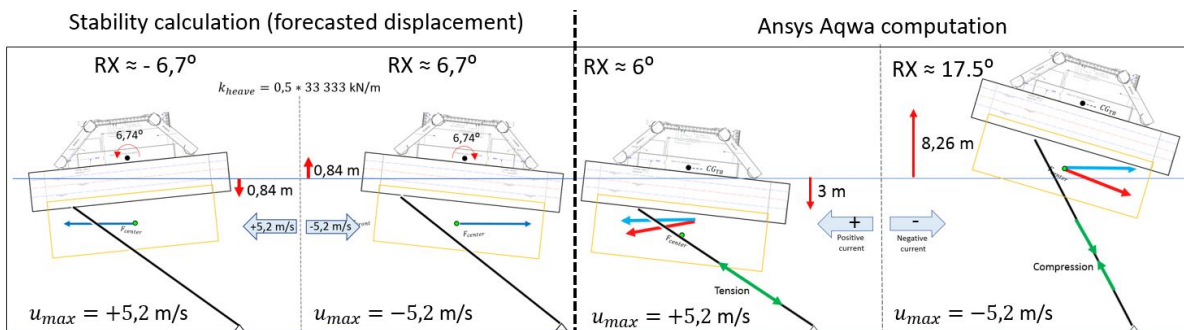


Figure 9.8: Forecasted displacement versus displacement computed by Ansys Aqwa. Both seen with respect to the middle two floaters

Design suggestions are proposed to stabilise the dynamic response of the bridge. The two most favourable design alternatives are implemented in Ansys Aqwa: the improved spudpole design and the full rotation of the present design. The improved Tidal Bridge design approaches the estimated serviceability limits and the feasibility of the conceptual idea becomes more realistic. The dynamic response peaks are given in Table 9.6. Dampening of wave motion is still desired. However, it is likely that the dynamic response of the bridge will be more stable by implementing the correct hydrostatic data of the FishFlow turbines. It is probable that the roll-rotation, vertical displacement and pitch-rotation will reduce in this case. An overview of the maximum motion that originated in one tidal cycle is presented in Table 9.6. The percentage of decrease or increase with respect to the original design and the improved design is illustrated in Figures 9.9 and 9.10. The governing degrees of freedom show an optimisation of 70% compared to the original response.

		Surge		Sway		Heave		Roll		Pitch		Yaw	
		Along x-axis [m]	[m/s ²]	Along y-axis [m]	[m/s ²]	Along z-axis [m]	[m/s ²]	Around x-axis [°]	[°/s ²]	Around y-axis [°]	[°/s ²]	Around z-axis [°]	[°/s ²]
Serviceability limits		-	0,50	-	0,50	-	0,70	2,52	6,13	2,01	4,01	3,44	2,86
Original	Current only	0,15	0,02	20,27	0,15	8,41	0,05	19,68	0,28	4,38	0,09	8,16	0,10
	Wave+Current	0,17	0,37	20,47	0,32	8,53	0,78	20,49	2,87	4,44	0,90	8,26	0,33
Impr. spudpole	Current only	0,14	0,04	8,89	0,01	6,38	0,05	6,30	0,04	3,59	0,09	4,39	0,01
	Wave+Current	0,16	0,51	9,10	0,32	6,60	0,78	7,90	2,86	3,68	0,82	4,48	0,21
Rotation	Current only	0,14	0,15	2,36	0,01	2,97	0,07	5,95	0,04	2,46	0,12	1,66	0,02
	Wave+Current	0,19	0,71	2,49	0,36	3,32	0,79	6,84	3,46	2,64	0,77	1,71	0,30

Table 9.6: The dynamic response of the Tidal Bridge

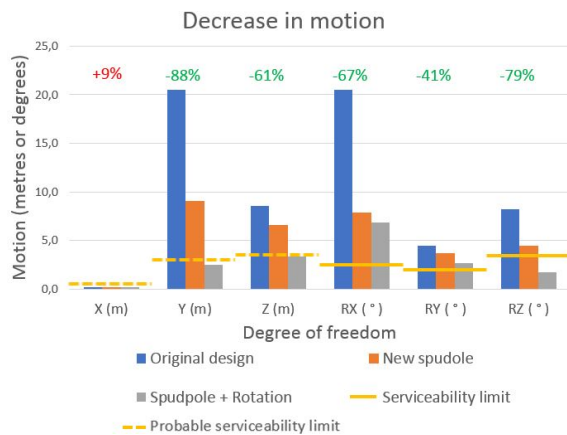


Figure 9.9: Bar diagram illustrating the decrease in motion to two design improvements

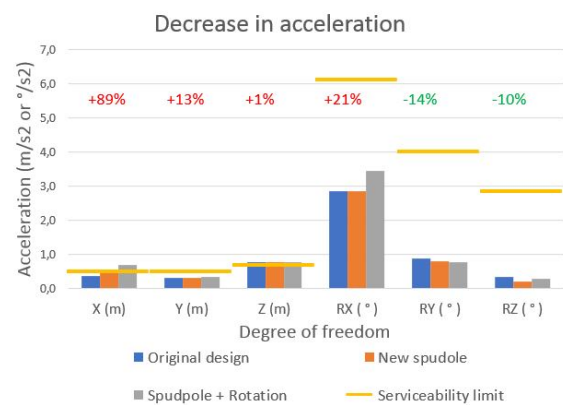


Figure 9.10: Bar diagram illustrating the decrease in acceleration to two design improvements

At the moment, the dynamic response of the Tidal Bridge is not of an acceptable magnitude to allow the safe passage of traffic. With this answer, the research question is defended. Continuing to the Front-End-Engineering-Design stage may prove whether the project can be technically feasible.

9.2. Recommendations

The research is based on a wide variety of (literature based) assumptions. An indication of the actual response of the Palmerah Tidal Bridge can solely be determined if additional data surveys are conducted. If the sea spectrum and current distribution are known, a real estimation of the downtime of the bridge can be found. In addition, the hydrostatic properties of the turbines are critical. At the moment, no data is available regarding the stabilising effect of the FishFlow turbines. The computed dynamic response of the Tidal Bridge is therefore not fully accurate. A list of the most important and uncertain assumptions and the substantiation behind these assumptions is presented.

Data uncertainties

- Sea spectrum in the Strait of Larantuka.
 - Data is based on hourly maximum wind speeds.
- Extended survey on the maximum flow speeds and the current distribution.
 - Flow speeds are based upon maximum tolerable roll-moment.
- Subsoil research to indicate tolerable foundation stiffness.
- Determination of additional loads: wind, eddies, non-uniform waves and the current distribution.
 - One irregular wave group is analysed per model run, instead of an actual sea state.
 - Solely a perpendicular current with a constant water level is defined.
- Determination of the hydrostatic properties of the FishFlow turbines.
 - Drag coefficient is based upon a static CFD-model with perpendicular flow speed.
- Determining and verifying the serviceability limits for a highly dynamic bridge.

The Ansys Aqwa model is not verified or calibrated as any information regarding the magnitude of likely motion is absent. The capabilities of the computational software package of Ansys Aqwa are restricted as well. For example, all structures are infinitely stiff and hence the deformation effects are excluded. The most critical limitation of the virtual model are listed.

Model inaccuracies

- All bodies are seen as infinitely stiff.
 - Torsion, bending and other structural factors are excluded.
- The current drag force on non-tube-shaped elements should be defined manually.
 - All implementation methods act at the centre of gravity of the structure.
 - The drag force 'moves' with the structure.
- Inaccurate FishFlow turbine implementation.
 - Extreme unrealistic motion.
- Solely an uniform current can be implemented.
 - Non-uniformities in the flow distribution a result of the bathymetry are absent.
- The waterlevel is set, the tidal range can not be defined.

In addition, the scope limits the extent of the research. In reality, the technical feasibility should be proven by including all failure possibilities and load combinations. Many other combinations of factors influence the feasibility of the project, some problematic examples are given.

Failure possibilities that are out of the scope

- Fatigue of all components.
- The transfer of forces through the mooring system.
- Failure of structural components: spudpoles, mooring system, connections.
- Failure during construction or transportation.
- Possibilities for maintenance and repair of parts.
- Failure as a result of extreme weather: tsunamis, cyclones, earthquakes, volcanic eruptions.
- Collapse with ships.
- Effect of sea level rise.
- Turbine resistance during extreme sudden (oblique) flow speeds.
- Vortex induced vibrations.

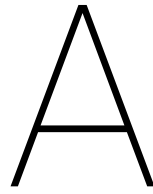
An additional recommendation is to improve the overall design and to optimise the geometry. Steps that could form the base for an improved realistic floating bridge design are given. If the additional design steps are executed, it can be officially concluded whether the realisation of worlds largest tidal water power plant will be feasible.

1. Collecting data.
2. In-depth design study to prove technical feasibility.
3. Scale model tests.
4. Structural analysis for the design, construction stage and maintenance plan.

V

Appendices

Appendix A:	The Palmerah Tidal Bridge
Appendix B:	Determination of serviceability limits
Appendix C:	Boundary conditions
Appendix D:	Load index
Appendix E:	Structural dynamics
Appendix F:	Ansys Aqwa
Appendix G:	Model set-up
Appendix H:	Wave results
Appendix I:	Current results
	Lists of symbols
	References



The Palmerah Tidal Bridge

This appendix contains confidential information and is therefore not included in the public version of the report at the repository of Delft University of Technology.

B

Determination of serviceability limits

This Appendix elaborates upon the magnitudes of tolerable motion limits with respect to traffic, the *serviceability limits*. A serviceability limit is the condition beyond which the structure does not fulfil the relevant function or design criteria. The serviceability limits of the Tidal Bridge imply the condition beyond which the bridge will not be serviceable and should be closed. For the research the limits are not verified or approved as valid reasonable limits, but function as a measuring scale. The estimated serviceability limits are relevant to evaluate and validate the outcome of the dynamic response of the bridge. The magnitudes of the allowable deflections, rotations and accelerations create an impression of realistic motion magnitudes. Nevertheless, additional research should determine whether the tolerable motion assumptions are correct.

B.1. Introduction to motion limits

The Tidal Bridge is designed to provide a safe connection between the islands of Larantuka and Adonara. The serviceability limits indicate whether safe passage is possible to cross the bridge. Verified guidelines are absent, as a highly moving bridge that allows traffic is not incorporated in any code.

Serviceability limits of general fixed bridges can not be compared to dynamic floating bridges. A floating bridge follows the induced motions of the floating 'foundations': the pontoons. As a result, floating bridges allow more deflection and acceleration than fixed bridges. Acceleration limits for floating bridges are stated in a couple of norms. Unfortunately, the applicability of the norms is questionable. Four cases are compared to indicate the possible range of limits. Serviceability limits should be defined in every degree of freedom, Table B.1 and Figure B.1.

1. NEN-ISO 2613: The design code for floating bridges.
2. Research of the University of Singapore. Studybook *Large Floating Structures* by Wang and Wang (2015).
3. The Sognefjord bridge: A design for a floating bridge that will serve as a part of a highway in Norway.
4. The Bergsøysund bridge: A floating bridge that is part of the E39 highway in Norway.

DOF	Symbol	Name	Motion path	Unit
1	x	Surge	Along x-axis	[m]
2	y	Sway	Along y-axis	[m]
3	z	Heave	Along z-axis	[m]
4	ϕ	Roll	Around x-axis	[rad]
5	θ	Pitch	Around y-axis	[rad]
6	ψ	Yaw	Around z-axis	[rad]

Table B.1: Degrees of freedom and directions/rotations

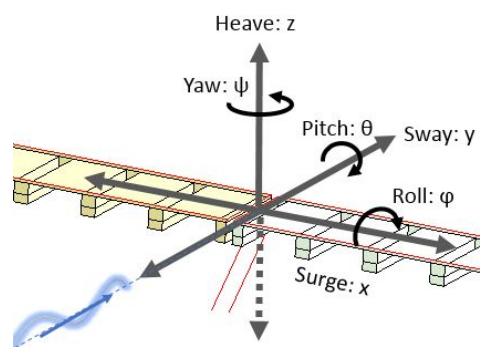


Figure B.1: Visualisation of the motion of a single floating bodies (Heuberger, 2018)

Another aspect of uncertainty regarding the serviceability limits of the Tidal Bridge is the motion plane, Figure B.2. In general, floating bridges experience motion by deformation of the superstructure. The outer bridge ends are rigidly connected and the bridge superstructure is supported by pontoons. Motion occurs by bending, torsion or elongation of the superstructure. An illustration of this type of motion is presented in Figure B.2. The scope of the research assumes infinitely stiff element, hence the bridge components can not bend, twist or elongate, but move as body. It is probable that the motions are 'damped' by structural deformation in the model, the result is an overestimation of the actual motion.

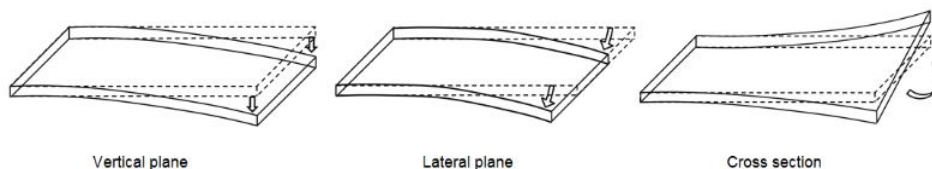


Figure B.2: The different planes in which accelerations and deflections can occur (Wang and Wang, 2015)

B.2. International standard

According to the international norm NEN-ISO 2631, the acceleration limits of floating bridges are based on comfortable driving on the bridge deck during a normal (1-year) storm. The motion limits are based on the objective that people will not experience discomfort walking or driving over the bridge (NEN-EN 2631, 2010) and are presented in Table B.2. The norm is intended for floating highway bridges where a speed limit of approximately 120 km/h is tolerated. The speed limit on the Tidal Bridge is set to 20 km/h, suggesting that the norm is highly conservative for the research.

	Loading condition	Deflection or motion	Max. Deflection	Max. Motion
NEN-ISO 2613	Vehicular load	Vertical	$L/800=0,125$ m	
		Roll (around x-axis)	$0,5^\circ$	$0,05$ rad/s ²
		Sway (along y-axis)	$0,3$ m	$0,50$ m/s ²
	Waves - dynamic	Heave (along z-axis)	$0,3$ m	$0,50$ m/s ²

Table B.2: Serviceability limits floating bridge according to NEN-ISO2631 (2010)

B.3. Requirements obtained from test results (University of Singapore)

A study, that indicates the limits for safe traffic passage over a highly dynamic floating bridge, is conducted by professor Wang in 2015. A professor at the Department of Civil and Environmental Engineering at the National University of Singapore. The study is conducted for research on the book *Large Floating Structures - Technological Advance*, of the serie *Ocean Engineering & Oceanography*.

Driving on top of a floating bridge was simulated with passengers in a bus that drove over existing long-span bridges in Osaka, Japan. Vibration accelerations were measured in the bus and the 36 passengers filled in a questionnaire on riding comfort. Figure B.3 indicates the correlation between the riding comfort index and mean/maximum vertical acceleration measured on the bus floor at the front wheels (Wang and Wang, 2015). However, the test is conducted on a small scale and the outcome is not significant, it only gives an indication of the vertical motion. Extended research on driving comfort is recommended. The pre-feasibility study, conducted by Antea Group, assumes a vertical acceleration of $0,30 g = 3$ m/s². The motion limits according to professor Wang are presented in Table B.3.

Prof. Wang	Deflection or motion	Max. Deflection	Max. Motion
	Roll	2°	$0,035$ rad/s
	Sway (y-axis)	-	3 m/s ²
	Heave (z-axis)	-	3 m/s ²

Table B.3: Serviceability limits floating bridge according to professor Wang (Wang and Wang, 2015)

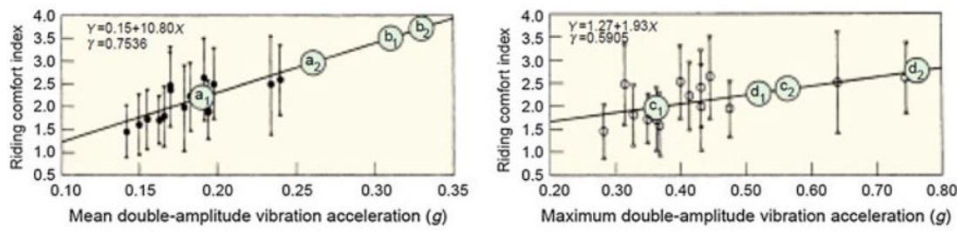


Figure B.3: Correlation between dynamic acceleration and riding comfort index (Wang and Wang, 2015)

With corresponding legend:

1. No peculiar vibration is felt
2. Some vibration is felt, no dis-comfortable vibration is felt
3. Obviously peculiar vibration is felt
4. Considerably large and uncomfortable vibration is felt
5. Extremely large, uncomfortable and uneasy vibration is felt

- a_1 & c_1 Accelerations at MSL under good surface conditions.
- a_2 & c_2 Accelerations at LAT under good surface conditions.
- b_1 & d_1 Accelerations at MSL under bad surface conditions.
- b_2 & d_2 Accelerations at LAT under bad surface conditions.

As a reference for this research, the lecture notes of course "MT2433 Shipmovements" of Delft University of Technology are consulted. Figure B.4 and B.5 indicate correlation between ship accelerations and the degree of motion sickness. In here, 0,3 g indicates an 'unbearable' feeling of motion and can lead to 20 % of sailors getting sick. Suggesting that the test results of The University of Singapore are probably over estimated.

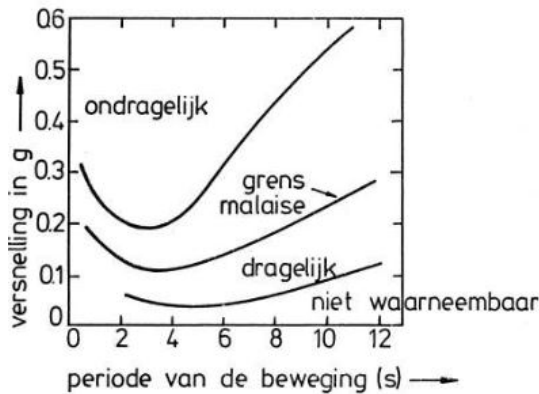


Figure B.4: Human valuation of accelerations with specific periods (Gerritsma, 2003)

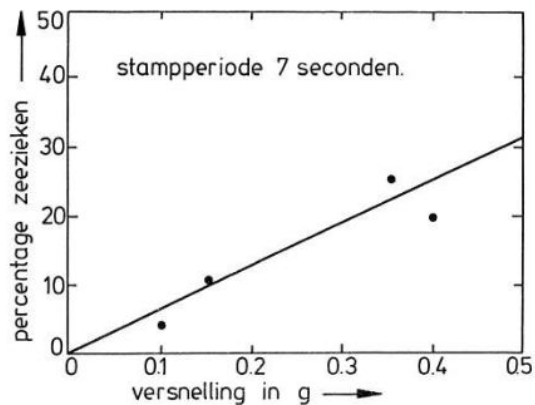


Figure B.5: Percentage of motion sickness during vertical acceleration (Gerritsma, 2003)

B.4. E39 Coastal Highway Project (Norway)

In Norway, many fjords are present with very deep waters in between. The coastal highway E39 is the main transport route of Norway and crosses eight of the deep waters. Currently, the 1 100 km route takes approximately 22 hours as eight ferry connections are located along the highway. Norway wants to eliminate the ferries and construct floating bridges to reduce the travelling time to 9 hours and increasing the trade and industry of the region.

Two bridge design studies of the Norway highway are consulted to compare serviceability limits of floating bridges, the *Sognefjord bridge* and the *Bergsøysund bridge*, both appointed in Figure B.6. The main distinction between the Tidal Bridge and the E39 bridges is the function of a power plant. The bridge mimics the tidal range in order to attain the highest current velocity and hence the maximum power output. This vertical motion is accompanied by horizontal motion induced by the mooring system. All in all, the Tidal Bridge is highly dynamic with respect to the floating bridges along the E39 coastal highway.



Figure B.6: Coastal highway route E39 (Hendriksen, 2018)

Sognefjord bridge

The Sognefjord bridge, is designed as a 3 700 m long bridge that will be supported by 22 floating pontoons. Connecting the highway between Lavik and Oppedal across the Vartdalsfjorden. The bridge will be the longest bridge of the E39 project and the bridge design is part of an ongoing feasibility study of IV Groep. Serviceability limits for this floating highway are set for the rotations, deformations and accelerations, Table B.4 (Hendriksen, 2018).

	Deflection or motion	Max. Deflection	Max. Motion
Sognefjord Bridge	Surge (x-axis)		0,50 m/s ²
	Sway (y-axis)	L/200	0,50 m/s ²
	Heave (z-axis)	L/200	0,70 m/s ²
	Roll (x-axis)	0,044 rad	0,107 rad/s ²
	Pitch (y-axis)	0,006 rad	0,007 rad/s ²
	Yaw (z-axis)	0,06 rad	0,05 rad/s ²

Table B.4: Serviceability limits floating bridge of the Sognefjord Bridge (Hendriksen, 2018)

Bergsøysund bridge

The Bergsøysund bridge is comparable with the Sognefjord bridge but smaller, the bridges are both located in Norway to cross fjords. This bridge is already constructed and opened in 1992. The bridge covers a span of 931 m and is supported with seven concrete pontoons and a steel superstructure. Every 20 years excessive maintenance is required to prevent corrosion, fatigue and brittle failure. The considered serviceability limits are presented in Table B.5 (Heuberger, 2018).

	Deflection or motion	Max. Deflection	Max. Motion
Bergsøysund Bridge	Sway (y-axis)	L/350	0,50 m/s ²
	Heave (z-axis)	L/350	0,70 m/s ²
	Roll (x-axis)	0,044 rad	0,107 rad/s ²
	Pitch (y-axis)	0,035 rad	0,07 rad/s ²
	Yaw (z-axis)	0,03 rad	0,05 rad/s ²

Table B.5: Overview of all serviceability limits of floating bridges

B.5. Serviceability limits of the Tidal Bridge

An estimation regarding the serviceability limits for the Tidal Bridge is based on the four reference cases. A deliberation between the applicability of each case with respect to the Tidal Bridge properties and conditions is made to estimate an indication of limits. Nevertheless, it is strongly suggested to conduct an additional study for this specific case.

Reference case	Applicability to Tidal Bridge	Specifically applied for:
NEN-ISO 2631	Too conservative	Highway (120 km/h), European norm
Prof. Wang	Over-estimated	Bus acceleration
Sognefjord	Conservative	Highway (120 km/h)
Bergsøysund	Conservative	Highway (120 km/h)

It is assumed that the floating bridges in Norway are most representative for the limits of the Tidal Bridge, yet to conservative as the bridges are designed for a highway with a speed limit of 120 km/h, while the speed limit on the Tidal Bridge is 20 km/h. The highest values of the NEN-ISO, the Sognefjord and the Bergsøysund bridge are assumed to be correct. The maximum displacement of the Tidal Bridge will be of a higher magnitude as the bridge is designed to move freely and allows motion. A maximum value for the vertical displacement is set to 3 meters, this is the distance for which the pontoon will be fully submerged. An overview is provided in Table B.6.

	Surge		Sway		Heave		Roll		Pitch		Yaw	
	Along x-axis		Along y-axis		Along z-axis		Around x-axis		Around y-axis		Around z-axis	
	[m]	[m/s ²]	[m]	[m/s ²]	[m]	[m/s ²]	[rad]	[rad/s ²]	[rad]	[rad/s ²]	[rad]	[rad/s ²]
NEN-ISO 2613	-	-	0,3	0,5	0,3	0,5	0,010	0,050	-	-	-	-
University of Singapore	-	-	-	3	-	3,0	0,010	0,040	-	-	-	-
Sognefjord	-	0,5	L/200	0,5	L/200	0,7	0,044	0,107	0,006	0,07	0,06	0,05
Bergsøysund	-	-	L/350	0,5	L/350	0,7	0,044	0,107	0,035	0,07	0,03	0,05
-	-	-	-	-	-	-	-	-	-	-	-	-
Tidal Bridge (rad)	-	0,5	-	0,5	3,0	0,7	0,044	0,107	0,035	0,07	0,06	0,05
(degrees)	-	0,5	-	0,5	3,0	0,7	2,521	6,131	2,005	4,01	3,44	2,86

Table B.6: Overview of all serviceability limits of floating bridges

The serviceability limits will not function as definite limits that can not be exceeded, but as an indication of a logical tolerable amount of motion. The real acceptable motion for the Tidal Bridge should be found and validated by extensive research and experiments.

C

Boundary conditions

The Tidal Bridge design is subjected to the boundary conditions at the reference case of the Palmerah Tidal Bridge in Indonesia. The Appendix elaborates on the surroundings and the hydraulic and environmental conditions, to be able to formulate the initial boundary conditions that are implemented in the final model.

C.1. Seismic activity

Indonesia is located at the intersection of four tectonic plates: the Sunda Plate, Indo-Australia Plate, the Pacific Plate and the Philippine Sea Plate. The region is called the *Ring of Fire* and suffers frequent earthquakes. In Figure C.1 the large green dots indicate earthquakes higher than factor M7.0 on the Richter scale since 1800. In December 1992 Flores Island was hit by a tsunami, though Larantuka was hardly affected as a result of the protected position in the Strait of Larantuka. The volcanoes that are located nearby are presented in Figure C.3, all volcanoes in the area are non-active.

Every year the *United Nations Office for the Coordination of Humanitarian Affairs* determines the Disaster Risk Index. Hazards are scaled between 1 (low risk) and 10 (high risk), the scales are based on historical events. Figure C.2 indicates that Indonesia is vulnerable for a tsunami, earthquake and floods.

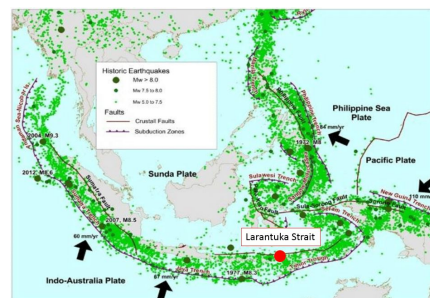


Figure C.1: Active faults and seismicity (Wan Ahmad et al. (2019))

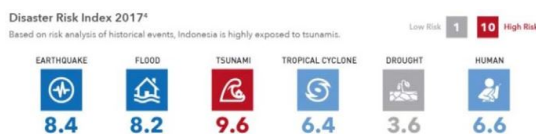


Figure C.2: Disaster Risk Index 2017 (OCHA, 2017)

The typical geotechnical aspects of a volcanic subsoil is a top layer that consists of very brittle materials bound in lava containing of lot of air bubbles. The seabed probably consists of very hard diorite and is partly covered by a brittle layer. The precise content of the soil is not determined yet.

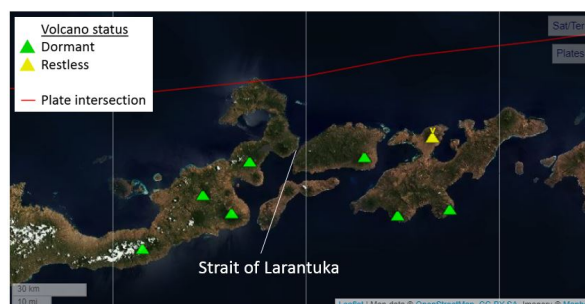


Figure C.3: Volcanoes near Strait of Larantuka and activity (Volcano Discovery, 2019)

C.2. Bathymetry

The optimal bridge location is based upon a bathymetry study performed on data of the Indonesian Hydrodynamics Laboratory and field measurements conducted by Aquaterra. Along the proposed bridge path the maximum depth is 34 m, Figure C.5. Due to the non-uniform bathymetry profile the pendulum mooring system is connected to the bottom at different depths and has a variable length. To maintain a normalized system, only the pendulum length is variable, the tripod connection and angle between the pendulum and seabed remains 40 degrees at MSL. The varying pendulum lengths are given in Table C.1. For the analysis, the average depth of 25 m along the floating span of the bridge is used, Figure C.4. The depth corresponds with the average depth seabed level underneath the floating bridge part. The smallest depth results in a higher percentage of flow blocking by the submerged parts of the bridge and will be governing. Hence, the average depth is used instead of the maximum depth.

Mooring number	Pendulum length	Bottom depth	Neutral angle
10	31,05 m	20,79 m	40°
11	40,07 m	25,20 m	40°
12	45,71 m	30,28 m	40°

Table C.1: Mooring dimensions (Vos, 2017)

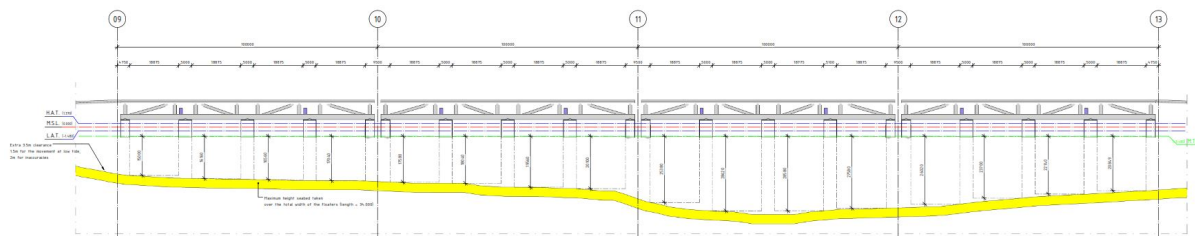


Figure C.4: Available turbine space (Tasma, 2017)

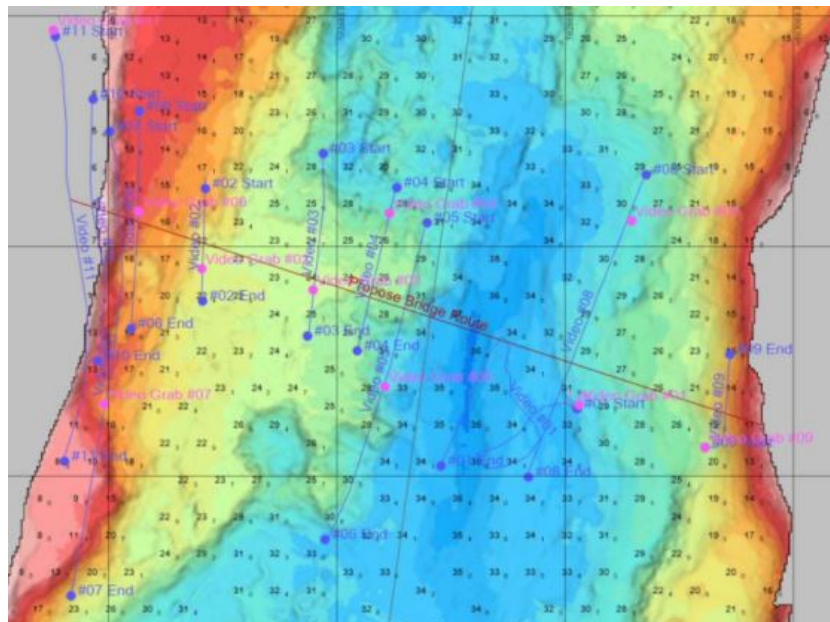


Figure C.5: Field measurements (Aquaterra, 2017)

C.3. Wind

The Larantuka Strait is sheltered by the islands of Flores and Adonara. Wind speeds up to approximately 11 m/s (≈ 40 km/h) occur annually. The highest winds arise in the wet season, especially in January and February. Figure C.6 shows that the annual mean wind speed over the past 12 years was relatively constant, fluctuating around 4 m/s. The software company EMD International A/S (2017) measured the maximum wind velocity every hour during a period of twelve years, from 2007 till 2015. The reports can be downloaded from <http://indonesia.windprospecting.com>. One column in the dataset provides annual report with the maximum wind velocity and its direction at a height of 10 meters every hour. An overview of the characteristics of the data is given in Table C.2.

Time period	2004 - 2015	[12 years]
Median	2,93	[m/s]
Average	3,03	[m/s]
Standard deviation	1,74	[m/s]
Maximum wind speed	11,56	[m/s]
Minimum wind speed	0,00	[m/s]
Number of records	105 168	[-]

Table C.2: Overview of wind data characteristics

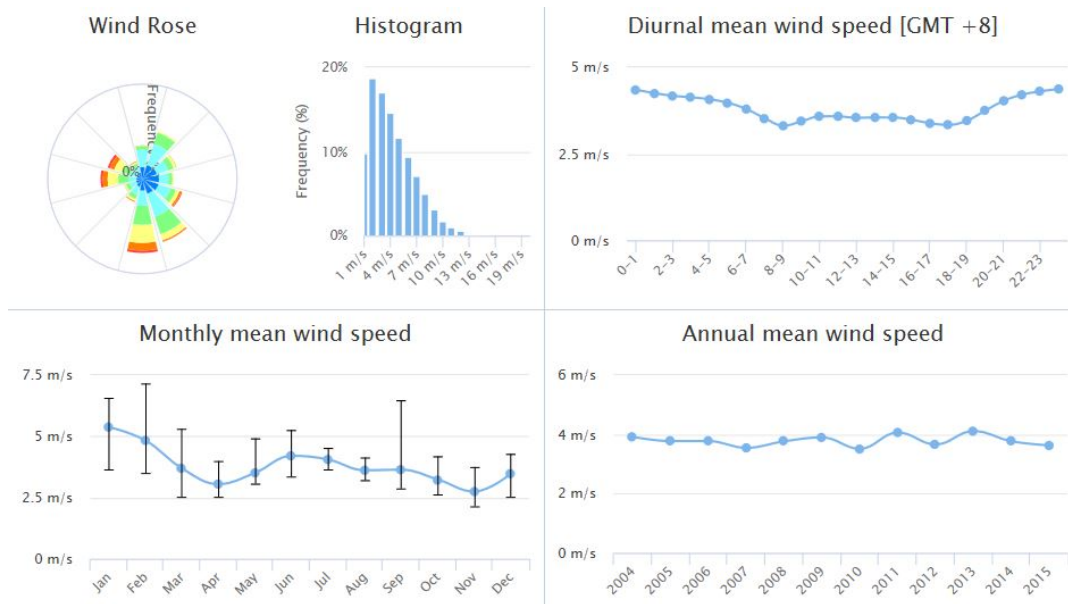


Figure C.6: Overview of wind data; S08.320, E122.997, mainland West of Larantuka Strait (EMD International A/S, 2017)

The wind data should be thoroughly analysed to be able to find the maximum wind speed with a return period of 100 years. This return period wind speed is later used to calculate the significant wave height in the Strait of Larantuka. EMD International A/S (2017) measured the hourly maximum wind speeds at the mainland at the West side of the Strait of Larantuka during the years 2004 till 2015. The dataset consists out of over 105 000 rows with more than 35 columns. One column represents the maximum wind gust at 10 m height and the direction of the wind. The return period of the maximum wind gust that occurs within 1, 50 and 100 years can be found with the extreme value distribution. The extreme value distribution of wind speeds can be accurately described by a Gumbell or Weibull distribution according to Jonkman et al. (2017). A check whether the correct distribution is chosen is based on plots of the histogram with the datapoints and the probability density function of the *Gumbell distribution*, *Weibull distribution* and the *Generalized Extreme Value distribution (GEV)*, Figure C.7 (Overkamp and Van Wierst (2018)). The analysis is computed with the programming software *Matlab*. Comparing the figure with the characteristic wind data values of Table C.2 verifies the accuracy of the plot. The plot of Figure C.7 may suggest that the GEV distribution has the best fitting shape on the dataset.

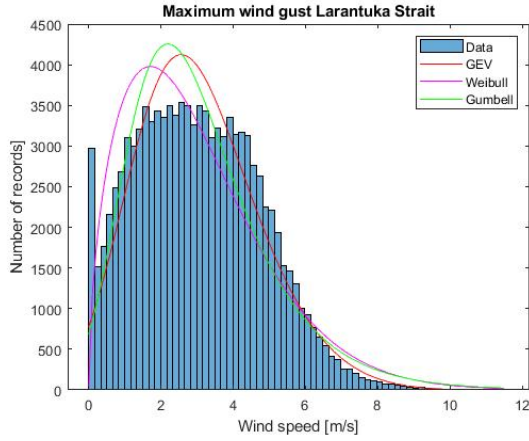


Figure C.7: Histogram with maximum wind gusts in the Larantuka Strait

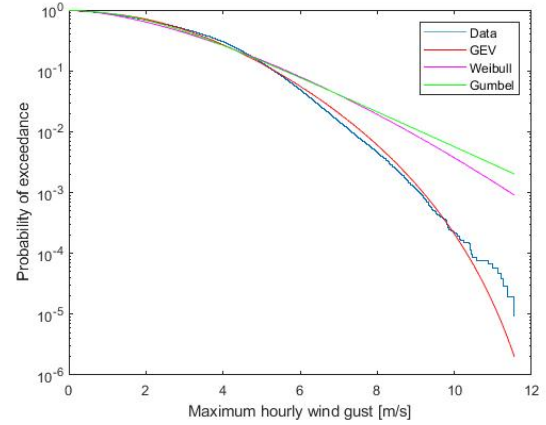


Figure C.8: Probability of exceedance of wind gust

Visually the accuracy of all distributions is doubtful. Hence, the distributions are converted on a log-scale plot with the probability of exceedance on the other axis, Figure C.8. It is clear that the GEV-distribution is more closely approximation than the Gumbell distribution. Yet, the best fitting distribution is depending on the dataset values and the amount of extreme datapoints that are present.

The distribution functions that are used for the computation of the probability of exceedance are stated in the following equations C.1 till C.3 . The theory behind the function is written in the book *Probabilistic Design Risk and Reliability Analysis in Civil Engineering* by Jonkman et al. (2017). The characteristics of the distributions projected to the total dataset are provided in Table C.3.

$$F_{x,Gumbell}(x) = \exp(-e^{-a(x-u)}) \quad (C.1)$$

$$F_{x,Weibull}(x) = 1 - \exp\left(-((x-u)/\alpha)^k\right) \quad (C.2)$$

$$F_{GEV}(s; \xi) = \begin{cases} \exp(-(1 + \xi s)^{-1/\xi}) & \xi \neq 0 \\ \exp(-e^{-s}) & \xi = 0 \end{cases} \quad (C.3)$$

Distribution	St. deviation σ [m/s]	Mean μ [m/s]	Shape factor ξ [-]	$U_{10,max 1 year}$ [m/s]	$U_{10,max 50 year}$ [m/s]	$U_{10,max 100 year}$ [m/s]
Gumbell	-2,19419	1,50886		15,8916	21,7943	22,8403
Weibull	3,30677	1,55695		13,6477	17,1818	17,7655
GEV	2,31445	1,57480	-0,14497	10,2640	11,5251	11,6830

Table C.3: Characteristic Dataset distributions for total dataset (Matlab)

Next step is to extrapolate the data to find the maximum wind gust for a specific return period larger than the 12 year period indicated in the data. The dataset is measured every hour during a period of 12 years, indicating a maximum hourly return period possible to find with the data of $1/(12 \cdot 365 \cdot 24) = 9,51 \cdot 10^{-6}$. The data is extrapolated for all distribution types to find the maximum wind speed for larger return periods. Figure C.9 represents a plot of the extrapolated distribution data. It is clear that in the scenario, the GEV distribution is the most accurate approximation of the magnitude of the wind speed for a specific return period.

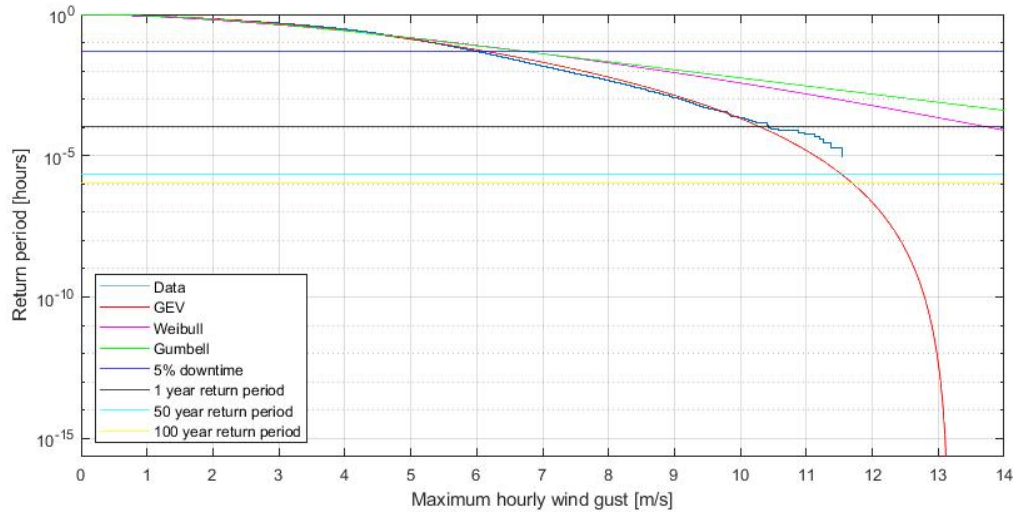


Figure C.9: Extrapolation of the dataset according to the three types of distribution

The direction of the wind speed is of importance to indicate the direction of the waves. Therefore, the dataset is narrowed to data that considers a specific direction range only. An overview of the magnitudes of the wind speeds for every 20 degrees and for the whole dataset is provided in Table C.4. The narrowed datasets are coupled to the best fitting distribution for each specific set. This is done with a visual analysis which line is closest to the actual data. In some cases none of the distributions seem near an approximation. If this occurs, a value is estimated by means of an imaginary distribution line. The offset of the distribution lines can be explained by extreme values within the dataset. The shape of the extrapolated distribution lines are created along the extreme value. Hence, the line adopts to another shape. In the table the non accurate extrapolation lines are denoted with 'Best fitting distribution: *None*'. In addition, the number of records for the narrowed dataset is a fraction of the total dataset. The return periods are calculated with the amount of records for each of the narrowed datasets. The plots of the datasets are provided in the Figures C.10 to Figure C.27.

Direction [°]	Records [-]	Return period			Best fitting distribution	$U_{10,max5\%}$ [m/s]	$U_{10,max 1 year}$ [m/s]	$U_{10,max 50 year}$ [m/s]	$U_{10,max 100 year}$ [m/s]
		1 year	50 year	100 year					
Total dataset	105141	0,00011	0,0000023	0,0000011	GEV	6,1151	10,2640	11,5251	11,6830
0-20	9548	0,00126	0,0000251	0,0000126	Weibull	5,4850	7,8032	9,5596	9,8284
20-40	6556	0,00183	0,0000366	0,0000183	GEV	5,7289	7,4832	8,3692	8,6655
40-60	3092	0,00388	0,0000776	0,0000388	<i>None</i>	3,9395	5,4770	8,9255	9,5360
60-80	1844	0,00651	0,0001302	0,0000651	Gumbell	3,2405	9,0400	12,4856	13,0962
80-100	1646	0,00729	0,0001458	0,0000729	Gumbell	3,7773	4,7571	7,8087	8,3490
100-120	2358	0,00509	0,0001018	0,0000509	GEV	5,6359	5,4589	8,1351	8,5690
120-140	5353	0,00224	0,0000448	0,0000224	GEV	6,0133	8,0646	9,8983	10,1390
140-160	11000	0,00109	0,0000218	0,0000109	GEV	6,3017	7,7708	8,4289	8,4906
160-180	17536	0,00068	0,0000137	0,0000068	GEV	6,5860	8,2065	8,8262	8,8858
180-200	11839	0,00101	0,0000203	0,0000101	GEV	4,6601	8,8669	9,8155	9,9133
200-220	4422	0,00271	0,0000543	0,0000271	GEV-cons.	4,6601	7,1417	9,7522	10,1458
220-240	2986	0,00402	0,0000804	0,0000402	GEV	3,9247	6,2242	9,6451	10,2374
240-260	3074	0,00390	0,0000781	0,0000390	Gumbell-cons.	4,7738	7,7499	12,2741	13,0753
260-280	4310	0,00278	0,0000557	0,0000278	<i>None</i>	6,9342	9,5000	10,5000	11,0000
280-300	5225	0,00230	0,0000459	0,0000230	GEV	7,6620	10,4049	12,1230	12,3093
300-320	4000	0,00300	0,0000600	0,0000300	<i>None</i>	7,2996	10,5000	13,0000	12,5000
320-340	3469	0,00346	0,0000692	0,0000346	Gumbell	5,5083	8,9583	14,0094	14,8822
340-360	6883	0,00174	0,0000349	0,0000174	Weibull	5,4158	8,0769	10,3873	10,7678

Table C.4: Approximation of the maximum wind gusts with a return period of respectively 1, 50 and 100 years

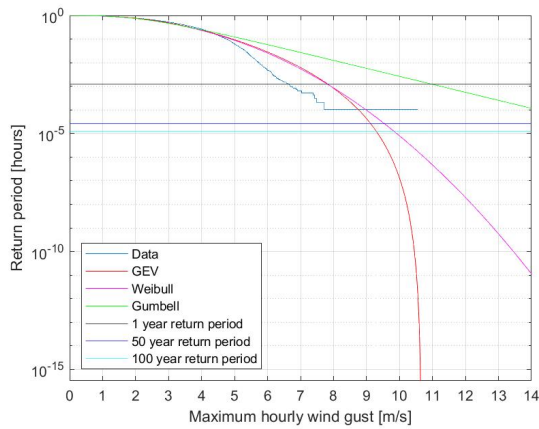


Figure C.10: Dataset with direction range: 0 - 20 degrees
best fitting distribution: Weibull

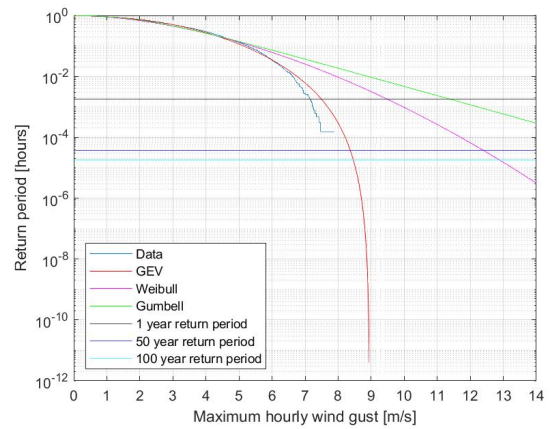


Figure C.11: Dataset with direction range: 20 - 40 degrees
best fitting distribution: GEV

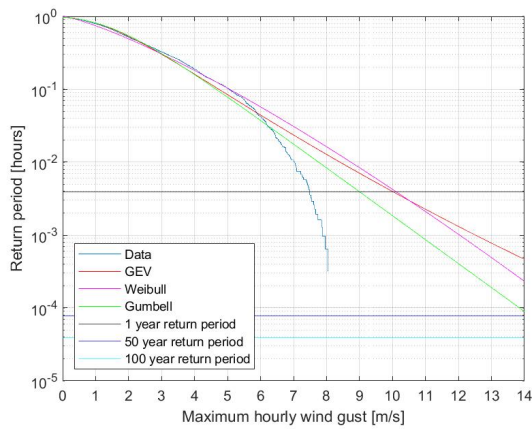


Figure C.12: Dataset with direction range: 40 - 60 degrees
best fitting distribution: None

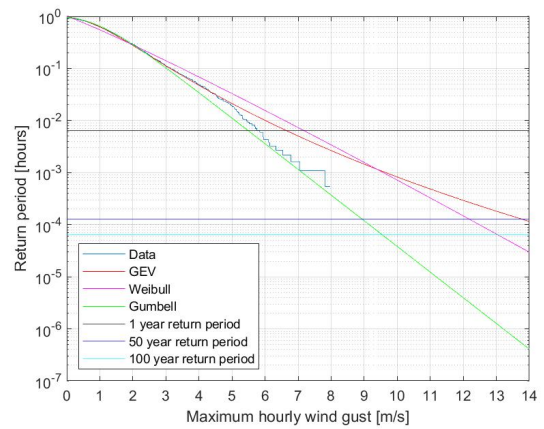


Figure C.13: Dataset with direction range: 60 - 80 degrees
best fitting distribution: Gumbell

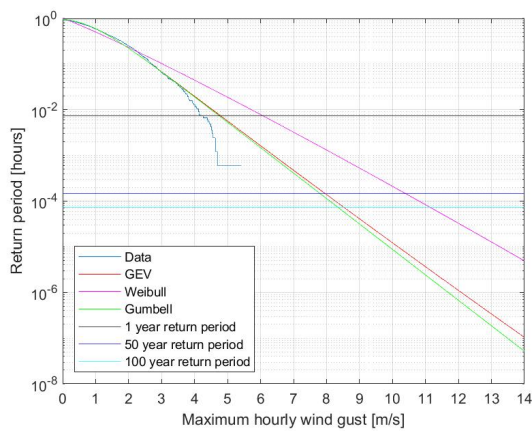


Figure C.14: Dataset with direction range: 80 - 100 degrees
best fitting distribution: Gumbell

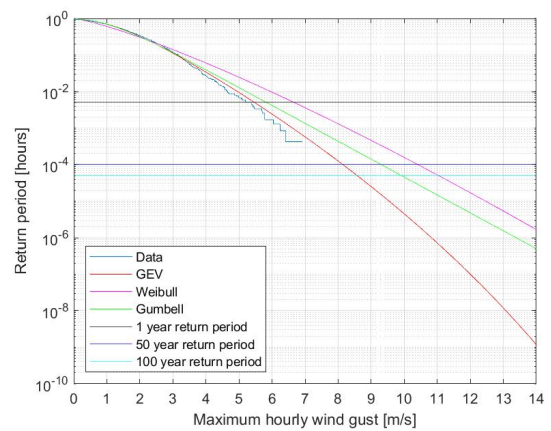


Figure C.15: Dataset with direction range: 100 - 120 degrees
best fitting distribution: GEV

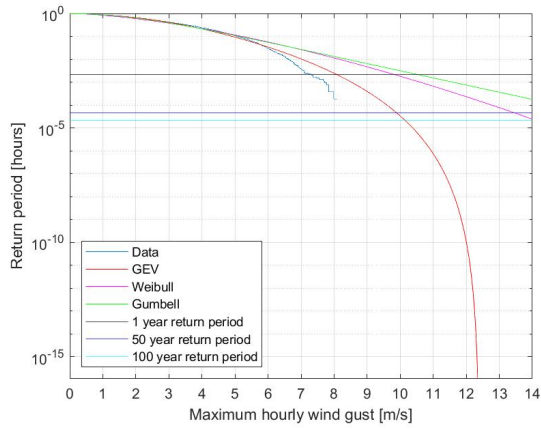


Figure C.16: Dataset with direction range: 120 - 140 degrees
best fitting distribution: GEV

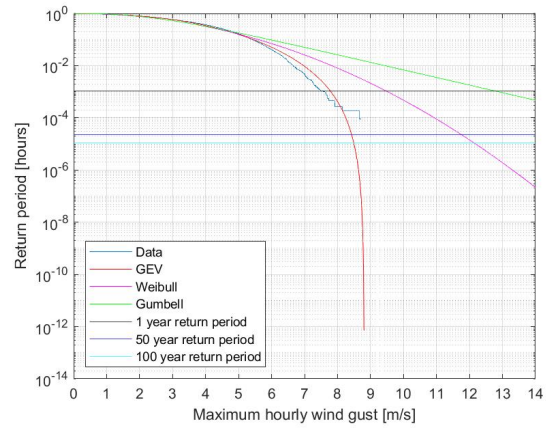


Figure C.17: Dataset with direction range: 140 - 160 degrees
best fitting distribution: GEV

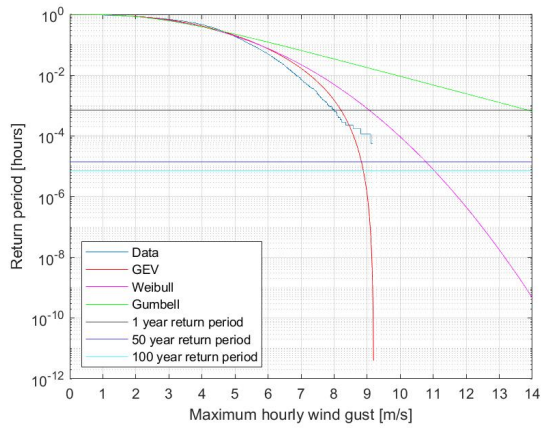


Figure C.18: Dataset with direction range: 160 - 180 degrees
best fitting distribution: GEV

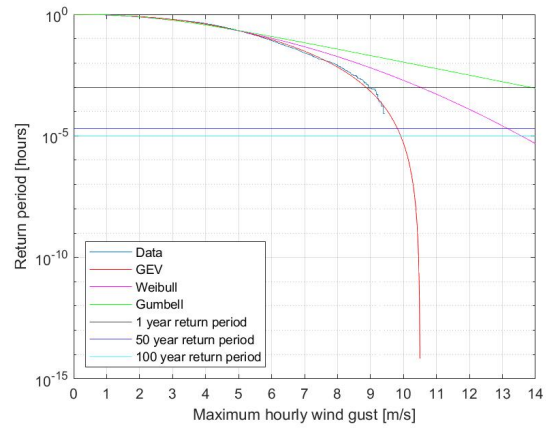


Figure C.19: Dataset with direction range: 180 - 200 degrees
best fitting distribution: GEV

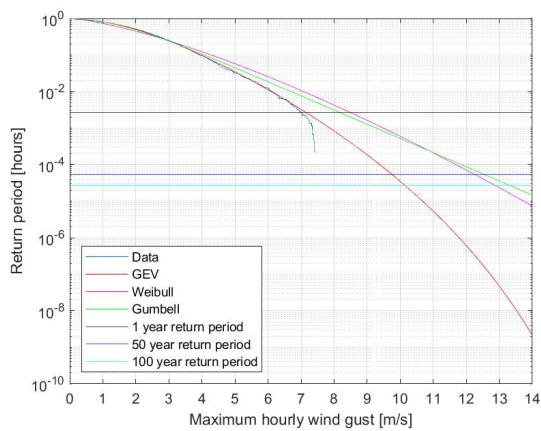


Figure C.20: Dataset with direction range: 200 - 220 degrees
best fitting distribution: GEV - conservative

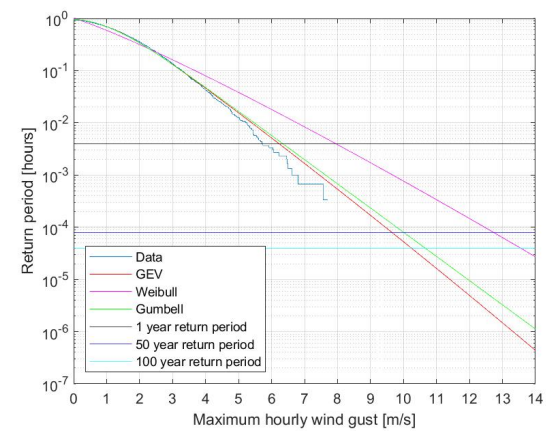


Figure C.21: Dataset with direction range: 220 - 240 degrees
best fitting distribution: GEV

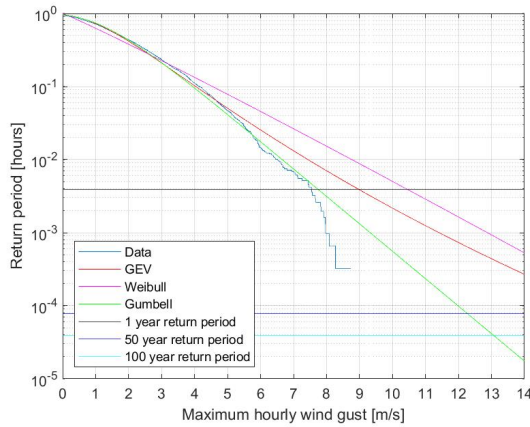


Figure C.22: Dataset with direction range: 240 - 260 degrees
best fitting distribution: Gumbell - conservative

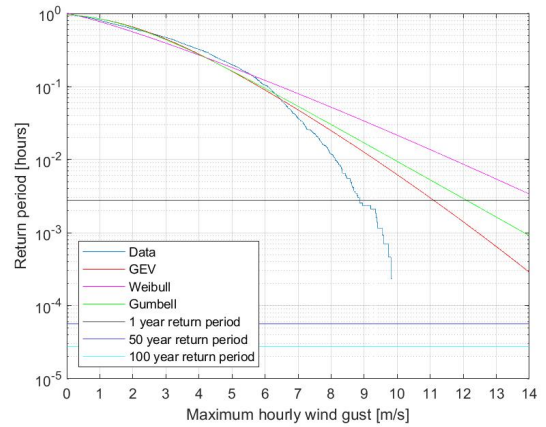


Figure C.23: Dataset with direction range: 260 - 280 degrees
best fitting distribution: *None*

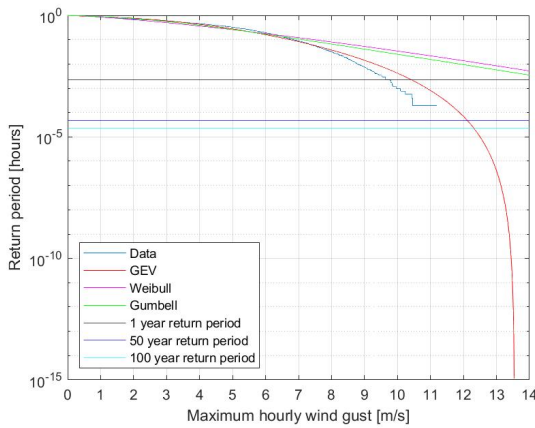


Figure C.24: Dataset with direction range: 280 - 300 degrees
best fitting distribution: GEV

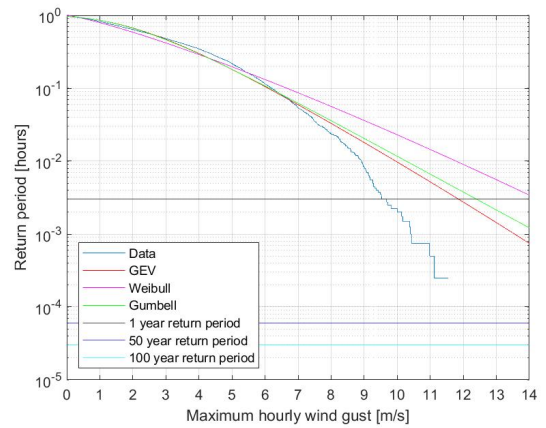


Figure C.25: Dataset with direction range: 300 - 320 degrees
best fitting distribution: *None*

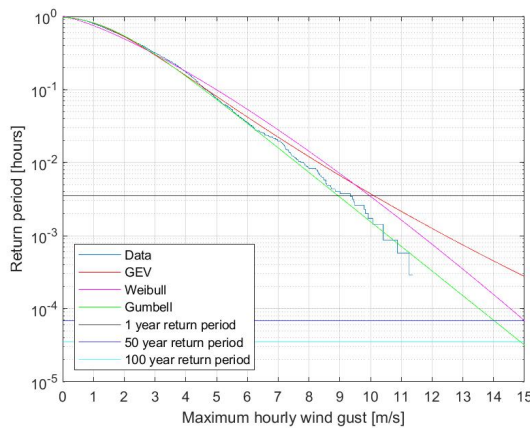


Figure C.26: Dataset with direction range: 320 - 340 degrees
best fitting distribution: Gumbell

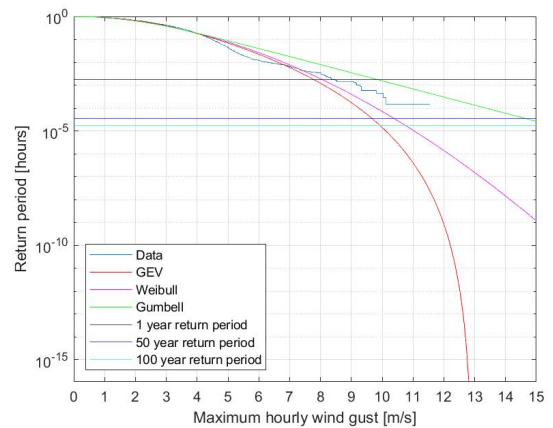


Figure C.27: Dataset with direction range: 340 - 360 degrees
best fitting distribution: Weibull

C.4. Wave height

Transformation of the maximum wind speed to significant wave height for deep water is done according to the formula's of Bretschneider that are improved by Young and Verhagen (1998), formula C.4 and C.5, (Molenaar and Voorendt, 2018). The fetch lengths and average water depths are based on Figure C.28.

$$\tilde{H} = \tilde{H}_\infty \cdot \left[\tanh(0,343 \cdot \tilde{d}^{1,14}) \cdot \tanh\left(\frac{4,41 \cdot 10^{-4} \cdot \tilde{F}^{0,79}}{\tanh(0,343 \cdot \tilde{d}^{1,14})}\right) \right]^{0,527} \tag{C.4}$$

$$\tilde{T} = \tilde{T}_\infty \cdot \left[\tanh(0,10 \cdot \tilde{d}^{2,01}) \cdot \tanh\left(\frac{2,77 \cdot 10^{-7} \cdot \tilde{F}^{1,45}}{\tanh(0,10 \cdot \tilde{d}^{2,01})}\right) \right]^{0,187} \tag{C.5}$$

$$\tilde{H} = \frac{g \cdot H_s}{U_{10}^2} \tag{C.6} \qquad \tilde{T} = \frac{g \cdot T_p}{U_{10}^2} \tag{C.8}$$

$$\tilde{F} = \frac{g \cdot F}{U_{10}^2} \tag{C.7} \qquad \tilde{d} = \frac{g \cdot d}{U_{10}^2} \tag{C.9}$$

$$L = \frac{g \cdot T_p^2}{2 \cdot \pi} \cdot \tanh\left(\frac{2 \cdot \pi \cdot \tilde{d}}{L}\right) \tag{C.10}$$

In which:

F	Fetch		[m]
d	Water depth		[m]
U_{10}	Wind velocity at 10 meters altitude		[m/s]
g	Gravitational acceleration	9,81	[m/s ²]
\tilde{H}_∞	Dimensionless wave height at deep water	0,24	[-]
\tilde{T}_∞	Dimensionless wave height at deep water	7,69	[-]
H_s	Significant wave height		[m]
T_p	Wave period		[s]

Figure C.28 provides an overview of the bathymetry of the project location on a larger scale. In the second part of the figure an overview of the fetch length with respect to the seas is provided. Table C.5 gives the variables that are implemented in the equation of Young and Verhagen (1998), the wave height distribution is visualised in Figure C.29. The wave heights computed with the Young and Verhagen equation may be inaccurate as a result of large water depths.

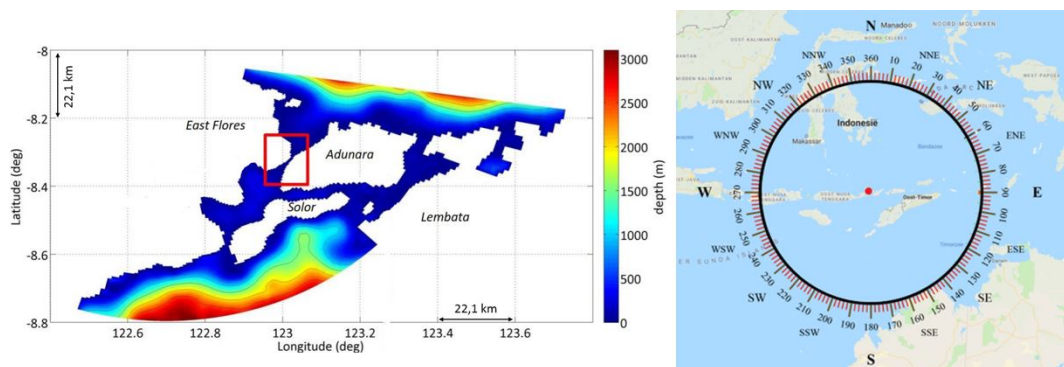


Figure C.28: Overview on estimated Fetch and average water depth data (Orhan et al., 2015)

Direction [°]	$U_{max, 1year}$	Fetch [m]	Av. depth [m]	\bar{d}	\bar{F}	\bar{H}	\bar{T}	H_s [m]	T_p [s]	L [m]
0-20	7,803	316 000	2 000	322,22	50 911	0,24	7,62	1,47	6,06	57,35
20-40	7,483	750 000	2 000	350,37	131 388	0,24	7,69	1,37	5,87	53,73
40-60	5,477	660 000	2 000	654,05	215 838	0,24	7,69	0,73	4,29	28,78
60-80	9,040	800 000	2 000	240,08	84 029	0,24	7,69	2,00	7,09	78,40
80-100	4,757	315 000	2 000	866,99	136 551	0,24	7,69	0,55	3,73	21,71
100-120	5,459	1 000	18	5,93	329	0,04	2,20	0,12	1,22	2,34
120-140	8,065	1 000	18	2,72	151	0,03	1,78	0,18	1,46	3,34
140-160	7,771	1 000	18	2,92	162	0,03	1,82	0,18	1,44	3,23
160-180	8,207	1 000	18	2,62	146	0,03	1,76	0,19	1,47	3,40
180-200	8,867	1 000	18	2,25	125	0,03	1,69	0,21	1,53	3,64
200-220	7,142	1 000	18	3,46	192	0,03	1,90	0,16	1,38	2,99
220-240	6,224	32 000	18	4,56	8103	0,16	5,24	0,63	3,32	16,35
240-260	7,750	3 000	18	2,94	490	0,05	2,45	0,29	1,94	5,83
260-280	9,500	1 000	18	1,96	109	0,02	1,63	0,22	1,58	3,87
280-300	10,405	1 000	18	1,63	91	0,02	1,55	0,24	1,64	4,19
300-320	10,500	1 000	18	1,60	89	0,02	1,54	0,25	1,65	4,22
320-340	8,958	480 000	2 000	244,48	58 676	0,24	7,66	1,95	6,99	76,39
340-360	8,077	350 000	2 000	300,75	52 632	0,24	7,63	1,58	6,28	61,63

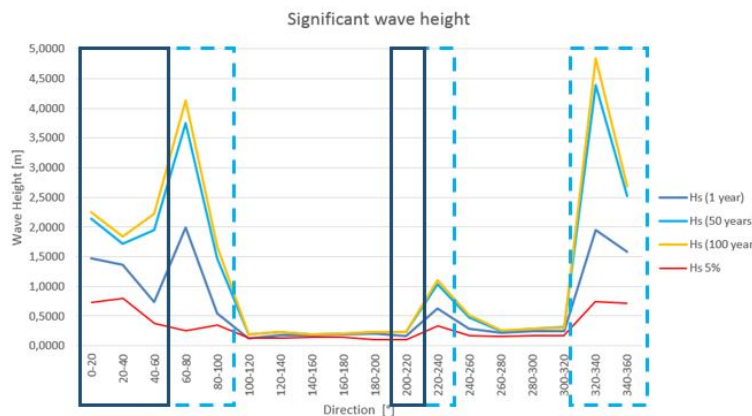
Table C.5: Computed wave height for wind speed $U_{max, 100 years}$ [m/s]

Figure C.29: All computed wave heights per direction

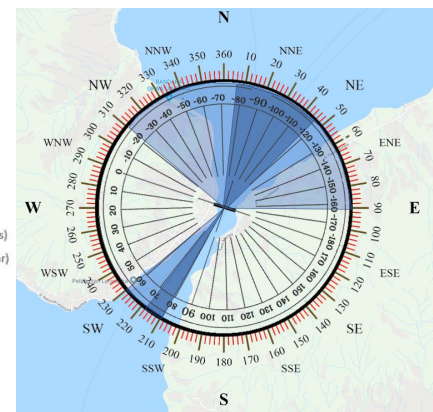


Figure C.30: Significant incoming wave angles area (blue) according to Table C.29

Figure C.30 indicates that the governing incoming wave directions are in a range of $8^\circ - 45^\circ$ and $210^\circ - 220^\circ$. The corresponding wave heights of the waves in the range are provided in Table C.6, the dynamic response of the bridge to waves will be checked. The largest significant wave height of a wave that arises once a year in the direction range is 1,47 m.

In general, the significant wave height indicates the mean of the highest one-third of waves in the wave record. The value is often used as it is close to the visually estimated wave height (Holthuijsen, 2007). A rule of thumb that is that the maximum wave height in storms is approximately two times the significant wave height. The distribution of characteristic wave heights is presented in Figure C.31. The modelling software accepts implementation of the significant wave height (H_s) and of individual waves (H_{max}). The rule of thumb is assumed as a correct indication of the maximum wave height of the forecasted waves. Collecting actual wave data should verify whether the assumption can be validated.

$$H_{max} \approx 2H_s \quad (\text{C.11})$$

	Direction [°]	U_{max} [m/s]	H_s [m]	H_{max} [m]	T_p [s]	L [m]	f [Hz]
Downtime of 5%	0-20	5,49	0,74	1,47	4,30	28,86	0,23
	20-40	5,73	0,80	1,61	4,49	31,49	0,22
	200-220	4,66	0,10	0,20	1,14	2,02	0,88
	220-240	3,92	0,33	0,67	2,66	11,01	0,38
1 year	0-20	7,80	1,473	2,95	6,06	57,35	0,16
	20-40	7,48	1,370	2,74	5,87	53,73	0,17
	200-220	7,14	0,162	0,32	1,38	2,99	0,72
	220-240	6,22	0,630	1,26	3,32	16,35	0,30
50 year	0-20	9,56	2,147	4,29	7,14	79,62	0,14
	20-40	8,37	1,713	3,43	6,56	67,20	0,15
	200-220	9,75	0,228	0,46	1,60	3,96	0,63
	220-240	9,65	1,039	2,08	4,06	17,33	0,25
100 year	0-20	9,83	2,256	4,51	7,28	82,76	0,14
	20-40	8,67	1,836	3,67	6,79	72,04	0,15
	200-220	10,15	0,238	0,48	4,09	4,09	0,62
	220-240	10,24	1,109	2,22	17,34	17,34	0,24

Table C.6: Significant waves with corresponding characteristics for governing directions

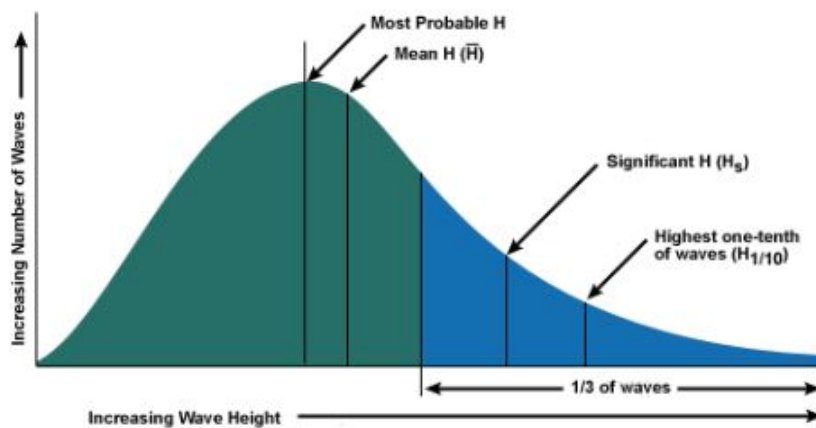


Figure C.31: Statistical wave distribution (Wulff Wathne, 2012)

C.5. Tidal data

The tidal range is based on data conducted by Aquatera during 11th and 16th of June 2017. An overview of the tidal water level is provided in Table C.7. Tidal range occurs mainly due to the gravitational pull of the sun and the moon with spring tides during full moon and new moon. At spring tides the tidal range is largest. However, the survey is conducted after a Micro Full Moon (June 9, 2017) and before the Third Quarter moon phase (June 17, 2017). The phenomenon of Micro Full Moon happens when a Full Moon coincides with an apogee, the point where the Moon's elliptical orbit is farthest away from earth. Due to this event, apogean spring tides occur that have around 5 cm smaller variation than regular spring tides (Time and Date, 2017). Combining the fact of the Micro Full Moon and a survey near the Third Quarter moon phase, the tidal range is assumed approximately 15cm larger, being 3,00m.

		[+ MSL]	[+ LAT]
Highest Astronomical Tide	HAT	1.37 m	2.85 m
Mean High Water Spring	MHWS	0.89 m	2.37 m
Mean High Water Neap	MHWN	0.39 m	1.87 m
Mean Sea Level	MSL	0.00 m	1.48 m
Mean Low Water Neap	MLWN	-0.40 m	1.08 m
Mean Low Water Spring	MLWS	-0.91 m	0.58m
Lowest Astronomical Tide	LAT	-1.48 m	0.00 m

Table C.7: Water level project location (Aquatera, 2017)

The type of tide can be determined with the Form Factor (F), equation C.12. The Form Factor is a function with the main amplitudes of the tidal constituents as variables and describes the type of tide. In this case the form factor is in the range of 0,25 - 1,5, which indicates a mixed, mainly semidiurnal tide (Bosboom and Stive, 2015). Two high and two low tides are present at the location every day.

$$F = \frac{K_1 + O_1}{M_2 + S_2} = 0,51 \quad (\text{C.12})$$

	Tidal constituents	Amplitude (m) a_n	Phase (°) α_n	Period (hr) ω_n
M_2	Semidiurnal lunar, moon	0,702	321,3	12,42
O_1	Diurnal lunar, moon	0,189	276,6	25,82
S_2	Semidiurnal solar, sun	0,295	26,1	12,00
K_1	Diurnal solar, sun	0,315	312,0	23,93
Total		1,501		

Table C.8: Main tidal constituents at bridge axis (Aquatera, 2017)

Tidal wave slope

Table C.8 indicates that a maximum amplitude of the tidal waves is approximately 1,5 m, this is in agreement with the estimated tidal range (TR) of 3 m (low tide + high tide = 1,5 + 1,5 = 3,0). The tides come and go predictably, with a mainly semi-diurnal tide profile ($T \approx 12$ hours = 43 200 sec). Hence, the maximum angle of the wave slope is $2 \cdot 10^{-9}$, equation C.13. Implying that the rotation induced by the incoming tidal wave is negligibly small.

$$\angle = \frac{TR}{0,5L_{tide}} = \frac{3}{0,5 * \frac{gT^2}{2\pi}} = 2,06 * 10^{-9} \quad (\text{C.13})$$

C.6. Current profile

The difference in water level as a result of the tides creates a flow stream through the Strait of Larantuka. If high tide changes to low tide, an incoming current from the north is present. If low tide change to high tide, the flow direction changes as well. The change of direction occurs harmonically and very gradual. Aquaterra conducted a vessel survey to indicate the flow pattern. During the 23th till the 26th of July a vessel zigzagged along a transect to indicate the most suitable placement of the bridge with respect to high flow speeds that may result in optimal generation of electricity. The zigzagging transect is presented in Figure C.32. In this Figure, the two black circles indicate the areas with highest flow speeds, the northern area is selected. Two measurement devices, *Acoustic Doppler Current Profilers (ADCP)* at different survey points (red dots), measured the current velocity during 28 days for each 5 m depth profile. An overview of the survey data of the Western ADCP measure point is presented in Figures C.32 to C.37, the absolute flow velocities are given. Tale C.38 presents the extreme characteristics of the ADCP survey.

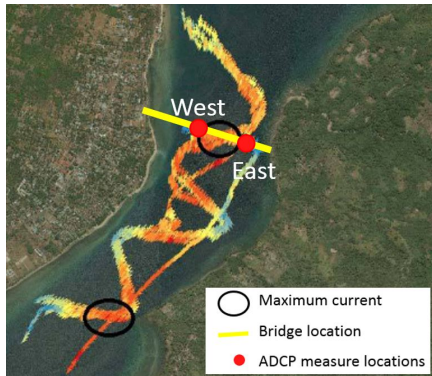


Figure C.32: Location of Aquaterra survey points (Aquaterra, 2017)

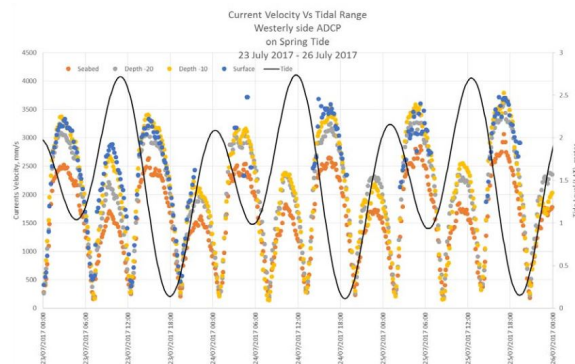


Figure C.33: Current speed and tide at the western ADCP (Aquaterra, 2017)

	Current velocity [m/s]										Total [%]	
	0-0,5	0,5 - 1	1 - 1,5	1,5 - 2	2 - 2,5	2,5 - 3	3 - 3,5	3,5 - 4	4 - 4,5	4,5 - 5		5 - 5,5
N	1,364	3,049	5,029	5,363	4,841	3,088	1,050	0,167	0,014	0,000	0,000	23,97
NE	1,632	4,083	7,065	7,494	5,768	2,463	0,551	0,058	0,005	0,000	0,000	29,12
E	1,079	0,658	0,140	0,021	0,004	0,001	0,000	0,000	0,000	0,000	0,000	1,90
SE	1,058	0,616	0,146	0,037	0,012	0,004	0,002	0,001	0,001	0,000	0,000	1,88
S	1,500	2,740	2,968	4,267	5,784	5,804	4,951	3,028	0,802	0,108	0,009	31,96
SW	1,246	1,407	1,107	1,142	1,373	1,322	1,022	0,512	0,135	0,024	0,002	9,29
W	0,684	0,168	0,026	0,005	0,001	0,000	0,000	0,000	0,000	0,000	0,000	0,88
NW	0,696	0,233	0,046	0,016	0,005	0,001	0,001	0,000	0,000	0,000	0,000	1,00
Total	9,259	12,953	16,526	18,345	17,789	12,683	7,577	3,766	0,956	0,133	0,011	100,00

Figure C.34: Current speed distribution at western ADCP with respect to direction at a depth of 0-5 m below MWL [%] (Vos, 2017)

	Current velocity [m/s]										Total [%]	
	0-0,5	0,5 - 1	1 - 1,5	1,5 - 2	2 - 2,5	2,5 - 3	3 - 3,5	3,5 - 4	4 - 4,5	4,5 - 5		5 - 5,5
0-5 m	9,259	12,953	16,526	18,345	17,789	12,683	7,577	3,766	0,956	0,133	0,011	100
5-10 m	12,300	15,783	17,928	17,910	16,750	12,119	5,023	1,614	0,432	0,107	0,025	100
10-15 m	11,014	15,197	16,666	15,363	15,049	12,599	8,393	4,374	1,135	0,176	0,027	100
15-20 m	9,702	13,368	16,936	17,245	16,883	12,826	8,095	3,870	0,931	0,122	0,014	100
20-25 m	10,810	16,264	18,219	18,167	15,815	11,182	6,510	2,487	0,488	0,053	0,005	100
25-30 m	13,879	21,407	21,172	18,307	13,149	7,781	3,334	0,847	0,113	0,010	0,001	100
Overall	11,161	15,829	17,908	17,556	15,906	11,532	6,489	2,826	0,676	0,100	0,014	100
Hours per year	978	1387	1569	1538	1393	1010	568	248	59	9	1	8760

Figure C.35: Current speed distribution at western ADCP with respect to depth [%] (Vos, 2017)

A combined overview of the percentages per direction and the magnitudes is presented in Figure C.36 and C.37. In the research, the directions east, south-east, west and south-west are omitted as the flow is low in magnitude and percentage. In addition, Figure C.35, suggest that the maximum flow speeds is around 5 m/s, yet the maximum speed is only present during approximately 1 hour in a whole year.

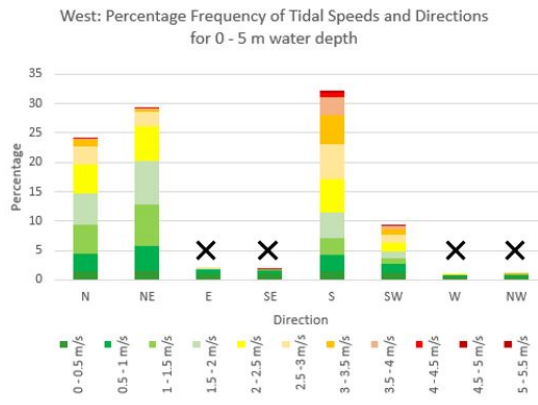


Figure C.36: Current distribution along different directions on the Western survey point, crosses indicate omitted directions (Vos, 2017)

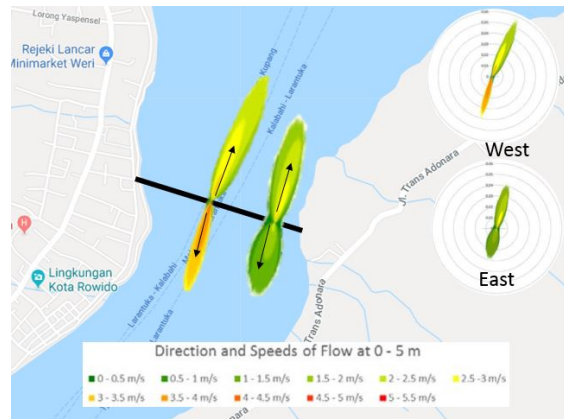


Figure C.37: Current speed at 0-5m depth at both survey points (Aquaterra, 2017)

The companies Bintang Subsea and Aquaterra performed a survey in July 2017 providing data about the correlation of the depth specific absolute current velocity to the tidal range, Figure C.39. The current velocity is plotted as absolute valued, while in reality the current switches direction (and sign) as result of the tide. The arrows indicate the actual current direction. Considering this, the correlation between the current and the tide can be found, Figure C.40. The derivative of the tide estimates the magnitude of the current. When the slope of the Tidal range is positive, the current velocity is positive. Illustrating that a positive current is primarily present at high tide. The maximum flow speed that is measured in the survey of Aquaterra is 7,48 m/s and arises during 0,0001 % of the measurements at a small local spot, Figure C.38. The considered maximum flow speed is a flow speed that is present at least 0,011 % of a day, respectively a flow speed of 5,2 m/s (Figure C.35). The maximum magnitude is based upon the requirement regarding the maximum moment around the x-axis induced by the drag force and is elaborated in Chapter 4.

	West ADCP	East ADCP
Average speed	1,70 m/s	1,04 m/s
Maximum speed	7.48 m/s	5,56 m/s
Minimum speed	0,00 m/s	0,00 m/s
Median speed	1,64 m/s	1,00 m/s

Figure C.38: Absolute valued ADCP survey points (Vos, 2017)

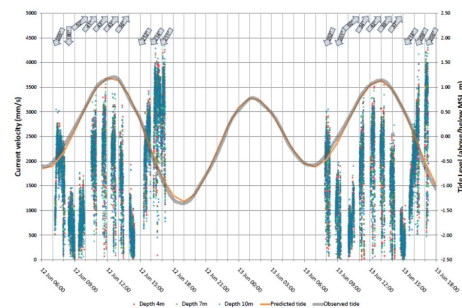


Figure C.39: Current velocity versus the tidal range (Vos, 2017)

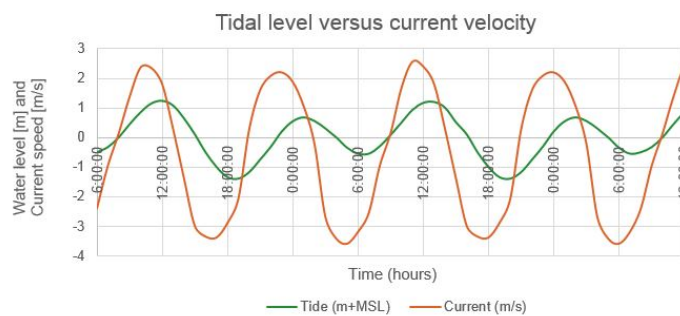


Figure C.40: Extrapolation of the current velocity and the tidal water level



Load index

This Appendix calculates the loads that are acting on the bridge and induce motion. First, the general loads as the weight of the structure and traffic distribution are discussed and later the main variable loads are indicated. With the data, realistic critical load combinations are determined that can be analysed in the model.

D.1. Static loads

The bridge is subjected to a wide variety of horizontal and vertical forces, however, as the vertical forces are in balance with the upwards water pressure, the horizontal forces are the principle forces. Nevertheless, the main loads are elaborated and it is discussed whether the effect on the stability of the system will be significant.

Self-weight

In general, the main load acting on a bridge is the vertical load induced by the mass of the bridge and traffic. In the Tidal Bridge scenario, the vertical load is not the main load component as the upwards water pressure equals is in balance with the vertical. Yet, the mass of the system influences the stability and is therefore significant for the analysis. The weight of the components of on one floating 100 m element are presented in Table D.1, (Vos, 2017). The estimated mass is based on the present design, though the mass can be easily adjusted by adding ballast or with the use of less heavy material, for example composites.

			Nr. on element	Total	
Deck	400 000	kg/100m	4	400 000	[kg]
Turbines	150 000	kg/turbine	4	600 000	[kg]
Pontoon	68 000	kg/pontoon large	3	204 000	[kg]
	48 000	kg/pontoon small	2	96 000	[kg]
Truss structure	900 000	kg/100m	1	900 000	[kg]
Container	40 000	kg/turbine	3	120 000	[kg]
			<i>Total mass</i>	$2,32 * 10^6$	[kg]

Table D.1: Mass of one Tidal Bridge element (Vos, 2017)

Buoyancy Force

The bridge floats on the water thanks to the upward water pressure created by the displaced water volume: the pontoon volume underneath the water line, Figure D.1. To determine the draught of the pontoons the upwards buoyancy force $F_{buoyancy}$ and the total mass of the bridge are set equal with *Archimedes' law*. With a total mass of 2 320 tonne and a pontoon surface area of 748 m², the draught of the pontoon becomes 3,03m. The corresponding buoyancy force becomes 22,7 MN or 7,52 d_p [MN].

$$d_p = \frac{M_{TB}}{\rho_w A_p} = 3,03 \quad (D.1)$$

$$F_{buoy} = \rho_w g A_p d_p = 7\,521 d_p \quad (D.2)$$

In which;

d_p	Draught of pontoon	[m]
M_{TB}	Total mass of one Tidal Bridge element	[kg/100 m]
A_p	Cross-sectional area of all five pontoons	[m ²]
F_{buoy}	The buoyancy force	[kN/m]

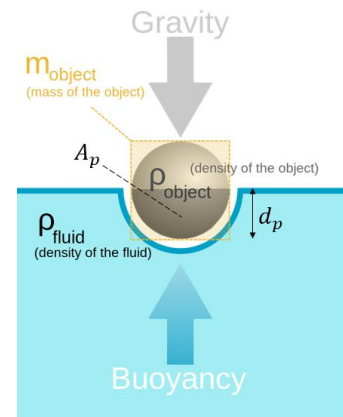


Figure D.1: Illustration of the Archimedes' principle

D.2. Traffic

Traffic loads are based on the Eurocode, NEN-EN 1991-2, European norms are used instead of Indonesian standards as the Indonesian norms are written in Indonesian. Due to the remote area, the traffic intensity is expected to be limited, with a small amount of heavy traffic in the design lifetime. An estimation for the traffic intensity is based upon the Eurocode NEN-EN 1991-2, according to traffic-category 3 "*Roads with limited cargo traffic*", the annual number of heavy vehicles per lane is $N_{obs,a,ai} = 125 \cdot 10^3$. Figure D.2 indicates the traffic distribution on the bridge deck, an illustration of traffic distribution that may be present on the deck is given in Figure D.3. Two types of load cases are analysed: uniform traffic and eccentric traffic.

Load	Parameter	Application	Value	Additional information	
Uniform distributed	q	Lane 1	9	[kN/m ²]	Loading by vehicle
		Lane 2	2,5	[kN/m ²]	Loading by vehicle
Uniform distributed	q_p	Pedestrian paths	5	[kN/m ²]	Loading by pedestrians

Table D.2: Traffic loads (NEN-EN 1991-2)

For the uniform traffic distribution the product of the length and the magnitude of the load is calculated. This point load indicates the vertical force acting on the deck. With the load combination, the most unfavourable rotations due to traffic along the x-axis can be analysed.

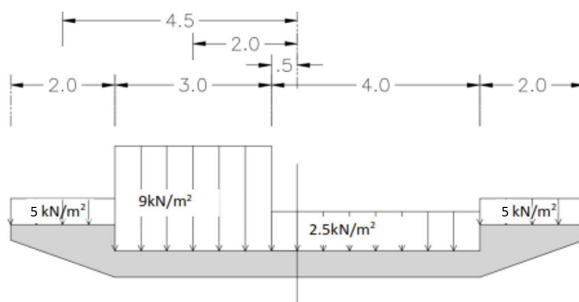


Figure D.2: Traffic loads on steel deck (Antea Group, 2018)



Figure D.3: Illustration of traffic driving over the Tidal Bridge deck (Tidal Bridge, 2018)

$$F_{traffic,1} = \begin{Bmatrix} 2 \\ 3 \\ 4 \\ 2 \end{Bmatrix} [m] \cdot \begin{Bmatrix} 5 \\ 9 \\ 2,5 \\ 5 \end{Bmatrix} [kN/m^2] \cdot 100 [m] = 57 \text{ kN/m} \quad (D.3)$$

The application point for the forces is taken in the most unfavourable part of the total structure, at connection 2 and 4, (red lines in Figure D.4). The point force is the sum of the distributed load acting on half the length of both floaters. The next situation, in which the loads are situated at 1 and 5, indicates the steepest slope of the roll-on roll-off construction due to traffic induced loads, blue lines in the figure. In here, the force is acting on half of the 30 m roll-on roll-off plate and half of the 100 m long floater.

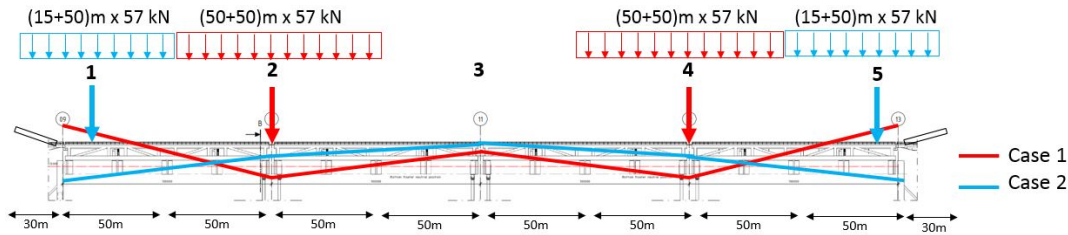


Figure D.4: Traffic attachment points (not to scale)

The largest roll-rotation of the deck is when all traffic is located on one side of the deck. The maximum moment occurs if traffic is solely present on the left side of the deck (Figure D.2). The maximum eccentric moment is calculated with equation D.4 and D.5. The point of action of the maximum eccentricity force is determined by dividing the maximum moment by the maximum force, equation D.6.

$$F_{traffic, eccentric} = \begin{Bmatrix} 2 \\ 3 \\ 0,5 \end{Bmatrix} [m] \cdot \begin{Bmatrix} 5 \\ 9 \\ 2,5 \end{Bmatrix} [kN/m^2] \cdot 100 [m] = 3\,825 \text{ kN} \quad (D.4)$$

$$M_{traffic, eccentric} = \begin{Bmatrix} 2 \\ 3 \\ 0,5 \end{Bmatrix} [m] \cdot \begin{Bmatrix} 5 \\ 9 \\ 2,5 \end{Bmatrix} [kN/m^2] \cdot \begin{Bmatrix} 4,5 \\ 2 \\ 0,25 \end{Bmatrix} [m] \cdot 100 [m] = 9931 \text{ kNm} \quad (D.5)$$

$$e = \frac{9931}{3825} = 2,60 \text{ m} \quad (D.6)$$

If the bridge is fully occupied with traffic, for example during a traffic jam, the ratio between the mass of the bridge structure and the mass of traffic is 1:0,25. The maximum traffic weight results in an increase in draught of approximately 60 cm. The influence of traffic distribution on the stability of the system is checked in the sensitivity study in Chapter 7.

1. Maximum rotation around the y-axis: Point forces of 5 700 kN acting at points 2 and 4
2. Maximum rotation around the y-axis: Point forces of 2 705 kN acting on points 1 and 5
3. Maximum rotation around the x-axis: The eccentric point load, 3 825 kN, (equation D.4) with an eccentricity of 2,60 m acting in the middle of each floater.

D.3. Wave induced loads

The significant wave height is estimated, Appendix C, resulting in a maximum wave in 100 years with a wave height of $H_S = 2,26 \text{ m}$ and a wave period of $7,28 \text{ s}$. The wave properties can indicate what type of wave theory may be valid at the project location. The *Shallowness characteristic* (equation D.7) and *Steepness characteristic* (equation D.8), are calculated and implemented in Figure D.5. The wave theory that may be applicable in the Strait of Larantuka is the *Third order Stokes theory*, a wave theory often used for wind waves.

$$\frac{d}{T_p^2} = \frac{25 * 3,28}{7,28^2} = 1,55 \text{ [Ft/s}^2\text{]} \quad (\text{D.7})$$

$$\frac{H_S}{T_p^2} = \frac{2,25 * 3,28}{7,28^2} = 0,14 \text{ [Ft/s}^2\text{]} \quad (\text{D.8})$$

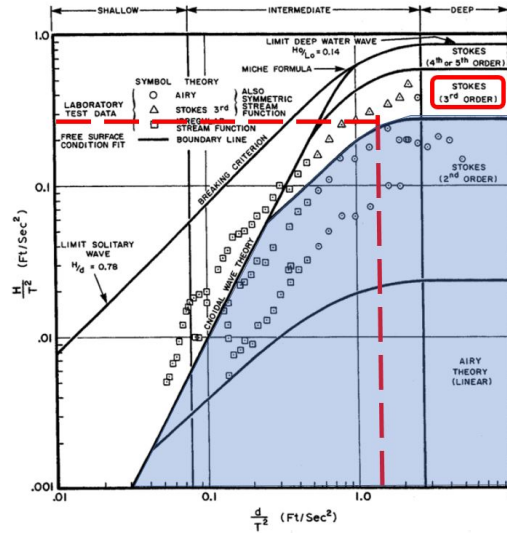


Figure D.5: Ranges of validity of wave theories (Det Norske Veritas, 2010a)

The valid wave theory is the *third order Stokes theory*, implying that the three harmonic wave components are summed. Figure D.6 visualises waves up to the 5^{th} order. A Stokes wave is characteristic for its wave shape: steep narrow crests and flat wide troughs. The shape of the wave will become more exact with a higher order wave, yet computations will become a lot more complex. The difference between a second and third order wave is small and validation wave data is absent, for that reason only up to second order Stokes waves are considered in the analysis.

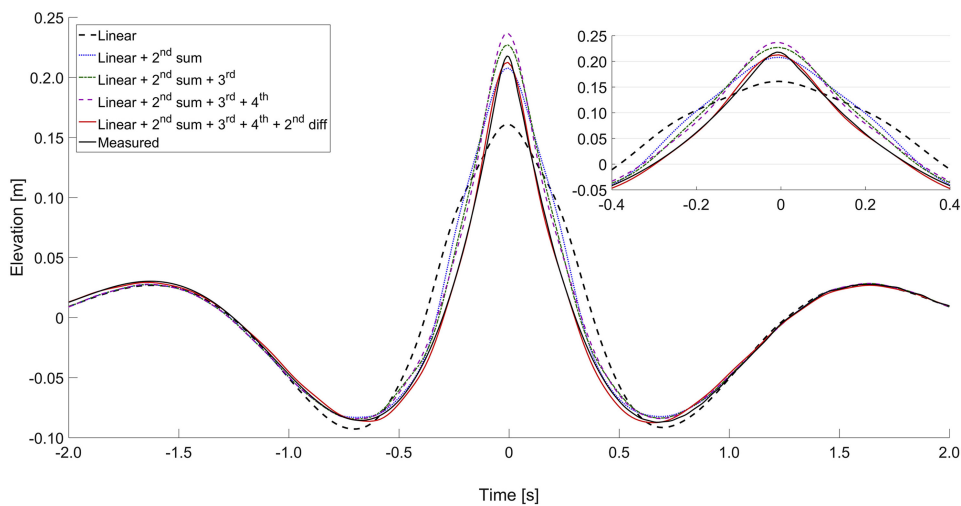


Figure D.6: N^{th} order waves (Vyzikas et al., 2018)

Diffraction load

If waves collide with a surface, the surrounding fluid flow modified. The modified wave pattern is accompanied with a pressure field that results in a diffraction load. If the fluid accelerates with respect to the body and the wave is not modified, inertia loads are present. The inertia load can be considered as an individual type of diffraction load and is dependent on the added mass coefficients. The *maximum* wave height that may occurs in 100 years is approximately 4,51 m. The length of the bridge is 100 m, placing the wave load in the diffraction regime, Figure D.7.

Next to small wind waves, long tidal waves are present. Tidal waves can be described as harmonic functions of a propagating sinusoidal wave, equation D.9 (Holthuijsen, 2007). Tides can be described as long waves and the wind-generated waves as short waves, both with corresponding amplitude and frequency. The surface elevation of waves can be described according to equation D.9.

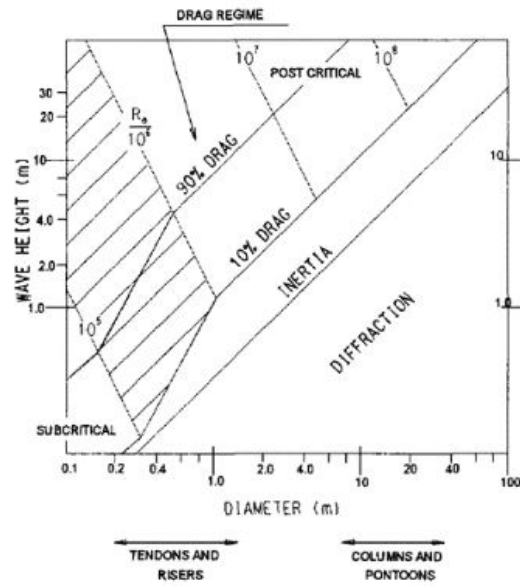


Figure D.7: Wave loading regime (Bartrop, 1998)

$$\eta(x, t) = a \sin(\omega t - kx) \tag{D.9}$$

$$\omega = \frac{2\pi}{T} \tag{D.10}$$

$$k = \frac{2\pi}{L} \tag{D.11}$$

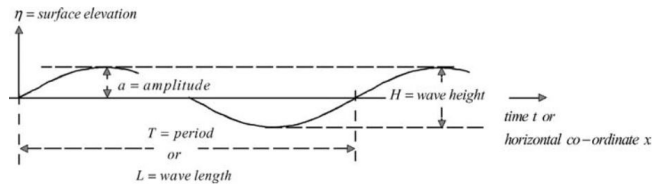


Figure D.8: Sine Wave (Holthuijsen, 2007)

Next to the increase in magnitude of wave crest height of a Stokes wave (approximately 0,03 m, Chapter 4), data on the actual wave spectrum is absent. Therefore, the linear theory of deep water waves is used to compute wave loading. The wave loads can be described by the formula's of the wave potential and the surface elevation (Journée and Massie, 2008).

$$\psi = \frac{-\zeta_a g}{\omega} e^{kz} \sin(\omega t - kx) \tag{D.12}$$

$$\zeta = \zeta_a \cos(\omega t - kx) \tag{D.13}$$

In which the abbreviations are illustrated in Figure D.8 and explained in the list.

$\eta(x, t)$	Surface elevation in time (t) and space (x) domain	[m,s]
ω	Radian frequency	[rad/s]
a	Amplitude ($H_s/2$)	[m]
k	Wave number	[-]
T	Wave period	[s]
L	Wave length	[m]
z	Depth below water level	[m]

D.4. Current induced loads

The current changes in magnitude and direction as a result of ebb and flood: the tides. In addition, the current can approach the bridge under an angle of 22 degrees. According to the data of Appendix C the flow speed is harmonic with a maximum velocity around 4 m/s. The main force that is induced by the current is the drag force. Drag forces are present at all elements of the structure that are located beneath the water level. The magnitude of drag is linearly dependent on the shape of the submerged structure and the surface that faces the flow. The submerged components of the Tidal Bridge are the pontoons, the turbines and the mooring system. Each component experiences a different type of drag. The mooring pendulums are relatively small compared to the rest of the structure and are therefore neglected. Estimation of the drag coefficient for the combined pontoon-turbine system is difficult as the shape is not definitive and the turbine resistance influences the system majorly. According to the data of Appendix C, the measured flow velocity and the tidal range are in relation as shown in Figure D.9.

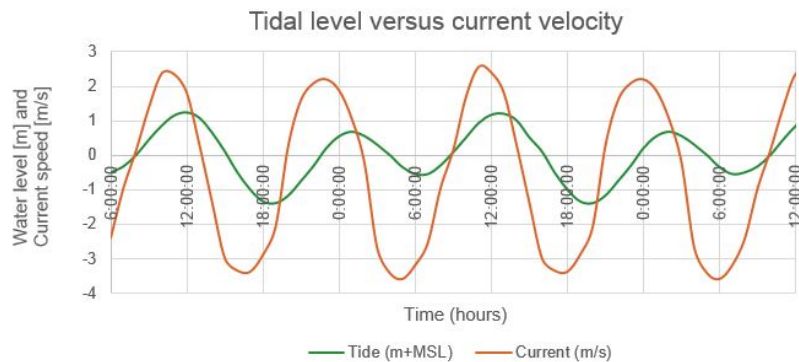


Figure D.9: Current velocity versus Tidal Range during the 12th and 13th of June 2017

D.4.1. Drag on 'tube-elements'

The steel tubes, the six pendulums and the two spud piles, are present along the whole depth. The drag forces on the tubes is calculated with the Morison equation, an equation widely used for evaluating the wave load on cylindrical structures. The submerged area of the pendulums is only a fraction of the total submerged area and with the cylindrical shape of the pendulums the influence of the drag on the 'tubes' is assumed to be small. The Morison equation considers the inertia force and the drag force in an oscillatory flow. In this equation, the inertia force is represented by equation D.14 and the drag force by equation D.15. The inertia force is the sum of the hydrodynamic mass force and the Froude Krylov force.

$$F_{drag, tube} = \rho_w C_m \frac{\pi D^2}{4} \dot{u} \quad (D.14)$$

$$+ 0,5 \rho_w C_d D u |u| \quad (D.15)$$

$$F_{drag, tube 1,5} = 23623 \dot{u} + 769 u |u| \quad (D.16)$$

In which:

$F_{drag, tube}$	Force inline with the current direction		[N]
C_m	The inertia coefficient, $C_m = 1 + C_a$		[-]
C_a	Added mass coefficient, Figure D.10	1,0	[-]
C_d	Drag coefficient of tube	1,0	[-]
\dot{u}	Flow acceleration $\frac{du}{dt}$		[m/s ²]
u	Flow velocity		[m/s]
D_p	Diameter of tube (pendulum)	1,5	[m]
D_{sp}	Diameter of tube (spudpole)	3	[m]

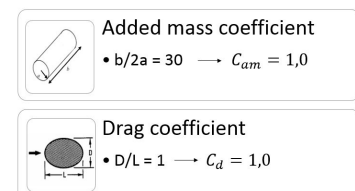


Figure D.10: Added mass and drag coefficients for pendulum (Det Norske Veritas, 2010b)

D.4.2. Drag on pontoons

The drag force on the pontoons and turbines is depending on the shape of the structures. Slender streamlined structure experiences less drag than a robust structure. The shape is represented in the drag force equation with the drag coefficient. Multiple guidelines indicate the order-size of the drag coefficient. Figure D.13 represents an overview with additional information. Important items to consider are the aspect that the structure is 'floating' and hence not rigidly connected to the bottom. This indicates the importance of the waterdepth-draught ratio, in here $25/13 = 1,92$. The draught of the FishFlow turbines is considered as governing as the turbines span the main length of the structure and its area is almost 14 times larger than the pontoon area, Figure D.11. Yet, the pontoons are solid and the turbines allow flow to pass through, Figure D.12. First the drag coefficient of the pontoons is considered and later the coefficient of the turbine. In addition, the coefficients vary when the current comes in under an angle. The maximum incoming current angle is $45 / 2 = 22,5^\circ$, generally the flow will be perpendicular on the structure.

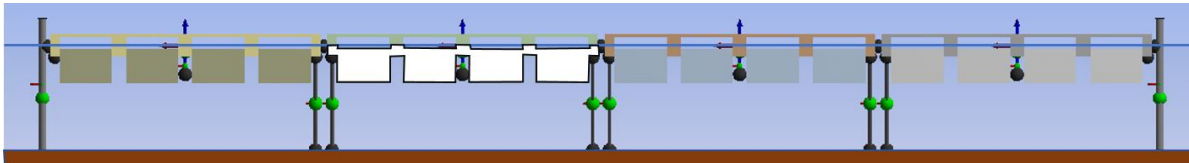


Figure D.11: Surface area facing perpendicular flow; $\alpha = 0$



Figure D.12: Surface area facing perpendicular flow; $\alpha = 0$ (Vos, 2017)

British Standard 1898	DNV-RP-H103	DNV-RP-H103	DNV-RP-H103	DNV-RP-H103	DNV-RP-H103	OCIMF - 2017
Rectangular pontoon	2D: thin square	3D: Rectangular slender plate	3D: Square rod	Pile: rectangle with rounded corners	Two thin plates, side by side	LNG Tanker
L/B = 2,4 [0,34] B/D = 6 [7,69] WD/D = 3 [1,92] Fr = 0,1 (U=2 m/s)	L/B = 1 [0,34] $\Theta = 0$	B/h=10 [8,33]	L/D=1 [0,34]	L/D = 0,5 [0,34] R/D = 0,25 [0,21]	E/D = 0,5 [0,22]	WD/d = 2,73 [1,92]
$C_D = 0,83$	$C_D = 2,20$	$C_D = 1,5$	$C_D = > 1,15$	$C_D = 1,6$	$C_D = 1,42 - 2,2$	$C_D = 0,04$
Slightly too low Lower L/B	Too high TB is floating	Too high TB less slender	Too low L/D is smaller than 1	Too high TB is floating	Too high/ In between Floating + smaller gap	Too low TB: Less streamlined

Figure D.13: Comparison of drag coefficients, [...] indicates the Tidal Bridge ratio ((Det Norske Veritas, 2011), (Vroegrijk, 2017) and (British Standards Institution, 1989))

Observing the data in Figure D.13, the drag coefficients vary significantly. The exact drag coefficient should be determined with a scale model. Yet, for the analysis a comparison has been made between the considered literature. Different types of ratios are of importance when determining the drag coefficient. First, the type of shape is currently assumed as rectangular, the final design will be more streamlined, reducing the drag coefficient. Next, a significant difference between coefficients can be related to a 'floating' structure or a pile over the whole depth. All DNV-RP-H103 examples are representations of structures that

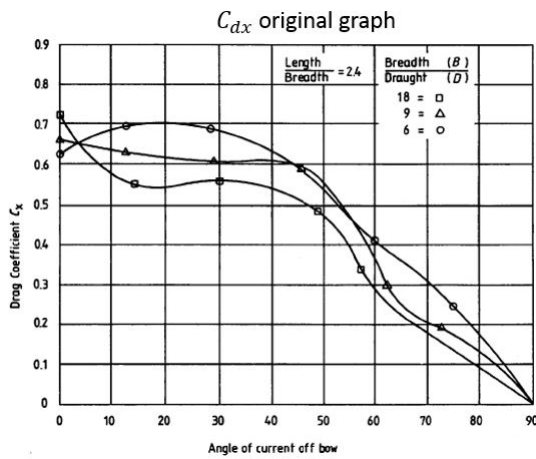


Figure D.16: Original graph of pontoon drag coefficients, C_{dx} (British Standards Institution, 1989)

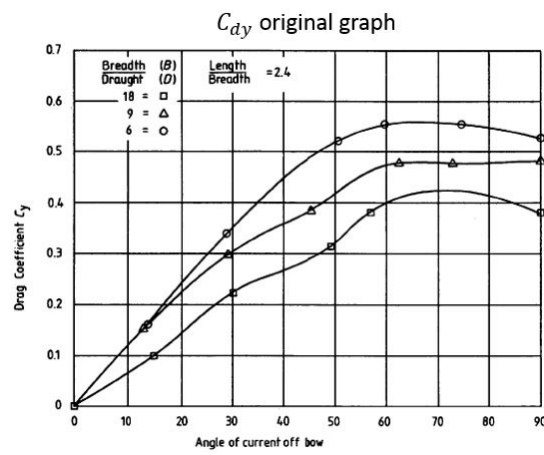


Figure D.17: Original graph of pontoon drag coefficients, C_{dy} (British Standards Institution, 1989)

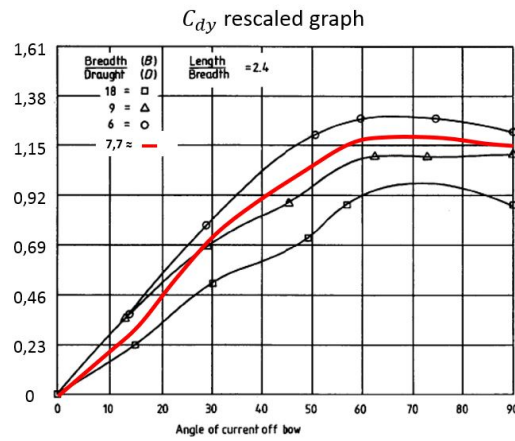
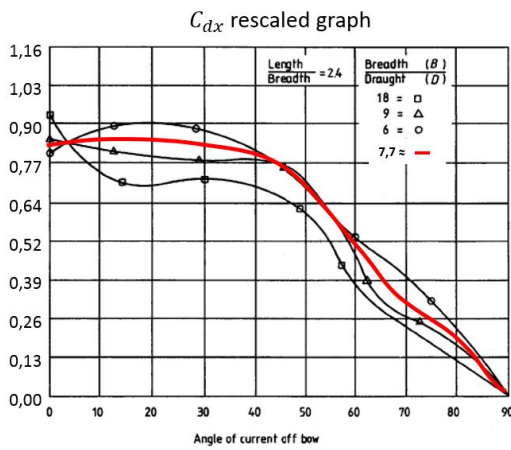


Figure D.18: Rescaled graphs of longitudinal (C_{dx}) and transverse (C_{dy}) drag coefficient for rectangular pontoon.

The coefficients are implemented in formula D.18 in the virtual model for each direction. The formula is dependent on the area that is normal to the flow, the amount of area is computed with formula D.21.

$$F_D = F_{DX} + F_{DY} = \frac{1}{2} * \rho_w * C_D * u^2 * A_n \tag{D.18}$$

$$F_{DX} = \frac{1}{2} * \rho_w * C_{DX} * u^2 * A_{front} \tag{D.19}$$

$$F_{DY} = \frac{1}{2} * \rho_w * C_{DY} * u^2 * A_{side} \tag{D.20}$$

$$A_n = \cos \alpha * A_{front} + \sin \alpha * A_{side} \tag{D.21}$$

F_D	Drag force parallel to flow direction	[N]
u	Incident current velocity	[m/s]
C_D	Drag coefficient	[-]
A_n	Area normal to the current	[m ²]
A_{front}	Area normal to the x-axis	[m ²]
A_{side}	Area normal to the y-axis	[m ²]
α	Incoming current angle	[°]

D.4.3. Turbine induced loads

One of the requirements set by Tidal Bridge is that the maximum moment induced by the currents on the turbine, including resistance, drag and velocity potential difference, does not exceed a value of 21 000 kNm per 100 m of element. It is assumed that the turbine manufacturers deliver a product that does not exceed this limit. First, the annual energy field is considered, the field is based on the flow speed measurements with an ADCP (Acoustic Doppler Current Profiler) at the West and East measurement points on the seabed beneath the proposed project location. Estimation of the possible energy generation with the tidal turbines is determined with an CFD-model (Computational Fluid Dynamics) by the company Dynasim Engineering (2017), Figure D.19. First, the pressure field around the turbine is analysed, two relationships between the force and the moment are found and given in equation D.23 and D.24.

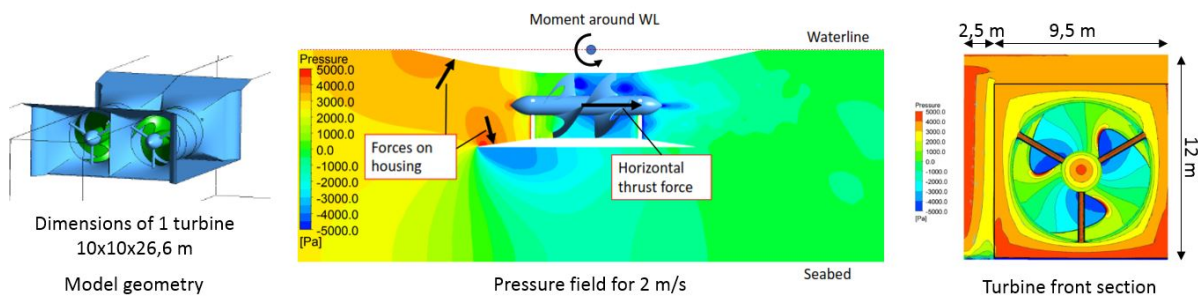


Figure D.19: Results from CFD model with a flow velocity of 2 m/s (Dynasim Engineering, 2017)

	Moment (2 m/s) [Nm/m]	Ratio moments [-]	Moment (1 m/s) [Nm/m]	Arm [m below MWL]	F-section [N/m]	F-m [N/m ²]
Turbine	1 200 000	3,16	300 000	7,00	511 607	42 857
Housing	-800 000	-2,16	-205 000	6,86	-356 607	-29 873
Total	400 000	1,00	95 000	7,32	155 000	12 984

Table D.3: Cursive values indicate the results of the output of the dynasim moments and values (Dynasim Engineering, 2017), straight values are correlated values computed in Excel

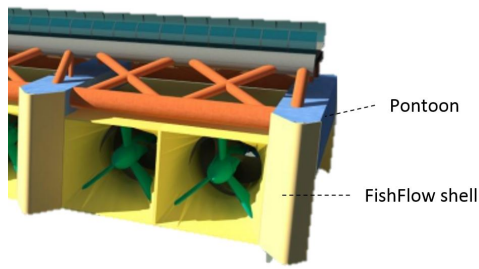
$$M = F * a \quad [\text{Nm}] \quad \text{General formula} \quad (\text{D.22})$$

$$F_x = 155\,000 \, u^2 \quad [\text{N}] \quad \text{Total point force of whole section (143 m}^2) \quad (\text{D.23})$$

$$M = 95\,000 \, u^2 \quad [\text{Nm}] \quad \text{Total moment around x-axis at MWL} \quad (\text{D.24})$$

The CFD-model includes the drag force induced by flow on the pontoons and the turbines. For an optimal flow potential a 'shell' is placed in front of the pontoons, Figure D.20. Dynasim included the shell in the CFD-model. The impermeable shell is placed over the pontoons, indicating that the drag forces on the pontoons itself will not be present. Nevertheless, Dynasim only considered an perpendicular flow. The study regarding the pontoon drag coefficients can not be used to indicate the possible influence of an oblique flow. The forces that act on one total bridge element (100 m) are presented in Table D.21. The moment around the x-axis is calculated with formula D.22, in the formula a indicates the distance between the waterline of the structure and the point of action of the point load, being 7,32 m (Table D.3). The requirement regarding the maximum moment induced by the turbines around the x-axis (at waterlevel) is 2,1 MNm/m. This moment is proportional to a drag force of approximately 34 MN. The flow velocity maximum moment occurs is then 5,2 m/s. Turbines have the possibility to reduce the amount of resistance if high flow velocities are present. The turbine efficiency will decrease, but the maximum tolerable moment is not exceeded. With the information, it is possible to inverse calculate the drag coefficient of the combined Fishflow - Pontoon structure, this results in a drag coefficient of C_d is 2,11. The value is higher than estimated in the previous section. This is explained by the blockage of the water flow through the turbines and as a result of the FishFlow shell. The drag coefficient of 2,11 is assumed as correct.

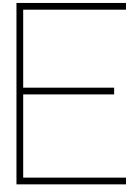
It is uncertain how the combined turbine-pontoon structure will react to an oblique flow. This should be estimated with extensive research or scale-model and implemented in a new model.



Perpendicular flow velocity		Force [MN/100 m]	Moment around x-as [MNm/100 m]
1	m/s	1 265 969	7,76
2	m/s	5,06	31,01
3	m/s	11,39	69,83
4	m/s	20,26	124,14
5	m/s	31,65	193,98
5,202	m/s	34,26	210,00
5,5	m/s	38,29	234,71

Figure D.20: Implemented geometry of FishFlow by Dynasim (Dynasim Engineering, 2017)

Figure D.21: Drag forces on the total submerged part for a 100 m long Tidal Bridge element



Structural dynamics

The method to indicate the motion of the bridge is based on the theory of dynamics of structures. Every moving mechanism can be described with an equation of motion consisting out of four variables and a time and/or space function. The basics of dynamics that are of importance in the research are explained in this Appendix.

E.1. Introduction to dynamics

In general, the response of a bridge span section is considered as a three-degrees-of-freedom response in every point along the bridge. In here, the three degrees of freedom correspond with displacement in horizontal direction, vertical direction and rotation about the shear centre axis of the bridge cross-section (x-axis), Figure E.1. The response of the bridge may be considered in terms of a quasi-static and dynamic part. The quasi-static part is constant throughout the duration of the analysis. The response is determined through traditional static response analysis by applying the environmental loading that may be regarded as static within the time interval of the analysis.

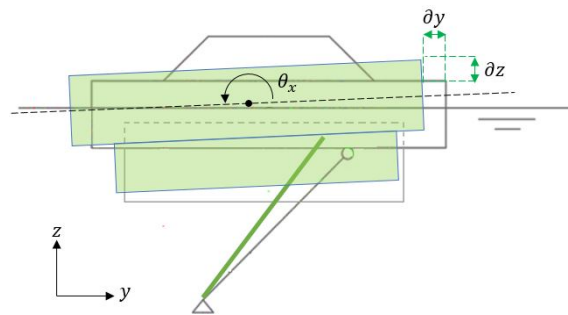


Figure E.1: three-degrees-of-freedom system

The static deflection is considered to represent the position of the bridge span at which the dynamic response takes place. The dynamic response of the bridge is viewed to oscillate about the quasi-static position. The dynamic response arises from the time-dependent parts of the environmental loading. The Tidal Bridge experiences motion in all six degrees of freedom. The dynamic response in a single degree of freedom can be described with a mass-spring-damper system excited to an external forces, the type equation is called the Equation of Motion, equation E.1.

$$m\ddot{x} + c\dot{x} + kx = f(x) \tag{E.1}$$

Where:

$$\begin{aligned} x &= a \sin(\omega t) \\ \dot{x} &= a\omega \cos(\omega t) \\ \ddot{x} &= -a\omega^2 \sin(\omega t) \end{aligned}$$

In equation E.1, m represents the mass of the system, c the damping, k the stiffness and $f(x)$ the excitation force on the system. All variables are depending on the motion x , this motion is for example a wave at the frequency (ω).

The Tidal Bridge system consists of multiple separate 'individual' construction systems. Each system has specific structural properties that influence the stability and hence the dynamic response. A schematic overview of the Tidal Bridge including the direction of the axis is presented in Figure E.2. The combined equation of motion for the total dynamic response of one 100 m long Tidal Bridge element can be written as:

$$[\mathbf{M} + \mathbf{M}_a(\omega)]\ddot{\mathbf{x}} + \mathbf{C}\dot{\mathbf{x}}(\omega) + \mathbf{K}\mathbf{x} = \mathbf{F}_i(\omega) + \mathbf{F}_d(\omega) \quad (\text{E.2})$$

Where:

$$\mathbf{x} = \begin{pmatrix} x \\ y \\ z \\ \varphi \\ \theta \\ \psi \end{pmatrix} = \begin{pmatrix} \text{Surge} \\ \text{Sway} \\ \text{Heave} \\ \text{Roll} \\ \text{Pitch} \\ \text{Yaw} \end{pmatrix} \quad (\text{E.3})$$

In which,

\mathbf{M}	System Mass Matrix	[kg]
\mathbf{M}_a	System Added Mass Matrix	[kg]
\mathbf{C}	System Damping Matrix	[kN/m]
\mathbf{K}	System Stiffness Matrix	[kN/m ²]
$\mathbf{x}(\omega)$	Displacement of the system	[m]
\mathbf{F}_i	Initial forcing function	
\mathbf{F}_d	Dynamic forcing function	

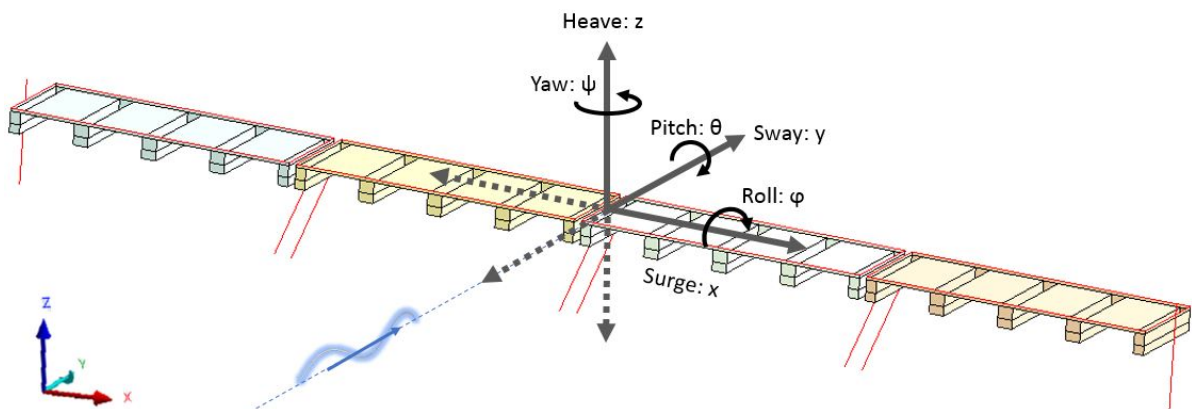


Figure E.2: Six-degrees-of-freedom system with positive axes

E.1.1. Example: floating body in water

To determine the movements of floating structures in water the system characteristics need to be identified. Examples of the characteristics are the mass, stiffness and damping of the structures. To indicate what types of characteristics are necessary to determine the dynamic response of the system, a short example of the motion in one-degree-of-freedom without an external force is considered for a floating body in water, Figure D.1.

In the example, the vertical movement (along z-axis) is considered with a buoy that floats in water. During every moment in time, the Second Newtons law: $F = ma$, is valid for a constant mass (Gerritsma, 2003). In this equation Z represents the sum of all vertical forces acting on the buoy. m is the mass of the buoy [kg] and k represents the 'stiffness' of the vertical motion, in the example this is the upwards water pressure.

$$m\dot{z} = Z \tag{E.4}$$

$$\begin{aligned} Z &= -F_{buoy} + \rho g T A_w - c\dot{z} - a\ddot{z} \\ &= -F_{buoy} + \rho g (T - Z) A_w - c\dot{z} - a\ddot{z} \end{aligned} \tag{E.5}$$

$$\begin{aligned} F_{buoy} &= \rho g T A_w \\ m &= \rho T A_w \\ k &= \rho g A_w \end{aligned}$$

The formula can be reduced to the standard form of the Equation of Motion:

$$(m + a)\ddot{z} + c\dot{z} + kz = 0 \tag{E.6}$$

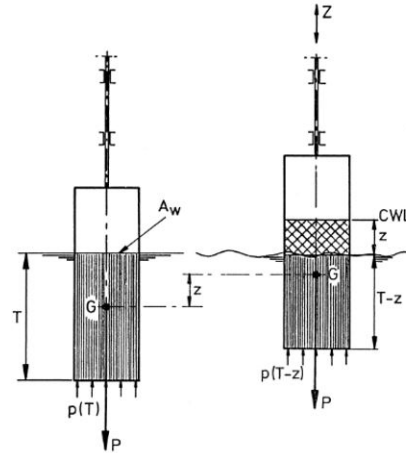


Figure E.3: Schematic representation of displaced buoy in water (Gerritsma, 2003)

The terms $c\dot{z}$ and $a\ddot{z}$ are originated by the hydrodynamic reaction of the movement of the buoy compared to the water surface. Assuming frictionless and incompressible water, indicates that damping is present as result of surface waves. The wave damping is linearly dependent on z by small movement amplitudes. The other part of the hydromechanic reaction, $a\ddot{z}$, is proportional with the vertical acceleration of the buoy movement and occurs as water particles near the buoy are accelerated by the movement. Energy is transferred from the buoy to the water particles and energy dissipation occurs by initiated waves. The coefficient a has a dimension of mass. Implementing the information, the equations can be rewritten.

$$\ddot{z} + 2v\dot{z} + \omega_0^2 z = 0 \tag{E.7}$$

In which;

$$2v = \frac{c}{m + a} \quad \text{and} \quad \omega_0^2 = \frac{k}{m + a} \tag{E.8}$$

In which;

$m + a$	The virtual mass		[kg]
a	Hydrodynamic mass		[kg]
ω_0	The undamped eigenfrequency	$\omega_0 = \frac{2\pi}{T_0}$	[rad/s]
T_0	The undamped eigenperiod		[s]
ω_z	The eigenfrequency	$\sqrt{\omega_0^2 - v^2}$	[rad/s]

The solution of these equations is: $z = Ce^{\alpha t}$, with:

$$\begin{aligned} \alpha &= -v \pm \sqrt{v^2 - \omega_0^2} \\ &= -v \pm i\sqrt{\omega_0^2 - v^2} \\ &= -v \pm i\omega_z \end{aligned} \tag{E.9}$$

Combining all equations, the solution can be rewritten into:

$$z = e^{-vt} (C_1 \cos \omega_z t + C_2 \sin \omega_z t) \tag{E.10}$$

Equation E.9 has an imaginary part and therefore no particular solution of the equation of motion can exist when $v \geq \omega$, as the square root will become real. When formulating initial boundary conditions the constants

C_1 and C_2 can be found and the problem can be solved. As an example for the initial boundary conditions Figure E.4 is used. The initial boundaries are defined at $t=0$ seconds, and may be the position $z = z_a$ and the velocity $\dot{z} = 0$. The time-dependent boundary condition is formulated with the function $z(t) = z_a - e^{-\nu t}$.

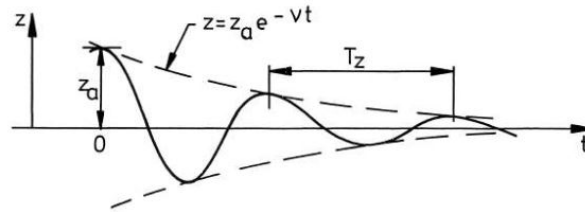


Figure E.4: Damping curve with coefficients and parameters (Gerritsma, 2003)

E.1.2. Floating pontoon bridge

Converting the wave pressure to a dynamic response is done by computing the steady state displacement of the structure under an uniform harmonic load. The systems eigenmodes and corresponding modal frequencies are computed first. After this, the systems equation of motion is combined with said results and transformed to the modal form. The expression includes the sum of all modal responses and an actual response of the structure for all degrees of freedom in the same time function. The equation of motion for the final response can be reduced to the following equation (Spijkers et al., 2006).

$$M\ddot{u} + C\dot{u} + Ku = F(t) \quad (\text{E.11})$$

u	System displacement; system velocity	[m]
\dot{u}	First derivative of time; system acceleration	[m/s]
\ddot{u}	Second derivative of time	[m/s ²]
M	System mass matrix [6x6]	[kg]
C	System damping matrix [6x6]	[N s/m]
K	System stiffness matrix [6x6]	[N/m]
$F(t)$	External (harmonic) force depending on time	

$$u(t) = \sum_{i=1}^n \hat{x}_i u_i(t) \quad (\text{E.12})$$

$u(t)$	System response
n	Number of eigenmodes of the system
\hat{x}_i	Eigenvector of mode i (Mode shape)
$u_i(t)$	Modal response of mode i

$$u_i(t) = \hat{u}_i \sin(\Omega t - \phi_i) \quad (\text{E.13})$$

\hat{u}_i	Response amplitude for mode i	[m]
Ω	Frequency of the force	[rad/s]
ϕ_i	Phase shift	[rad]

Combination of equation E.11 and E.12 the total equation of motion of the system is formulated:

$$\ddot{u}_i + 2\zeta_i \omega_i \dot{u}_i + \omega_i^2 u_i = \frac{F^*(t)}{m_{ii}^*} \quad \text{for } i = 1 \dots n \quad (\text{E.14})$$

$$\zeta_i = \frac{c}{\sqrt{k/m}} \quad (\text{E.15})$$

u_i	Modal displacement of mode i , particular solution	[m]
ζ_i	Modal damping factor for mode i	[-]
ω_i	Modal eigenfrequency of mode i	[rad/s]
$F^*(t)$	Generalized force i	[N]
m_{ii}^*	Modal mass matrix entry for mode i	[kg]

The theory is based on a linear system, while in reality non-linearities in the system are present. The steady state response may be an approximation of the amount of motion that a moving body will experience.

With the information system characteristics as the natural frequencies can be found. The type of frequency indicates at which forcing frequencies large motion may occur and whether the system is sensitive for resonance. The next sections apply the information of the theory to the Palmerah Tidal Bridge case and its properties.

E.2. System properties

The Tidal Bridge elements will be modelled as an infinitely stiff structures. The structural elements have structural properties as mass, centre of gravity and moments of inertia, that determine the stability of the system. The section determines the most important system properties of an individual 100 m long Tidal Bridge element. First, the technical drawings and individual properties of the system components are analysed in Figure E.1. Second, the combined properties are computed and the moments of inertia are calculated.

Element	Mass	Dimensions of element [m]			Vector to midpontoon		
		Length	Width	Height	x	y	z
Pontoon (large)	204 000 kg	34,00	5,00	6,55	23,87 & 0,00 & -23,87	0,00	0,00
Pontoon (small)	96 000 kg	34,00	3,50	6,55	47,87 & -47,87	0,00	0,00
Turbine support structure	600 000 kg	28,80	9,44	10,00	0,00	0,00	-13,49
Equipment	120 000 kg	12,00	2,30	3,00	0,00	0,00	4,40
Truss	900 000 kg	22,00	100,00	5,50	0,00	0,00	7,28
Road	400 000 kg	11,00	100,00	1,00	0,00	0,00	10,52
Total (Equation E.17)	2 320 000 kg				0,00	0,00	3,36

Table E.1: Properties different components Tidal Bridge

With a total mass of 2320 tonne and a pontoon surface area of 748 m², the draught of the pontoon is 3,03m. The buoyancy force becomes 2,06 * 10⁴ kN. The structure as whole will not experience major rotation angles as the limits are set. As a check, the distance the centre of buoyancy and the metacentre, \underline{BM} , is computed with formula E.16. With small angles, for example $\phi = 2$ degrees, $\tan \phi^2$ reduces to almost zero, making small rotations negligible.

$$\underline{BM} = \frac{I_{TB}}{V_{d,w}} (1 + 0,5 * \tan \phi^2) \quad (\text{E.16})$$

In which;

\underline{BM}	Distance between centre of buoyancy \underline{B} and the metacentre \underline{M}	[m]
I_{TB}	Moment of inertia	[m]
$V_{d,w}$	The pontoon volume under the water line (displaced volume)	[m ³]
ϕ	Rotation angle	[°]

In the formula I_t indicates the moment of inertia of the total floating structure. To determine the centre of gravity of the bridge, the mass and distances, seen from the centre of gravity of the mid pontoon, of all main elements are summed and divided by the total mass.

$$CG_{total} = \frac{\sum M_i [z_i]}{\sum M_i} = \begin{Bmatrix} 0 \\ 0 \\ 3,36 \end{Bmatrix} m \quad (E.17)$$

Figure E.5 considers the centre of gravity of the total Tidal Bridge (CG_{TB}), of the pontoon (CG_p) and the buoyancy centre (CB).

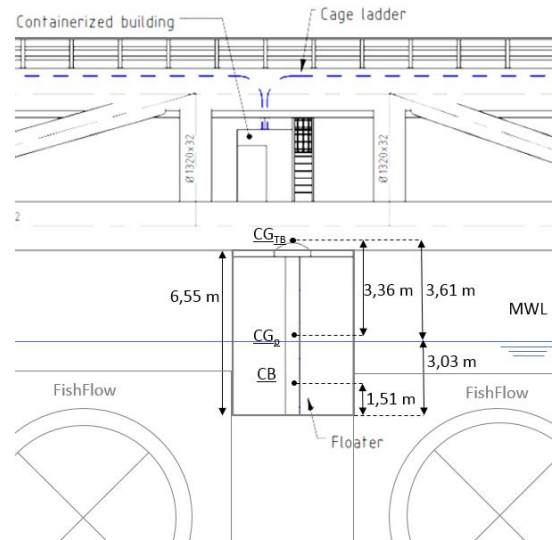


Figure E.5: Centres of gravity Tidal Bridge, side view pontoon

Next, with the information the mass moments of inertia of the combined bridge can be determined according to the *Parallel Axis Theorem*, Peraire and Widnall (2008). First, the theorem is discussed and secondly the moments of inertia are calculated. The components are located at different coordinates along the Fixed Reference Axis (FRA), the tensor of inertia about different axis should be found to calculate the combined moment of inertia. In Figure E.6 two axis are considered, the black axis is the original FRA and the gray axis is the central axis of component i . Peraire and Widnall (2008) state that the moment of inertia with respect to the FRA can be computed by equation E.18.

$$(I_{xx})_{FRA} = I_{xx} + m(y_G^2 + z_G^2) \quad (E.18)$$

In here I_{xx} can be calculated according to the general rules and should be multiplied by the distance between both axes in each direction respectively. Table E.1 indicates that the central axis of all components only differ in z -direction, indicating that only a vector z_G will exist.

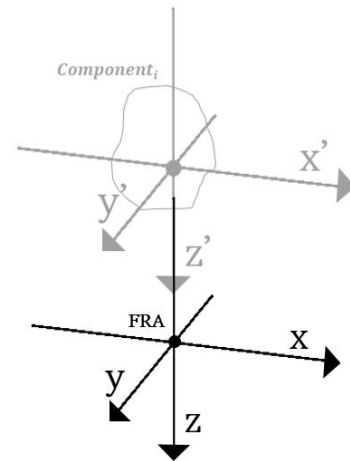


Figure E.6: Example of translated axis of the Tidal Bridge components

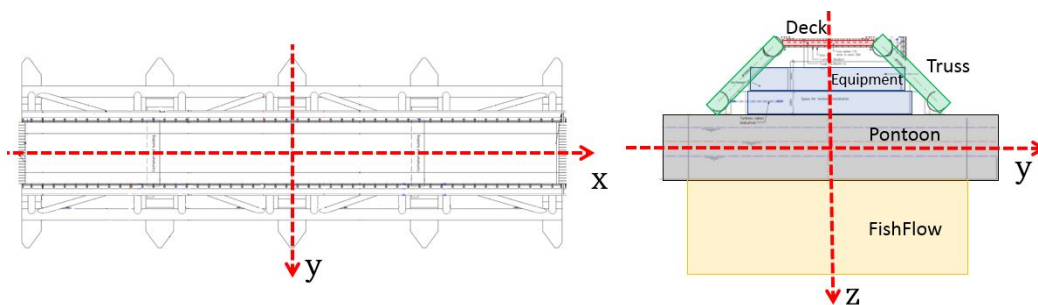


Figure E.7: Symmetry of axis system, symmetric around all axis

A Tidal Bridge element is symmetric along all axis, Figure E.7. With a translation along the z -axis all normal axis centres can be found. In addition, each component is symmetric as well, indicating that the I_{xy} , I_{xz} , I_{yz} values are zero. The the distances between axis centra is zero for δx and δy , the considered moments of inertia are all products of the multiplication to one of the distances and are therefore zero.

With the theorem and the general rules for the inertia values, the moment of inertia of a 100 m long Tidal Bridge element is computed, E.19 and E.20. Equation E.21 presents the final mass moments of inertia with respect to the main axis. In this case, the main axis is located at the centre of gravity of the combined system indicating that z_{Gi} can be calculated by $z_i - z_{TB}$.

$$I_{TB} = \begin{Bmatrix} I_{xx} & I_{xy} & I_{xz} \\ I_{yx} & I_{yy} & I_{yz} \\ I_{zx} & I_{zy} & I_{zz} \end{Bmatrix} \tag{E.19}$$

$$= \begin{Bmatrix} \sum \frac{1}{12} m_i (w_i^2 + h_i^2) + m_i z_{Gi}^2 & I_{xy} & I_{xz} \\ I_{xy} & \sum \frac{1}{12} m_i (l_i^2 + h_i^2) + m_i z_{Gi}^2 & I_{yz} \\ I_{xz} & I_{yz} & \sum \frac{1}{12} m_i (w_i^2 + l_i^2) \end{Bmatrix} \tag{E.20}$$

$$= \begin{Bmatrix} 2,14 * 10^8 & 0 & 0 \\ 0 & 1,73 * 10^9 & 0 \\ 0 & 0 & 1,76 * 10^9 \end{Bmatrix} [\text{kg m}^2] \tag{E.21}$$

In which;

- m_i Mass of component i [kg]
- w_i Width of component i [m]
- h_i Height of component i [m]
- l_i Length of component i [m]
- z_{Gi} Vector between axis component i and central axis [m]

E.3. Connections

This section indicates en calculates all types of hinges and connection. Figure E.8 shows a two-dimensional image with a schematic view of two tidal bridge elements attached to the civil bridge. In the figure four different connections are considered, three of them are hinges and one is the 'rigid' connection to the mainland (green point). The properties of the connections are considered in the section.

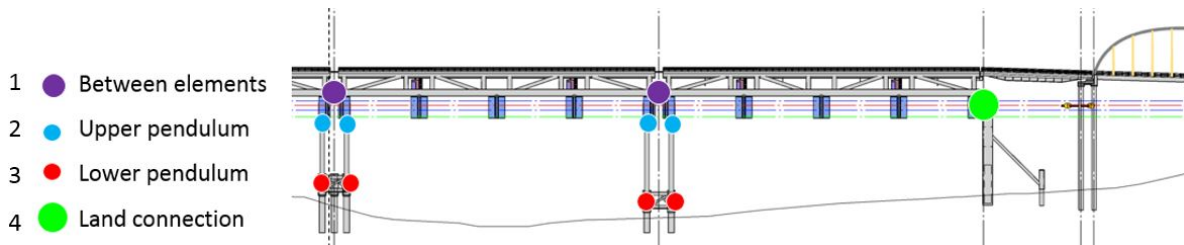


Figure E.8: Different types of connections present in the Tidal Bridge, sideview of half the span of the bridge

E.3.1. Connection between elements

The current hinge design is able to rotate along every axis and is assumed as infinitely stiff with a minimum amount of friction. The hinge design is proposed by Drie-D (2017), a company that supplies mechanical connections for the offshore industry. According to their expertise, the assumption of an infinitely stiff and frictionless hinge is validated. The negligible amount of friction is possible to the use of the material *D-glide*.

E.3.2. Upper pendulum hinge

The hinge at the upper part of the pendulum is the same type of hinge as the hinge between the elements. An infinitely stiff, frictionless hinge that rotates in every degree of freedom.

E.3.3. Lower pendulum hinge

The bottom hinge consists of a more complex design as the hinge functions as the connection between a structure and a foundation. The pendulum is connected to the bottom hinges by means of grouting with shear keys. Three piles function as foundation in the seabed, the piles have a length of 6,5 m above water. The tripod connection functions as a sleeve on top of the piles and grout will fill the area between the transition piece and the monopiles, figure E.9. This type of construction is comparable to offshore wind turbines as is illustrated in Figure E.10. The governing stiffness is given by the grouted connection. According to Det Norske Veritas (2014) the stiffness of a grouted connection with multiple foundation piles connected to another structure can be calculated with formula E.22

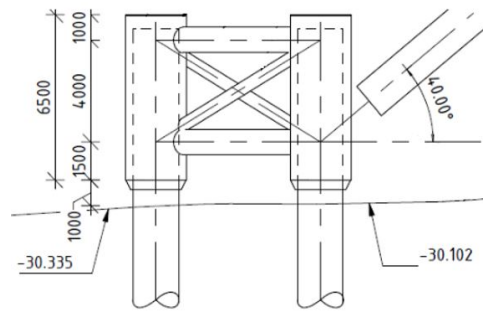


Figure E.9: Tripod connection with 'sleeve' and piles (Antea Group, 2018)

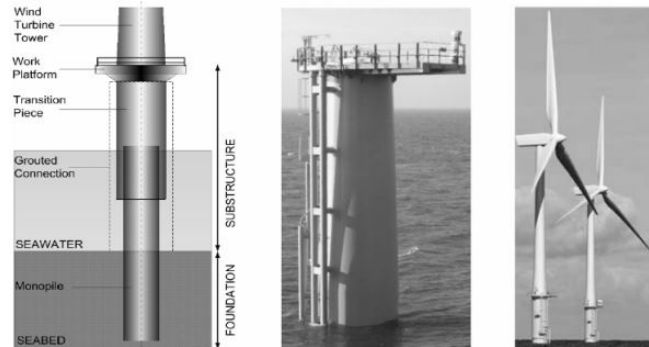


Figure E.10: Wind turbine with grouted monopile foundation (Gupta et al., 2015)

$$k_f = \frac{2 t_{TP} s_{eff}^2 n E_s \Psi}{4 \sqrt[4]{3(1-\nu_s^2)} t_g^2 \left(\left(\frac{R_p}{t_p} \right)^{3/2} + \left(\frac{R_{TP}}{t_{tp}} \right)^{3/2} \right) t_{tp} + n s_{eff}^2 L_g} = 944 \text{ kN/m} \quad (\text{E.22})$$

In which,

k_f	Effective spring stiffness foundation construction	944	[kN/m]
t_{TP}	Wall thickness transition piece	36	[mm]
s_{eff}	Effective vertical distance between shear keys; s-w	670	[mm]
s	Vertical ctc distance between two consecutive shear keys	750	[mm]
w	Width of shear key	80	[mm]
n	Number of effective shear keys	3	[-]
E_s	Young's modulus of steel	210 000	[MPa]
Ψ	Design coefficient for maximum nominal radial contact pressure	0,5	[-]
ν_s	Poisson's ratio for steel	0,3	[-]
t_g^2	Grout thickness	250	[mm]
R_p	Outer radius of inner tube	711	[mm]
t_p	Wall thickness of pile	36	[mm]
R_{TP}	Outer radius of transition piece	997	[mm]
t_{tp}	Wall thickness of transition piece	36	[mm]
L_g	Effective length of grouted section, $L_g = L - 2t_g$	6 000	[mm]
L	Full length grouted section	6 500	[mm]

In general, these type of connections are not always as efficient as designed. Nevertheless, the stiffness value is used to check whether the forces in the mooring pendulums according to the computer model are of a correct order size. The consistence of the seabed is still uncertain, yet the volcanic area indicates granite- and basalt-type rocks. Slopes of volcano's are most times covered by a very brittle type of mixed materials bound in lava containing a lot of air bubbles. Three cobble samples taken from the beach, no the bedrock, are tested on the uniaxial compressive strength (UCS), results vary between a compressive strength of 11,6 MPa to 72,5 MPa. The large range can be explained by the degree of weathering and erosion of the cobbles. One of the samples, with the highest compressive strength, belongs to the strongest and hardest natural rock

mix you can find worldwide. A plate test, to measure a modulus of subgrade reaction, would probably test the stiffness of steel (de Rijke et al., 2017). The bedrock is assumed to be less weathered and eroded, probably comparable to the cobble sample with a high compressive strength. The soil stiffness is assumed as $K_{soil} = 60 \text{ MPa} = 60\,000 \text{ kN/m}^2$ to be conservative. In the research it is assumed that the very stiff soil is sufficiently strong to hold the foundation in place. Nevertheless, an additional soil survey and analysis is recommended.

E.3.4. Spudpoles to mainland

The spudpole is the main connection between the Tidal Bridge and the mainland and transfers high forces. The connection between the pole and the floating body is able to move in vertical and limited horizontal directions, illustrated in Figure E.11. Horizontal displacement of the spudpole is required to let the mooring system function. Without the displacement, an elongation and shrinkage of the bridge will happen continuously. With high or low tide, the floating elements move along the radius of the pendulum, indicating a horizontal movement with a vertical movement. For the movement, elongation of the bridge 'necklace' is required, visualised in Figure E.11. The necessary elongation is calculated in Table E.2, The amount of displacement, in combination with the moment of inertia of the spudpoles can be converted to a spring stiffness.

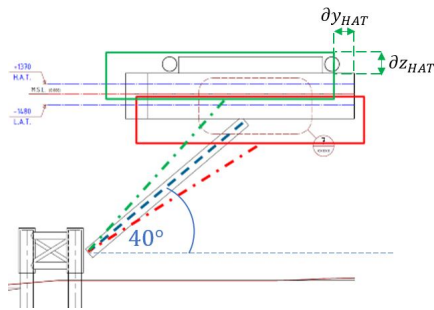


Figure E.11: Displacement due to high tide, cross section

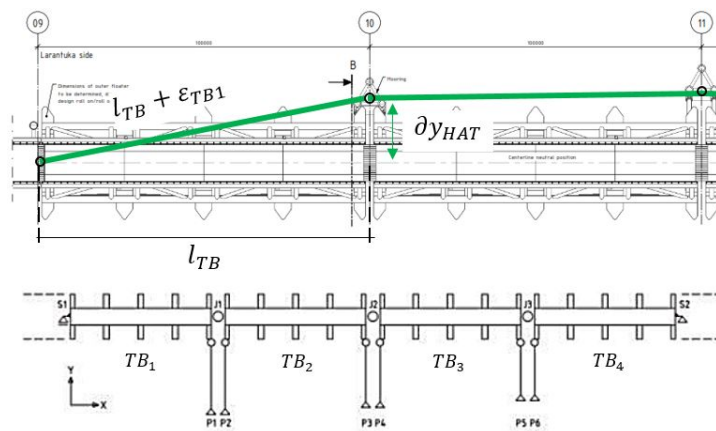


Figure E.12: Displacement due to high tide, top view

Item	Length pendulum	LAT			HAT		
		dz [m]	dy [m]	Angle [°]	dz [m]	dy [m]	Angle [°]
S1	-	-4,85	0	-	3,51	0	-
P1& P2	29,87	-4,85	3,34	28,71	3,51	-3,48	49,49
P3& P4	38,89	-4,85	3,49	31,20	3,51	-3,34	47,14
P5& P6	44,53	-4,85	3,55	32,27	3,51	-3,28	46,19
S2	-	-4,85	0	-	3,51	0	-

Table E.2: Displacement due to tides

Element (100 m)	δy_{LAT} [m]	$\delta \epsilon_{LAT}$ [cm]	δy_{HAT} [m]	$\delta \epsilon_{HAT}$ [cm]
TB1	3,27	5,36	3,52	6,19
TB2	0,22	0,02	0,20	0,02
TB3	0,04	0,00	0,11	0,01
TB4	3,53	6,23	3,40	5,78
Total		11,61		12,00

Table E.3: Elongation of bridge elements

Table E.3 suggests that a total elongation of 12 cm over 400 m is obligatory to realise the horizontal movement of the bridge induced by the mooring system. This elongation is obtained by the deformation of the steel elements and the bending or movement of the spudpoles at the outer bridge ends. Two different types of spudpoles are designed, one rigid spudpole that allows vertical motion (z-axis) and the other spudpole that also allows horizontal movement (along the x-axis), Figure E.13. The design is assumed to be strong enough to adapt to the horizontal forces.

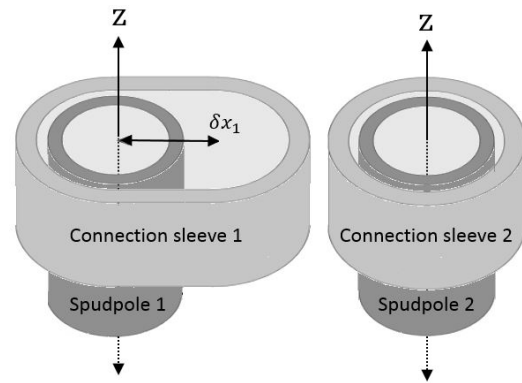


Figure E.13: Spudpole translations

E.4. Stiffness characteristics

The structural properties of the system are obtained by simplifying the system to a floating body in stagnant water. Without a current or surface elevation the body is in a stable equilibrium position. The buoyancy force is in ratio with the mass of the body. The force can be seen as a hydrostatic 'stiffness' contribution as is explained in the first section of the chapter. The hydrostatic stiffness for a floating body is expressed in terms of the associated mode of motion, (Wulff Wathne, 2012).

In general ship engineering the combined heave-roll motion is not included, yet the rectangular shape of the pontoons and turbines the heave and pitch motion are regarded as coupled with roll motion. The stiffness modes represent a force if a displacement in that mode is present.

$$F_{\Delta,stat,i}(t) = k_i * u_i \quad (E.23)$$

$k_{33} = \rho_w g A_w$	In which;	
$k_{34} = k_{43} = -\rho_w g I_{Mxx}$	A_w	Water plane area [m ²]
$k_{35} = k_{53} = -\rho_w g I_{Myy}$	∇	Displaced water volume due to roll motion [m ³]
$k_{44} = \rho_w g \nabla \overline{GM}_T$	\overline{GM}_T	The transverse metacentric height [m]
$k_{45} = k_{54} = -\rho_w g I_{Mzz}$	I_{ii}	Moment of inertia about the i -axis [kg m ²]
$k_{55} = \rho_w g \nabla \overline{GM}_L$	I_{Mii}	Area moments of the water plane around i -axis [m ⁴]

$$\mathbf{K}_{hys} = \begin{pmatrix} 0 & 0 & 0 & 0 & 0 & 0 \\ 0 & 0 & 0 & 0 & 0 & 0 \\ 0 & 0 & k_{33} & k_{34} & k_{35} & 0 \\ 0 & 0 & k_{43} & k_{44} & k_{45} & 0 \\ 0 & 0 & k_{53} & k_{54} & k_{55} & 0 \\ 0 & 0 & 0 & 0 & 0 & 0 \end{pmatrix} = \begin{pmatrix} 0 & 0 & 0 & 0 & 0 & 0 \\ 0 & 0 & 0 & 0 & 0 & 0 \\ 0 & 0 & 7\,518\,1758 & ? & ? & 0 \\ 0 & 0 & ? & 607\,767\,558 & k_{45} & 0 \\ 0 & 0 & ? & k_{54} & 7\,299\,345\,191 & 0 \\ 0 & 0 & 0 & 0 & 0 & 0 \end{pmatrix}$$

When all the stiffness modes are found, the natural frequencies of the system can be computed. The equilibrium situation allows unlimited motion in every degree of freedom, this counteracts with reality. Surge and yaw will be small and the amount yaw is limited, Figure E.14. Roll motion will be the most crucial motion direction as the incoming waves front is perpendicular to the axis. That is the reason pitch will probably be limited as well, no incoming waves are present along the x-axis. The critical hydrostatic stiffness and corresponding frequencies (E.24) are calculated with the modelling software MathCad and presented in Table E.4. The MathCad code is elaborated in section E.6 of this appendix.

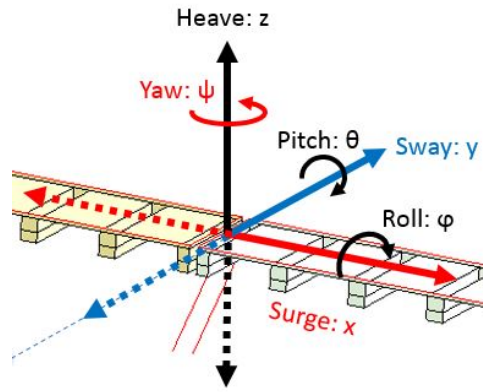


Figure E.14: Restricted or limited degrees of freedom

$$f_i = \frac{1}{2\pi} \sqrt{\frac{k_i}{M_{TB}}} \quad \text{and} \quad f_{\alpha,i} = \frac{1}{2\pi} \sqrt{\frac{k_{\alpha,i}}{I_{tii}}} \quad (\text{E.24})$$

Mode	Axis	Hydrostatic stiffness	Frequency [Hz]	Period [s]
Heave	z	k_z 7 518 758 [N/m]	0,287	3,49
Roll	x	k_ϕ 607 767 558 [Nm/rad]	0,268	3,73
Pitch	y	k_θ 7 299 345 191 [Nm/rad]	0,327	3,06

Table E.4: Hydrostatics computed with Mathcad

A frame of reference for the natural frequencies of the system is to compare the frequencies to the waves present on the sea. Figure E.15 presents multiple types of waves with their frequency range and the amount of arbitrary energy. The red line indicates approximately the natural frequencies of the Tidal Bridge elements. In here, it can be seen that wind sea waves may be of the same frequency and may induce heavy displacements. The frequency of the tides is very small and will induce very gradual displacement and this motion will be less critical for the dynamic response.

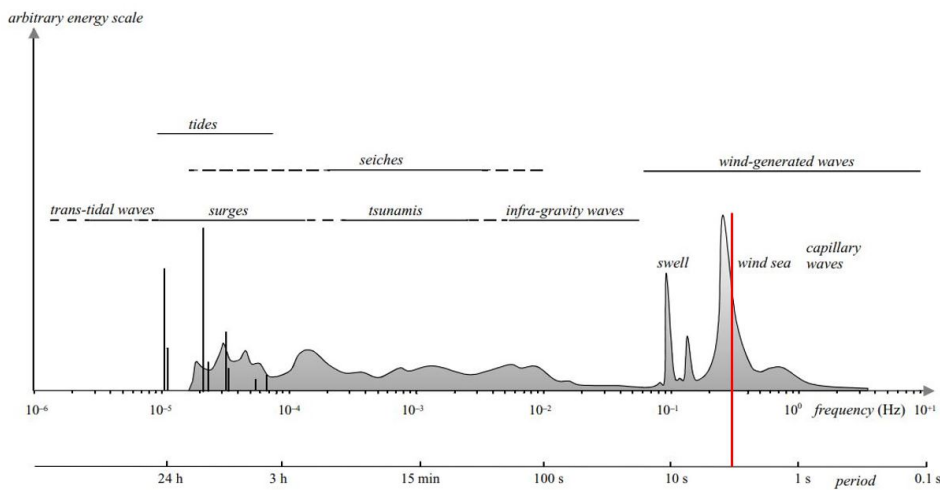


Figure E.15: Frequencies of the vertical motions of the ocean surface (Holthuijsen, 2007)

E.5. Rotation of individual floater

An estimation of the roll-rotation of the floater induced by the flow velocity is calculated with the hydrostatic stiffnesses. The estimation presents an indication of the magnitude of rotation that will be induced by a constant uniform drag force. The rotation is checked for one single 100 metre long floater connected to two pendulums. The drag force is simplified to a constant distributed load acting at a distance of 7.32 m from the waterlevel. The floater is simplified to a plane (97,5x34x1) constructed through a truss girders in *Matrixframe*. A truss girder is defined beneath the floater plane to create an application point for the drag force. An overview of the construction is presented in Figure E.16. The girder profiles for the truss structure are defined as very thick steel tubes: S355 2000x800 mm. The strong profile is chosen to prevent additional rotations as a result of bending of the truss structure. The pendulum has dimension corresponding to the technical drawings: S355 1320x36 mm. The hydrostatic stiffnesses, that are a result of the upwards water pressure and the mass of the bridge, are designed at the outer ends of the pendulum on the x-axis (the centre line of the bridge). The implemented stiffnesses are presented in Table E.5.

The drag force is computed in Chapter 4 and has a value of $13 \cdot u^2$ kN/m. The maximum moment that is allowed around the x-axis (2,1 MNm/m) is present at 5,2 m/s. The maximum distributed drag force is thus $q_{\text{drag}} = 13 \cdot 5,2^2 = 351$ kN/m.

k_X	150 000	kN/m	Spudpole stiffness (found in Chapter 7)
k_Z	3 759	kN/m	$0.5 \cdot k_{\text{heave}}$
k_{RX}	303 833	kNm/rad	$0.5 \cdot k_{\text{roll}}$
k_{RY}	3 564 610	kNm/rad	$0.5 \cdot k_{\text{pitch}}$

Table E.5: Stiffness of $k_{\text{hydrostatic}}$

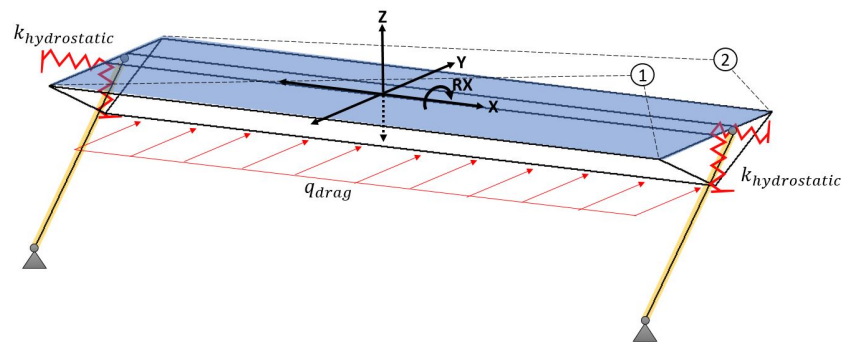


Figure E.16: Schematic representation of one floater with drag force en pendulum system, created in Matrixframe

The displaced system is calculated by Matrixframe for a positive and negative distributed drag force. The displacement of the outer plane points, points 1 and 2 in Figure E.16, are presented in Table E.6. The rotation for a positive and negative drag force is counter-equivalent. This is explained by the length pendulum, the floater moves along the radius of the pendulums. The direction of the radius is dependent on the direction of the drag force. An illustration of the cross sections of the displaced bodies is presented in Figure E.17. In the figure it can be seen that the draught of the floater varies significantly. The response is not probable, the mass of the structure will secure the structure around the water line. The response in Matrixframe may be a result of the heave stiffness. The heave stiffness is defined with equation E.25. The floater is floating on top of five pontoons with a total area of 748 m². The length and width of the bridge suggest a significant increase in area: $100 \cdot 34 = 3400$ m². With the second area, the heave stiffness with a factor 4,5. The option with the increased heave stiffness is defined in Matrixframe as well and the results are presented in the table. With the increased hydrostatic stiffness, the vertical displacement decrease from 3,69 m to 0,84 m, which is more probable. The roll-rotation remains counter-equivalent as the hydrostatic stiffness for the roll-rotation does not change. This is doubled checked as the difference between the vertical displacement of point 1 and point 2 remains 3,98 m between both points.

$$k_{\text{heave}} = \rho \cdot g \cdot A_{\text{submerged}} \quad (\text{E.25})$$

k_{heave} (kN/m)	q_{drag} (kN/m)	Point 1			Point 2			Displacement centre point			Rotation RX [°]
		X [m]	Y [m]	Z [m]	X [m]	Y [m]	Z [m]	dX [m]	dY [m]	dZ [m]	
3 759	351	0,0006	2,4051	-5,6824	-0,0004	2,4051	-1,7011	0,0005	2,4051	-3,6918	-6,7400
3 759	-351	-0,0006	-2,4051	5,6824	0,0004	-2,4051	1,7011	0,0005	-2,4051	3,6918	6,7400
16 666	351	0,0006	0,0954	-2,8289	-0,0004	0,0953	1,1524	0,0005	0,0954	-0,8383	-6,7400
16 666	-351	-0,0006	-0,0954	2,8289	0,0004	-0,0953	-1,1524	-0,0005	-0,0954	0,8383	6,7400

Table E.6: Displacement of points 1 and 2 to a horizontally distributed drag force.

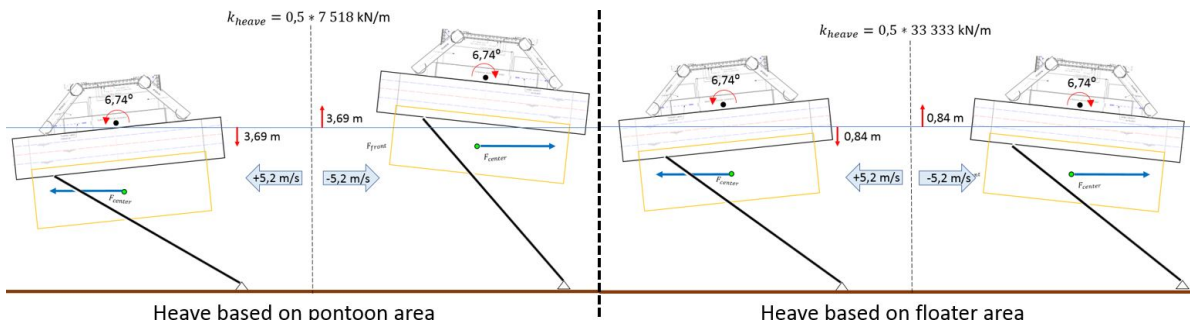


Figure E.17: Illustration of displaced floater with computed values from Table E.6

An inaccuracy in the Matrixframe model is that the force moves with the structure. If the structure moves vertically, the force moves as well. In the figure this is visualised with the blue arrow that represents the drag force. The inaccuracy in the model effects the vertical displacement, a screenshot of the displaced floater for a negative flow speed is presented in Figure E.18. In addition, the water body that flows through the turbines will probably secure the floaters below the waterline. The roll-rotation is of the same magnitude for both computations and is of a reasonable amount. The second option is assumed as a correct estimation of the probable response of the floater.

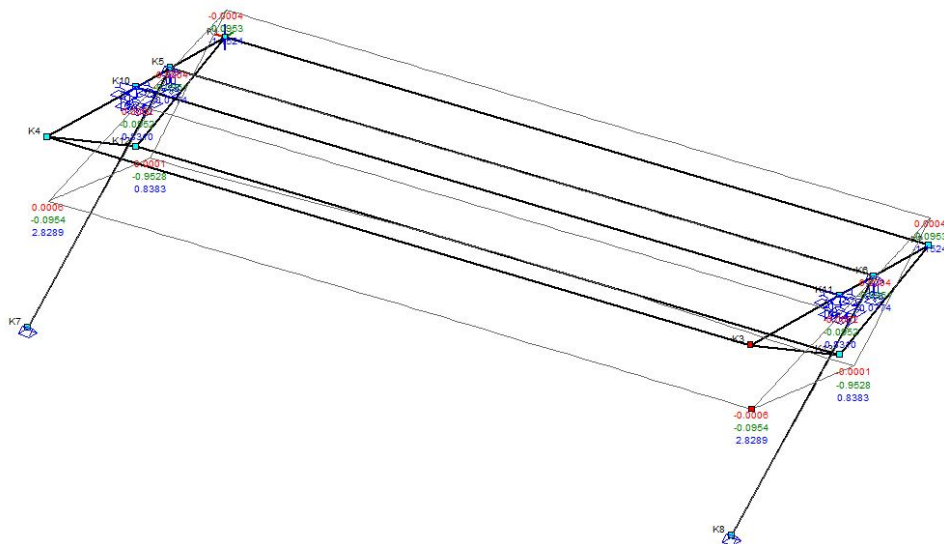


Figure E.18: Screenshot from the Matrixframe model for a negative flow speed

E.6. MathCad file

Computation of the moments of inertia, centres of gravity, frequencies and other equations is done with the help of the computer software *MathCad*. The input files are presented in here.

Input data

Density water	: $\rho_{\text{water}} := 1025 \frac{\text{kg}}{\text{m}^3}$
Dimensions and structures	
Bequip	: $B_{\text{equip}} := 12\text{m}$ # als het over de container building haat is het 12x3x16.5
Hequip	: $H_{\text{equip}} := 3\text{m}$
Lequip	: $L_{\text{equip}} := 2.3\text{m}$
Mass of equipment	: $M_{\text{equip}} := 120\text{tonne}$
Bturbine supportstruc.	: $B_{\text{ts}} := 3\text{m}$
Hturbine supportstruc	: $H_{\text{ts}} := 25\text{m}$
Total mass of turbines	: $T_{\text{Mturbines}} := 600\text{tonne}$
Hfloaters supportstruc	: $H_{\text{fl}} := 6.55\text{m}$
Length of the floaters	: $L_{\text{floaters}} := 34\text{m}$
Mass of large floater	: $M_{\text{Lfloater}} := 68\text{tonne}$
Number of large floaters	: $N_{\text{L}} := 3$
Mass of small floater	: $M_{\text{MSfloater}} := 48\text{tonne}$
Number of small floater	: $N_{\text{S}} := 2$
Length of the bridge	: $L_{\text{bridge}} := 100\text{m}$
Whidth of truss	: $W_{\text{truss}} := 22\text{m}$
High of truss	: $H_{\text{truss}} := 5.5\text{m}$ #is geen rechthoek, maar vakwerk met schuine wanden
Mass of truss structure	: $M_{\text{truss}} := 900\text{tonne}$
Whidth of the road	: $W_{\text{road}} := 11\text{m}$
Mass of trafic road	: $M_{\text{road}} := 400\text{tonne}$
Total mass bridge	: $T_{\text{Mbridge}} := M_{\text{road}} + M_{\text{truss}} + M_{\text{equip}} + N_{\text{L}} \cdot M_{\text{Lfloater}} + N_{\text{S}} \cdot M_{\text{MSfloater}} + T_{\text{Mturbines}} = 2.32 \times 10^6 \text{ kg}$

Centers of gravity

Center of gravity Road	: $g_{\text{r}} := \begin{pmatrix} 0 \\ 0 \\ 10.525 \end{pmatrix} \text{m}$
Center of gravity truss	: $g_{\text{t}} := \begin{pmatrix} 0 \\ 0 \\ 7.2775 \end{pmatrix} \text{m}$
Center of gravity floaters total	: $g_{\text{f}} := \begin{pmatrix} 0 \\ 0 \\ 0 \end{pmatrix} \text{m}$ #mid-mid floater (niet tov waterlijn)
Center of gravity floaters individually	: $g_{\text{fi}} := \begin{pmatrix} 49.5 - \frac{3.5}{2} \\ 23.875 \\ 0 \\ -23.875 \end{pmatrix} \text{m} \cdot \begin{pmatrix} 0 \\ 0 \\ g_{\text{f}_2} \\ 0 \end{pmatrix} = \begin{pmatrix} 47.75 & 0 & 0 \\ 23.875 & 0 & 0 \\ 0 & 0 & 0 \\ -23.875 & 0 & 0 \\ -47.75 & 0 & 0 \end{pmatrix} \text{m}$
Center gravity small floater	: $g_{\text{fsf}} := \begin{pmatrix} 0 \\ 0 \\ 47.75 \end{pmatrix} \text{m} = \begin{pmatrix} 0 \\ 0 \\ 47.75 \end{pmatrix} \text{m}$
Center of gravity large floater:	: $g_{\text{flf}} := \begin{pmatrix} 0 \\ 0 \\ 23.875 \end{pmatrix} \text{m} = \begin{pmatrix} 0 \\ 0 \\ 23.875 \end{pmatrix} \text{m}$
Center of gravity turbines total	: $g_{\text{tur}} := \begin{pmatrix} 0 \\ 0 \\ -7.5 \end{pmatrix} \text{m}$
Center of gravity equipment	: $g_{\text{e}} := \begin{pmatrix} 0 \\ 0 \\ 4.4 \end{pmatrix} \text{m}$
Center of gravity total bridge:	: $g_{\text{b}} := \frac{g_{\text{r}} \cdot M_{\text{road}} + g_{\text{t}} \cdot M_{\text{truss}} + g_{\text{tur}} \cdot T_{\text{Mturbines}} + g_{\text{e}} \cdot M_{\text{equip}}}{(T_{\text{Mbridge}} - M_{\text{Lfloater}} \cdot N_{\text{L}} - M_{\text{Sfloater}} \cdot N_{\text{S}})} = \begin{pmatrix} 0 \\ 0 \\ 3.36 \end{pmatrix} \text{m}$
Center of gravity 2:	: $g_{\text{b2}} := \frac{g_{\text{r}} \cdot M_{\text{road}} + g_{\text{t}} \cdot M_{\text{truss}} + g_{\text{tur}} \cdot T_{\text{Mturbines}} + g_{\text{e}} \cdot M_{\text{equip}} + 0}{(T_{\text{Mbridge}})} = \begin{pmatrix} 0 \\ 0 \\ 2.926 \end{pmatrix} \text{m}$

Vertical Translation stiffness

Width of large floater	: WLfloater := 5m
Width of small floater	: WSfloater := 3.5m
Projected surface large floater	: APL := WLfloater·Lfloaters = 170 m ²
Projected surface small floater	: APS := WSfloater·Lfloaters = 119 m ²
Verticle stiffness total	: TCz := (APL·NL + APS·NS)· water·g = 7.519 × 10 ⁶ · $\frac{\text{N}}{\text{m}}$

Natural frequency heave

Natural frequency z-direction :

$$f_z := \frac{1}{2} \cdot \sqrt{\frac{TCz}{TM_{\text{bridge}}}} = 0.287 \cdot \text{Hz}$$

Periode time in z-direction : $T_z := \frac{1}{f_z} = 3.49 \text{ s}$

Angular mass moment of inertia

Mass moment of inertia truss around y-axis : $J_{ty} := \frac{1}{12} \cdot M_{\text{truss}} \cdot (L_{\text{bridge}}^2 + H_{\text{truss}}^2) + M_{\text{truss}} \cdot (g_{t_2} - g_{b_2})^2 = 7.661 \times 10^5 \cdot \text{tonne} \cdot \text{m}^2$

Mass moment of inertia truss around x-axis : $J_{tx} := \frac{1}{12} \cdot M_{\text{truss}} \cdot (W_{\text{truss}}^2 + H_{\text{truss}}^2) + M_{\text{truss}} \cdot (g_{t_2} - g_{b_2})^2 = 5.238 \times 10^4 \cdot \text{tonne} \cdot \text{m}^2$

Mass moment of inertia truss around z-axis : $J_{tz} := \frac{1}{12} \cdot M_{\text{truss}} \cdot (W_{\text{truss}}^2 + L_{\text{bridge}}^2) = 7.863 \times 10^5 \cdot \text{tonne} \cdot \text{m}^2$

Mass moment of inertia floaters around y-axis :

$$J_{fy} := NL \cdot \frac{1}{12} \cdot ML_{\text{floater}} \cdot (WL_{\text{floater}}^2 + H_{\text{fl}}^2) + NS \cdot \frac{1}{12} \cdot MS_{\text{floater}} \cdot (WS_{\text{floater}}^2 + H_{\text{fl}}^2) + (g_{f_2} - g_{b_2})^2 \cdot (ML_{\text{floater}} \cdot NL + NS \cdot MS_{\text{floater}}) = 4.983 \times 10^6 \cdot \text{m}^2 \cdot \text{kg}$$

Mass moment of inertia floaters around x-axis

$$J_{fx} := \frac{1}{12} \cdot (NS \cdot MS_{\text{floater}} + NL \cdot ML_{\text{floater}}) \cdot (L_{\text{floaters}}^2 + H_{\text{fl}}^2) + (NS \cdot MS_{\text{floater}} + NL \cdot ML_{\text{floater}}) \cdot (g_{f_2} - g_{b_2})^2 = 3.336 \times 10^4 \cdot \text{tonne} \cdot \text{m}^2$$

$$J_{fz} := NL \cdot \frac{1}{12} \cdot ML_{\text{floater}} \cdot (WL_{\text{floater}}^2 + L_{\text{floaters}}^2) + NS \cdot \frac{1}{12} \cdot MS_{\text{floater}} \cdot (WS_{\text{floater}}^2 + L_{\text{floaters}}^2) = 2.942 \times 10^7 \cdot \text{m}^2 \cdot \text{kg}$$

Mass moment of inertia road around the y-axis : $J_{ry} := \frac{1}{12} \cdot M_{\text{road}} \cdot L_{\text{bridge}}^2 + M_{\text{road}} \cdot (g_{r_2} - g_{b_2})^2 = 3.539 \times 10^5 \cdot \text{tonne} \cdot \text{m}^2$

Mass moment of inertia road around the x-axis : $J_{rx} := \frac{1}{12} \cdot M_{\text{road}} \cdot W_{\text{road}}^2 + M_{\text{road}} \cdot (g_{r_2} - g_{b_2})^2 = 2.457 \times 10^7 \cdot \text{m}^2 \cdot \text{kg}$

Mass moment of inertia road around the z-axis : $J_{rz} := \frac{1}{12} \cdot M_{\text{road}} \cdot (W_{\text{road}}^2 + L_{\text{bridge}}^2) = 3.374 \times 10^8 \cdot \text{m}^2 \cdot \text{kg}$

Mass moment of inertia turbines around the y-axis : $J_{ty} := \frac{1}{12} \cdot TM_{\text{turbines}} \cdot (L_{\text{bridge}}^2 + H_{\text{ts}}^2) + TM_{\text{turbines}} \cdot (g_{t_{ur_2}} - g_{b_2})^2 = 6.02 \times 10^5 \cdot \text{tonne} \cdot \text{m}^2$

Mass moment of inertia turbines around the x-axis : $J_{tx} := \frac{1}{12} \cdot TM_{\text{turbines}} \cdot (B_{\text{ts}}^2 + H_{\text{ts}}^2) + TM_{\text{turbines}} \cdot (g_{t_{ur_2}} - g_{b_2})^2 = 1.025 \times 10^8 \cdot \text{m}^2 \cdot \text{kg}$

Mass moment of inertia turbines around the z-axis : $J_{tz} := \frac{1}{12} \cdot TM_{\text{turbines}} \cdot (B_{\text{ts}}^2 + L_{\text{bridge}}^2) = 5.005 \times 10^8 \cdot \text{m}^2 \cdot \text{kg}$

Mass moment of inertia equipment around the y-axis : $J_{eqy} := \frac{5}{12} \cdot \frac{Me_{\text{equip}}}{5} \cdot (Le_{\text{q}}^2 + He_{\text{q}}^2) + 5 \cdot \frac{Me_{\text{equip}}}{5} \cdot (g_{e_2} - g_{b_2})^2 = 2.726 \times 10^5 \cdot \text{m}^2 \cdot \text{kg}$

Mass moment of inertia equipment around the x-axis : $J_{eqx} := \frac{5}{12} \cdot \frac{Me_{\text{equip}}}{5} \cdot (Be_{\text{q}}^2 + He_{\text{q}}^2) + 5 \cdot \frac{Me_{\text{equip}}}{5} \cdot (g_{e_2} - g_{b_2})^2 = 1.66 \times 10^6 \cdot \text{m}^2 \cdot \text{kg}$

Mass moment of inertia equipment around the z-axis : $J_{eqz} := \frac{5}{12} \cdot \frac{Me_{\text{equip}}}{5} \cdot (Be_{\text{q}}^2 + Le_{\text{q}}^2) = 1.493 \times 10^6 \cdot \text{m}^2 \cdot \text{kg}$

Resume angular massmoment of inertia

Total mass of inertia around the y-axis : $J_y := J_{ty} + J_{fy} + J_{ry} + J_{eqy} + J_{ty} = 1.727 \times 10^6 \cdot \text{tonne} \cdot \text{m}^2$

Total mass of inertia around the x-axis : $J_x := J_{tx} + J_{fx} + J_{rx} + J_{eqx} + J_{tx} = 2.144 \times 10^5 \cdot \text{tonne} \cdot \text{m}^2$

Total mass of inertia around the z-axis : $J_z := J_{tz} + J_{fz} + J_{rz} + J_{eqz} + J_{tz} = 1.655 \times 10^6 \cdot \text{tonne} \cdot \text{m}^2$

Angular stiffness

$$\text{Draught pontoons - from bottom} : dz := \frac{TM_{\text{bridge}}}{\text{water} \cdot (APL \cdot NL + APS \cdot NS)} = 3.026 \text{ m}$$

$$\text{Distance Keel - center of buoyancy} : KBz := \frac{TM_{\text{bridge}}}{\text{water} \cdot (APL \cdot NL + APS \cdot NS) \cdot 2} = 1.513 \text{ m}$$

$$\text{Distance Keel - center of gravity} : KGz := \frac{Hfl}{2} + gb_2 = 6.635 \text{ m}$$

$$\text{Second moment of area x} : I_{tx} := L_{\text{floaters}}^3 \cdot \frac{1}{12} \cdot (NL \cdot WL_{\text{floater}} + NS \cdot WS_{\text{floater}}) = 7.206 \times 10^4 \text{ m}^4$$

$$\text{Second moment of area y} : I_{ty} := L_{\text{floaters}} \cdot \frac{1}{12} \cdot (NL \cdot WL_{\text{floater}}^3 + NS \cdot WS_{\text{floater}}^3) + (NL - 1) \cdot (gfi_{1,0})^2 \cdot APL + NS \cdot (gfi_{0,0})^2 \cdot APS = 7.378 \times 10^5 \text{ m}^4$$

$$\text{Angular stiffness around the y-axis} : ACy := \text{water} \cdot g \cdot \frac{TM_{\text{bridge}}}{\text{water}} \cdot \left(KBz + I_{ty} \cdot \frac{\text{water}}{TM_{\text{bridge}}} + -KGz \right) = 7.299345191 \times 10^3 \cdot \frac{\text{MN} \cdot \text{m}}{\text{rad}}$$

$$\text{Angular stiffness around the x-axis} : ACx := \text{water} \cdot g \cdot \frac{TM_{\text{bridge}}}{\text{water}} \cdot \left(KBz + I_{tx} \cdot \frac{\text{water}}{TM_{\text{bridge}}} + -KGz \right) = 607.767558 \cdot \text{MN} \cdot \frac{\text{m}}{\text{rad}}$$

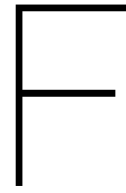
Angular frequencies

$$\text{Own frequency around the y-axis} : f_y := \frac{1}{2} \cdot \sqrt{\frac{ACy}{J_y}} = 0.327 \cdot \text{Hz}$$

$$\text{Periode time around the y-direction} : T_y := \frac{1}{f_y} = 3.056 \text{ s}$$

$$\text{Own frequentie around the x-axis} : f_x := \frac{1}{2} \cdot \sqrt{\frac{ACx}{J_x}} = 0.268 \cdot \text{Hz}$$

$$\text{Periode time around the a-direction} : T_x := \frac{1}{f_x} = 3.732 \text{ s}$$



Anslys Aqwa

F.1. Purpose of the Anslys Aqwa model

The modelling software Anslys Aqwa is based on numerical solution methods. This section addresses the modelling process shortly. Insight in the software indicates the applicability of the model for the unique Tidal Bridge system. Aqwa models various types of waves up to second order. For first order waves, for example small amplitude waves, the incident wave forces are computed with the linear Froude-Krylov force. Next, the force is corrected with a diffraction force to implement disturbance of the waves induced by the moving body. Second order waves, tides and long waves, can be implemented in Aqwa as well. The wave forces are solved for the complex geometries by three dimensional wave diffracting panel methods based on fluid potential theory, conserving mass and momentum. The potential theory assumes an incompressible, inviscid and irrotational fluid, similar to linear wave theory. The second order waves are of importance for the research and the implementation in Aqwa is elaborated in the next section.

The panels are defined on the surface of the complex geometry and split the body into many individual panels, creating a mesh. For each panel, the differential equations and boundary conditions governing the fluid motion around the structure can be solved. The fluid potential is hence solved by input conditions, *the boundary integration approach*. Greene's function requires that each panel contains a source term that can be solved with the hull wetted surface boundary condition. The radiation and diffraction problem can be solved by calculating the source terms.

Aqwa normally assumes that the Reynolds number, a dimensionless quantity to predict flow patterns in fluid dynamics, is sufficient large for the drag coefficient to be considered constant. The assumption is based on the statement that the drag is mainly due to skin friction as a function of the magnitude of the flow velocity.

If a current is defined in the analysis, drag forces on Morison elements ('tubes and discs') due to current velocity are computed by using the Morison equation. In this case the structural velocity is taken as zero. For static stability calculations, only the tube drag force term in the above equation is considered, since the structure and fluid accelerations are not included. The force arising from velocity components in line with the tube axis is assumed to be zero. Morison drag is applicable on tube shaped elements, for example the pendulum system en spudpoles in the Tidal Bridge. The drag forces on the pontoons and turbines should be defined manually as a function of the squared flow velocity.

F.2. Wave conditions

Aqwa can simulate up to two types of waves: Airy waves and second order Stokes waves. In addition, a set with uni- or multi-directional irregular waves can be formulated. Aqwa does not allow implementation of a varying water depth or very gradual changing wave slopes. Hence, the tidal range can not be defined or checked. Waves with a smaller period can be checked. The absence of the implementation of the tidal range is negligible as the maximum angle of the wave slope is $2 \cdot 10^{-9}$ degrees. Influence of high and low water level is checked by adjusting the seabed level and the geometry.

F.2.1. Linear regular wave (Airy wave)

The simplest ocean wave is a linear wave, based on homogeneous, incompressible and frictionless fluid in an irrotational flow. This simple ocean wave has a small amplitude compared to the water depth and wave length (a small wave steepness), applying that the free surface condition is valid. The waves can be referred to as an unidirectional train of waves with constant amplitude and frequency. The wave can be described as a sine wave. The water surface elevation of a linear wave at point (X, Y) is described in complex value form of equation E.1 (Ansys Inc., 2015).

$$\zeta = a_w e^{i(-\omega t + k(X \cos \chi + Y \sin \chi) + \alpha)} \quad (\text{E.1})$$

In which;

ζ	Water surface elevation	[m]
a_w	Wave amplitude	[m]
k	Wave number	[-]
X, Y	Velocity potential in finite water depth at location $\bar{X} = (X, Y, Z)$	
χ	Wave propagation direction	[rad]
α	Wave phase	[rad]

Considering the assumption of ideal and irrotational fluid, the flow is expressed by a velocity potential that satisfies the Laplace equation for the boundary conditions in the: linear free surface condition, the whole fluid domain and for the horizontal impermeable bottom condition. The *Aqwa Theory Manual* (2012) elaborates on the implementation of the condition into the modelling software equations in Section 2.1.

F.2.2. Second order Stokes waves

If a wave becomes steeper, the waves become non-linear or of finite amplitude. The outline of the wave is more peaked at the crests and flatter in the troughs. If non-linearities should be included in Ansys Aqwa, equation E.3 is used to compute a second order Stokes waves. The formula requires input of the estimated Froude-Koulov force over the instantaneous wetted surface. The smallness parameter ϵ represents ratio between the wave amplitude and the wave length and indicates the order size of the Taylor expansion computed by Aqwa (Ansys Inc., 2015). The wave conditions suggest that the Tidal Bridge is always in deep water as the waterdepth $> 0,5 \lambda$ in every scenario. In deep water, the second order Stokes wave potential consist of first order components only, implying absence of set-up and set-down (Ansys Inc., 2015).

$$\zeta = \zeta^{(0)} + \zeta^{(1)} + \zeta^{(2)} + O(\epsilon^3) \quad \text{with:} \quad \epsilon = \frac{a_w}{\lambda} \quad (\text{E.2})$$

$$\begin{aligned} \zeta(X, t) &= \zeta^{(1)}(X, Y; t) + \zeta^{(2)}(X, y; t) \\ &= a_w e^{i(\omega t + kX)} + \frac{1}{2} k a_w^2 e^{i(-2\omega t + 2kX + 2\alpha)} \end{aligned} \quad (\text{E.3})$$

In which;

ζ	Surface elevation	[m]
$O(\dots)$	Taylor order	[-]
ϵ	Smallness parameter	[-]

E.2.3. Irregular waves

Another common type of waves is the wind generated wave, the wave type that is contributing to the most energy at the ocean surface. Winds blow over the fluid surface, creating a wind induced wave system that is vulnerable for local winds. The latter is the main difference compared to swell waves, which are wind generated waves as well but not affected by local winds. Swell waves are developed some time ago at a different location and propagate towards the location. Most winds are non-uniform in velocity and direction, generating a non-uniform wave pattern. The wave pattern is transformed to be applicable in linear wave theory. The multi-directional sea waves are described by a summation of a number of wave components, equation E4 gives an example (Ansys Inc., 2015).

$$\zeta(X, Y, t) = \sum_{n=1}^{N_d} \sum_{j=1}^{N_m} a_{jm} e^{i(k_{jm}X \cos \chi_m + k_{jm}Y \sin \chi_m - \omega_{jm}t + \alpha_{jm})} \quad (\text{E4})$$

N_d	Number of wave direction	[-]
N_m	Number of wave components along each wave direction $\chi_m (m = 1, N_d)$	[-]
a_{jm}	Wave amplitude	[m]
ω_{jm}	Wave frequency	[rad/s]
k_{jm}	Wave number	[-]
α_{jm}	Phase angle of wave component $jm (j = 1, N_m)$	[rad]

Irregular seas can be represented by specification of wave spectra. A wave spectrum defines the distribution of wave energy among different wave frequencies of the sea surface. Different types of wave spectra exist, Aqwa can implement the most common types:

- JONSWAP Spectrum: accounts for imbalance of energy flow: not fully developed seas (input: H_s, f, f_m)
- Pierson-Moskowitz Spectrum: when the sea is fully developed and long crested (input: H_s, f_m, γ)
- Gaussian Spectrum: based on the normal probability density function. (input: H_s, f_m, σ)
- User Defined Wave-spectrum: for input of non-deterministic spectra
- Import Time History of Wave Elevation: is reproduction of model test wave conditions is required.

In here H_s is the significant wave height [m], f the frequency [rad/s], f_m the peak frequency [rad/s], γ the peak enhancement factor [-] and σ the standard deviation. For all spectra, cross swell details can be defined. The Aqwa Theory Manual considers a Table 2,2 for the different peak enhancement factors, in general $\gamma=1$ for the Pierson-Moskowitz spectrum and $\gamma>1$ for the JONSWAP spectrum with a mean peak factor of 3,3 (Barltrop, 1998). The ratio of the peak frequency (T_p) to the zero up-crossing period (T_z or $T_{m0,2}$) is not constant for every spectrum type. For the mean JONSWAP spectrum the ratio is 1:1,286 and for the Pierson-Moskowitz spectrum the ratio is 1:1,41. The spectral forms of these spectra are (Ansys Inc., 2015):

$$S_{JONSWAP}(f) = \alpha g^2 f^{-5} e^{-1,25(f/f_p)^{-4}} \gamma e^{-\frac{(f-f_p)^2}{2\sigma^2 f_p^2}} \quad (\text{E5})$$

$$S_{PM}(f) = 0,3125 H_s^2 \frac{f_p^4}{f^5} e^{-1,25(f/f_p)^{-4}} \quad (\text{E6})$$

E.3. Current

The current represents a horizontal water flow that may vary depending on the water depth. Two current options can be defined in Aqwa and are both dependent on the velocity U [m/s] and the direction θ [degrees].

- Uniform current: constant current velocity from seabed till water surface (input: U_0, θ_0)
- Non-uniform current: current velocity varies along depth, near surface velocity is maximal and at bottom minimal (U_z, θ_z)

The change in tidal current velocity in relation to depth is computed with equation E7 (Barltrop, 1998). With this formula, the surface current is approximately 1,07 times the depth averaged current. The reduction of the current is due to the friction of the seabed.

$$u_{t(z)} = u_{t(z=0)} \left(\frac{h+z}{h} \right)^{1/7} \quad (\text{E7})$$

$u_{t(z)}$	Depth averaged current that occurs at $0,32 h$	[m/s]
h	Total water depth	[m]
z	Distance from bottom, positive upward	[m]

The tidal current velocity for the Tidal Bridge varies along the depth, suggesting the second implementation option. However, the drag force that arises as a result of the current can solely be implemented as an uniform force. It is not possible to implement a current that varies over time in Ansys Aqwa. An alternative solution to analyse the impact of different flow velocities on the motion of the structure should be analysed and compared. The next section elaborated on the methods that are suggested to mimic the behaviour of a varying tide.

F.4. Wave and current interaction

The combination of the fluid particle velocity induced by waves and current may increase the drag force and affect the radiation and diffraction forces on especially the small components of the bridge. Wave-current interaction interpretation is complicated as it is complex to measure the current in fixed Eulerian axes in the presence of waves. Measurements of waves often already include influences due to current, for example Doppler shift or wave frequencies. Baltrop and Adams (1991) stated that this problem can be simplified if the water depth is constant and if the current is steady and constant, Aqwa follows their statement.

"A constant steady current with constant water depth, a regular wave travelling on the current can be modelled by the established wave theory, but the wave period relative to a stationary observer should be shifted as: " - Ansys Inc. (2012a)

$$\frac{\lambda}{T_e} = \frac{\lambda}{T} + U_c \cos \theta' \quad (\text{F8})$$

In here, λ is the wave length [m], T_e is the wave period relative to the stationary observer [s], T is the wave period relative to the current [s], U_c is the current speed amplitude [m/s] and θ is the angle between the current and the waves.

G

Model set-up

The modelling software *Ansys v.19 Academic* consists of many stand-alone sub-software programs. The dynamic response of a structure to wave and currents can be calculated with the *Hydrodynamic Diffraction* and *Hydrodynamic Response* function within *Ansys Aqwa*. Another possibility is to create a CFD model in *Ansys Fluent* to determine for example drag coefficients and stream patterns or to analyse the structural characteristics with *Ansys Structural*. Combining the software tools is possible, yet the different sub-programs do not allow implementation of more than the geometry in the model. The additional data, by example the connections, system characteristics and other implemented parameters, can not be coupled with another subprogram, but should be implemented manually.

Ansys Aqwa requires a significant amount of input parameters for a reliable output. The steps to develop a functioning virtual model will be discussed in this Appendix. In addition, the results of the model should be checked and iterated until a viable set-up is acquired. Next, the parameters and variables for different scenarios should be implemented, analysed and modified. The total process is visualised in Figure G.1.

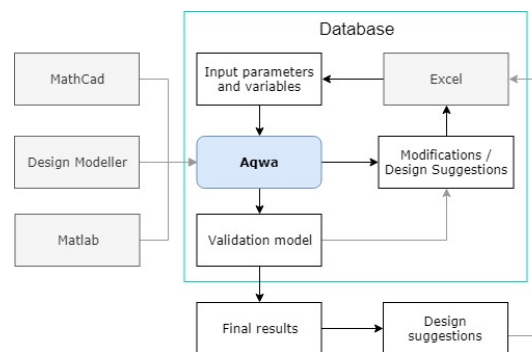


Figure G.1: Iteration process Ansys Aqwa

G.1. Geometry

First step is to create a geometry of the system within one of the 3D software packages that can be implemented in *Aqwa*, *Design Modeller* or *Spaceclaim*, and import the geometry. Ansys requests an empty shell geometry consisting of uncoupled bodies with the main axes at the waterline with the vertical z-axis upwards directed. Every submerged body is used by *Aqwa* to calculate the diffraction loads. The construction above the waterline is neglected in the computation of the model. For that reason, the structural elements of the Tidal Bridge that are located above the waterline, the bridge deck and steel frame, are neglected and not constructed in the geometry.

The bridge is divided into four floating parts of 100 meter. The four floating parts consist of five pontoons and the mooring system, Figure G.2. The turbines are not included in the geometry. The water flow through the turbines can not be modelled in *Aqwa*, hence external forces are implemented to represent the turbine pressures. The waterdepth is set to 25 m, water density is formulated ($\rho_w = 1025 \text{ kg/m}^3$) and the gravitational acceleration ($9,81 \text{ m/s}^2$) is defined. In the geometry, 12 different parts are defined: four Tidal Bridge floating bodies, six pendulum-tubes and the two spud constructions. *Aqwa* requires the input of structural characteristics to transpose the 'empty shell' to a 'floating body'. Obligatory data are the mass,

centre of gravity, radius of gyration and connection points of the particular element. The structural elements define the characteristics of the floating body. For example, the *Point Mass* is a representation of the weight of the element. The characteristics that are implemented are calculated in Appendix E, being: mass, moments of inertia, centre of gravity and the buoyancy point. In addition, connection points on the bodies are formulated to be able to couple individual parts into one system.

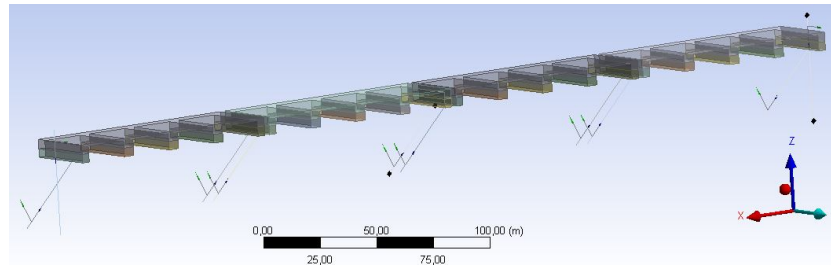


Figure G.2: Geometry input Design Modeller

	I_{xx} [kg m ²]	I_{yy} [kg m ²]	I_{zz} [kg m ²]	Z-coordinate CG	Mass [kg]
Tidal Bridge element	214 400 000	1 727 000 064	1 764 000 000	-3,61	2 323 106
Pendel	448 411 424	446 190 880	2 238 144	-14,01	47 940
Spudpole	20 811 694	208 116	430 125	-7,50	201 633

Table G.1: Input data Ansys Aqwa bodies

G.1.1. Mesh

The geometry step is followed by the generation of a mesh. The mesh size and tolerances and defines the computation time and the allowable frequencies, higher element sizes and tolerances reduce computation time significantly, yet reducing accuracy. For a valid outcome within a realistic computation time, the most important criteria is that the mesh sizes should be small compared to the wave lengths (Ansys Inc., 2015).

$$L_{max} = \frac{1}{7} \cdot \lambda \quad (G.1)$$

In which;

L_{max}	Mesh panel size	[m]
λ	Wave length	[m]

The wave length of the smallest 1-year estimated significant wave is approximately 3 m, Table C.5. Suggesting a maximum mesh element size of 0,42 m, a screenshot of the Ansys Aqwa model for this mesh size is given in Figure G.3. Generating a mesh with this maximum panel size results in over 405 000 panels, increasing computation time significantly. For that reason, an adjusted mesh size is considered for the iteration process. The mesh size is based on the highest frequency of the wave heights that are computed in Appendix C. This is a frequency of 0,72 Hz. Unfortunately, when the model is run with this mesh size, the maximum number of coordinates is exceeded. Hence, the mesh size is iterated until the maximum coordinate number is not exceeded, the third mesh size in the model, the mesh size distribution is visualised in Figure G.4.

	Max. element size	Tolerance	Nr. of Elements	Max. allowed frequency
High accuracy	0,42 m	0,21 m	405 392	0,940 Hz
Max. frequency of 0,72 Hz	0,70 m	0,30 m	149 164	0,728 Hz
Reduced computation time	2,00 m	0,30 m	20 084	0,436 Hz

Table G.2: Mesh input parameters

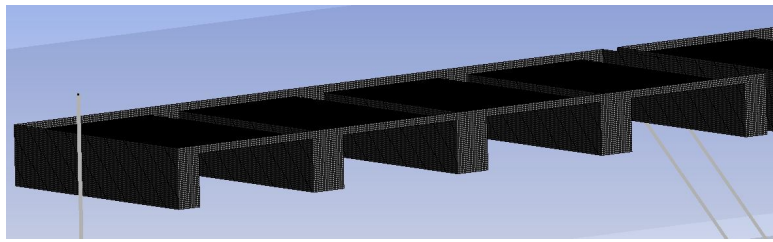


Figure G.3: High accuracy mesh

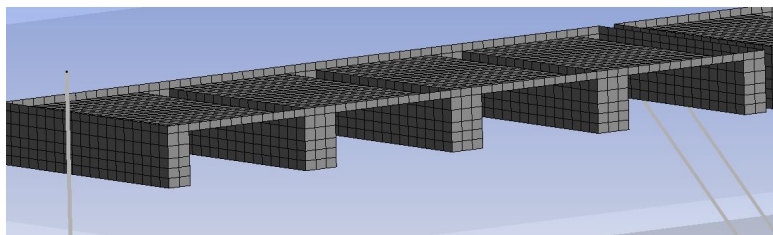


Figure G.4: Reduced computation time mesh

G.1.2. Connections

The geometry considers uncoupled 'bodies', not an interacting coupled mechanism. Connections between the bodies and 'fixed points' (by example points that represent the seabed) are obligatory to define. In Figure G.5, the four different type of 'connections' (hinges) are indicated. The tidal bridge uses ball-and-socket type hinges, hinges that are able to rotate in every degree of freedom. Aqwa allows the implementation of stiffness for all degrees of freedom of the hinges. The hinges are designed and constructed by an offshore construction company that is specialised in frictionless hinges. Hence, the stiffness of these 'hinges' is set to 0 Nm/rad.

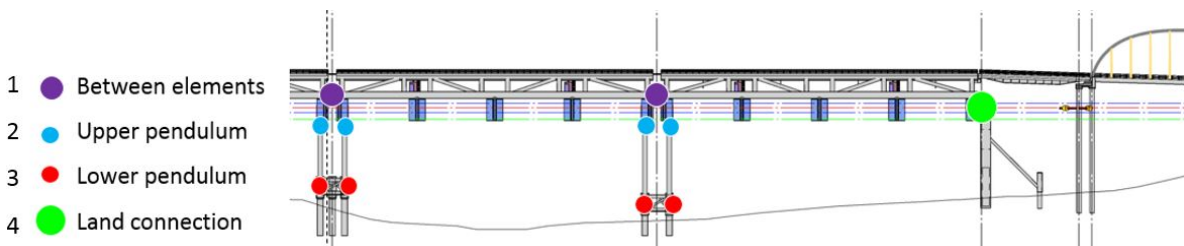


Figure G.5: Schematic overview of different hinge types

Another type of 'hinge' is present between the spud construction and the floating elements, number 4 and 5 in Figure G.6. The spudpoles allow vertical motion and rotations, yet the motion in x- and y- (horizontal) direction is limited. One spudpole should allow some motion in x-direction to create a mechanism, Figure G.7. In Aqwa this type of motion is simulated by deactivating degrees of freedom for the spudpoles. Spudpole 4 can move along the z-axis and x-axis and spudpole 5 only along the z-axis. To restrict the motion in x-direction, an imaginary cable is placed between the spudpole and a fictional 'fixed' point. The function and characteristics of this cable are elaborated in the next section.

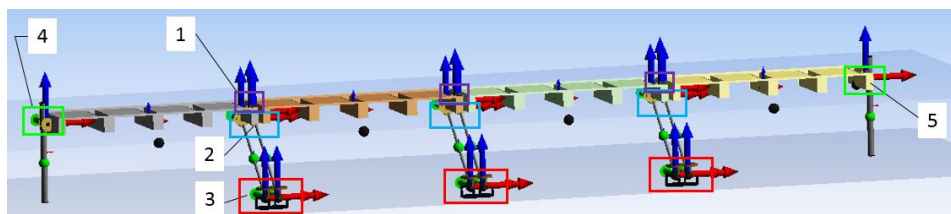


Figure G.6: Connections in Ansys Aqwa

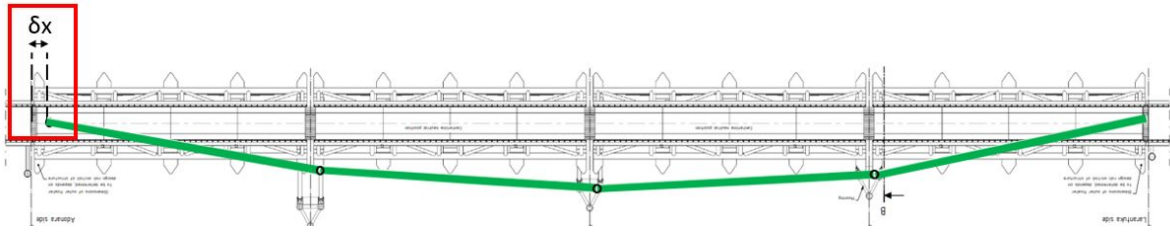


Figure G.7: Necessary displacement for spud construction

G.2. Wave implementation

The influence of waves on the dynamic response of the structure is more apparent to implement. Multiple types of waves can be chosen and characteristic parameters can be defined. The *Hydrodynamic Diffraction* analysis requires an implementation of a sequence of waves in multiple directions to be able to find the *Response Amplitude Operators* (RAO). The RAO indicate the expected response of a floating structure to a certain sea state. The accuracy of the RAO is depending on the amount of wave directions and frequencies, not amplitudes.

The wave data, Appendix C.4, indicates that waves are present in every direction, Table G.3. For an accurate RAO, a total of 50 wave frequencies are defined, equally distributed between 0,016 Hz and 0,44 Hz. The frequency range is depending on and limited by the mesh size. The maximum frequency of 0,44 Hz is accompanied by a wave length of approximately 7,5 m. The width of the bridge is 34 m, suggesting that a wave with a wave length smaller than 7,5 m will not induce large motions. Hence, the mesh size is not reduced. All 50 frequencies are checked for 35 incoming directions. The number of 35 is chosen to be able to check the RAO influence for every 10 degrees. In total, Ansys Aqwa computes and checks the RAO for $50 \cdot 35 = 1750$ wave combinations.

Direction [°]	1 year				50 years				100 years			
	H_s	T_p [s]	f [Hz]	L [m]	H_s	T_p [s]	f [Hz]	L [m]	H_s	T_p [s]	f [Hz]	L [m]
0-20	1,47	6,06	0,16	57,35	2,15	7,14	0,14	79,62	2,26	7,28	0,14	82,76
20-40	1,37	5,87	0,17	53,73	1,71	6,56	0,15	67,20	1,84	6,79	0,15	72,04
40-60	0,73	4,29	0,23	28,78	1,95	6,99	0,14	76,39	2,22	7,47	0,13	87,09
60-80	2,00	7,09	0,14	78,38	3,74	9,61	0,10	144,09	4,13	10,11	0,10	159,42
80-100	0,55	3,73	0,27	21,71	1,47	6,06	0,16	57,40	1,67	6,43	0,16	64,50
100-120	0,12	1,22	0,82	2,34	0,19	1,47	0,68	3,37	0,20	1,50	0,66	3,53
120-140	0,18	1,46	0,68	3,34	0,23	1,61	0,62	4,01	0,24	1,62	0,62	4,08
140-160	0,18	1,44	0,70	3,23	0,19	1,49	0,67	3,48	0,20	1,50	0,67	3,50
160-180	0,19	1,47	0,68	3,40	0,20	1,52	0,66	3,63	0,21	1,53	0,65	3,65
180-200	0,21	1,53	0,65	3,64	0,23	1,60	0,62	3,98	0,23	1,61	0,62	4,01
200-220	0,16	1,38	0,72	2,99	0,23	1,60	0,63	3,96	0,24	1,63	0,62	4,09
220-240	0,63	3,32	0,30	16,35	1,04	4,06	0,25	17,33	1,11	4,17	0,24	17,34
240-260	0,29	1,94	0,52	5,83	0,48	2,39	0,42	6,99	0,52	2,46	0,41	6,96
260-280	0,22	1,58	0,63	3,87	0,25	1,65	0,61	4,21	0,26	1,69	0,59	4,35
280-300	0,24	1,64	0,61	4,19	0,29	1,76	0,57	4,71	0,29	1,78	0,56	4,76
300-320	0,25	1,65	0,61	4,22	0,31	1,82	0,55	4,94	0,30	1,79	0,56	4,82
320-340	1,95	6,99	0,14	76,39	4,39	9,83	0,10	150,73	4,84	10,17	0,10	161,04
340-360	1,58	6,28	0,16	61,63	2,52	7,68	0,13	92,19	2,68	7,87	0,13	96,70

Table G.3: Significant wind wave characteristics for 1, 50 and 100 years. Governing wave directions are highlighted.

The limit of 0,44 Hz in the Hydrodynamic Diffraction analysis is not relevant with respect to the critical dynamic response. This can be explained by the likely response of the bridge to certain wave lengths. The dimensions of the floating structure determine the sensitivity for swaying on the waves. A rule of thumb that indicates the sway is if the wave length is approximately 0,7 times the width of the structure (depending on the wave direction): $L_0 \leq 0,7 \cdot 34 = 23,8$ m (Molenaar and Voorendt, 2018). Figure G.8 illustrates the sensitivity to certain wave lengths. Equation G.2 indicates that an increase wave period is an exponential increase in wave length. Frequency is the inverse of the wave period $f = 1/T$, implying that a high frequency is contributed by a small wave length.

$$L_0 = \frac{gT^2}{2\pi} \approx 1,56 T^2 \quad (\text{G.2})$$

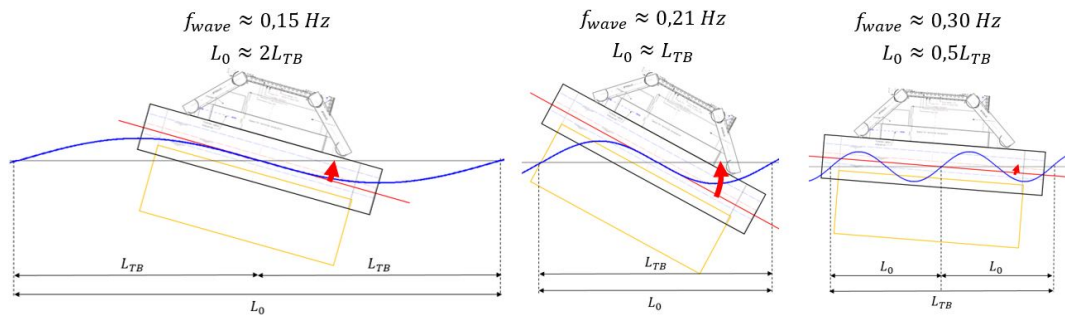


Figure G.8: Influence of motion induced by waves with respect to the wave length

The RAO of the amount of likely rotation about the x-axis RX in [°/m] with respect to wave frequency and direction is presented in Figure G.9. Two clear peaks can be distinguished at a frequency of 0,213 Hz. This frequency is proportional to a wave length of 34 m, confirming the validity of the model. The peaks are present at +90° and -90°. In the rotated axis system of Aqwa, this indicates a perpendicular flow. The outcome of the *Hydrodynamic Diffraction* analysis can be substantiated and the wave input is assumed as correctly implemented. All RAO results will be extensively elaborated in the Chapter 6.4 about the results from Ansys Aqwa.

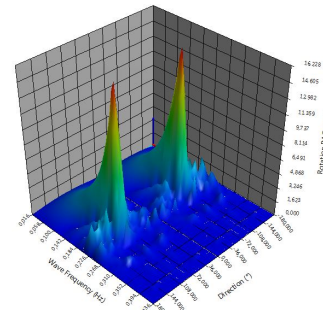


Figure G.9: Response Amplitude Operator: motion [m/m] vs. frequency [Hz] and direction [degrees]

The second wave analysis, *Hydrodynamic Response*, is a time-dependent analysis. The dynamic response for a specific set of waves is computed for a requested defined duration. The type of wave can be chosen, the wave height, period and direction are required and the shape of the wave should be implemented. The absence of actual wave records at the project location suggests that the computed wind waves are estimation and not checked. Therefore, the simplest wave type is considered: the *JONSWAP wave*. The requested input parameters for a JONSWAP wave are the significant wave height (H_s [m]), the peak period (T_p [s]), the direction and gamma [-]. The gamma represents the peak enhancement factor and an average value for the factor for experiment data is 3,3 according to Det Norske Veritas (2011). The values for the *Hydrodynamic Response* analysis are implemented in the sensitivity analysis. As a check the wave surface elevation is computed for a JONSWAP wave spectrum with characteristics: $H_s=2,26$ m, T_p is 7,28 s. The surface elevation is plotted in Figure G.10. During a one hour (3600 seconds) period a wave with a crest height of 2,5 m and a trough of -2,5 m is present. The heights are measured from the mean water level and represent the amplitude and not the actual wave height. The ratio between the significant wave height ($H_s = 2,26$ m) and the maximum wave height ($H_{max} = 2,5 + 2,5 = 5$ m) is 1:2,12. According to the distribution of the significant wave height and the maximum wave height, Figure C.31, the value is very reasonable. The maximum wave height is approximately two times the significant wave height. All in all, it can be concluded that the waves are correctly implemented in the Ansys Aqwa model.

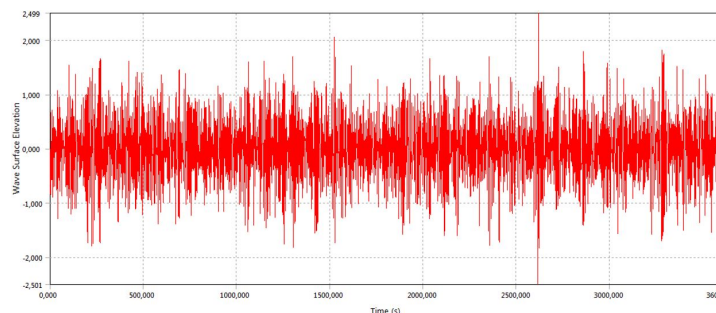


Figure G.10: Wave Surface Elevation of the Jonswap wave over a period of 3600 seconds

G.3. Current implementation

Aqwa has limitations concerning the input of a current. A constant magnitude and direction can be adjusted for a current. Indicating that a varying current velocity can not be implemented. Nevertheless, the maximum velocities induce the largest displacements. Another restriction is the computation method that is used to calculate drag forces in Ansys Aqwa. The drag force is solely computed for 'tube' elements with the Morison equation. Bodies without a cylindrical shape are not included in any drag force computations. The influence of the submerged part to a specific current velocity is neglected and calculated as a drag force of zero. Nonetheless, with a detour the inclusion of the drag force can be implemented for all submerged bodies. This section discusses the possibilities to implement the current induced loads.

G.3.1. Drag force on 'tube-elements'

The pendulum system consists of cylindrical shaped 'tube' elements. Hence, the drag force is calculated by the Morison equation (equation D.14). The Morison-equation calculates the force on a body in oscillatory flow by adding two force components: the drag force and the inertia force. Automatically, the Morison drag coefficient and added mass coefficient are set to 1. The scale factor in Aqwa for the constant is not adjusted as in appendix D.4 the coefficients are estimated as 1,0. Table G.4 considers the Morison drag force on the 'tube-elements' computed in Aqwa for a current of 1 m/s. Only the tube-shaped elements experience Morison drag: the pendulums and the spudpoles. The Morison drag on the floater is zero.

'Tube-element'	Diameter	Ansyes Aqwa	Calculations
		Morison Drag	Morison Drag
Mooring pendulum	1,5 m	5 063 N	$3623 \cdot \dot{u} + 769 \cdot u^2$
Spudpole	3 m	28 8409 N	$14491 \cdot \dot{u} + 1538 \cdot u^2$

Table G.4: Morison drag force on the 'tube-elements' in Aqwa with a current of 1 m/s

In the table, \dot{u} indicates the acceleration potential between the current and the velocity of the tube. The influence of the drag of the 'tubes' is negligible compared to the drag that will be present on the floating elements (ordersize of 1 300 kN). Therefore, the complex acceleration potential is not computed to verify the drag on the cylindrical elements.

G.3.2. Drag force on floating bodies

The first paragraph of this section suggests that a couple of detour options are possible to implement drag forces into Aqwa for non tube-shaped bodies. All options consider the combined pontoon-turbine system. In total, three different methods are analysed, implemented and discussed. In the end, one method is selected to continue with the research. An overview of the three types of methods including their restrictions is presented in Table G.5. The response of the system is unknown and therefore the model can not be calibrated.

Method	Advantages	Disadvantages
1. Current force coefficient	- Direction sensitive - Depending on parametric flow	- Constant current velocity - Time-consuming
2. Structure force matrix	- Time-dependent force - Mimic 48-hours tide	- One force that acts on centre of body - Perpendicular flow
3. Horizontal point force	- Quick	- Constant force - Force moves with structure

Table G.5: Overview of implementation options of drag force in Aqwa

None of the methods mimics the exact behaviour of the bridge. Data is absent about the counteracting forces and moments that occur due to water body that flow through the turbines. It is probable that the moving water body stabilises the rotations around the X-axis. Part of the effect is already implemented in the calculations of the drag coefficients in the CFD-model. This is the counteracting moment that occurs through the housing of the turbines, illustrated in Figure G.11. Nonetheless, the absence of the actual data indicates a non-realistic approximation of the displacement. The influence of this important factor is

discussed in every model implementation option. The options are run for a flow speed with a maximum magnitude of 5,2 m/s, the velocity where the maximum turbine pressure is present.

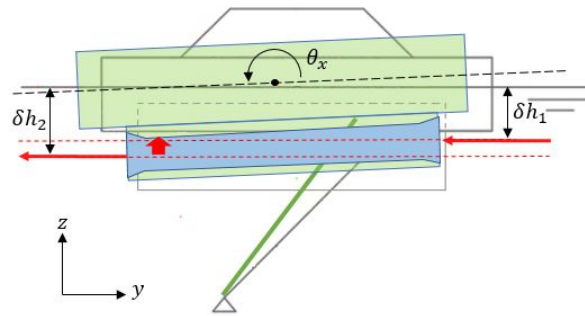


Figure G.11: Visualisation of the stabilising effect of the water body

Method 1: Current Force Coefficient

One of the methods to implement the drag force on the submerged bodies is the "Current Force Coefficient Matrix". The coefficients are considered as the force or moment per unit velocity squared, equation G.3 (Ansys Inc. (2012b)). The moment acts at the centre of gravity of the particular body. The coefficients are functions of the relative velocity between the current and the structure velocity. Aqwa requires an input matrix for an incoming current direction (α) between a range of $+180^\circ$ and -180° . For a valid estimation of the dynamic response the forces or moments for every degree of freedom are indicated in the matrix. Aqwa multiplies the current force coefficients with the magnitude of the current that is defined in a particular direction. The drag force coefficients are estimated in Appendix D.4 and calculated with Excel. A non accurate estimation of the drag coefficients under an angle is obtained by rescaling the graph of British Standards Institution (1989) that represents the drag coefficients for pontoons in deep water.

$$F_{yc} = F_y U^2 = 0,5 \rho_w C_y A_{surface} \tag{G.3}$$

Aqwa does not consider the forces in the direction of the current, but in the direction of the local axes system. A current perpendicular on the pontoon front, is defined in Aqwa with a rotation angle of 90° . In Table G.6 the rotations are transposed to the correct Aqwa input, visualised in Figure G.12. In addition, as a result to the rotation of the axes system, the drag force perpendicular to the bridge is denoted as F_y instead of the general notation F_x .

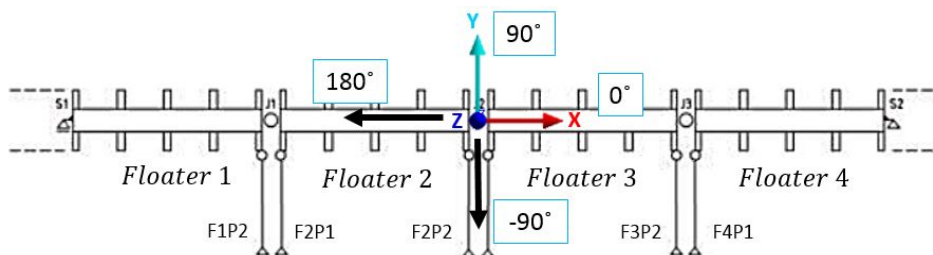


Figure G.12: Rotated axis system Ansys Aqwa

The fundamental input parameters are the force coefficients Y direction and the rotation around the x-axis. The structure will be tested mainly on a perpendicular flow. An incoming flow under an angle will induce other dynamic behaviour. Yet, unfortunately not enough data is conducted to indicate a valid approximation of the drag coefficients and hence a realistic estimation.

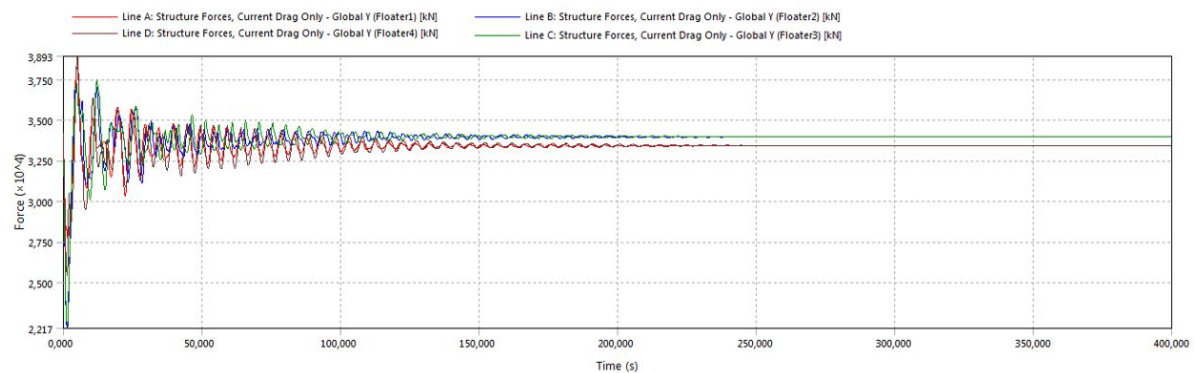
α [°]	Aqwa α [°]	C_x	C_y	C_{xy}	Surge (X) F_x [$\frac{N}{m/s^2}$]	Sway (Y) F_y [$\frac{N}{m/s^2}$]	Heave (Z) F_z [$\frac{N}{m/s^2}$]	Roll (RX) M_x [$\frac{Nm}{m/s^2}$]	Pitch (RY) M_y [$\frac{Nm}{m/s^2}$]	Yaw (RZ) M_z [$\frac{Nm}{m/s^2}$]
0	90	2,11	0,00	0,00	0	1 265 969	0	13 826 317	0	0
10	80	2,02	2,02	0,00	-62 722	1 020 056	0	11 140 580	-685 016	0
20	70	1,73	1,73	0,00	-130 401	1 027 400	0	11 220 785	-1 424 175	0
30	60	1,25	1,25	0,00	-220 733	1 096 361	0	11 973 942	-2 410 742	0
40	50	1,82	1,82	0,00	-309 566	1 057 951	0	11 554 443	-3 380 935	0
50	40	2,02	2,02	0,00	-371 617	894 201	0	9 766 046	-4 058 631	0
60	30	2,11	2,11	0,00	-420 119	695 565	0	7 596 636	-4 588 347	0
70	20	2,21	2,21	0,00	-455 856	475 794	0	5 196 405	-4 978 648	0
80	10	2,30	2,30	0,00	-477 742	241 567	0	2 638 284	-5 217 675	0
90	0	2,40	2,40	0,00	485 112	0	0	0	5 298 166	0
100	-10	2,32	2,32	0,00	477 742	-241 567	0	-2 638 284	5 217 675	0
110	-20	2,32	2,32	0,00	455 856	-475 794	0	-5 196 405	4 978 648	0
120	-30	2,32	2,32	0,00	420 119	-695 565	0	-7 596 636	4 588 347	0
130	-40	2,32	2,32	0,00	371 617	-894 201	0	-9 766 046	4 058 631	0
140	-50	2,32	2,32	0,00	309 566	-1 057 951	0	-11 554 443	3 380 935	0
150	-60	2,32	2,32	0,00	220 733	-1 096 361	0	-11 973 942	2 410 742	0
160	-70	2,32	2,32	0,00	130 401	-1 027 400	0	-11 220 785	1 424 175	0
170	-80	2,32	2,32	0,00	62 722	-1 020 056	0	-11 140 580	68 5016	0
180	-90	2,32	2,32	0,00	0	-1 265 969	0	-13 826 317	0	0

Table G.6: Input data drag coefficient Ansys Aqwa for a flow velocity of 1 m/s

The *Hydrodynamic Response Analysis* is run for a current of 5,2 m/s in a direction of 90 degrees. To verify whether the drag force is correctly implemented in Aqwa, the "Structure Forces, Current Drag Only" is plotted in Y-direction and compared with a hand-calculation with a current of 5,2 m/s perpendicular on the pontoon.

The plot on Figure G.13 indicates that the drag force in Y-direction acting on the submerged parts of the bridge is of the same order as the handcalculation and the Aqwa output. The equilibrium situation in the Aqwa plot has a value of 33 978 kN, an absolute difference of 1,5%. The plot shows oscillations that dampen out during time. The oscillations are a consequence of the impulse load of the current at $t = 0$. In reality, the current varies harmonious with the tide and will not appear abruptly. The equilibrium situation indicates the final drag force on the pontoons. This suggests that the first 250 seconds of all results computed by Aqwa will be trivial. The maximum rotations that occur by the drag induced pressure (for $u=5,2$ m/s) are $RX=5,88^\circ$ and $RY=3^\circ$. The sensitivity analysis will discuss the outcome of the analysis.

$$F_{D,y} = \frac{1}{2} \rho_w C_D A_s u^2 = 34\,232 \text{ kN} \quad (\text{G.4})$$

Figure G.13: Drag force [kN] in Y-direction on every pontoon in Ansys Aqwa ($\alpha = 90^\circ$; $u = 5,2$ m/s)

Method 2: Structure Force Matrix

The second option to mimic the drag force is the implementation of a *Structure Force Matrix*. The matrix represents a time history of structure forces and is applied at the centre of gravity of the structure (Ansys Inc., 2012a). The columns in the matrix indicate what force is acting on what structure for every six degrees of freedom. In the section *Structure Selection* in the *Hydrodynamic Diffraction analysis* the order of structures is displayed and can be changed. In Table G.7 the first floater is indicated with S_1 , all other structures are denoted with S_i . The Structure Force Matrix is calculated for a perpendicular directed flow. The input of a flow under an angle is possible, but time-consuming as a new matrix should be calculated and implemented in the model. The main advantage of this type of analysis is the possibility to vary the magnitude of the structure force, and thus the magnitude of the current.

Time (s)	$F_x S_1$	$F_y S_1$	$F_z S_1$	$M_x S_1$	$M_y S_1$	$M_z S_1$	$F_x S_i$	$F_y S_i$	$F_z S_i$	$M_x S_i$	$M_y S_i$	$M_z S_i$
0	0	0	0	0	0	0
70	0	837	0	9151	0	0
140	0	3268	0	35712	0	0
210	0	7055	0	77080	0	0
280	0	11826	0	129207	0	0
350	0	17115	0	186991	0	0
420	0	22404	0	244774	0	0
490	0	27176	0	296901	0	0
560	0	30962	0	338270	0	0
630	0	33394	0	364830	0	0
700	0	34231	0	373982	0	0
...

Table G.7: Input data drag coefficient Ansys Aqwa for a flow velocity of 1 m/s

The Structure Force Matrix has a maximum number of timesteps that can be implemented. In between the timesteps the forces are interpolate to match the defined timestep. For the interpolation Aqwa uses a *cubic spline interpolation technique*, Ansys Inc. (2012b). The maximum current speed of 5,2 m/s is converted to a sinusfunction to represent the tide. In reality, the tide also varies harmonically and very gradually. The acceleration of the bridge will be small as a result of the gradual change in current magnitude. The rotations will be governing with respect to the current. Figure G.14 provides the relation between the current velocity (left vertical axis) and the force and moment induced by drag (right vertical axis).

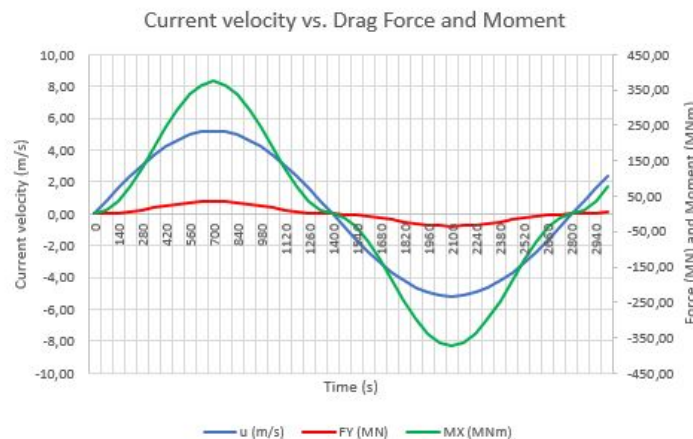


Figure G.14: Current induced drag force [kN] and moment [kNm] for a perpendicular flow

A problem arises when the model is run. The error notification appears *"The structure exceeded 75% of its original position. The Aqua server stopped abruptly."* and the run aborts. The core of the problem is that the structure exceeds its original position with a significant amount that the software is not able to calculate the response based from the equilibrium position. The error-notification occurs at a timestep of 1900 seconds,

when a negative current is present. The only possibility to exceed 75% of the equilibrium position is when the bridge is 'flipped' over in the radius of the pendulum. A restriction of the possible displacement is obligatory. A mechanism is created by allowing one spudpole to 'move freely' along the x-axis, while in reality the displacement will be limited according to the dimensions of the frame of the spud construction, δx in Figure G.15.

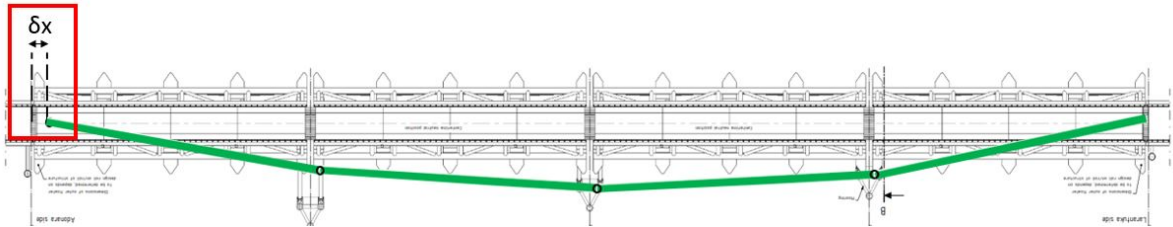


Figure G.15: Spudpole that allows movement along the x-axis and the actual limited displacement

Aqwa considers all bodies as infinitely stiff and thus not able to bend. The characteristics of the spud constructions are 'imitated' by defining a cable. A short cable is placed at a "Fixed Point" and the connection point of spudpole 1. The cable properties define the properties of the spud construction, for a first check a random cable stiffness and elongation is applied:

- Cable elongation = 0,20 m
- Cable stiffness = 30 000 kN/m (very high)

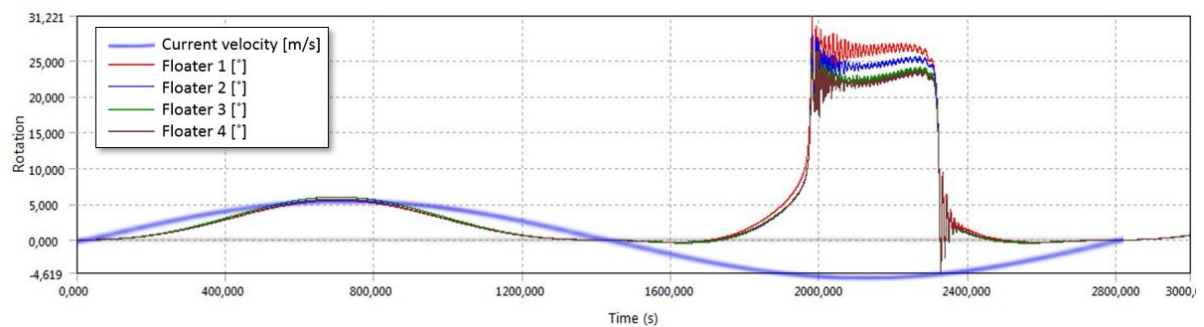


Figure G.16: Rotation as a result of the *Structure Force Matrix* and a cable

Figure G.16 suggests that the assumed core of the problem was correct and as is visualised in Figure G.17 and G.18 the floating part will 'flip' over and 'levitate'. The first rotation peak that occurs by the positive current velocity is of the same order size as computed in *Method 1: Drag Force Coefficient*. In the structure force matrix the maximum rotation around the x-axis for a positive current is $6,00^\circ$ (compared to $5,88^\circ$ in Method 1). If Method 1 is run with a negative current, the same error-notification emerges. The same problem is present. An accurate approximation of the cable forces is elaborated in the next section.

Probably, the 'flipping over' will not occur in reality as the water body that flows through the turbines has a stabilising effect as discussed previously. The effect is complex to implement in the model and based on assumptions only.

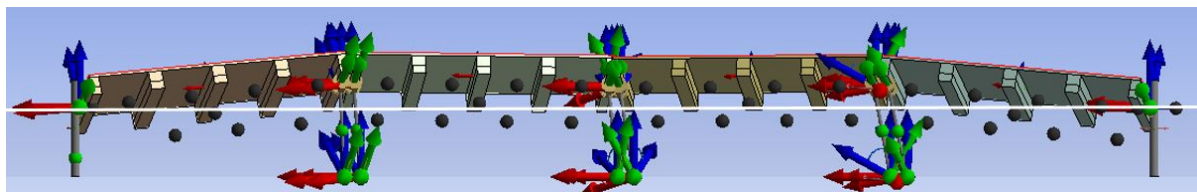


Figure G.17: Front view of the system at $t=2100$ s, white line indicates the waterline.

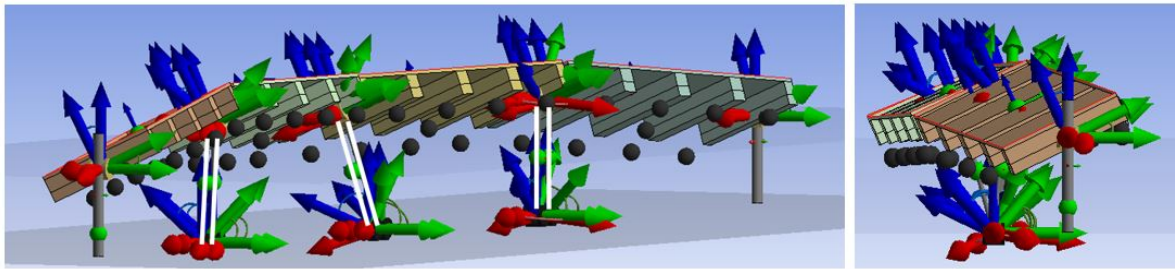


Figure G.18: Response of the system at $t=2100$ s, cable system is applied. Mooring pendulums are displayed in white.

Method 3: Horizontal Point Forces

The last manner to imitate the drag on the structure is with *Horizontal Point Forces*. In the middle of the pontoons at an arm of 7,32 m below the Fixed Reference Axis horizontal point forces are defined. Again, the point forces are acting on the centre of gravity of the specific structure. Four turbine areas are present in between the bridge. The magnitude of the point forces is calculated by computing the drag force at a current magnitude of 5,2 m/s for a total bridge element and divide it by four.

$$F_{\text{Point Force}} = \frac{0,5C_d A_n \rho_w u^2}{4} = 8\,558 \text{ kN} \tag{G.5}$$

Within a point force a selection of options can be selected. Along every axis a force can be defined, indicating that a force induced by a current under an angle can also be defined. In the model, solely the horizontal force is implemented. Another element that should be selected is if the *force should move with the structure* or if the *force direction should remain constant*. In total 16 point forces are considered, suggesting that a combination of selections may also be possible. The combination is the most probable scenario. Generally, the water flow is horizontal directed, but as the ar between the structure and the force is fixed, the force will move upwards when the structure moves up. The arm of the force can not be set as a variable, hence the upwards displacement of the force is counteracted by the additional vertical force that arises when the structure rotates, Figure G.19. In addition, the application point of the point force is of influence for the dynamic response. If the system rotates, the 'arm' of the system changes and the moment will change accordingly: a_1 , a_2 and a_3 . In Figure G.19 two application possibilities and difference in 'arm lengths' are visualised for a *positive* current direction: F_{center} and F_{front} . In the other figure, Figure G.20, screenshots of the Aqwa model are included. The yellow arrows indicate the point force and is in this scenario applied at the centre.

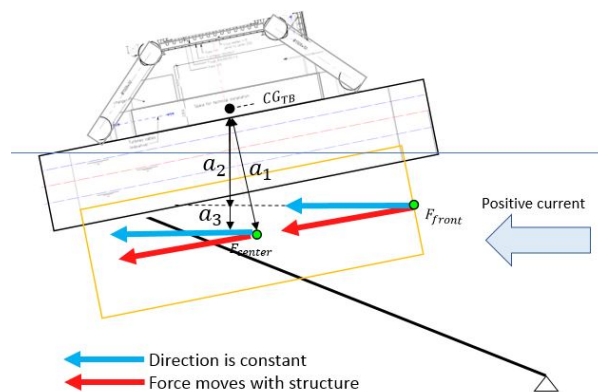


Figure G.19: Application possibilities and selection options for the Point Forces (visualisation is not to scale)

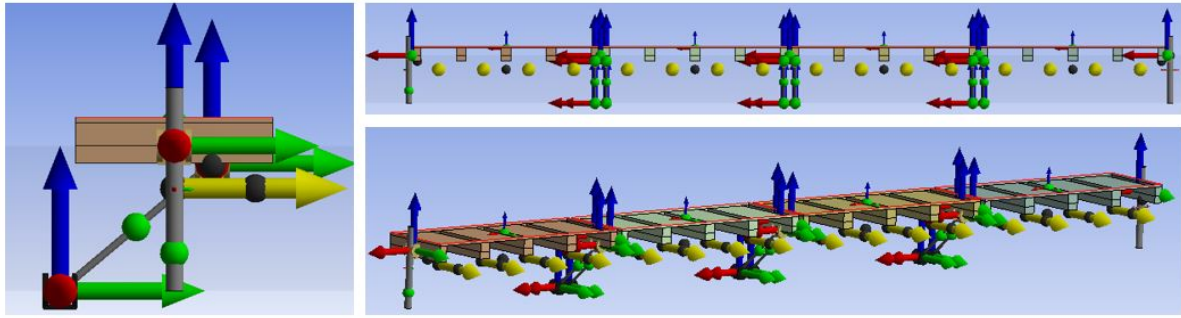


Figure G.20: Screenshot of the Ansys Aqwa model including point forces

The situation with a *positive* current is checked to be able to compare the rotations with the rotations of the other two elaborated methods. All combinations are checked and the maximum rotations around the x-axis are indicated in Table G.8. The final position of the most extreme combinations, *Case 1*, is visible in Figure G.21. The constant direction of the current in combination with the force application at the front of the turbine 'pulls' the bridge under its rotation point. In reality this is not probable, the water flow through the turbine bodies will counteract the effect. Hence, *Case 1* is not realistic. *Case 2, 4, 5 and 6* induce the same order of rotations as the first two methods. The front of the turbine will experience higher pressures than the back of the turbine, indicating that the attachment point of F_{front} is more suitable. A force that *moves with the structure* is partly realistic. In general, the water body will flow horizontally, but within the turbine, the water body will follow the central axis of the turbine system. Thus, when rotated, the water body will travel in a rotated direction as well.

	Attachment point	Property selection	Maximum RX [°]	Realistic?
Method 1	Current drag coeff.	-	5,88	-
Method 2	Structure force matrix	-	6,00	-
Method 3	Horizontal point forces			
Case 1	F_{front}	Constant Direction	21,8	Too high
Case 2	F_{front}	Moves with Structure	6,07	Probable
Case 3	F_{front}	Combination	9,97	Conservative (Combi. Case 1)
Case 4	F_{center}	Direction is constant	6,03	Probable
Case 5	F_{center}	Moves with Structure	6,07	Probable
Case 6	F_{center}	Combination	6,06	Probable

Table G.8: Add caption

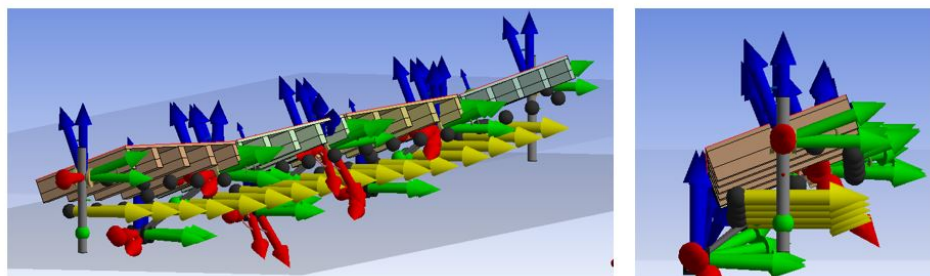


Figure G.21: Most extreme scenario: Case 1; Constant direction and attachment point at front

The *Horizontal point force method* is time-consuming. All sixteen point forces need to be manually defined and changed individually. In addition, if a *negative* current is applied and the structure starts to levitate and act like a kite in the air, the response with *forces that move with the structure* is even more drastic. The negative current should be analysed, concluding that the method is not suitable.

G.3.3. Implementation of mainland connection

In the drag implementation section, it became clear that the displacement of the spudpole should be limited in x-direction. The 'stiffness' of the spudpole is computed by analysing the technical drawings of the spud constructions, Figures G.22 and G.23. The technical drawing only consider the main frame of the spudpoles, a design for the connection element between the spudpole and the floater is absent. According to the COO of the company Tidal Bridge, Andre Hoogeveen (2019), one of the spudpole connections should be designed with some tolerable initial x-displacement and the other spudpole should be restricted to solely vertical z-displacement. The initial 'first-order' displacement is indicated in Figure G.24 with δx_1 . An indication of the magnitude of the x_1 displacement is not designed or calculated.

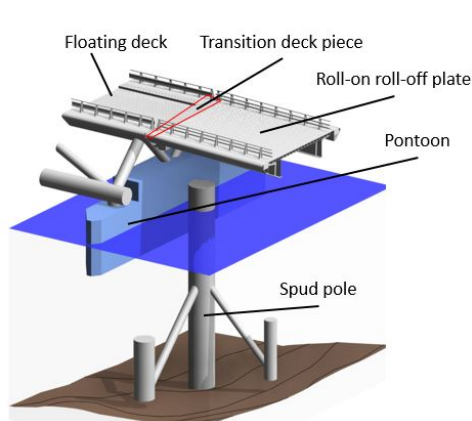


Figure G.22: Present design of the spud construction: d=3 m and t=50 mm

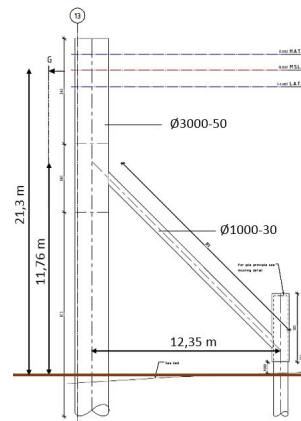


Figure G.23: Technical drawing of spud connection (Antea Group (2018))

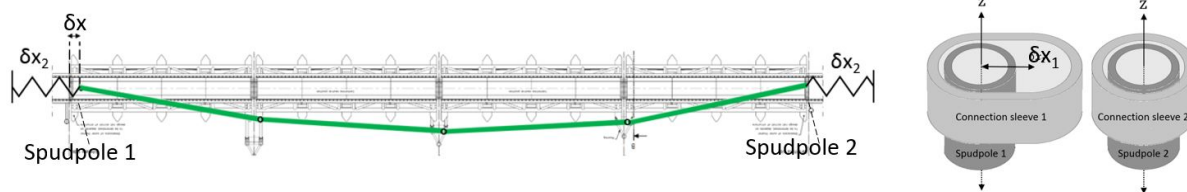


Figure G.24: Spudpole that allows movement along the x-axis and the actual limited displacement

Next to the first-order displacement, bending of the steel spud construction results in 'second-order' displacement. An estimation of the order size of the amount of bending, that may occur by the maximum horizontal force in the spud connection, is computed in *Matrixframe*. The second order effect is indicated with δx_2 in Figure G.25. A horizontal force of 21,8 MN is proportional to a displacement δx_2 of 0,30 m.

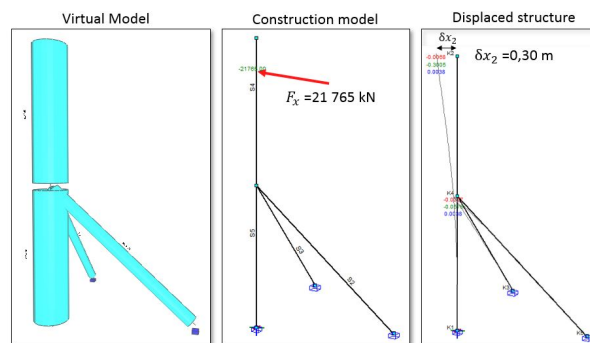


Figure G.25: Matrixframe model to indicate bending stiffness of spudpole according to dimensions in technical drawing G.23

A linear elastic cable can be described by the relation between force F [kN], displacement x [m] and stiffness k [kN/m]: $F = k \cdot x$. The characteristic data found in the Matrixframe model can be converted to a stiffness that can be implemented as the cable between a 'fixed point' and the infinitely stiff spudpole. The corresponding cable stiffness is 72,55 MN/m. The second order displacement, the bending of the spudpole, is present at both spudpoles. Cables are defined for both spudpoles with a stiffness of 72,55 MN/m and without an additional cable elongation. The Ansys Aqwa model is run and the rotation around the x-axis, the displacement of both spudpoles and the maximum tension forces in the cable are computed and presented in Table G.9 and the rotation of the floaters around the x-axis is plotted in Figure G.26.

		Peak during positive current		Peak during negative current	
		Spudpole 1	Spudpole 2	Spudpole 1	Spudpole 2
Displacement spudpole X-axis	[m]	0,12	0,12	1,51	1,51
Tension force in cable	[kN]	12 640	12 640	108 477	108 477
Z-displacement		1,11	1,11	-0,84	-0,84
		Floater 1&4	Floater 2&3	Floater 1&4	Floater 2&3
Maximum rotation x-axis	[degrees]	5,63	5,96	17,51	17,46
Maximum rotation y-axis	[degrees]	2,54	0,42	4,23	1,62
Maximum rotation z-axis	[degrees]	0,99	0,29	7,30	5,10
Maximum z-displacement	[m]	-1,13	-2,98	3,24	8,26

Table G.9: Maximum values that arise at the positive and negative current velocity peaks for both spudpoles

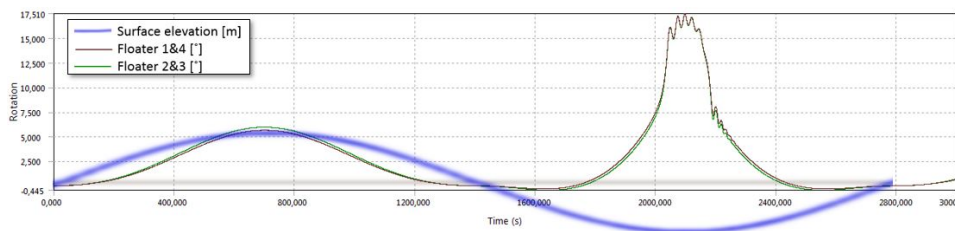


Figure G.26: Rotation around x-axis with two cables that imitate the bending stiffness of the spudpoles

The Aqwa solver is able to complete the run for the negative current velocity, but an exponential increase is still present if the current velocity reaches a certain negative magnitude. If the cable stiffness is increased, the peak will become smaller. The sensitivity with respect to cable stiffness and magnitude of motion is analysed in the Sensitivity analysis for the current in Chapter 7. The maximum rotation that is induced by the positive current velocity is $5,96^\circ$, suggesting that the cable will dampen the system slightly compared to the situation without cables elaborated in section G.3. At the negative current a maximum rotation of $17,51^\circ$ is present, the z-displacement of the floaters is considerably high: 8,26m. Indicating that the bridge is located above water level, Figure G.27. The counteracting stabilising effect of the water body through the turbine is not in the scope of the research. Therefore, the model with two cables is assumed as a correct approximation of the dynamic response for a positive current velocity. The sensitivity study elaborates on both the positive and negative current velocity with respect to the cable stiffness.

The first order displacement, δx_1 can be implemented in the Aqwa model by increasing the *unstretched cable length*. Hence, the *point to point distance* between the two cable attachment points is smaller than the actual *unstretched length*. An initial displacement along the x-axis, δx_1 , is allowed before stress in the cable is induced. The best suitable distance for δx_1 is elaborated in the sensitivity analysis.

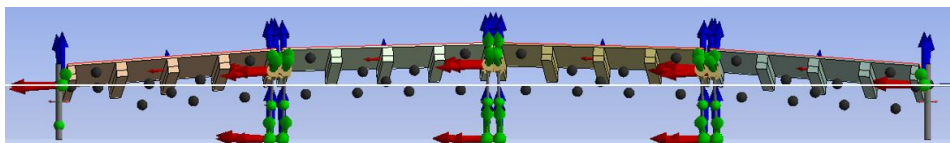


Figure G.27: Screenshot of maximum bridge displacement, white line indicates water level



Wave results

This Appendix elaborates and discusses the results of the wave sensitivity study computed in Ansys Aqwa. With the results and observations the sensitivity of the bridge to many wave combinations is substantiated and formed. First, the critical modes are indicated with the *Response Amplitude Operators* in the Frequency Domain. Secondly, the actual dynamic response of the fully coupled bridge is computed in the Time Domain. The results are discussed and the likely motion of the Tidal Bridge is determined.

H.1. Hydrostatics

The properties that determine the likely response of the Tidal Bridge are based on the hydrostatic characteristics of the four main floating elements. An overview of the hydrostatic characteristics is presented in Table H.1. Although each floater consists of the same geometry, the characteristics vary slightly as the dynamic response is based on the interacted system. The most important values with respect to the likely behaviour are identical:

- Heave: 7,52 MN/m
- Roll: 10,61 MNm/°
- Pitch: 124,43 MNm/°

The magnitude of the force indicates the amount of motion or rotation that may arise. Nonetheless, the Hydrostatic analysis is based on uncoupled floating bodies with absence of hinges or the connection to the mooring system. The motion of the coupled system will be influenced by all connected parts and elements and will differ from the equilibrium floating characteristics.

				Z	RX		RY		
Floater 1	Heave	Z	z	7,518	MN/m	0,07	N/°	-0,06	N/°
	Roll	RX	φ	4,06	Nm/m	10,61	MNm/°	-0,38	Nm/°
	Pitch	RY	θ	-3,60	Nm/m	-0,38	Nm/°	124,43	MNm/°
Floater 2	Heave	Z	z	7,518	MN/m	-0,16	N/°	-0,61	N/°
	Roll	RX	φ	-9,31	Nm/m	10,61	MNm/°	-0,53	Nm/°
	Pitch	RY	θ	34,97	Nm/m	-0,53	Nm/°	124,43	MNm/°
Floater 3	Heave	Z	z	7,518	MN/m	-0,16	N/°	-0,98	N/°
	Roll	RX	φ	-9,45	Nm/m	10,61	MNm/°	0,15	Nm/°
	Pitch	RY	θ	-56,37	Nm/m	0,15	Nm/°	124,43	MNm/°
Floater 4	Heave	Z	z	7,518	MN/m	0,07	N/°	-0,50	N/°
	Roll	RX	φ	4,06	Nm/m	10,61	MNm/°	-0,26	Nm/°
	Pitch	RY	θ	-28,37	Nm/m	-0,26	Nm/°	124,43	MNm/°

Table H.1: Hydrostatic characteristics of 100 m long floating elements

H.2. Response amplitude operators

The *Response Amplitude Operator* (RAO) of the free floating structures of the system are determined to indicate the combination of wave direction and frequency that induce large motion. The harmonic response of the body is computed through Aqwa by solving linear algebraic equations with regular waves. The response characteristics are proportional to the wave amplitude. The magnitude motion is plotted with respect to the original position of the centre of gravity of the structure (Ansys Inc., 2015).

The two-dimensional version of the motional RAO is generally in the shape of Figure H.1. Within the graph, three sections can be distinguished that are sensitive for one specific characteristic of the Equation of Motion: spring stiffness, damping and mass (Journée and Massie, 2008). The graph is plotted for the heave response for a cylinder in water.

1. Low frequency section: Motion dominated the spring stiffness
2. Natural frequency section: Motion dominated by damping. Small damping results may result in a high resonance magnitude amount of motion.
3. High frequency section: Mass dominated motion.

$$1. \quad \omega^2 \ll \frac{c}{m+a} \quad (\text{H.1})$$

$$2. \quad \omega^2 \approx \frac{c}{m+a} \quad (\text{H.2})$$

$$3. \quad \omega^2 \gg \frac{c}{m+a} \quad (\text{H.3})$$

In which, c is the spring coefficient and m the mass. a represents the value of the potential mass and damping at the natural frequency (ω_0) of the system: $a = (c - \omega_0^2) - m$.

The RAO for motional behaviour is general in the form of $\frac{z}{\zeta_a}(\omega)$, which is equal to the displacement (z) at frequency (ω) divided by the surface elevation (ζ_a) at the same frequency.

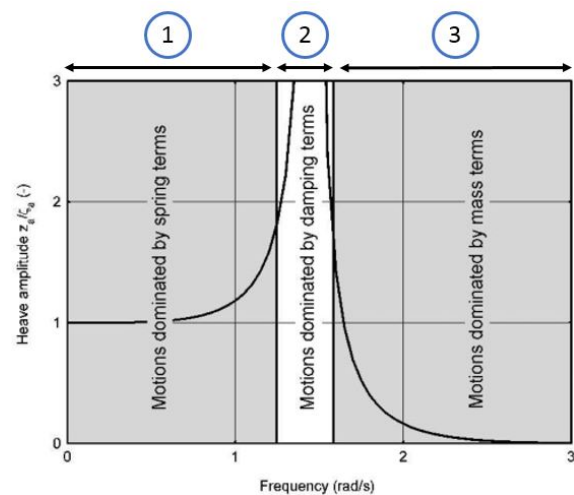


Figure H.1: General form of the Response Amplitude Operator for motional behaviour (Journée and Massie, 2008)

The Response Amplitude Operators for the motional behaviour for the floating 100 meter long Tidal Bridge bodies in steady state are computed. Figure H.2 to H.7 present 3D-plots with on the vertical axis the amount of motion or rotation and on the horizontal axes the frequency and direction. An overview of the peak values with corresponding frequencies and directions is given in Table H.2. The same shape as in Figure H.1 can be distinguished in all plots, indicating the different frequency sections.

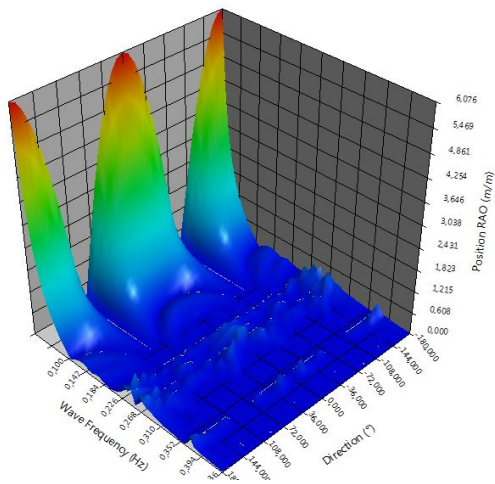


Figure H.2: RAO Motion along X-axis [m/m]

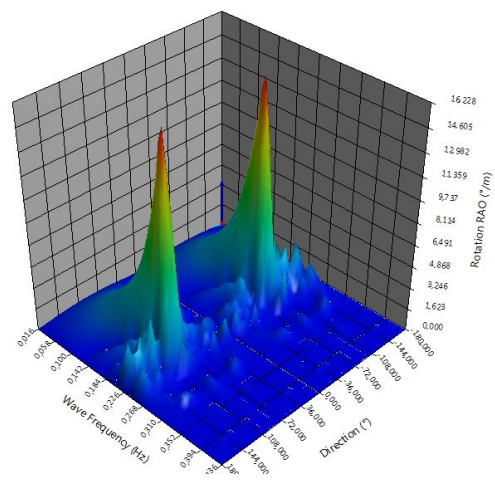


Figure H.3: RAO: Rotation around X-axis [°/m]

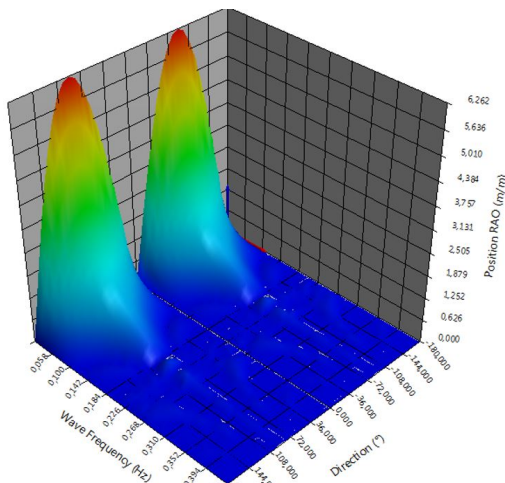


Figure H.4: RAO Motion along Y-axis [m/m]

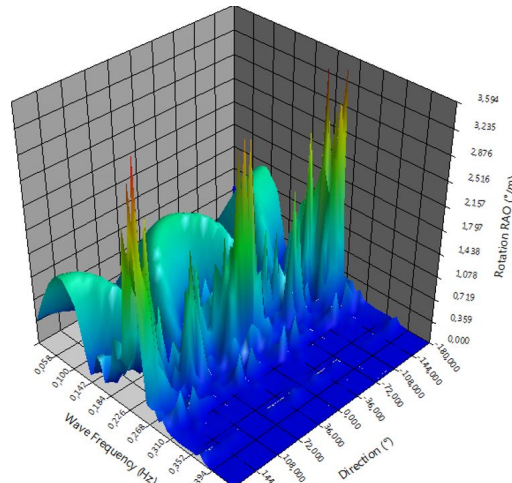


Figure H.5: RAO: Rotation around Y-axis [°/m]

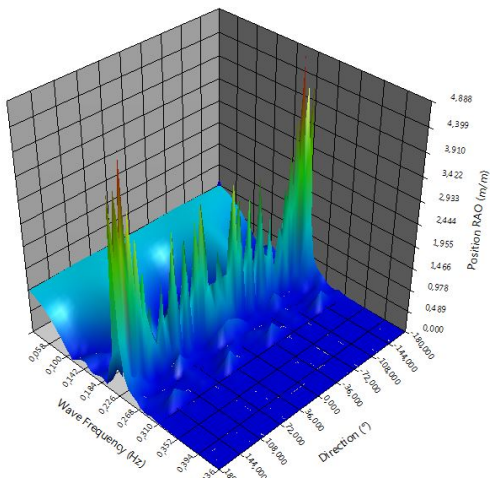


Figure H.6: RAO Motion along Z-axis [m/m]

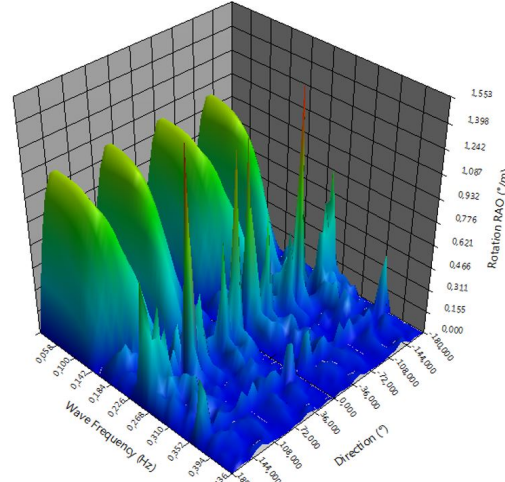


Figure H.7: RAO: Rotation around Z-axis [°/m]

	Directions [°]	Frequencies [Hz]	Value RAO	
X	180, 0, -180	0,016	6,076	[m/m]
Y	90,-90	0,016	6,262	[m/m]
Z	160, -160	0,222	4,888	[m/m]
RX	90, -90	0,213	16,228	[° /m]
RY	160, 0, -160	0,230	3,594	[° /m]
RZ	100, -100	0,255	1,553	[° /m]

Table H.2: Peak values of the RAO with respect to motion or rotation

The peak values for the X and Y displacement are directed along their governing axis, Figure H.8. The most important frequency is the range of the natural frequencies, between 0,213 and 0,255 Hz. The small frequencies correspond to long wave lengths that are not realistic for the project location. In addition, the possible incoming wave directions are limited, illustrated in Figure H.9. The governing incoming wave directions are varying between 50° and 130°. The bridge is symmetric, implying that the RAO's should be symmetrical. This indicates that a direction of 80° induces the same dynamic response as a direction of 100°. The RAO's of the 'direction-couples' in the governing incoming wave range are presented in Figures H.12 till H.15 and discussed in the end of the section.

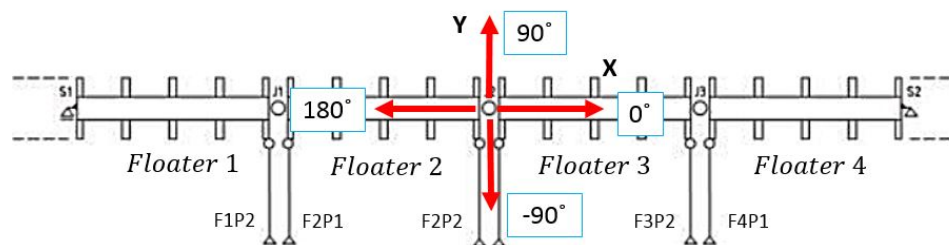


Figure H.8: Schematic overview of directions in Ansys Aqwa

First notable observation is the symmetry around 0° (and 180°) degrees. This is explained by the symmetrical geometry of the system. The deck is aligned with the x-axis and will move similarly for a positive and negative directed wave. Some plots are also approaching symmetry at 90 degrees. The symmetry simplifies the complexity of the dynamic response of the coupled system. Nevertheless, the incoming wave directions are not necessarily perpendicular directed as is visualised in Figure H.9. In the figure, the inner circle represents the Ansys Aqwa axis and the outer circle indicates the actual direction rose.

The symmetry in the RAO plots suggests that the system behaves analogues for a positive or negative directed current. Waves that enter under an angle of 80 or 100 degrees have a variation of 10 degrees seen from the governing perpendicular axis. As a result of symmetry, the likely motion for a 80 or 100 degree waves is equivalent, therefore this set is called a 'direction-couple'. The following 'direction-couples' are analysed: 80 and 100°, 70 and 110°, 60 and 120° and 50 and 130°) degrees. The RAO's for all direction couples are computed for waves with frequencies between 0,02 Hz and 0,43 Hz. Within estimated wave heights the governing frequency is 0,14 Hz. Therefore, this frequency is seen as a lower limit. The RAO peak values for every degree of freedom are presented in Table H.3.

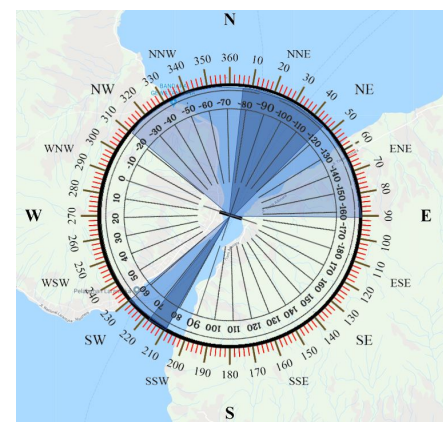


Figure H.9: Rotated axis system Ansys Aqwa versus actual angle and governing wave directions

Direction	X [m/m]	f_{peak} [Hz]	Y [m/m]	f_{peak} [Hz]	Z [m/m]	f_{peak} [Hz]	RX [°/m]	f_{peak} [Hz]	RY [°/m]	f_{peak} [Hz]	RZ [°/m]	f_{peak} [Hz]
90°	0,23	0,25	0,58	0,14	1,13	0,22	16,23	0,21	2,08	0,25	0,58	0,25
80 & 100°	0,16	0,22	0,53	0,14	2,85	0,22	11,17	0,21	1,37	0,22	0,54	0,25
70 & 110°	0,10	0,14	0,38	0,14	0,61	0,22	2,97	0,15	0,96	0,15	0,62	0,14
60 & 120°	0,18	0,37	0,21	0,14	2,58	0,22	2,04	0,20	1,54	0,22	0,71	0,14
50 & 130°	0,18	0,28	0,07	0,14	0,96	0,22	1,62	0,19	1,57	0,21	0,63	0,14

Table H.3: Maximum motion response for Range of direction in between 0,14 - 0,43 Hz. Highest value of direction couple is provided.

Displacement in the X, Y and Z direction will not cause inconvenient motion, more important are the accelerations. In addition, roll-rotation may cause unfavourable driving experiences, discomfort and possible accidents. Table H.3 indicates high amount of rotation around the x-axis for a perpendicular wave. Most peak values are present in this direction. This suggests that this is the governing wave direction regarding the magnitudes of motion. The graphs for the direction couples are presented in Figures H.10 to H.15.

The wave frequency that is proportional to a wave length of 34 m, the width of the bridge, is 0,214 Hz. Table H.3 and Figure H.10 substantiate that a peak value is present at this frequency. Nonetheless, the governing critical frequency differs slightly for each degree of freedom.

The scenario with a perpendicular incoming wave, a wave under an angle of 90° or -90°, is elaborated. The RAO's for every degree of freedom are presented in one plot, Figure H.10. In the plot the X, Y and Z lines are linked to the left axis in [m/m] and the rotations RX, RY and RZ are corresponding to the right axis in [°/m]. Immediately, the peak of RX in the realistic wave frequency range can be distinguished. The peak has a value of 16,22 °/m and is a significantly higher than the other peak values. Nonetheless, the other degrees of freedom show peaks in the same frequency range, Figure H.11. Hence, the range of 0,21 to 0,30 Hz is most sensitive and will be checked in the model.

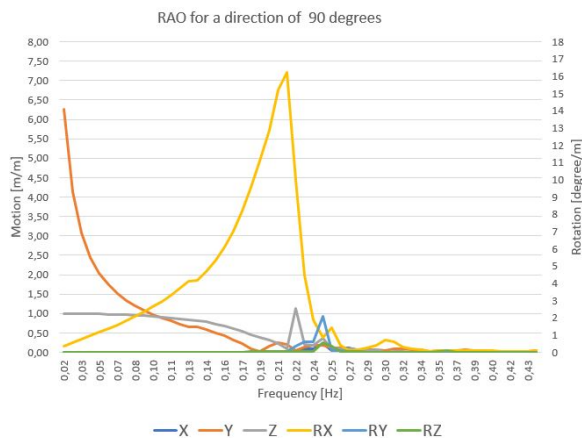


Figure H.10: RAO for direction of 90° in six degrees of freedom

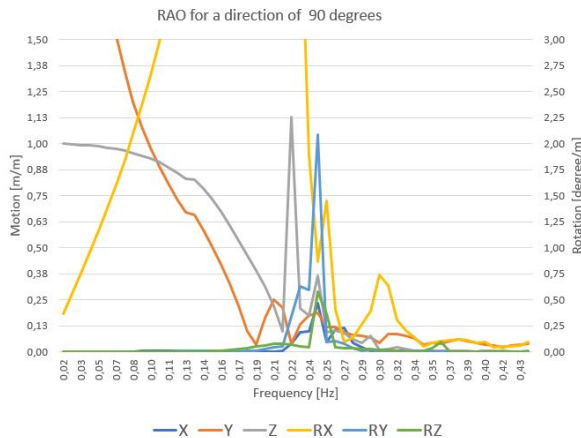


Figure H.11: RAO for direction of 90°. Rescaled vertical axis.

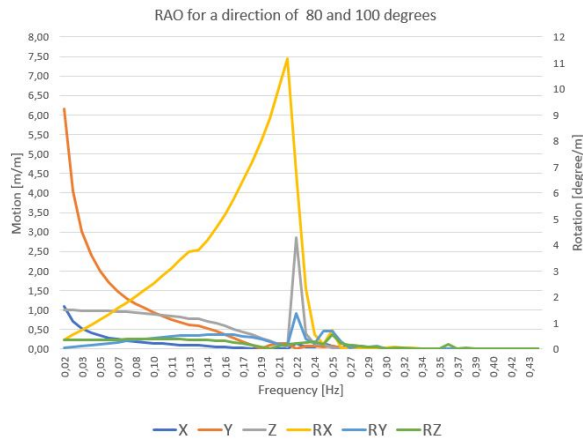


Figure H.12: RAO for direction of 80° and 100°

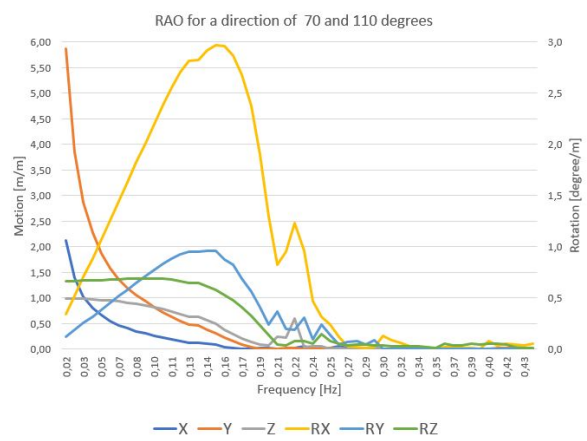


Figure H.13: RAO for direction of 70° and 110°

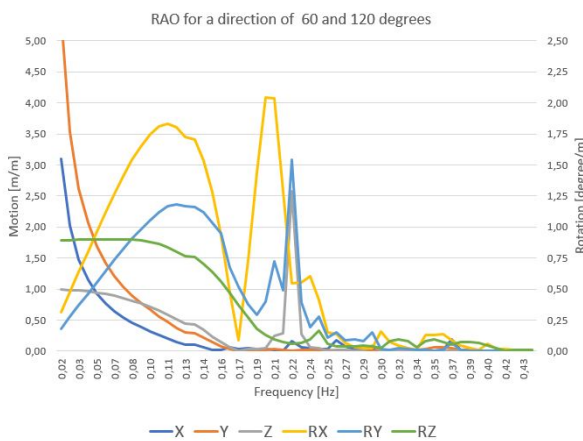


Figure H.14: RAO for direction of 60° and 120°
Six degrees of freedom

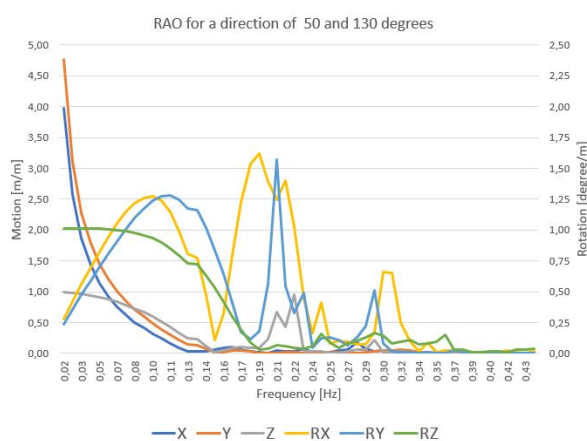


Figure H.15: RAO for direction of 50° and 130°
Six degrees of freedom

The response of the bridge with respect to the a specific rotation is visualised in Figure H.16. The Response Amplitude Operators for the rotation around the x-axis will induce the highest amount of discomfort. Rotation around the Y-axis is analogous to driving up or down a hill. Rotation around the z-axis can be compared to the X, Y and Z-displacement and, if stable, may not induce discomfort for driving. Nonetheless, a combination of rotations may enhance unfavourable positions and decrease comfort. The influence of the incoming wave angle versus the rotation about the x- and y-axis is plotted in Figures H.17 and H.18. It is clear that the rotation around the x-axis decreases significantly with an increase in angle variation. The peak of the rotation about the y-axis decreases with an increase in angle variation as well. Contradictory, the response RY for low frequencies increases with an increase in angle.

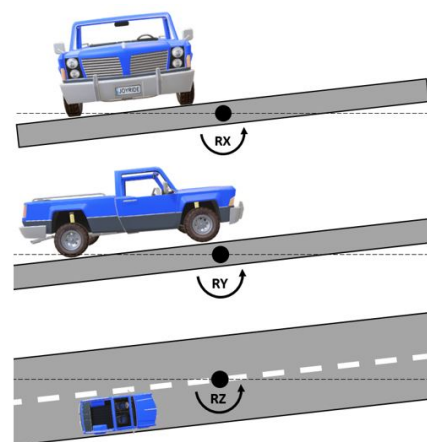


Figure H.16: Visualisation of the same rotation angle with respect to a car position

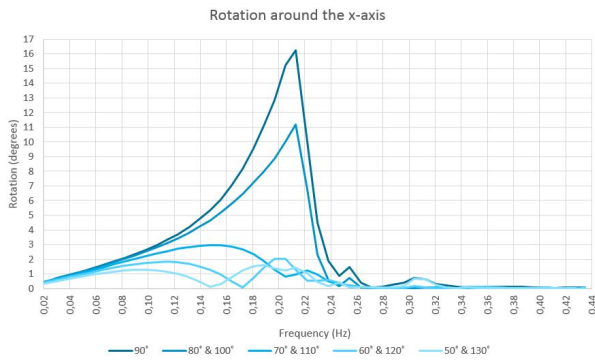


Figure H.17: RAO: Rotation around the **x-axis** for sequence of incoming flow angles

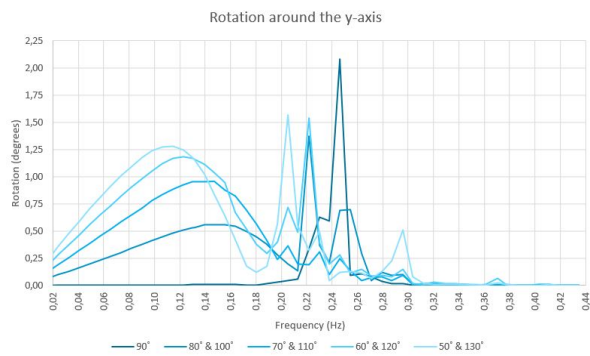


Figure H.18: RAO: Rotation around the **y-axis** for sequence of incoming flow angles

The actual dynamic response of the fully connected system differs from the computed RAO's of the individual unconnected freely floating floaters. The RAO's are computed for the equilibrium state of an individual floater, the mooring system does not influence the floating behaviour. If the system is exposed to waves the mooring system manipulates the RAO-based motion. The influence of the mooring system is checked by running the *Hydrodynamic Response* analysis for a *regular* Second order Stokes wave with a wave height of 1 m (wave amplitude = 0,5 m), a frequency of 0,21 Hz and directed perpendicular to the bridge deck (90°).

The RAO-based response and the response of the fully coupled bridge (the '*actual response*') are computed and presented in Figure H.19 along with the wave surface elevation. The ratio between the RAO-based response and the actual response is approximately 2,65:1 for the rotation around the x-axis. Indicating that the freely floating RAO-based response is damped with approximately a factor 2,5 for the rotation around the x-axis.

The difference in response suggests that the mooring pendulum stabilises the coupled system. The response induced by the waves is limited by the maximum radius of the pendulum. The actual response to a wave with the wave height of 1 m is 3,3° and higher than the estimated serviceability limit for roll of 0,044 rad ≈ 2,52°. The rotation is accompanied by an acceleration of 5,94 °/s. The estimated serviceability limit for roll-acceleration is 6,13°/s, being just within the limit. An overview of the estimated serviceability limits and the actual displacement of floater 1 is given in Table 7.3 in Chapter 7.

Maxima of wave amplitude	-0,478 to 0,522 m
Maximum Actual response	3,30°
Maximum RAO-based response	8,73°
Maximum Low frequency response	0,08°

Table H.4: Peak values of Figure H.19

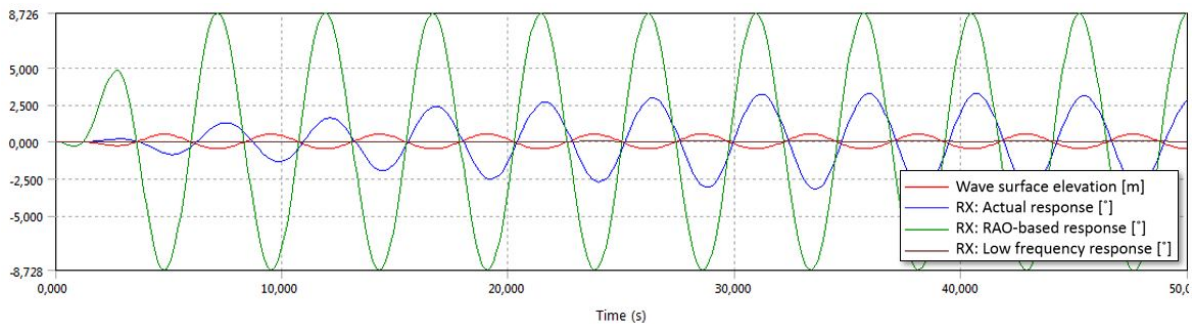


Figure H.19: Relation between wave surface elevation and rotation around the x-axis (RAO-based vs. Actual vs. Low frequency response)

H.3. Determination of critical waves

The critical wave directions and frequency parameters are defined in the JONSWAP wave spectrum of Ansys Aqwa. A total of 28 combinations is analysed, equation H.4 described the possible combinations of the system. Considering the wave characteristics of section C.4 and Table H.5, the governing incoming wave angles are in between 80° to 100° and -80° to -100° . The four critical frequencies based on the RAO's are 0,14, 0,21, 0,22 and 0,25 Hz. Next to these frequencies, the natural frequencies of the bridge, computed in Chapter 5, are also checked. The sensitivity analysis requires data that can be scaled. Hence, the significant wave height is set to 1 m and γ (the peak enhancement factor) is set at 3,3 for all combinations. The wave directions and nomenclature of the Ansys Aqwa model is visualised in Figure H.20. The results are presented in Figures H.21 to H.26. Within the plots a distinction is made between the rotation of the individual floaters. The rotations of floater 1 and floater 4 are identical, as are the rotations of floater 2 and 4.

$$\text{Wave combinations} = \alpha \cdot f^T \quad (\text{H.4})$$

Time	400 s
Wave height (H_s)	1 m
Peak enhancement factor (γ)	3,3
RAO frequencies (f)	0,14, 0,21, 0,22 and 0,25 Hz
Natural frequencies (f_n)	0,287 (Z), 0,268 (RX), 0,327 (RY)
Direction (α)	$90, -90, 100$ and -100°
Wave height range	$-0,80$ to $0,73$ m ($H_{max}=1,53$ m)

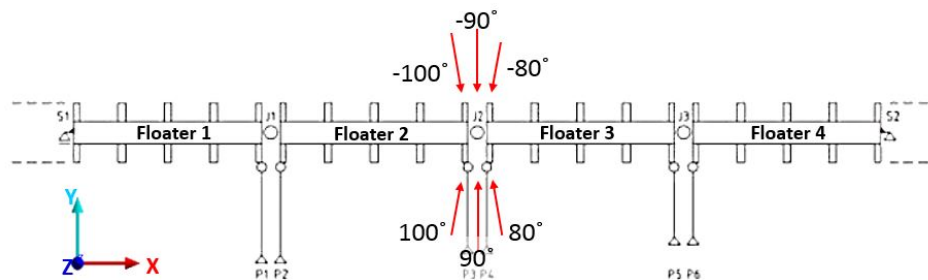


Figure H.20: Overview of the implemented wave parameters in Ansys Aqwa

The actual rotations differ significantly from the RAO-based rotations. An explanation is that the RAO-based motions are computed for an uncoupled system, while the actual motion is computed for the total system. The influence of the hinges and the mooring system is significant.

The left graphs indicate the response of the individual floaters. Symmetry at the centre of the bridge results in the same behaviour of floaters 1 & 4 and floaters 2 & 3. Data values in Ansys Aqwa confirm the identical dynamic response of the floater couples. The plots show the response of the coupled floater sets. The waves approach the bridge deck primarily perpendicular, explaining that the rotation around the x-axis is nearly identical for the floater couples. The difference in rotation that is present between the floater couples for the other rotations can be justified by the juncture points. The outer side of the floater is secured in y-direction, while the other end is free to move. Hence, the outer floaters experience an overall higher rotation around the y-axis than the middle floaters. The rotation around the z-axis is of the same magnitude for both floater sets.

The plots on the left, Figures H.22, H.24 and H.26, show the maximum actual rotations versus the RAO-based rotations. The effect of the mooring system becomes visible with plots. The forecasted rotation around the x-axis, dashed lines in Figure H.22, is shifted to lower frequencies. The effect is advantageous, waves with higher frequencies are expected to occur during most times. The low frequency waves are corresponding to the maximum waves that are computed.

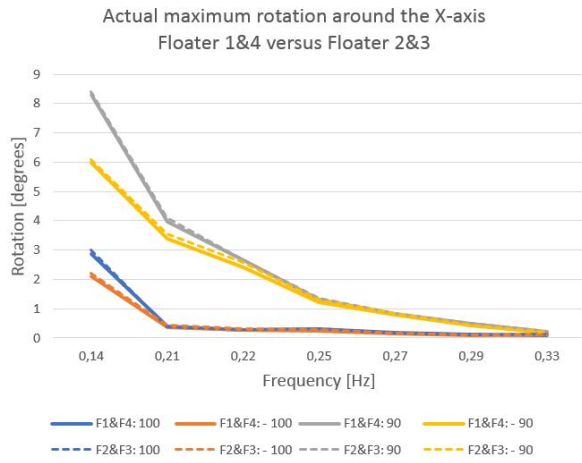


Figure H.21: Rotation around the X-axis
Actual rotation Floater 1 and Floater 4 versus Floater 2 and Floater 3

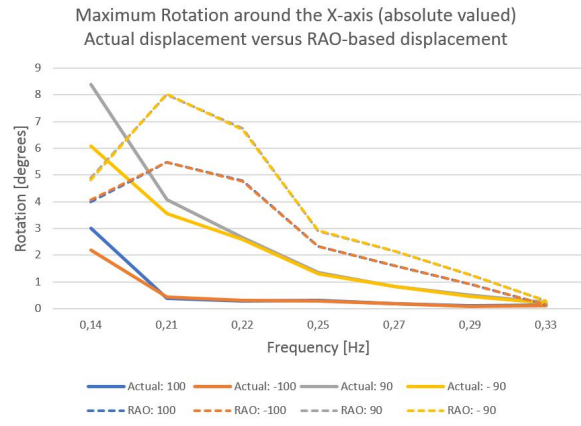


Figure H.22: Rotation around the X-axis
Actual rotation versus RAO-based rotation

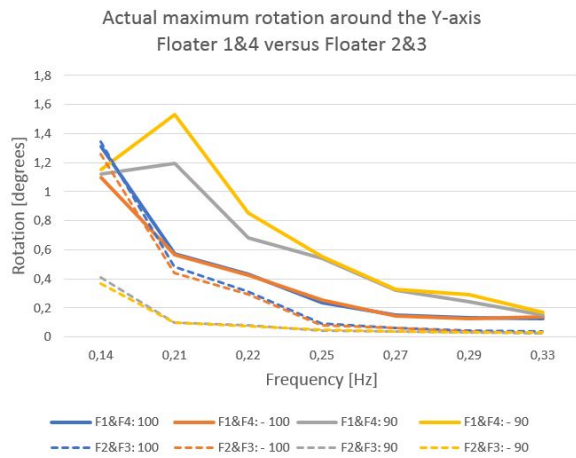


Figure H.23: Rotation around the Y-axis
Actual rotation Floater 1 and Floater 4 versus Floater 2 and Floater 3

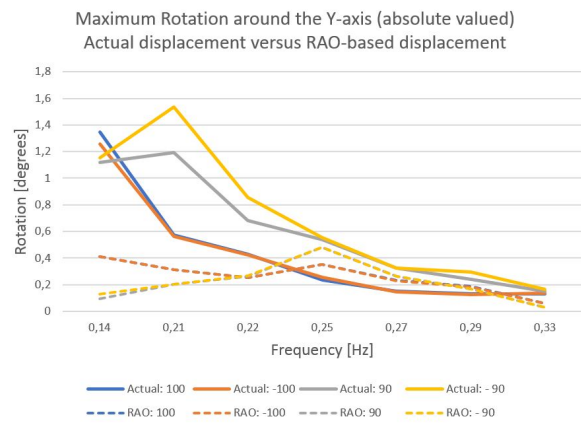


Figure H.24: Rotation around the Y-axis
Actual rotation versus RAO-based rotation

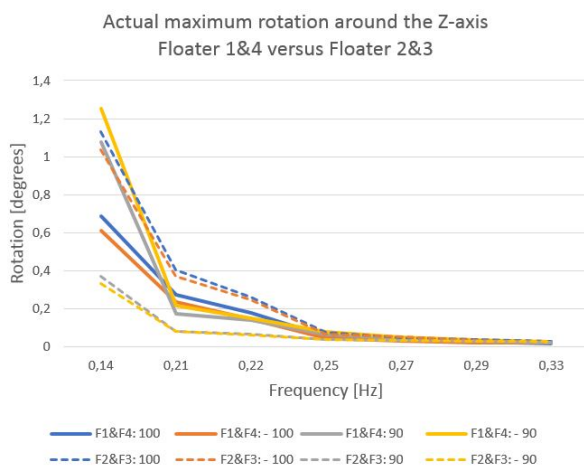


Figure H.25: Rotation around the Z-axis
Actual rotation Floater 1 and Floater 4 versus Floater 2 and Floater 3

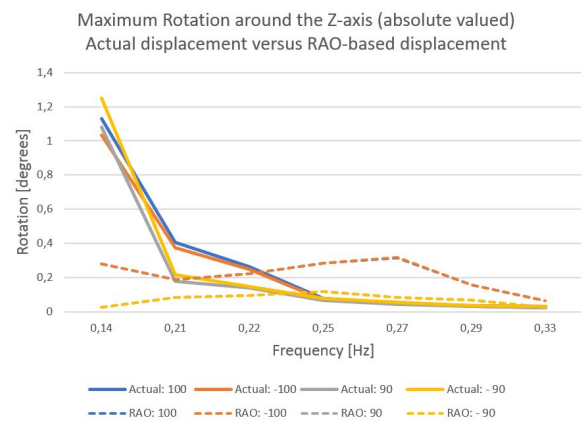


Figure H.26: Rotation around the Z-axis
Actual rotation versus RAO-based rotation

H.4. Time response analysis

A realistic load combination in the Larantuka Strait will consist of a combination of loads. The highest amount of motion induced solely by waves arises if the current velocity reaches zero. The current induces high drag forces that will overpower the motion induced by waves. Four times during a day the current magnitude approaches zero m/s, waves present during the time-interval will have free play on the bridge. The sensitivity analysis concluded that low frequency waves perpendicular directed to the bridge induce maximum displacement. Table H.5 shows the wave heights that are computed in Appendix C.4 and corresponding direction in the Ansys Aqwa axis system, Figure H.27.

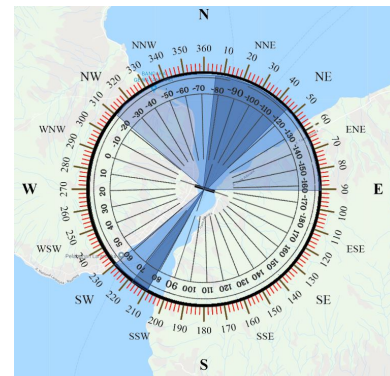


Figure H.27: Ansys Aqwa axis system versus compass directions

Windrose	direction [°]	Aqwa axis[°]	H_s [m]	H_{max} [m]	T_p [s]	L [m]	f [Hz]
5% of time	0-20	-78	0,74	1,47	4,30	28,86	0,23
	20-40	-102	0,80	1,61	4,49	31,49	0,22
	200-220	78	0,10	0,20	1,14	2,02	0,88
	220-240	58	0,33	0,67	2,66	11,01	0,38
1 year	0-20	-78	1,473	2,95	6,06	57,35	0,16
	20-40	-102	1,370	2,74	5,87	53,73	0,17
	200-220	78	0,162	0,32	1,38	2,99	0,72
	220-240	58	0,630	1,26	3,32	16,35	0,30
50 year	0-20	-78	2,147	4,29	7,14	79,62	0,14
	20-40	-102	1,713	3,43	6,56	67,20	0,15
	200-220	78	0,228	0,46	1,60	3,96	0,63
	220-240	58	1,039	2,08	4,06	17,33	0,25
100 year	0-20	-78	2,256	4,51	7,28	82,76	0,14
	20-40	-102	1,836	3,67	6,79	72,04	0,15
	200-220	78	0,238	0,48	4,09	4,09	0,62
	220-240	58	1,109	2,22	17,34	17,34	0,24

Table H.5: Significant waves with corresponding characteristics for governing directions

Two types of wave analyses are elaborated. The dynamic response to the individual floaters with respect to the highest hourly *significant* wave height. The analysis considers a time response of 3 600 seconds (1 hour) with an irregular JONSWAP wave spectrum. The other analysis type is focussed on the shape of the wave. The validity of wave theories indicated that the Third Order Stokes theory will be valid. Ansys Aqwa can calculate regular waves up to Second Order Stokes, the influence of the shape is checked for second order stokes wave with the *maximum* wave height. The wave parameters that are implemented to compute the dynamic response with respect to waves are presented in Table H.6.

	JONSWAP wave spectrum			Second order Stokes wave		
	Direction	H_s [m]	f [Hz]	Direction	H_{max} [m]	f [Hz]
1 year	90°	1,473	0,16	90°	2,95	0,16
50 years	90°	2,147	0,14	90°	4,29	0,14
100 years	90°	2,256	0,14	90°	4,51	0,14

Table H.6: Input parameters for maximum wave response at particular time period.

In the analysis the significant wave height (H_s) is implemented in the *Time Response Analysis* for irregular waves during a time period of 3 600 seconds. The maximum significant wave heights are based upon hourly

wind data records. Hence, the time response for an irregular waves with the corresponding significant wave height is computed during a time period of 1 hour (3 600 seconds). The wave surface elevation for the irregular JONSWAP wave is indicated in Figure H.28. The blue line indicates the induced rotation around the x-axis. Both plots indicate peak values at the same timesteps, showing the correlation of the surface elevation with the rotation. The rotation lags approximately 0,5 seconds behind for the rotation. The peak crest height of the wavegroup is 2,5 m and the maximum trough height -2,49 m. Corresponding to a wave height of $H_s \approx 5\text{m}$ and thus a ratio of $2,2 H_s = H_{max}$. This is of the same order size of the assumed ratio of 2:1 elaborated in Appendix C.4. The ratio for the 1 and 50 year surface elevation plots is of the same order, respectively 1:2,21 and 1:2,19.

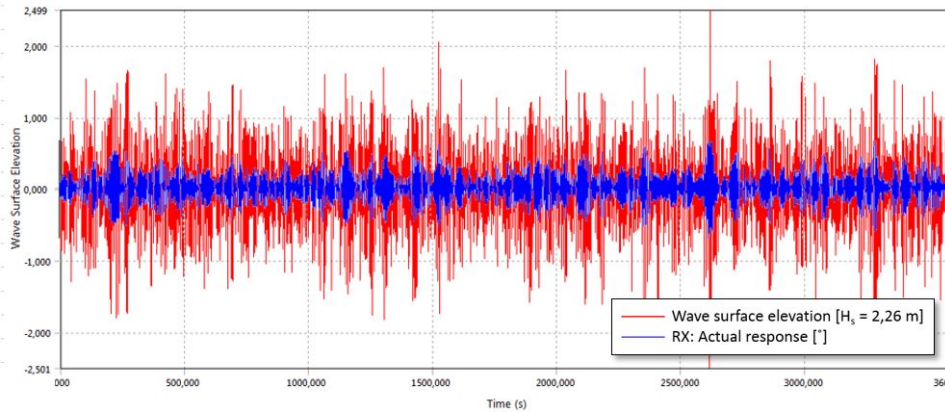


Figure H.28: Surface elevation of irregular wave with 100 year-properties during one hour (3 600 s)
Vertical axis for rotation around X axis is not present, degree range of -25° to 26°

According to the valid wave theory, the computed waves are *Third Order Stokes Theory waves*. The shape of such a wave changes, the peak becomes steeper and narrower. In addition, the wave height increases slightly. The increase in wave height is less than 2 cm for the 100 year wave. The form of the wave slope can have an effect on the dynamic response of the system. Ansys Aqwa is able to compute the dynamic response up to a second order (regular) Stokes wave. The difference between a second and third order wave is limited and the second order Stokes wave is assumed to give a correct approximation of the dynamic response. The Stokes waves can solely be implemented as regular wave, waves with a constant frequency and wave height. The response of the maximum wave height (H_{max}) is determined for a *regular second order Stokes wave*. The implemented parameters are given in Table H.6. The relation between the wave surface elevation and the rotation around the x-axis for the analysis is presented in Figure H.29. The timestep of the analysis is set to 300 seconds as the wave is constant. The maximum wave height is computed according to the ratio found in literature ratio of $2 H_s = H_{max}$ (Wulff Wathne, 2012). The plot indicates that the rotation angle of the response is counter directed to the positive values of the wave surface elevation. The first part of the plot indicates a phase lag of the rotation with respect to the wave height. An explanation for the phenomenon is that the surface elevation is measured underneath the Fixed Reference Axis (FRA), at the centre of the bridge axis. Rotation starts as the initial wave travelled past the width of the bridge. The wave with a period of 7,15 seconds (0.14 Hz) is proportional to wave with wave length of approximately 80 m. Indicating that after 3 seconds ($(34/80)*7,15=3,05\text{ s}$) the initial floater rotations arise. Hence, the phase lag of ≈ 3 seconds along the whole time sequence can be clarified.

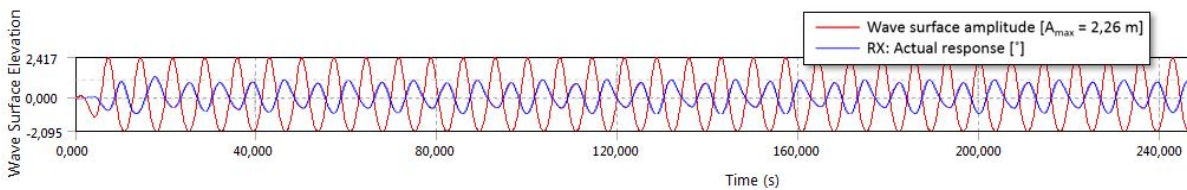


Figure H.29: Surface elevation of regular second order Stokes wave with 100 year-properties during 300 seconds
Corresponding rotation around the x-axis [degrees]
Vertical axis for rotation around X axis is not present, degree range of -21° to 29°

Realistic wave spectrum

In reality, a sea spectrum will not consist of regular waves or one irregular wave group. Many irregular wave groups coming from plenty direction will form the sea state. In the previous analysis the dynamic response of only one irregular wave group is analysed, if multiple wave groups are combined the total response will be different. In Figure H.30 two irregular wave groups are presented in the frequency and time domain (Journée and Massie, 2008). For each wave the form of waves for the specific frequency is plotted and the corresponding irregular wave responses over time are presented at the bottom of the figure. The final RAO with respect to heave is indicated with the red line in the centre of the image.

In the Strait of Larantuka, the wave spectrum is unknown. Therefore, the research is conducted for solely one irregular wave group at a time and not a combined sequence.

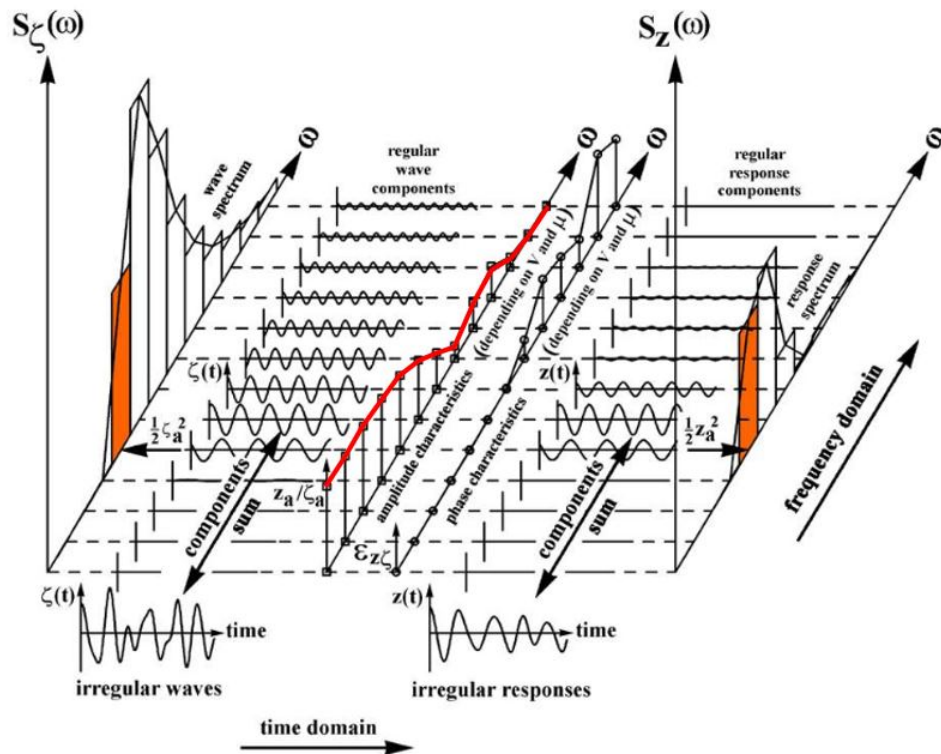


Figure H.30: Irregular wave group consisting of two waves (Journée and Massie, 2008 p.224)

Current results

The current is implemented with the *Structure Force Matrix* method in Ansys Aqwa. The method allows gradual variation of the drag force instead of an impulse load at $t=0$ s that result in high unrealistic oscillations. The model input section (Chapter 6 and Appendix G), indicated that the Ansys Aqwa model is inaccurate for high negative current velocities. With high negative current velocities the bridge deck tends to act like a flying kite. For that reason, the sensitivity analysis with respect to motion induced by the current is divided into two separate parts that consider respectively the negative and the positive current velocity.

I.1. Initial problems

The tidal water body travels through the narrow passage of the Strait of Larantuka and by adapting the tidal range, high magnitudes in the flow speed arise. The high flow speeds are desired for an optimal use of the tidal water power turbines. A counteracting result is that extremely high horizontal forces are induced on the submerged parts of the Tidal Bridge. The turbine suppliers should fulfill the requirement that the maximum moment around the x-axis does not exceed 2,1 MNm/m. The probable turbine type is the FishFlow turbine. According to a CFD-model, analysed by the company *Dynamicsim Engineering* to indicate the efficiency of the turbine, a force distribution on the turbines is found. Conversion of the data led to an estimation of the drag coefficient $C_d = 2,11$. The current magnitude that approaches the maximum moment with drag coefficient of 2,11 is 5,2 m/s. The magnitude seems realistic as a survey of *Aquaterra* measured maximum current velocities of this magnitude. The scope of the project assumes that the maximum moment is not exceeded. Therefore, the maximum current velocity checked in the analysis is set to 5,2 m/s. The relation between the current and the tide is analysis in Chapter C and presented in Figure I.1. The other figure, Figure I.2, shows the rescaled current velocity (maximum of 5,2 m/s) and corresponding drag force and moment that arise with the current. The figure indicates that the magnitude of forces and moments increases exponential to the current velocity.

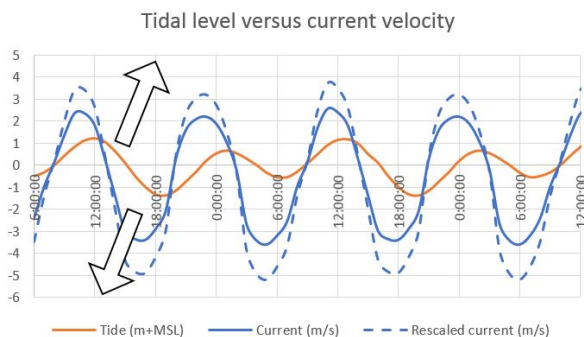


Figure I.1: Relation between Tidal Range, *average* current velocity and rescaled *maximum* current velocity (Aquaterra (2017)). Arrows indicate the direction of the current

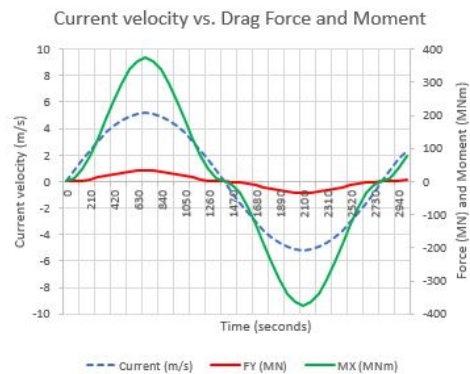


Figure I.2: *Maximum* current velocity with corresponding maximum drag force (MN) and Rotational x-moment (MNm)

The extreme rotations that are indicated in the model input sections were a result of the unrealistic situation that the floating bridge part will act like a kite. A visualisation of the probable reaction to both current directions is presented in Figure I.3. The right scenario represents the critical scenario in which the bridge may act like a kite. In reality the water body that flow through the turbine will have a stabilising effect, that counteracts the rotation induced by the current and the forces of the pendulum system. The flipping of the floater to the other side induces 'error' notification that result in abortion of the solve in Ansys Aqwa. The model is adjusted to prevent flipping of the system. The spudpole that allows some horizontal motion (along the x-axis) is restricted with a cable that acts like a spring, Figure I.4. The cable consists of first and second order displacement effects (δx_1 and δx_2). The first order effect is the initial displacement that may arise by the connection sleeve between the floater and the spudpole. The second order displacement is induced by the bending stiffness of both steel spudpole frames. The sensitivity of the response is checked for different values of the cable stiffness and the initial displacement δx_1 .

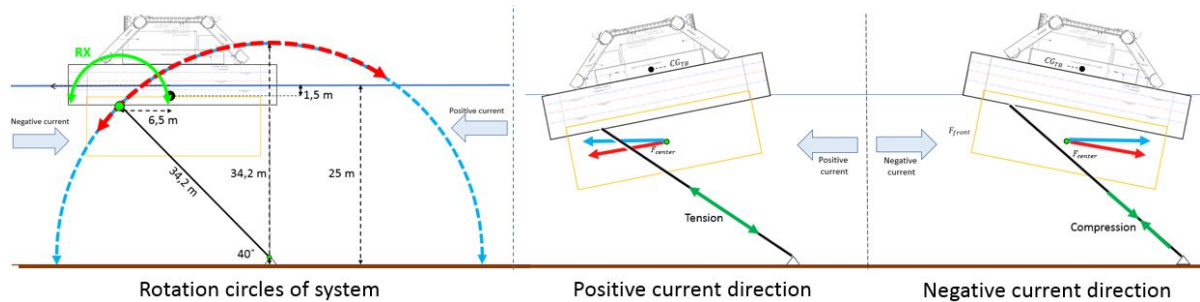


Figure I.3: Probable reaction of the system with respect to the current (no change in water level)

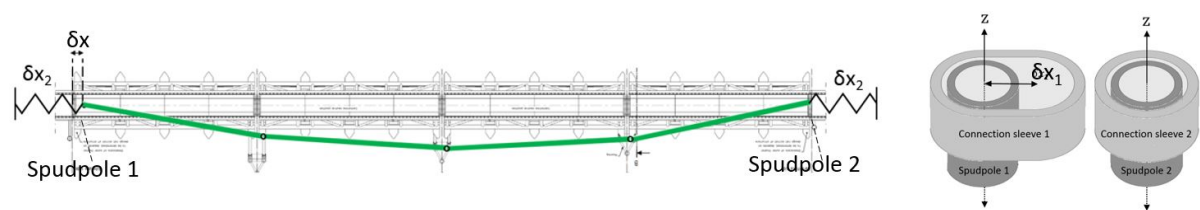


Figure I.4: The spudpole system. Left: Topview displaced bridge with spring on the left side. Right: Topview of both spudpoles.

I.2. Cable properties

A short *linear elastic cable* is defined between the spudpole that is able to move in x-direction and a 'Fixed point'. The cable requires definition of two cable properties: unstretched length and cable stiffness. The unstretched length may represent the first order effect, the possibility of the spudpole connection to move along the length δx_1 , Figure I.4. The length of δx_1 is unknown and should be estimated. The second order effect is the bending of the spudpole constructions, Figure I.6. The present spudpole design is implemented in Matrixframe and with a horizontal point force of 21,8 MN (representing the drag force) a displacement of 0,30 m is induced. The computed characteristics are converted to an indication of the cable stiffness: $k = F/x = 72,55$ MN/m. At both bridge ends a spudpole connects the floating bridge part to the mainland. Bending may occur at both bridge ends. Within the Ansys Aqwa model the bending is mimicked with cables with a stiffness of 72,55 MN/m attached to the 'infinitely stiff' spudpoles. If the rotation around the x-axis is plotted for one tidal cycle and cables at both bridge ends, a peak will be present at a negative current velocity, Figure I.5.

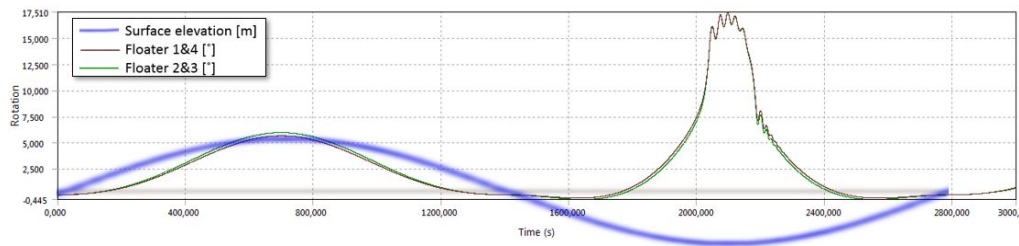


Figure I.5: Rotation around the x-axis for one tidal cycle with two implemented cables

Graph G.24 indicates that the rotation of the bridge deck will be positive during both a positive and a negative current velocity. This is contradictory to the initially forecasted response. The two situations are visualised in Figure I.7. Another observation is that during the negative flow velocity, Aqwa calculates the steady state response of the two centre floaters above the water level, Figure I.8.

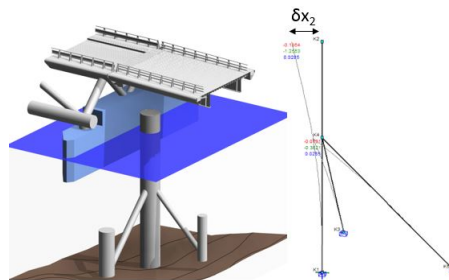


Figure I.6: Second order effect of the spudpole

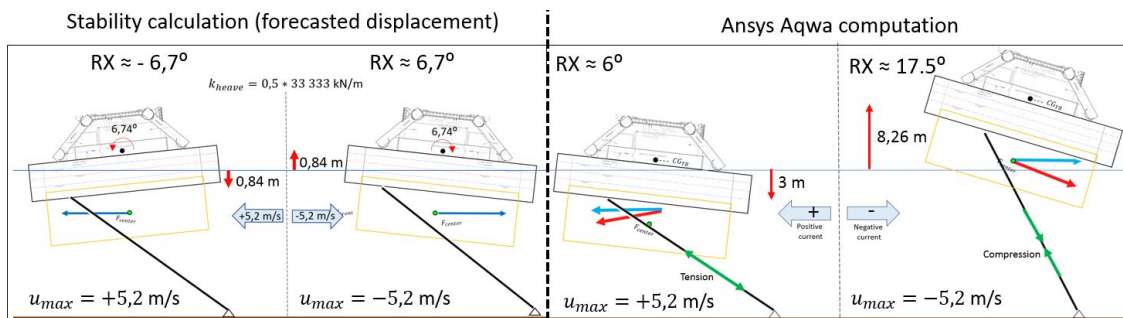


Figure I.7: Forecasted displacement versus Displacement computed by Ansys Aqwa. Both seen with respect to the middle two floaters

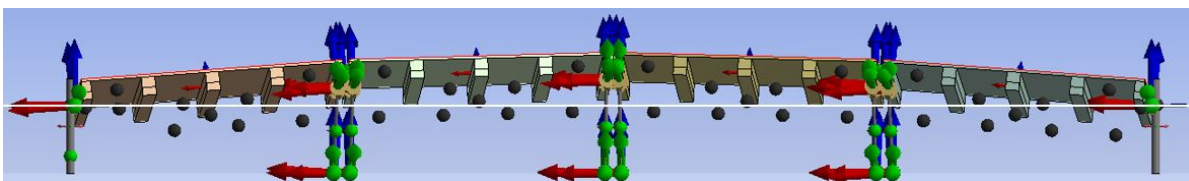


Figure I.8: Screenshot of displaced Tidal Bridge. Middle two pontoons are located above the water line. Water line is presented as the white horizontal line

The induced unrealistic rotations are a result of the attachment point of the Structure Force Matrix. For every manually defined drag force method, the attachment point of the force is at the centre of gravity of the structure. If the centre of gravity of the structure is adjusted, the hydrostatic properties will change and the new geometry will not match with the calculated dynamic characteristics. The rotational moments are defined by multiplying the horizontal drag force with the distance from the centre of gravity to the force position. If the system moves vertically, the 'arm' remains constant and the drag force moves upwards, the arrows in Figure I.7 indicate the (displaced) drag force. The sensitive degrees of freedom for a the current sensitivity study are thus the rotation around the X-axis and the vertical displacement along the Z-axis.

In addition, the displacement along the x-axis for the spudpoles indicates the amount of bending of the spudpole. High displacement suggest that the spudpole might collapse. The relation between the amount of rotation and the displacement of the spudpole if one spudpole is not restricted by cable is checked for a *positive* current velocity. The results of the 'original' model, without cables and one spudpole that is free to move along the x-axis, is presented in the plot in Figure I.9. The positive current induces a displacement of the spudpole of 35 cm. The relatively small displacement might function as a base for the order size of the δx_1 displacement of the connection sleeve.

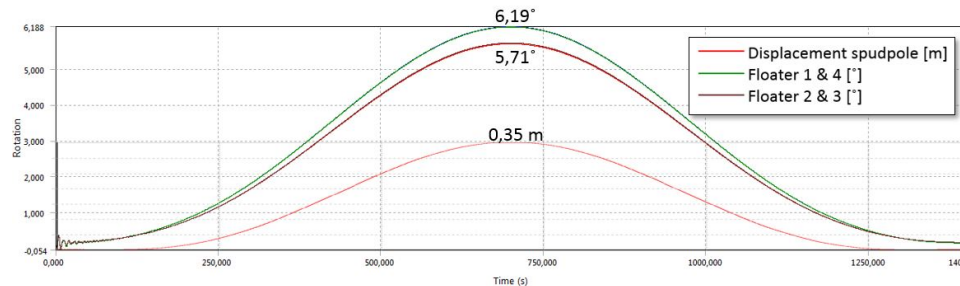


Figure I.9: Displacement of the spudpole and rotation around the x-axis for a positive current force ($u_{max} = 5,2$ m/s).

The distribution of the forces in the mooring system at the maximum *positive* flow speed, is examined and an overview is presented in Figure I.10. The force distribution is symmetric for a perpendicular directed flow speed. The sum of the forces in y-direction is almost zero verifying Newtons third law: *For every action there is an opposite and equal reaction*, equation I.1. The slight difference can be explained by the transfer of forces between the spudpole and the cable. The tension force in the cable is the sum of all combined forces and a small part, approximately 0,3 MN is included in the cable tension force.

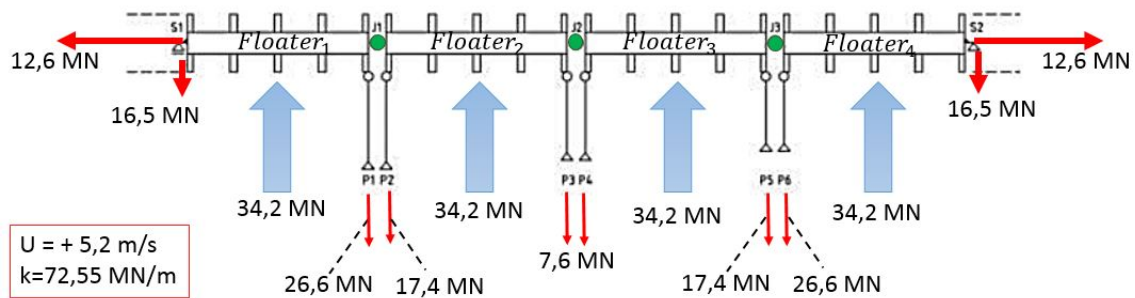


Figure I.10: Distribution of the horizontal forces in the mooring elements as a result of a *positive* current velocity of 5,2 m/s

$$\begin{aligned}
 F_{\text{action}} &= F_{\text{reaction}} & (I.1) \\
 \sum F_h &= 0 \\
 4 \cdot 34,2 &= 2 \cdot (16,5 + 26,6 + 17,4 + 7,6) \\
 136,8 &\approx 136,2
 \end{aligned}$$

Another observation is the high forces present in the mooring pendulums, especially the two outer pendulums. The pendulum needs to transfer tension and compression forces of approximately this magnitude. Steel is distinctive for the high tension and compression strength, but after a certain limit, the pendulum will collapse. In addition, another failure mechanism may be the buckling of the pendulum or fatigue. The scope of the research does not include the technical feasibility of the construction materials, but an additional study is definitely obligatory.

The sensitivity of the system to a certain flow speed is checked for a variation of properties of the spudpole. First, the sensitivity to an increased bending stiffness is analysed and secondly the effect on an initial displacement due to the connection sleeve is determined.

I.3. Spudpole design iterations

The final cable stiffness is based upon the possibilities to increase the spudpole design. With an iterative process in Matrixframe it is checked if the bending stiffness of the spudpole can be adjusted easily. The base of the adjusted design is to move the connection point of both supporting beams upwards, point 1 in Figure I.11. Another option is to displace the application point of the supporting beams, points 2 and 3. Or to increase the diameter or thickness of the beams. A couple of adjustments in the design are examined and presented in Table I.1. With slight improvements of the design, a duplication of bending stiffness can be reached. A conservative stiffness design is suggested to prevent failure in extreme conditions. Hence, the design improvements that result in a stiffness of 160 MN/m is suggested for the spudpole design.

Design	Change in design	Force [MN]	δx_2 [m]	Stiffness [MN/m]	Sensitivity
1	Original design	70	0,96	72,55	-
2	Move point 1, 1 m up	70	0,64	109,38	High
3	Move point 1, 2 m up	70	0,57	123,89	Medium
4	Move point 2, 1 m	70	0,73	96,42	Low
5	Increase thickness 30 mm to 50 mm	70	0,60	116,67	High
6	Move point 1, 2 m up+ increase thickness	70	0,44	159,45	High

Table I.1: Sensitivity to design changes within spudpole construction (Matrixframe)

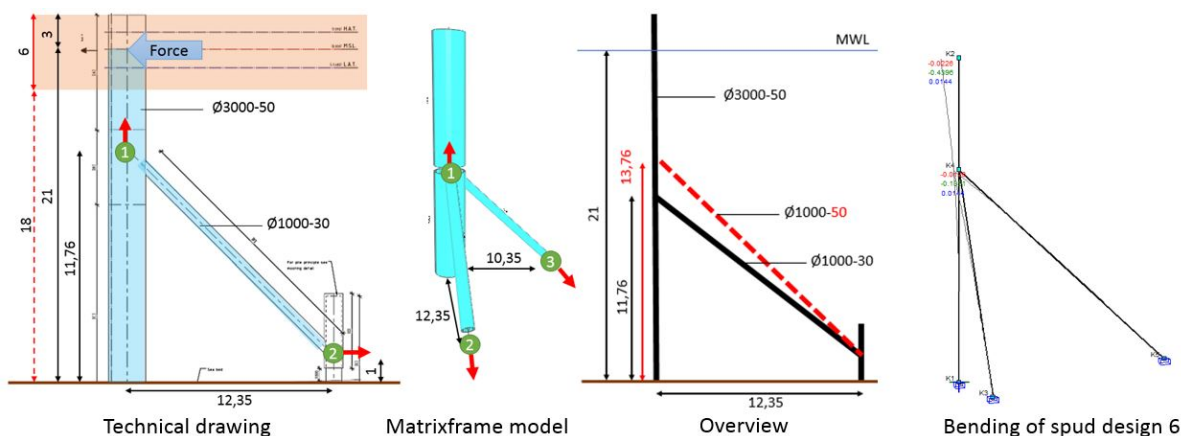


Figure I.11: Possibilities to improve spudpole design. Red shaded area in left image indicates area that should be available to adjust to displacements. Right images shows possible final design with bending stiffness of 160 MN/mm

The force distribution with the suggested spudpole design is checked and presented for a positive and negative current in Figures I.12 and I.13. Comparing both images, it can be seen that the force distribution in the pendulum system remains approximately equal, except for the vertical forces. This is verified by the unrealistic extreme upwards displacement that arises for the floaters. The forces that should be transferred are high and the deformation of the system will be essential in the technical feasibility of the bridge.

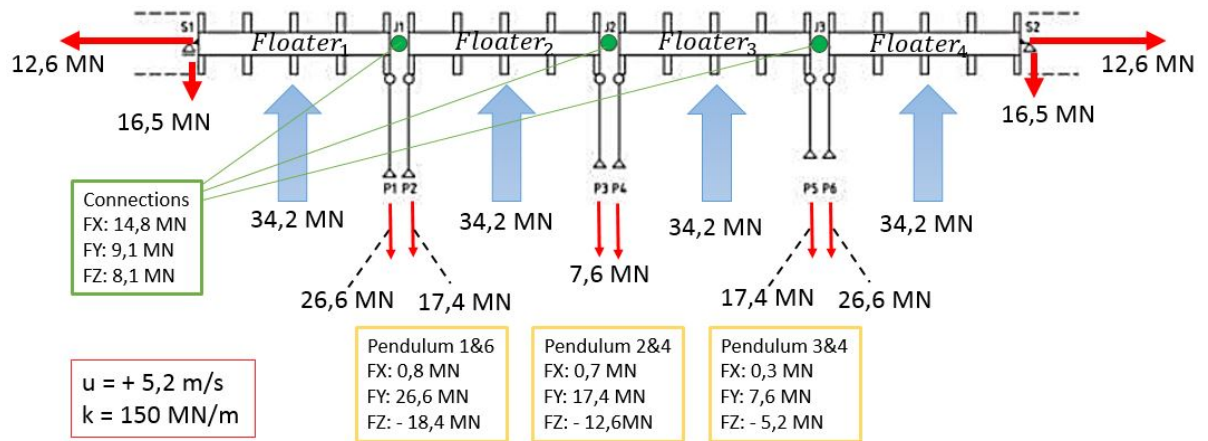


Figure I.12: Force distribution for a *positive* maximum flow speed and spudpole with stiffness of 150 MN/m and initial displacement of 0,12 m.

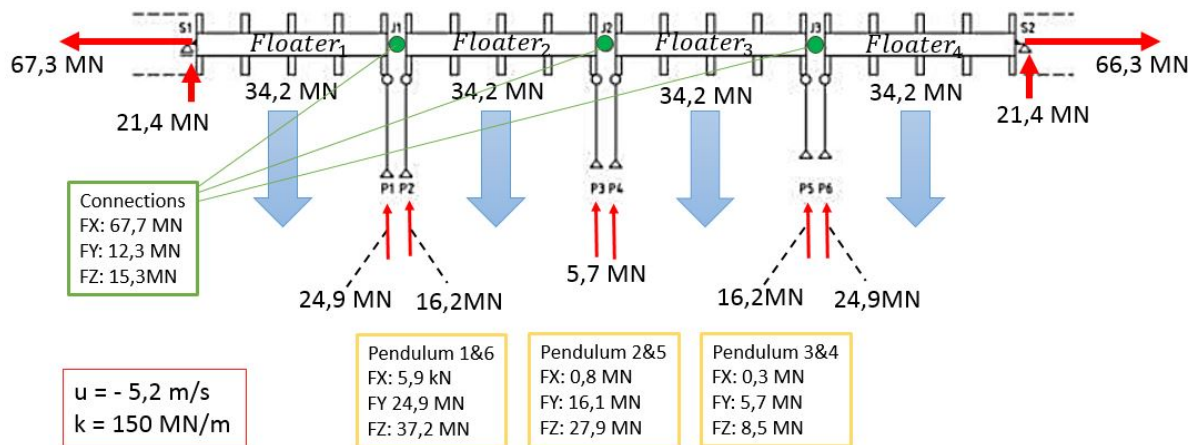


Figure I.13: Force distribution for a *negative* maximum flow speed and spudpole with stiffness of 150 MN/m and initial displacement of 0,12 m.

Lists of symbols

List of Latin symbols

Symbol	Description	Units
A_i	Area of element i	[m ²]
C	Damping matrix	[kN/m]
C_D	Drag coefficient (static)	[-]
D	Diameter	[m]
E_{cm} or E_s	Modulus of elasticity	[N/mm ²]
F_i	Force induced by i	[kN]
H	Height	[m]
H_{max}	Maximum wave height	[m]
H_s	Significant wave height	[m]
I_{ii}	Moment of inertia in direction ii	[mm ⁴]
K	Stiffness matrix	[kN/m]
J_i	Angular mass moment of inertia	[kg m ²]
L	Wave length	[m]
M	Moment	[kNm]
M_a	System added mass matrix	[kg]
M_i	Mass of element i	[kg]
N_i	Number of elements of element i	[-]
Q	Concentrated load	[kN]
S	Strouhal number	[-]
T	Period	[s]
T_p	Significant wave period	[s]
T_0	Undamped eigenperiod	[s]
U	Wind velocity	[m/s]
U_{10}	Wind velocity at 10 meters altitude	[m/s or km/h]
V_i	Volume of element i	[m ³]
W	Width	[m]
a	Amplitude	[m]
c	Damping ratio	[m/s ²]
d	Water depth	[m]
d_p	Draught pontoons	[m]
e_i	Eccentricity of element i	[m]
f	Frequency	[Hz]
f_n	Natural frequency	[Hz]
g	Gravitational acceleration	9,81 [m/s ²]
h	Average water depth	[m]
k	Wave number	[-]
k_i	Stiffness of element i	[m/s]
m	Mass	[kg]
$m + a$	Virtual mass	[kg]
p_i	Pressure due to element i	[Pa]
q	Uniform distributed load	[kN/m]
t	Time	[s]
u	Flow velocity	[m/s]
x	Displacement along x-axis, surge	[m]
x_r	Rotational distance	[m]

y	Displacement along y-axis, sway	[m]
z	Displacement along z-axis, heave	[m]
z_i	Distance between components	[m]

List of Greek symbols

Symbol	Description	Units
α_i	Angle or phase angle of element i	[°]
ϵ_{su}	Ultimate steel strain	[%]
ζ_i	Modal damping factor for mode i	[-]
η	Surface elevation	[m]
ϕ	Rotation in roll direction, around x-axis	[°]
ξ	Phase shift	[°]
ψ	Rotation in yaw direction, around z-axis	[°]
θ	Rotation in pitch direction, around y-axis	[°]
ρ_w	Density of water	1025 [kg/m ³]
ω	Radian frequency	[rad/s]

Notations

Symbol	Description	Units
x	Displacement	[m]
\dot{x}	Velocity	$\frac{dx}{dt}$ [m/s]
\ddot{x}	Accelerations	$\frac{d^2x}{dt^2}$ [m/s ²]

List of abbreviations

Symbol	Description
ADCP	Acoustic Doppler Current Profiler
CG_i	Centre of Gravity of element i
DOF	Degrees of Freedom
FD	Frequency Domain
FEED phase	Front End Engineering Design phase
FRA	Fixed Reference Axis
GEV	General Extreme Value distribution
HAT	Highest Astronomical Tide
LAT	Lowest Astronomical Tide
MHWN	Mean High Water Neap
MHWS	Mean High Water Spring
MSL	Mean Sea Level
MLWN	Mean Low Water Neap
MLWS	Mean Low Water Spring
NTT	Nusa Tenggara Timur government
RAO	Response Amplitude Operator
TD	Time Domain

References

- Ansys Inc. (2012a). AQWA User Manual. Technical report, Ansys Inc., Canonsburg.
- Ansys Inc. (2012b). Introduction to Hydrodynamic Analysis with ANSYS Aqwa. Technical report, Ansys Inc.
- Ansys Inc. (2015). Ansys Aqwa Theory Manual.
- Antea Group (2018). Ontwerptoelichting feasibility study Palmerah Tidal Bridge. Technical report, Antea Group.
- Aquatera (2017). Larantuka Straits, NTT - Metocean survey. Analysis results of tidal data from Tide Gauge and ADCO observatuib. Technical report, Bintang Subsea and Aquatera, Larantuka Strait Indonesia.
- Bartrop, N. (1998). *Floating structures: a guide for design and analysis*. CMT and OPL, volume 1 edition.
- Bitter, J. and Hoogeveen, A. (2014). Design Responsibility - Tidal Bridge. Technical report, Strukton and Antea Group.
- Bosboom, J. and Stive, M. (2015). *Coastal Dynamics I - Lecture notes CIE4305*. Delft University of Technology, Faculty of Civil Engineering and Geosciences - Section of Hydraulic Engineering, Delft University of Technology, version 0. edition.
- Bridge Management System (1992). Bridge Design Manual - Volume 1. Technical report, Directorate General of Highways Ministry of Public Works Republic of Indonesia.
- British Standards Institution (1989). BS6349: British Standard Code of practice for Maritime Structures, Part 6: Design of inshore moorings and floating structures. Technical report, British Standards Institution, England.
- Brito e Melo, A. and Luis Vilate, J. (2016). Annual report Ocean Energy Systems 2016. Technical report, The Executive Committee of Ocean Energy Systems.
- CBS (2018). Trends in the Netherlands 2018.
- CROW (2004). ASVV 2004 - Aanbevelingen voor verkeersvoorzieningen binnen de bebouwde kom. Technical report, Stichting Centrum voor de Regelgeving en Onderzoek in de Grond-, Water- en Wegenbouw en de Verkeertechniek.
- de Rijke, S., Koot, J., and Sengers, F. (2017). Design Report Palmerah bridge - Civil Structure. Technical report, Tidal Bridge and Strukton.
- Det Norske Veritas (2010a). Environmental Conditions and Environmental Loads. Technical report, Recommended Practice DNV-RP-C205.
- Det Norske Veritas (2010b). Environmental conditions and Environmental Loads - Recommended Practice DNV-RP-C205. Technical report, Det Norske Veritas, Norway.
- Det Norske Veritas (2011). Modelling and analysis of marine operations - Recommended practice DNV-RP-H103. Technical report, Det Norske Veritas.
- Det Norske Veritas (2014). Design of Offshore Wind Turbines Structures. Offshore Standard: DNV-OS-J101. Technical report, Det Norske Veritas.
- Drie-D (2017). D-glide Spherical SD360L1 and Concept bottom connector uni-joint. Technical report, Drie-D Lagertechniek, Berkel en Rodenrijs.

- Dutch Water Sector (2017). Tidal Bridge shifts gear for floating bridge with tidal power plant in Larantuka Strait, Indonesia.
- Dynasim Engineering (2017). Tidal Bridge performance with FishFlow Innovations Turbine. Technical report, Dynasim Engineering.
- EMD International A/S (2017). Wind Energy Resources of Indonesia.
- European Commission (2015). Paris Agreement (COP21).
- Gerritsma, J. (2003). *MT3408 - Hydromechanica 4: Scheepsbewegingen, sturen en manoeuvreren*. Werktuigbouwkunde en Maritieme Techniek Sectie Scheepshydrodynamica, Delft University of Technology.
- Gupta, S., Stoddart, E., Sanderson, D., and Morrison, A. (2015). Condition Monitoring of Offshore wind turbines with scour and grout damage in monopile foundations. Technical report, SECED 2015 Conference: Earthquake Risk and Engineering towards a Resilient World, Cambridge.
- Hendriksen, E. (2018). *Dynamic behaviour of the Sognefjord Bridge*. Master's thesis, Delft University of Technology & IV Groep.
- Heuberger, C. (2018). *Assesment of the dynamic response of a floating pontoon bridge with a fiber reinforced polymer superstructure*. Master's thesis, Delft University of Technology & Royal HaskoningDHV.
- Holthuijsen, L. (2007). *Waves in Oceanic and Coastal Waters*. Cambridge University Press, New York.
- Jarquín-Laguna, A. (2018). *CIE5304 - Waterpower engineering. "Energy at sea: wind, wave and tidal energy"*. Offshore Engineering, Delft.
- Jonkman, S., Steenbergen, R., Morales-Napoles, O., Vrouwenverlder, A., and Vrijling, A. (2017). Probabilistic Design: Risk and Reliability Analysis in Civil Engineering. (Lecture notes CIE430).
- Journée, J. and Massie, W. (2008). *Offshore Hydromechanics*. Delft University of Technology, Faculty of Civil Engineering and Geosciences - Section of Offshore Technology, Delft, 2 edition.
- Molenaar, W. and Voorendt, M. (2018). *Manual Hydraulic Structures - February 2018*. Delft University of Technology, Delft, february 2 edition.
- Noveltis (2015). Tide Prediction Service from high resolution modelling.
- Ocean Energy Systems (2011). An International Vision for Ocean Energy. Technical report, Dutch Marine Energy.
- Orhan, K., Mayerle, R., and Widodo Pandoe, W. (2015). Assesment of energy production potential from tidal stream currents in Indonesia. Technical report, European Geosciences Union General Assembly 2015, EGU, Division Energym Resources and Environment, Germany.
- Overkamp, N. and Van Wierst, B. (2018). Assignment: Data Analysis, Expert Judgement and Bayesian Networks. Technical report, CIE5310: Delft University of Technology, Probabilistic Design in Hydraulic Engineering.
- Peraire, J. and Widnall, S. (2008). Lecture L26 - 3D Rigid Body Dynamics: The Inertia Tensor. Technical report, Massachusetts Institute of Technology, Massacusetts.
- Singgih, V. (2018). Indonesia to build world's biggest tidal power plant.
- Spijkers, J., Vrouwenvelder, A., and Klaver, E. (2006). *Dynamics of Structures - Part 1: Vibration of Structures*. Faculty of Civil Engineering and Geosciences, Delft University of Technology, Delft.
- Tasma, T. (2017). Technical drawings - pre-feasibility study Tidal Bridge Larantuka. Technical report, Tidal Bridge and Antea Group, Larantuka.
- Tidal Bridge (2018). Introduction Tidal Power Plant. Technical report, Eindhoven.

- Time and Date (2017). Moon Phases 2017 - Lunar Calendar for Denpasar, Bali, Indonesia.
- van den Eijnden, E. and Middelweerd, H. (2017). PODCAST: Tidal Bridge en de kracht van getijdenenergie.
- Viecili, G., Halim, A., Braimah, A., and El-Desouky, O. (2014). Transportation Optimization of Ribbon Floating Bridges: Analytical and Experimental Investigation. *The Open Civil Engineering Journal*, 8:42–56.
- Volcano Discovery (2019). Volcanoes of Indonesia.
- Vos, R.-J. (2017). Palmerah Tidal Bridge - Feasibility Study. Technical report, Tidal Bridge and Antea Group.
- Vroegrijk, E. (2017). OCIMF - CFD Current Drag. Technical report, OCIMF Technical Investigation Department.
- Vyzikas, T., Stagonos, D., Buldakov, E., and Greaves, D. (2018). The evolution of free and bound waves during dispersive focusing in a numerical and physical flume. *Coastal Engineering*, 132:95–109.
- Wan Ahmad, S., Qing, L., Adnan, A., and Ramli, M. (2019). Unity check of typical offshore wellhead platform in Malaysia using Aceh earthquake loading data and SAP2000. *IOP Conference Series Earth and Environmental Science*, 244(012048).
- Wang, C. and Wang, B. (2015). *Large Floating Structures - Technological Advances*. Springer Science+Business Media, Singapore, 3 edition.
- Wulff Wathne, A. (2012). *Dynamic modelling and analysis of floating bridges (Dynamisk modellering of analyse av flytebruer)*. Master's thesis, NTNU - Norwegian University of Science and Technology.